



Ministério da
**Ciência, Tecnologia
e Inovação**



sid.inpe.br/mtc-m19/2014/01.15.12.56-TDI

**A MULTI-OBJECTIVE MEMETIC APPROACH FOR
THE AUTOMATIC DESIGN OF OPTICAL SYSTEMS
(UMA ABORDAGEM MEMÉTICA E MULTI OBJETIVA
PARA O PROJETO AUTOMÁTICO DE SISTEMAS
ÓPTICOS)**

Braulio Fonseca Carneiro de Albuquerque

Doctorate Thesis Course Graduate in Space Engineering and Technology/Space Systems of Management and Engineering, guided by Dr. Fabiano Luis de Sousa, approved in February 05, 2014.

URL of the original document:

<<http://urlib.net/8JMKD3MGP7W/3FJ6RME>>

INPE
São José dos Campos
2014

PUBLISHED BY:

Instituto Nacional de Pesquisas Espaciais - INPE

Gabinete do Diretor (GB)

Serviço de Informação e Documentação (SID)

Caixa Postal 515 - CEP 12.245-970

São José dos Campos - SP - Brasil

Tel.:(012) 3208-6923/6921

Fax: (012) 3208-6919

E-mail: pubtc@sid.inpe.br

BOARD OF PUBLISHING AND PRESERVATION OF INPE INTELLECTUAL PRODUCTION (RE/DIR-204):**Chairperson:**

Marciana Leite Ribeiro - Serviço de Informação e Documentação (SID)

Members:

Dr. Antonio Fernando Bertachini de Almeida Prado - Coordenação Engenharia e Tecnologia Espacial (ETE)

Dr^a Inez Staciarini Batista - Coordenação Ciências Espaciais e Atmosféricas (CEA)

Dr. Gerald Jean Francis Banon - Coordenação Observação da Terra (OBT)

Dr. Germano de Souza Kienbaum - Centro de Tecnologias Especiais (CTE)

Dr. Manoel Alonso Gan - Centro de Previsão de Tempo e Estudos Climáticos (CPT)

Dr^a Maria do Carmo de Andrade Nono - Conselho de Pós-Graduação

Dr. Plínio Carlos Alvalá - Centro de Ciência do Sistema Terrestre (CST)

DIGITAL LIBRARY:

Dr. Gerald Jean Francis Banon - Coordenação de Observação da Terra (OBT)

DOCUMENT REVIEW:

Marciana Leite Ribeiro - Serviço de Informação e Documentação (SID)

Yolanda Ribeiro da Silva Souza - Serviço de Informação e Documentação (SID)

ELECTRONIC EDITING:

Maria Tereza Smith de Brito - Serviço de Informação e Documentação (SID)

Luciana Manacero - Serviço de Informação e Documentação (SID)



Ministério da
**Ciência, Tecnologia
e Inovação**



sid.inpe.br/mtc-m19/2014/01.15.12.56-TDI

**A MULTI-OBJECTIVE MEMETIC APPROACH FOR
THE AUTOMATIC DESIGN OF OPTICAL SYSTEMS
(UMA ABORDAGEM MEMÉTICA E MULTI OBJETIVA
PARA O PROJETO AUTOMÁTICO DE SISTEMAS
ÓPTICOS)**

Braulio Fonseca Carneiro de Albuquerque

Doctorate Thesis Course Graduate in Space Engineering and Technology/Space Systems of Management and Engineering, guided by Dr. Fabiano Luis de Sousa, approved in February 05, 2014.

URL of the original document:

<<http://urlib.net/8JMKD3MGP7W/3FJ6RME>>

INPE
São José dos Campos
2014

Cataloging in Publication Data

Albuquerque, Braulio Fonseca Carneiro de.
Al15a A multi-objective memetic approach for the automatic design of optical systems (Uma abordagem memética e multiobjetiva para o projeto automático de sistemas ópticos) / Braulio Fonseca Carneiro de Albuquerque. – São José dos Campos : INPE, 2014.

xxii + 184 p. ; (sid.inpe.br/mtc-m19/2014/01.15.12.56-TDI)

Thesis (Doctorate in Space Engineering and Technology/Space Systems of Management and Engineering) – Instituto Nacional de Pesquisas Espaciais, São José dos Campos, 2014.

Guiding : Dr. Fabiano Luis de Sousa.

1. evolutionary optimization. 2. optical design. 3. multi-objective. 4. memetic. I.Título.

CDU 629.7:535.8



Esta obra foi licenciada sob uma Licença [Creative Commons Atribuição-NãoComercial 3.0 Não Adaptada](https://creativecommons.org/licenses/by-nc/3.0/).

This work is licensed under a [Creative Commons Attribution-NonCommercial 3.0 Unported License](https://creativecommons.org/licenses/by-nc/3.0/).

Aprovado (a) pela Banca Examinadora
em cumprimento ao requisito exigido para
obtenção do Título de **Doutor(a)** em

**Engenharia e Tecnologia
Espaciais/Gerenciamento de Sistemas
Espaciais**

Dr. Mário Luiz Selingardi



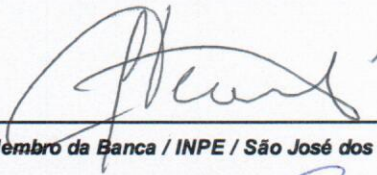
Presidente / INPE / SJC Campos - SP

Dr. Fabiano Luis de Sousa



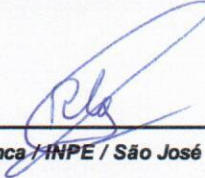
Orientador(a) / INPE / SJC Campos - SP

Dr. Leonel Fernando Perondi



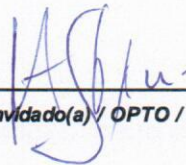
Membro da Banca / INPE / São José dos Campos - SP

Dr. Roberto Luiz Galski



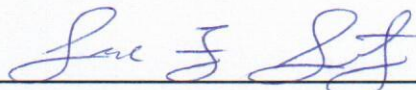
Membro da Banca / INPE / São José dos Campos - SP

Dr. Mário Antônio Stefani



Convidado(a) / OPTO / São Carlos - SP

Dr. Lucas Fugikawa Santos



Convidado(a) / UNESP / São José do Rio Preto - SP

Este trabalho foi aprovado por:

maioria simples

unanimidade

Aluno (a): **Bráulio Fonseca Carneiro de Albuquerque**

São José dos Campos, 05 de Fevereiro de 2014

ACKNOWLEDGEMENTS

First of all, I thank God for blessing me with wisdom, strength, perseverance and determination to carry out this work.

I would like to express my gratitude to my advisor Dr. Fabiano Luis de Sousa for introducing me to the topic of evolutionary optimization, inspiring me in the definition of the theme of this thesis, and for his useful ideas, comments, remarks and engagement through the developing process of this Ph.D. thesis.

A Special thanks goes to M.Sc. Amauri Silva Montes for the valuable guidance and advice in the optics field involved in this work. Mr. Amauri has helped in this thesis as a co-advisor from the very early stage of this research, providing ideas and supporting this work with his remarkable experience.

I express my special appreciation and thanks to Professor José M. Sasián for being my host during my year abroad in the Ph.D. program at the University of Arizona. Dr. Sasián has provided me with outstanding academic and professional opportunities. Moreover, I appreciate the feedback offered by Dr. Sasián about my Ph.D. thesis document.

Thanks to my deceived friend Dr. Juan Rayces for the illuminating discussions on classical optimization methods in lens design and glass selection. Dr. Rayces inspired me to pursue the studies about optimization in lens design.

I'm grateful to all friends and coworkers who have somehow helped me in my thesis, special thanks to M.Sc. Marcos Eduardo Borges for helping me out in the speed performance improvements of my codes used in this thesis and to Dr. Lin-Yao Liao for helping me in the implementations of some subroutines.

I would also like to thank my committee members for the valuable comments and suggestions to improve the level of my work.

I gratefully acknowledge the Kidger Optics Associates, Tina Kidger and the selection committee for awarding me the Michael Kidger Memorial Scholarship in Optical Design of 2010. This prize was a turning point in my career, providing me with unexpected and priceless opportunities.

Finally, I would like to thank my beloved families, specially my wife, for their understandings and supports on me in completing this project.

ABSTRACT

An innovative, evolvable hardware method for the automatic design of optical systems is presented and verified. The proposed method is based on a multi-objective memetic optimization algorithm. The multi-objective approach simultaneously, but separately, addresses the image quality, tolerance, and complexity of the system. The memetic technique breaks down the search for optical designs in three different parts or phases: optical glass selection, exploration, and exploitation. The optical glass selection phase is based on the unification of two previously published methods with new contributions to repair practical implementation issues and incorporates a multi-objective approach. This new glass selection method supports the choice of the most appropriate set of glasses for the system under design. The glass selection phase limits the available glasses from hundreds to just a few, drastically reducing the design space and significantly increasing the efficiency of the automatic design method. The exploration phase is based on an evolutionary algorithm (EA), more specifically, on a problem-tailored generalized extremal optimization (GEO) algorithm named optical GEO (O-GEO). The new EA incorporates many features customized for lens design such as optical system codification and diversity operands. The non-dominated systems found in the exploration phase are refined by a local search based on the damped least square method in the exploitation phase. As a result, the method returns a set of non-dominated solutions generating a Pareto front. Our method resulted in alternative and useful insights about the trade-off solutions for a lens design problem. The efficiency of the proposed method is verified through examples, showing excellent results for both simple systems and real-world problems.

UMA ABORDAGEM MEMÉTICA E MULTIOBJETIVO PARA O PROJETO AUTOMÁTICO DE SISTEMAS ÓPTICOS

RESUMO

Método inovador de hardware evolutivo para o projeto automático de sistemas ópticos é apresentado e validado. O método proposto se baseia em um algoritmo memético multiobjetivo de otimização. A abordagem multiobjetivo busca otimizar simultaneamente, mas de forma separada, a qualidade da imagem, a tolerância e a complexidade do sistema. A investida da técnica memética divide a busca por projetos de sistemas ópticos em três fases distintas: seleção de vidros ópticos, exploração e intensificação. A fase de seleção de vidros ópticos é baseada na unificação de dois métodos previamente publicados, incorporando novas contribuições que contornam problemas de implementação prática e faz uso de uma abordagem multiobjetivo. Este novo método de seleção de vidros auxilia na escolha ótima do conjunto de vidros mais apropriado para o sistema sendo projetado. A fase de seleção de vidros restringe os tipos de vidros ópticos disponíveis de centenas para alguns poucos tipos, desta forma, reduzindo drasticamente o espaço de projeto e conseqüentemente aumentando significativamente a eficiência do método de projeto automático. A fase de exploração é baseada em um algoritmo evolutivo, mais especificamente em uma versão customizada do algoritmo de otimização extrema generalizada (GEO), a qual foi nomeada O-GEO. Este novo algoritmo evolutivo incorpora várias características personalizadas para o projeto de lentes, como a codificação usada para representar um sistema óptico e os operadores de diversidade. Os sistemas não-dominados encontrados durante a fase de exploração são refinados por um algoritmo de busca local baseado no algoritmo de mínimos quadrados amortecidos durante a fase de intensificação. Como resultado, o método retorna um conjunto de soluções não-dominadas que formam a fronteira de Pareto. O método proposto retorna um conhecimento profundo, alternativo e extremamente útil acerca das soluções de compromisso envolvidas no projeto de sistemas ópticos. A eficiência do método proposto é comprovada através de exemplos que mostram excelentes resultados, tanto para o projeto de sistemas simples como para problemas reais.

LIST OF FIGURES

	<u>Pág.</u>
Figure 2.1 - Example of optical aberrations in the image formation of an infinitesimal object point.	10
Figure 2.2 - The most common design variables in an image forming optical system.....	12
Figure 2.3 - Chromatic aberration schematic representation.....	14
Figure 2.4 - Schematic representation for the partial chromatic aberration correction in an achromatic doublet.	14
Figure 3.1 - Generic evolutionary algorithm flowchart.	24
Figure 4.1 - GEO candidate solution representation. Each bit can be interpreted as a species within an ecosystem. Four bits representation were used here just as an example. The number of bits used by each variable can be defined according to the problem needs.	30
Figure 4.2 - Canonical GEO flowchart.....	30
Figure 4.3- The graph shows solutions for a generic min-min multi-objective problem, plotted in the objective-functions space F1 and F2. Dominated solutions are represented in blue, while red dots represent non-dominated solutions.	32
Figure 4.4 - M-GEO flowchart (GALSKI <i>et al.</i> , 2005).....	35
Figure 4.5 - GEO _{real1} flowchart (MAINENTI-LOPES <i>et al.</i> , 2008).....	37
Figure 5.1 - Overview flowchart of the global search algorithm proposed for the automatic design of optical systems.	47
Figure 6.1 - Format of the table used to store the best aplanatic solution data for each glass arrangement.	59
Figure 6.2 - Flowchart of the proposed method of glass combination selection.....	60
Figure 6.3 - O-GEO solution representation.....	62
Figure 6.4 - O-GEO codification of the triplet lens shown in Figure 6.5.....	63
Figure 6.5 - Layout representations for the lens system codified in the string shown in Figure 6.4.....	63
Figure 6.6- O-GEO flowchart.	64
Figure 7.1 - Lens system variable representation in the Matlab simulator.....	77
Figure 7.2 - Layout representation for the lens system data shown in the Matlab simulator variables in Figure 7.1.	78

Figure 7.3 - Relationship between the OPD and ray transverse aberration.	81
Figure 7.4 - Gaussian quadrature ray distribution scheme for $N_r = 3$ and $N_\theta = 6$ (FORBES, 1988).....	88
Figure 7.5 - Uniform Cartesian ray distribution scheme (FORBES, 1988).	89
Figure 8.1 - Example of Cooke triplet solutions obtained from the following sources: a) Kidger (2004), b) Moore (1999), and c) ZEMAX (2011b).	98
Figure 8.2 - Layout of the triplet system types found by the automatic lens design algorithm.	101
Figure 8.3 - Layout of the triplet system types found by ZEMAX.....	104
Figure 8.4 - Layout of the telephoto system found by the proposed automatic design algorithm during executions 1–10.....	110
Figure 8.5 - Layout of the telephoto system found by the proposed automatic design algorithm during executions from 11–20.	110
Figure 8.6 - Layout and MTF curves for the best and worse telephoto systems found during the twenty independent executions of the algorithm. The left-hand side corresponds to the worst system found and the right-hand side corresponds to the best system.	111
Figure 8.7- Layout of the telephoto system found by ZEMAX global search algorithm during executions 1–10.	113
Figure 8.8- Layout of the telephoto system found by ZEMAX global search algorithm during executions 11–20.	114
Figure 8.9 - Layout and MTF curve for the telephoto system found by ZEMAX with the RMS WFE closest to the average RMS WFE value.	115
Figure 8.10 - Pareto front for the telephoto experiment using image quality and tolerance to drive the search.	116
Figure 8.11 – Layout, MTF and Seidel diagram plots for one of the non-dominated telephoto designs close to the knee region in the Pareto front. This system has an image quality metric of 0.207 waves and a tolerancing metric of 0.619 waves.....	117
Figure 8.12 - Layout, MTF and Seidel diagram plots for one of the non-dominated telephoto designs close to the knee region in the Pareto front. This system has an image quality metric of 0.221 waves and a tolerancing metric of 0.612 waves.....	117
Figure 8.13 - Layout, MTF and Seidel diagram plots for one of the non-dominated telephoto designs close to the knee region in the Pareto front. This system has an image quality metric of 0.229 waves and a tolerancing metric of 0.578 waves.....	118

Figure 8.14 - Layout , MTF and Seidel diagram plots for the best image quality system found during the experiment. This system has an image quality metric of 0.185 waves and a tolerancing metric of 10.09 waves.....	118
Figure 8.15 - Pareto front for the telephoto experiment using the image quality, tolerance, and number of lenses to drive the search.....	120
Figure 8.16 – Layout, MTF and Seidel diagram plots for one of the non-dominated telephoto designs selected from the Pareto front. This 6-lens system has an image quality metric of 0.207 waves and a tolerancing metric of 1.5616 waves.....	121
Figure 8.17 – Layout, MTF and Seidel plots for one of the non-dominated telephoto designs selected from the Pareto front. This 5-lens system has an image quality metric of: 0.212 waves and a tolerancing metric of 2.106 waves.	121
Figure 8.18 – Layout, MTF and Seidel diagram plots for one of the non-dominated telephoto designs selected from the Pareto front. This 5-lens system has an image quality metric of: 0.231 waves and a tolerancing metric of 0.537 waves.....	122
Figure 8.19 – Layout, MTF and Seidel diagram for the system pointed by a blue arrow in Figure 8.15. This nine-lens system corresponds to the best image quality system found in this experiment, with an image quality metric of: 0.19 waves and a tolerancing metric of 81.32 waves.	122
Figure 8.20 - Pareto front for the telephoto experiment using the image quality, tolerancing, and number of lenses to drive the search.....	127
Figure 8.21 – Layout, MTF and Seidel diagram plots for one of the non-dominated MUX designs selected from the Pareto front. This 10-lens system has an image quality metric of 0.039 waves and a tolerancing metric of 2.944 waves.	128
Figure 8.22 - Layout, MTF and Seidel diagram plots for one of the non-dominated MUX designs selected from the Pareto front. This 9-lens system has an image quality metric of 0.049 waves and a tolerancing metric of 3.179 waves.	129
Figure 8.23 - Layout, MTF and Seidel diagram plots for one of the non-dominated MUX designs selected from the Pareto front. This 8-lens system has an image quality metric of 0.0529 waves and a tolerancing metric of 4.328 waves.	129
Figure 8.24 - Layout, MTF and Seidel diagram plots for one of the non-dominated MUX designs selected from the Pareto front. This 9-lens system has an image quality metric of 0.057 waves and a tolerancing metric of 3.056 waves.	130

Figure 8.25 - Layout, MTF and Seidel diagram plots for the best image quality MUX system composed of less than twelve lenses. This 10-lens system has an image quality metric of 0.035 waves and a tolerancing metric of 5.26 waves.....	130
Figure 8.26 – Layout, MTF and Seidel plots for the least sensitive system that complies with MUX image quality requirement. This 9-lens system has an image quality metric of 0.0795 waves and a tolerancing metric of 1.86 waves.	131
Figure 8.27 – Layout, MTF and Seidel diagram plots for the MUX EM design. This 10-lens system has an image quality metric of 0.085 waves and a tolerancing metric of 7.633 waves.	132
Figure 8.28 - Layout, MTF and Seidel diagram plots for the MUX QM design. This 11-lens system has an image quality metric of 0.060 waves and a tolerancing metric of 5.035 waves.	132
Figure B.1 - Tuning experiment curves for $\sigma = 0.1$. The left-hand side shows the average objective function value evolution for the number of objective function calculations. The right-hand side shows final performance of the average objective function as a function of τ	177
Figure B.2 - Tuning experiment curves for $\sigma = 0.2$. The left-hand side shows the average objective function value evolution for the number of objective function calculations. The right-hand side shows the final performance of the average objective function as a function of τ	177
Figure B.3 - Tuning experiment curves for $\sigma = 0.3$. The left-hand side shows the average objective function value evolution for the number of objective function calculations. The right-hand side shows the final performance of the average objective function as a function of τ	178
Figure B.4 - Tuning experiment curves for $\sigma = 0.4$. The left-hand side shows the average objective function value evolution for the number of objective function calculations. The right-hand side shows the final performance of the average objective function as a function of τ	178
Figure B.5 - Tuning experiment curves for $\sigma = 0.5$. The left-hand side shows the average objective function value evolution for the number of objective function calculations. The right-hand side shows the final performance of the average objective function as a function of τ	179
Figure B.6 - Tuning experiment curves for $\sigma = 0.6$. The left-hand side shows the average objective function value evolution for the number of objective function calculations. The right-hand side shows the final performance of the average objective function as a function of τ	179
Figure B.7 - Tuning experiment curves for $\sigma = 0.7$. The left-hand side shows the average objective function value evolution for the number of objective	

function calculations. The right-hand side shows the final performance of the average objective function as a function of τ	180
Figure B.8 - Tuning experiment curves for $\sigma = 0.8$. The left-hand side shows the average objective function value evolution for the number of objective function calculations. The right-hand side shows the final performance of the average objective function as a function of τ	180
Figure B.9 - Tuning experiment curves for $\sigma = 0.9$. The left-hand side shows the average objective function value evolution for the number of objective function calculations. The right-hand side shows the final performance of the average objective function as a function of τ	181
Figure B.10 - Tuning experiment curves for $\sigma = 1$. The left-hand side shows the average objective function value evolution for the number of objective function calculations. The right-hand side shows the final performance of the average objective function as a function of τ	181
Figure B.11 - Performance of the algorithm as a function of σ for $\tau = 1$ and $\tau = 2$	182
Figure B.12 - Histograms for the number of objective function calculations necessary to achieve the minimum image quality defined in the Cooke triplet experiment.	184

LIST OF TABLES

	<u>Pág.</u>
Table 8.1 - Triplet system requirements and constraints.	99
Table 8.2 - Cooke triplet experiment results using the automatic lens design algorithm. From left to right, the columns contain the execution number, the number of merit function evaluations in the exploration phase, the number of merit function evaluations during exploitation phase, the total number of merit function evaluations, the RMS WFE achieved in waves, and the system type obtained.	101
Table 8.3 - Cooke triplet experiment results using ZEMAX global search. The columns, from left to right, describe the execution number, the number of evaluations of the objective function, the RMS WFE value achieved in waves, and the system type.	103
Table 8.4 - Summarized results comparison for Cooke triplet experiment where TMFC describes the total number of merit function evaluations and MF describes the RMS WFE value achieved in waves.	104
Table 8.5 - Telephoto system requirements and constraints.....	106
Table 8.6 - Telephoto lens problem output table from the glass selection method for 2 glasses sorted bygi.	107
Table 8.7 - Results for each independent execution of the Telephoto problem using the proposed automatic design algorithm. From left to right, the columns describe the independent execution number, the number of exploration merit function evaluations, the number of exploitation merit function evaluations, the total number of merit functions required to determine the best solution, and the RMS WFE achieved in waves.	109
Table 8.8 - Results for each independent execution of the telephoto problem in ZEMAX. From left to right, the columns identify the independent execution number, the approximately number of MF calculations reported, and the best RMS WFE found during the execution.....	112
Table 8.9 - Summarized results comparison for the first telephoto experiment.	114
Table 8.10 - Primary MUX first-order requirements from INPE (2006).....	124
Table 8.11 - First 10 lines of the glass selection method output table applied to the MUX design using 3 glasses sorted bygi.....	125
Table 8.12 - MUX System Requirements and constraints.	126

TABLE OF CONTENTS

	<u>Pág.</u>
1 INTRODUCTION	1
1.1. Objective	2
1.2. Motivation.....	3
1.3. Methodology and thesis structure	5
1.4. Contributions of this thesis	6
2 OPTICAL DESIGN PROBLEM.....	9
2.1. Optical aberrations.....	9
2.2. Optical system design variables	12
2.2.1. Chromatic aberration and glasses as variables	13
3 OPTIMIZATION METHODS IN LENS DESIGN	17
3.1. Classical optimization methods in optical design.....	18
3.1.1. The damped least square method in lens design.....	19
3.1.2. Final considerations about the classical optimization methods in lens design	22
3.2. Evolutionary optimization methods in optical design.....	23
4 GENERALIZED EXTREMAL OPTIMIZATION (GEO) ALGORITHM AND ITS VARIATIONS..	29
4.1. Canonical GEO.....	29
4.1.1. Multi-objective approach and M-GEO algorithm	31
4.1.2. Real-coded GEO (GEO_{real1})	35
5 AN OVERVIEW OF THE PROPOSED AUTOMATIC OPTICAL DESIGN METHOD	39
5.1. The multi-objective approach	39

5.2.	The memetic approach	42
5.2.1.	Glass selection	42
5.2.2.	Exploration	44
5.2.3.	Exploitation	45
5.3.	The method overview	46
6	DETAILING THE METHOD PHASES.....	49
6.1.1.	The glass selection phase	49
6.1.2.	Background for the method of glass selection	49
6.1.3.	The synthesis method of glass selection	56
6.1.4.	Post-Pareto analysis	60
6.2.	Exploration phase algorithm for optical GEO (O-GEO).....	61
6.2.1.	O-GEO candidate solution representation	62
6.2.2.	O-GEO steps	64
6.2.3.	O-GEO Step 1.....	65
6.2.4.	O-GEO Step 2.....	66
6.2.5.	O-GEO Step 3.....	70
6.2.6.	O-GEO Step 4.....	71
6.2.7.	O-GEO Step 5.....	71
6.2.8.	O-GEO Step 6.....	72
6.2.9.	O-GEO Step 7.....	72
6.2.10.	O-GEO Step 8.....	72
6.3.	Exploitation phase.....	72
7	SIMULATOR AND MERIT FUNCTIONS.....	75
7.1.	The simulator	75

7.1.1.	Lens system and glass catalog representation in the simulator	77
7.2.	The Optimization Metrics.....	80
7.2.1.	Image resolution metrics.....	80
7.2.2.	System sensitivity metrics	89
8	EXPERIMENTS RESULTS AND VERIFICATIONS	97
8.1.	The Cooke triplet problem	97
8.1.1.	Tuning the exploration phase.....	99
8.1.2.	Triplet experiment results	100
8.2.	The telephoto lens problem.....	104
8.2.1.	First telephoto design experiment	108
8.2.2.	Second telephoto design experiment	115
8.2.3.	Third telephoto design experiment.....	119
8.3.	The MUX lens design problem	123
9	LIMITATIONS OF THE METHOD AND FUTURE WORK IDEAS.	135
9.1.	Aspherical Surfaces	135
9.2.	Catoptric and Catadioptric Systems.	137
9.3.	Non-rotationally Symmetrical Systems.	139
9.4.	Cemented Lens.....	141
9.5.	System Thermal Stability.....	142
10	CONCLUSIONS.....	145
	REFERENCES.....	149
APPENDIX A	DETAILED SOLUTION FOR THE DLS METHOD	169
APPENDIX B	TUNING O-GEO.....	175
APPENDIX C	PAPER PUBLISHED IN OPTICS EXPRESS.....	185

1 INTRODUCTION

Optical systems are arrangements of distinct optical elements that together are able to manipulate light (visible, ultraviolet, and/or infrared electromagnetic waves) aiming to accomplish a specific task. The scope of this thesis is limited to discussing image-forming optical systems. In this class of systems, the main optical elements are lenses and mirrors, which are capable of changing the direction of the light wavefront by means of the refraction and reflection phenomena, respectively.

The task of the optical designer is to find the optical element shapes, materials, and arrangements that maximize the image quality as required. The optical designer must accomplish this optimization using the first-order optical requirements, such as the effective focal length, aperture, field of view, spectral range, object distance, and entrance and exit pupil position, while operating within the optical and mechanical constraints of the system.

Optical design is a branch of science that is more than three centuries old. In order to truly design an imaging optical system, it is necessary to be able to perform the ray path calculation through optical surfaces. The physical and mathematical backgrounds needed for ray path calculation were already available in the first half of 17th century. (HECHT, 1987; VASILJEVIC, 2002). However, until the beginning of 20th century, almost all optical system developments were made based on the empirical loop method of constructing, testing, and changing. This development technique was preferred due to the difficulties and time required for performing ray trace calculations, which had to be performed using only a log table. To make matters worse, the lack of accuracy in measuring the surface radii and the refraction index of materials would make the theoretical calculations useless.

With the simplification of the third-order aberration theory in the end of the nineteenth century, derived from the work of Philipp Ludwig von Seidel's work presented in 1857, and with the popularization of mechanical computing machine in the early part of the twentieth century, ray tracing techniques

became more popular for designing optical systems. The typical time spent by a trained person to trace a single ray through an optical surface, with the help of a mechanical calculating machine, is about ten minutes. Based on this, it takes a whole week of labor (40 hours) to trace twenty rays through a twelve surface (six lens) system. Note that twenty is the minimum number of rays necessary to diagnose an optical system with moderate aperture and field of view, while six lenses is the number of elements in an average optical system (VASILJEVIC, 2002). With this scenario, it would be nonsense to discuss the optimization of optical systems.

The arrival of the digital computer in the 1940s was a turning point for scientific calculation, in general, and for ray tracing, in particular. In a very short period, the typical time for tracing a ray through a single optical surface improved from ten minutes to one second. From this time on, optical system optimization was investigated, developed, and applied (VASILJEVIC, 2002; MALACARA; MALACARA, 2004).

Current personal computers are capable of tracing millions of rays per surface per second. For instance, the commercial optical design software ZEMAX running on an Intel Core 2 Quad6600 CPU can trace approximately thirty million rays per surface per second. With this considerable improvement in the speed of computation, evolutionary optimization (EO) methods, which are considered computationally heavy, have been used in optical design since the 1990s. This class of optimization algorithms has the potential to overcome some of the limitations faced by classical methods when applied to an optical design. The state of the art is to use EO methods not only for optimization but also for automatically designing systems from scratch.

1.1. Objective

The aim of this thesis is to present a novel evolvable hardware method for the automatic design of image-forming optical systems. The proposed methodology is based on a multi-objective (BRANKE, *et al.*, 2008; ZITZLER, *et al.*, 2004) memetic (MOSCATO, 1989; MOSCATO; COTTA, 2003) approach, which is

capable of addressing fabrication issues during the design phase such as the system complexity and tolerance, and which is able to determine the most appropriate glass materials for the system under design.

1.2. Motivation

The Brazilian National Institute for Space Research (INPE) has been working in the past decades to develop low orbit satellites for Earth observation. The main satellite programs currently under development are the China-Brazil Earth Resources Satellite (CBERS) and the Multi-Mission Platform (PMM), presently with the CBERS 3&4 and AMAZONIA-I missions, respectively. In both cases, Brazil plays an important role in the development of the payloads, which include remote sensing optical instruments that have been entirely developed in Brazil. The INPE has also invested in the development of satellite attitude optical sensors. One example is the Autonomous Star Tracker, currently under development at the Aerospace Electronics Division in the Institute.

The future development of optical payloads and optical attitude control instruments is supported by the INPE Master Plan 2011-2015 (INPE, 2011) as well as by the PNAE-National Program of Space Activities 2012-2021 (AEB, 2012) documents.

SABIA-Mar and AMAZONIA-II are examples of future missions that will carry optical remote sensing payloads. Despite not explicitly mentioning CBERS future missions, both documents point in the direction of CBERS program continuation, which will probably include satellites with optical remote sensing instruments.

Optical attitude sensors, as star trackers, are used on virtually any three-axis stabilized satellite. In this way, the missions foreseen in Brazilian space program provide a range of opportunities for the developments of this type of optical instruments.

These space optical instruments are very complex and sophisticated. The INPE has invested more than a hundred million reais (R\$) in the development of

multispectral (visible and near-infrared) medium spatial resolution remote sensing cameras MUX, WFI, and AWFI, which will be onboard the CBERS 3&4 and AMAZONIA-1 satellites, respectively. The amount of the investments demonstrates the complexity and sophistication of these subsystems. Based on the challenges that have been faced during the development of these cameras, it is possible to affirm, with confidence, that the optics of these instruments are one of the critical parts of the subsystem in terms of design, fabrication, assembling and testing.

The MUX contract, for instance, has suffered considerable delays due to difficulties in making the optical system perform as specified. The MUX optical design performs extremely well “on paper,” but the design is so sensitive that the development of the physical system is very complicated. The fabrication for the MUX engineering model (EM) optics began around October 2005. Only in September 2007 were the first optical results obtained which complied with the requirements. Even now, with the experience obtained from the fabrication of the EM, the qualification model (QM) and the first flight model (FM), this still not a straightforward task. Therefore, the optical fabrication continues in the project critical path.

Furthermore, to the best of our knowledge, there are no studies presenting design techniques that could address the issues and doubts faced during the developments of the mentioned projects in a complete, satisfactory, and accessible way. Therefore, we find it necessary to develop more effective optical design tools.

Based on the foreseen future of optical instruments development at INPE, together with the issues faced during past and current projects in this area, associated with the lack of optical design methods addressing our problems, It seems reasonable to affirm that development of new effective optical design techniques will be relevant and useful for current and future projects at INPE and that this effort is aligned with the Institute interests.

1.3. Methodology and thesis structure

This document is divided in two parts. The first part presents the necessary background for the comprehension of the proposed method. The second part presents the automatic design methodology, results, and conclusions.

In Chapter 2, we discuss the basics for understanding the optical design problem. Chapter 3 provides a brief discussion about the classical and evolutionary methods applied to the lens design. In Chapter 4, we present the generalized extremal optimization algorithm and some of its variants.

We used a top-down methodology to develop the automatic optical design methods presented herein. Based on a broad literature survey about the optimization methods applied in lens design with a special focus on evolutionary optimization methods, we identified some potential contributions to improve the current available methods.

From these points, we selected the most important and relevant topics to be developed in this Ph.D. research. As a result, we formulated an overview of the automatic lens design method and delineated the key focal points and phases of the proposed method. The methodology overview is presented in Chapter 5.

Our method is composed of three phases, which we describe in Chapter 6. All of these phases have relevant scientific contributions that are an important part of the method.

In order to put the method to work, it was necessary to develop an environment for the optical system simulation as well as define and develop the metrics for each objective considered in the different phases. The simulator and objective function descriptions can be found in Chapter 7.

The proposed method was verified step by step through examples, including a real case example. The description of each problem, the obtained results, and some comparisons and discussions about the obtained results are discussed in Chapter 8.

Chapter 9 brings discussions about the method limitations and insights for future work development, aiming to overcome the current method restrictions. Finally Chapter 10 wraps up this work with the conclusions.

1.4. Contributions of this thesis

This section provides a superficial overview of the scientific contributions of this thesis. The contributions cited at this point will be clarified and better understood along the development of the work. In the Conclusions Chapter, we get back to this topic where all the scientific contributions of this thesis will be summarized again.

In the novel approach for the automatic design of optical systems proposed in this thesis, many new things were explored, resulting in original scientific contributions in different levels.

The memetic and multi-objective approach is something not explored together before in lens design. The memetic line of attack is responsible for breaking the automatic design process in three phases: glass selection; exploration (global search) and exploitation (local search), as well as for incorporating in the exploration phase different problem domain knowledge.

The use of a glass selection phase is one of the contributions of the proposed automatic design algorithm. Moreover, the developed glass selection methodology has its own original contributions as the generalized formulation proposed, the metric for color correction evaluation and the multi-objective approach used.

The evolutionary optimization algorithm used in the exploration phase is based on the on Generalized Extremal Optimization algorithm (DE SOUSA *et al.*, 2003), but totally tailored for the problem of lens design. This algorithm named Optical GEO is one of the contributions of this work. One of the outstanding contributions of this algorithm is the possibility of changing the number of lenses in the system during the optimization.

The multi-objective approach used during the exploration phase takes into consideration fabrication aspects never explored before in this approach: system tolerancing and complexity (number of lenses used in the design).

The image quality metric as well as the tolerancing metric used during the exploration phase were developed with evolutionary algorithms in mind and are also original contributions of this work.

2 OPTICAL DESIGN PROBLEM

As mentioned in Chapter 1, the goal of the optical designer is to find the optical elements arrangement, formats, and materials that provide the best possible image quality by complying with the system first-order optical requirements and imposed mechanical and optical constraints.

Basically, two phenomena affect the image formation: diffraction and optical aberrations. Nothing can be done about the diffraction effects; its influence is fixed for a given system aperture. On the other hand, the optical aberrations are a function of the optical system construction parameters and can be changed. In this case, maximizing the image quality requires minimizing the optical aberrations.

2.1. Optical aberrations

Optical aberrations can be defined as the error or deviation in the interception position of a ray in the focal plane related to a specific reference coordinate, which is normally taken as the paraxial position of the principal ray (SHANNON; WYANT, 1980).

Figure 2.1 shows the optical aberration arising for a single lens optical system. Note that rays coming from the infinitesimal point (X_0, Y_0) from the object plane do not collapse into a single infinitesimal point (X'_F, Y'_F) in the focal plane.

If an optical system can be described by N construction parameters, any ray traveling through the system can be specified by six parameters: three specifying the Cartesian coordinates $X, Y,$ and $Z,$ and three specifying its direction cosines $L, K,$ and $M.$ Moreover, each ray must satisfy the following conditions:

- 1) $L^2 + K^2 + M^2 = 1;$
- 2) The Cartesian coordinates shall satisfy the equation of the surface the ray belongs to, $Z = f(X, Y).$

As a consequence of these conditions, the ray specification can be reduced to four parameters: (X, Y, L, K) .

If (X_0, Y_0) are the coordinates of an infinitesimal object point and if we have a perfect optical system, all rays traced through the system from this point will collapse in the coordinates (X', Y') in the image plane:

$$X' = M \cdot X_0 \quad (2.1)$$

$$Y' = M \cdot Y_0 \quad (2.2)$$

Here, M is defined as the optical system lateral or transverse magnification.

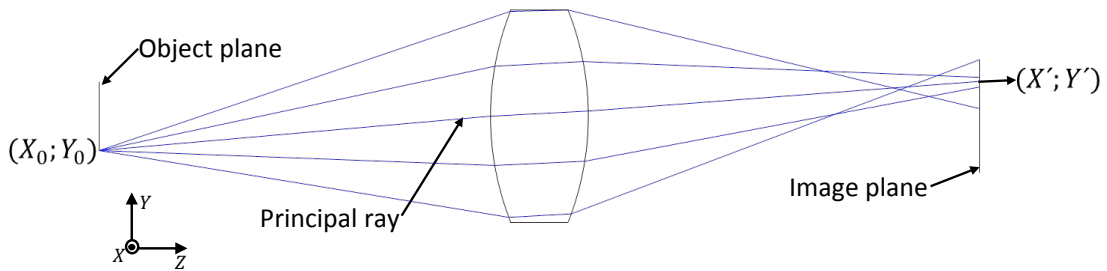


Figure 2.1 - Example of optical aberrations in the image formation of an infinitesimal object point.

Nevertheless, as perfect optical systems do not exist, each ray traced through the system will suffer some deviation from its expected position in the focal plane. This can be mathematically written in the following form:

$$X' = M X_0 + \delta X'(X_0, Y_0, L_0, K_0, x_1, x_2, \dots, x_n) \quad (2.3)$$

$$Y' = M Y_0 + \delta Y'(X_0, Y_0, L_0, K_0, x_1, x_2, \dots, x_n) \quad (2.4)$$

where (x_1, x_2, \dots, x_n) are the optical system construction parameters, and $\delta X'$ and $\delta Y'$ are so-called ray aberration functions.

From Equations (2.3) and (2.4), we can see that the image quality of an optical system can be evaluated by the mean square sum of the aberrations for all

possible rays that can be traced through the system. This can be written mathematically by the following equation (VASILJEVIC, 2002):

$$\Psi = \frac{\int \int \int \int (\delta X'^2 + \delta Y'^2) dX_0 dY_0 dL_0 dK_0}{\int \int \int \int dX_0 dY_0 dL_0 dK_0}. \quad (2.5)$$

Consequently, optimizing the image quality of an optical system requires **minimizing** the function Ψ .

Unfortunately, the function Ψ cannot be analytically computed. However, its value can be estimated through the trace of a set of m rays. In practice, some object points (3 or 5) are chosen, from which a finite number of rays are traced through the system. Therefore, instead of an integral over a continuous function, we have a sum over a discrete set of values (VASILJEVIC, 2002):

$$\Psi = \frac{1}{m} \sum_{i=1}^m (\delta X_i'^2 + \delta Y_i'^2), \quad (2.6)$$

where i represents a specific ray. The discrimination between $\delta X_i'$ and $\delta Y_i'$ is not relevant, so we can write Equation (2.6) as follows (VASILJEVIC, 2002):

$$\Psi = \frac{1}{m} \sum_{i=1}^m (f_i(x_1, x_2, \dots, x_n))^2. \quad (2.7)$$

However, the problem statement is still incomplete because the constructional parameters themselves are not entirely unconstrained. In this case, we need to minimize Ψ while fulfilling the boundary conditions represented by a set of k inequalities of the form (VASILJEVIC, 2002):

$$\begin{aligned} b_1(x_1, x_2, \dots, x_n) &\geq 0 \\ b_2(x_1, x_2, \dots, x_n) &\geq 0 \\ b_3(x_1, x_2, \dots, x_n) &\geq 0 \\ &\vdots \\ b_k(x_1, x_2, \dots, x_n) &\geq 0. \end{aligned} \quad (2.8)$$

These boundary conditions ensure that (i) all optical elements can be physically manufactured, (ii) the distance between successive optical elements is

physically feasible, (iii) the first-order optical requirements comply with the specified requirements, and (iv) the other optical, mechanical, and physical constraints are respected.

2.2. Optical system design variables

For an image-forming optical system, the most common construction parameters or design variables (x_1, x_2, \dots, x_n) are (i) the radius of curvature of each optical surface (lenses or mirrors). (ii) the lens central thicknesses, (iii) the air space between the optical elements, and (iv) the optical glass type used for the lens construction. Figure 2.2 shows examples of the most common design variables.

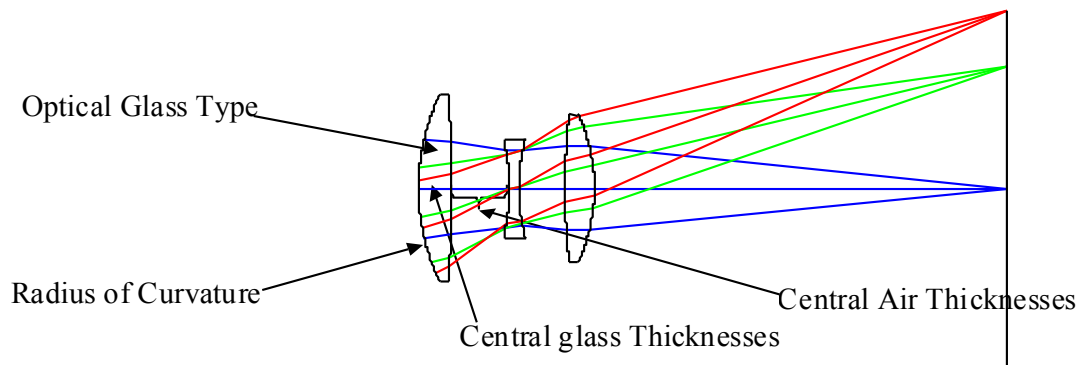


Figure 2.2 - The most common design variables in an image forming optical system.

Imaging optical systems may also have other variables including surface conic constants, coefficients of a polynomial equation describing a non-conic surface, decenter and tilt of the optical components in a non-rotationally symmetrical systems, and so on.

In general, the variables are real numbers with the exception of the optical glass materials. On the other hand, the glass materials are discrete variables. There are a finite number of glass types commercially available (on the order of hundreds). The optical characteristics of each type of glass is fixed and very well defined by the supplier. Therefore, the optical design must be limited to the materials available.

2.2.1. Chromatic aberration and glasses as variables

Glasses are solid, isotropic, homogeneous, dielectric, or non-conducting materials, which are transparent to a specific wavelength range of electromagnetic light. These materials are excellent for manipulating light through diffraction and are widely used in the construction of optical elements. However, glasses have an undesirable characteristic for lens design: the speed of light inside materials depends on the frequency. Therefore, the index of refraction (or dielectric constant) of an optical material is a function of the light frequency (or wavelength). This variation occurs due to the interaction of the electromagnetic waves with electric dipoles present in dielectric materials or glasses (HECHT, 2002). This difference in the refraction index makes different light wavelengths experience slightly different deviations when passing through the same optical element. This phenomenon gives rise to the so-called **chromatic aberration**. In Figure 2.3, the chromatic aberration from a single lens is illustrated. We can easily observe that the different wavelengths, which experience different deviations, form images at different positions.

The chromatic aberration in image-forming optical systems is a well-known issue studied since Isaac Newton's time (17th century). Around 1730, Chester Moor Hall, an amateur astronomer, concluded that the chromatic aberration of refractive (dioptric) optical systems could be reduced if two different kinds of glasses were used in the construction of a telescope objective. Hall used crown and flint, which are low and high index dispersion glasses, respectively, and the resulting lens is known today as an achromatic doublet (POLASHENSKI, 2001). As pointed out by Sigler (1986), the control of chromatic aberration has been one of the most studied issues in optical design.

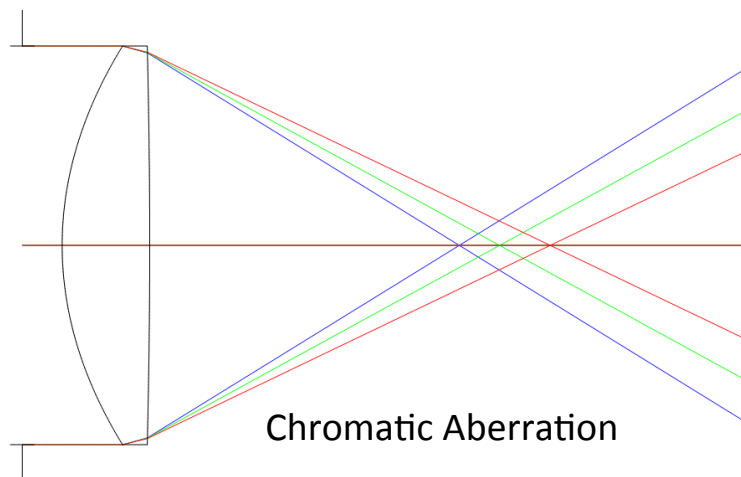


Figure 2.3 - Chromatic aberration schematic representation.

Figure 2.4 illustrates the combination of two glasses reducing the chromatic aberration. The negative lens (or divergent lens) is made out of flint glass, producing dispersion higher than the one generated by the positive lens (or convergent lens) made out of crown glass. In this way, the negative lens can partially compensate for the dispersion produced by the positive lens, keeping the light convergent.

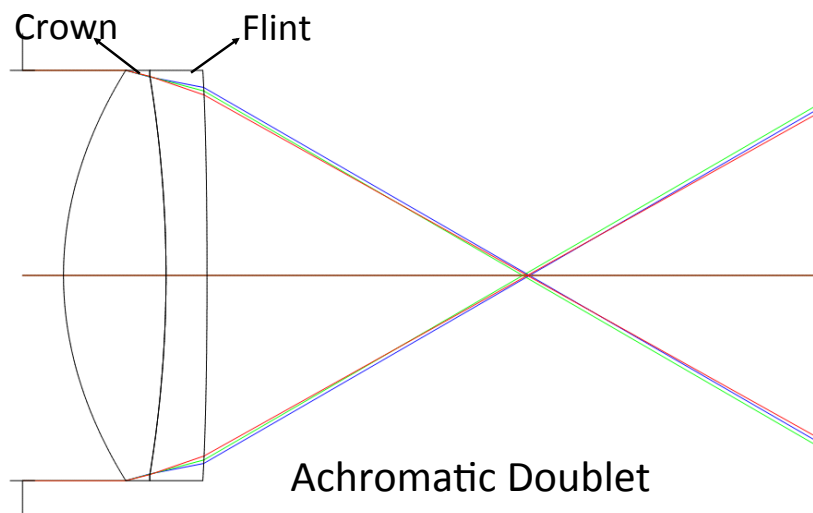


Figure 2.4 - Schematic representation for the partial chromatic aberration correction in an achromatic doublet.

In this way, glasses are very important design variables when a reduced achromatic aberration is desired, especially for systems covering a wide

spectral range, as is the case in remote sensing cameras. The glass selection for optical design is a science apart.

Glass materials in optical systems are discrete variables; therefore they cannot be directly optimized by classical methods, as we will show in the next chapter. For this reason, some optical design tools (ZEMAX, 2011a; ORA, 2009) and works in this area (RAYCES; ROSETE-AGUILAR, 1999) propose techniques for treating glasses as continuous variables. However, based on our own experience, this approach is not satisfactory, especially in the design of wide spectral range systems.

3 OPTIMIZATION METHODS IN LENS DESIGN

A lens system can be represented as a point (x_1, x_2, \dots, x_n) in an n -dimensional parameter space. Each point is associated with one objective function (OF) value, which is also called a merit function (MF) in optical design. The OF value defines the system performance. The optimization process of an optical system consists in transferring the initial point in the parameter space to another position that improves the MF, which, in our case, is a decrease in value. Repeating this process, the designer may eventually reach a satisfactory solution (RAYCES; ROSETE-AGUILAR, 2002).

The way the solution walks in the parameter space during the optimization process depends on the optimization method used. Generally speaking, these methods can be divided in two families: deterministic and metaheuristic methods.

Deterministic or classical optimization methods are analytical direct search-for-optimum methods, generally driven by OF gradient information. Therefore, deterministic methods can be only directly applied to continuous and differentiable functions (COLAÇO; DULIKRAVICH, 2011; LIN *et al.*, 2012; CAVAZZUTI, 2013).

Metaheuristic methods, on the other hand, are non-deterministic, generally stochastic, optimization methods that make few assumptions about the optimization problem being solved. Metaheuristics are normally used for global search purposes, but a globally optimal solution is not guaranteed. Natural, organic processes inspire many of these methods. Metaheuristics are recommended for highly nonlinear, multimodal, discontinuous and multivariate problems. Some examples of methods of this class are: simulated annealing, tabu search, evolutionary optimization (genetic algorithms, evolution strategies, genetic programming), ant colonies, particle swarms, scatter search, immune systems, and so on (BLUM; ROLI, 2003; GONZALEZ, 2007; BIANCHI *et al.*, 2009; TALBI, 2009).

In this thesis, our discussion is restricted to the most used classical and metaheuristic methods of optimization applied in optical design. To the best of our knowledge, the most common metaheuristic methods used are evolutionary optimization methods. Therefore, we will restrict our discussion of metaheuristic methods to only evolutionary methods of optimization.

3.1. Classical optimization methods in optical design

Based on a broad literature study, the first optimization method used in the optical design field was the classical least square method, proposed by Rosen and Eldert (1954). However, this method was quickly abandoned due to numerical instability problems, which arise from the inversion of the near singular matrix present in all practical cases. Some years later, Girard (1958) was the first author to suggest the damped least square (DLS) method, also known as the Levenberg–Marquardt algorithm, for the optimization of optical systems. The DLS is the most used optimization method in lens design (RAYCES; ROSETE-AGUILAR, 2004; MALACARA; MALACARA, 2004; VASILJEVIC, 2002). Other classical methods as the Spencer optimization method (SPENCER, 1963; RAYCES; ROSETE-AGUILAR, 2004), Grey orthonormal optimization method (VASILJEVIC, 2002), and the Glatzel adaptive optimization method (GLATZEL; WILSON, 1968, RAYCES; ROSETE-AGUILAR, 2002; 2004) have also been used in lens design.

Since these methods were presented during the 1950s and 1960s, they are well established and have been widely used for more than half century in optical systems design. The DLS method, for instance, is the main optimization tool in most of the optical design software commercially available today. For this reason, this method was selected as the local search algorithm used in the exploitation phase in this thesis. A detailed description of the DLS method is given in the next section.

3.1.1. The damped least square method in lens design

For all classical optimization methods, a valid initial input solution $P_0(x_{01}, x_{02}, \dots, x_{0n})$ must be provided. To start the optimization, the variables (or design parameters) and the MF need to be defined.

To apply the DLS method to the lens design problem, it is necessary to assume that the relationship between the design parameters (x_1, x_2, \dots, x_n) and the aberration functions $f_i(x_1, x_2, \dots, x_n)$ is continuous, differentiable, and real inside the allowed parameter domain.

In this case, the functions $f_i(x_1, x_2, \dots, x_n)$ at P_0 can be approximated by a linear function using a truncated Taylor series:

$$f_i(x_1, x_2, \dots, x_n) = f_i(P_0) + \sum_{j=1}^n \left. \frac{\partial f_i}{\partial x_j} \right|_{P_0} \cdot (x_j - x_{0j}). \quad (3.1)$$

Equation (3.1) is an approximation valid only in the neighborhood of P_0 . In this case, it is necessary to limit the absolute increment $(x_j - x_{0j})$ of each design parameter x_j to keep the solution inside the valid region. As a consequence, our goal is to minimize the optical aberration while restricting $(x_j - x_{0j})$ to a trusted region. Mathematically, this can be expressed by the following objective function:

$$\Psi = \frac{1}{\sum_{i=1}^m w_i} \sum_{i=1}^m w_i (f_i(x_1, x_2, \dots, x_n) - t_i)^2 + p \cdot \sum_{j=1}^n (x_j - x_{0j})^2. \quad (3.2)$$

The first part of Equation (3.2) is a general way of writing the merit function in Equation (2.7), where we included both the target values t_i and weighting factors w_i . The target values t_i allow us to include the problem constraints into the OF. Each one of the k inequalities shown in Equation (2.8) is transformed by an equation that assumes a zero value when the constraint is respected and that assumes a non-zero value when the constraint is violated. Therefore, the functions $f_i(x_1, x_2, \dots, x_n)$ do not represent only the optical aberrations that are

related with the image quality but also represent the problem constraints of other physical natures. For optical aberrations, t_i is normally zero. To overcome scaling problem from combining functions of different physical natures, the weighting factor w_i is included.

The second part of Equation (3.2) controls the change of the design variables, assuring the validity of the linearization of functions $f_i(x_1, x_2, \dots, x_n)$. Here, p is a positive real number called the damping factor. This number controls the compromise between minimizing the quadratic values of functions $f_i(x_1, x_2, \dots, x_n) - t_i$ and limiting the step size of the design variables in the solution space.

Substituting Equation (3.1) into Equation (3.2) we find:

$$\Psi = \frac{1}{\sum_{i=1}^m w_i} \sum_{i=1}^m w_i \left(f_i(P_0) + \sum_{j=1}^n \left. \frac{\partial f_i}{\partial x_j} \right|_{P_0} \cdot (x_j - x_{0j}) - t_i \right)^2 + p \cdot \sum_{j=1}^n (x_j - x_{0j})^2. \quad (3.3)$$

Now m in Equation (3.3) is not just the number of traced rays to access the system aberrations, but it is the number of traced rays plus the number of constraints included in the merit function equation.

It is possible to rewrite Equation (3.3) in a matrix form as follows:

$$\Psi = c \cdot (F_0 + A \cdot \Delta X)^T W_e (F_0 + A \cdot \Delta X) + p \cdot \Delta X^T \cdot \Delta X, \quad (3.4)$$

where $c = 1 / \sum_{i=1}^m w_i$ and

$$F_0 = \begin{bmatrix} f_1(P_0) - t_1 \\ f_2(P_0) - t_2 \\ \vdots \\ f_m(P_0) - t_m \end{bmatrix}, A = \begin{bmatrix} a_{11} & a_{12} & \cdots & a_{1n} \\ a_{21} & a_{22} & \cdots & a_{2n} \\ \vdots & \vdots & \ddots & \vdots \\ a_{m1} & a_{m2} & \cdots & a_{mn} \end{bmatrix}, \Delta X = \begin{bmatrix} x_1 - x_{01} \\ x_2 - x_{02} \\ \vdots \\ x_n - x_{0n} \end{bmatrix},$$

$$W_e = \begin{bmatrix} w_1 & 0 & \cdots & 0 \\ 0 & w_2 & \cdots & 0 \\ \vdots & \vdots & \ddots & \vdots \\ 0 & 0 & \cdots & w_m \end{bmatrix}$$

$$\text{and } a_{ij} = \left. \frac{\partial f_i}{\partial x_j} \right|_{P_0} \simeq \left. \frac{\Delta f_i}{\Delta x_j} \right|_{P_0}.$$

To minimize Ψ , we require $\frac{\partial \Psi}{\partial X} = 0$. Solving this equation, we find:

$$\Delta X = -(A^T \cdot W_e \cdot A + p \cdot I)^{-1} \cdot A^T \cdot W_e \cdot F_0, \quad (3.5)$$

where I is the identity matrix. For full details of the calculation, see Appendix A.

In practice, Equation (3.5) is applied successively in an iterative form. Matrixes F_0 and A are recomputed at each iteration. The final point $(P_0 + \Delta X)$ found in the current iteration is the initial point for the subsequent iteration. Normally, the iterations continue until there is no improvement in the OF or the algorithm has reached the maximum number of iterations.

This method is very stable numerically. The damping factor is added to the diagonal of matrix $(A^T \cdot W_e \cdot A)$. This reduces the difference between the largest and smallest eigenvalues, avoiding numerical errors during the matrix inversion.

A more general solution for the problem allows individual damping factors for each variable. In this case, a diagonal $n \times n$ damping matrix Q is used. The matrix elements q_j are real, positive values. In this case, the solution of the problem becomes

$$\Delta X = -(A^T \cdot W_e \cdot A + p \cdot Q)^{-1} \cdot A^T \cdot W_e \cdot F_0. \quad (3.6)$$

Many methods for calculating the individual damping factors have been proposed (VASILJEVIC, 2002). One of the simplest forms is given by

$$q_j = \sqrt{\sum_{i=1}^m a_{ij}^2}. \quad (3.7)$$

With this definition, the higher the sensitivity of the function f_i with respect to a construction parameter x_j , the greater the damping factor q_j and the smaller the step of x_j in the interaction.

The selection of the damping factors plays an important role in the DLS method because the damping factors can make the difference between good and bad convergence.

3.1.2. Final considerations about the classical optimization methods in lens design

As mentioned earlier, the classical methods are useful and have been used for a long time in optical design. However, they have some weaknesses that limit their performance:

- a) Classical methods are only able to find local minima. The methods are based on the gradient vector (or Jacobian matrix) asymptotically moving from the starting point to the local minimum in the design space that the starting point belongs to.
- b) The optical aberration functions are not linear with respect to the design construction parameters. This can cause numerical instability in methods that presume a linear behavior and can necessitate the definition of damping factors controlling the step variables in each iteration.
- c) The design space is complex. The problem is multimodal with many hills and valleys in the topography of the design space. Local valleys, which result in low performance optical systems, are traps in the design space for classical optimization methods. This complexity can also result in very close initial configurations having completely different solutions.
- d) It is necessary to provide an initial feasible solution before applying a classical optimization method. The final system performance depends on the initial solution provided. Normally, the system architecture does not change during the optimization process.

- e) Classical methods require continuous and differentiable variables. In this case, they cannot directly deal with glass as variables. Also, the number of elements used in an optical system cannot be changed during the optimization process.
- f) Classical methods cannot directly solve multi-objective problems.

3.2. Evolutionary optimization methods in optical design

In the last decades, evolutionary algorithms (EA) have been used for problem solving in several fields of knowledge. An estimated 3,000 or more papers are published every year in this area (FOGEL, 2006). Though the first known research using EAs occurred in the 1950s, EAs remained relatively unknown in the scientific community for more than thirty years. Because these methods are computationally demanding, this delay can be explained in part by the lack of powerful computers. Originally, these algorithms were proposed as machine learning problems and for the simulation of biological evolutionary processes (BACK *et al.*, 1997). In fact, in 1962, Hans-Joachim Bremermann was probably the first to claim that biological evolution is an optimization problem (EIBEN; SMITH, 2004). Currently, EAs are mostly applied for solving optimization problems (BACK *et al.*, 1997).

These algorithms attempt to mimic the evolution of living organisms using the natural selection theory proposed by Charles Darwin. According to the theory introduced in his 1859 book "On the Origin of Species", individuals that are better adapted to their environment are more likely to survive and reproduce than other members of the species (LACERDA; CARVALHO, 1999).

The basic principle of EA depends on the fact that the environmental pressure over the individuals of a species causes the natural selection that increases the quality of the population in subsequent generations. The basic elements of EA are (i) the process of individual selection based on the fitness in the environment, and (ii) the diversity operators (in general, recombination and mutation) responsible for generating new individuals (EIBEN; SMITH, 2003).

The generic flowchart for EA is shown in Figure 3.1. Generically speaking, EA starts by generating a random initial population. In the next step, the fitness of each individual in the population is computed. Then, a subset of individuals is selected stochastically to serve as parents. The parental selection is based on the individual fitness value; that is, individuals that are well adapted to the environment are more likely to be selected for the mating pool. Offspring are created by random variation of the parents in the form of mutations and/or genetic recombination. The fitness of each new individual is computed. From the population formed by parents and offspring, a subset of individuals is selected following a defined criterion. The selected subset forms the next generation. This process occurs repeatedly from generation to generation, which hopefully contains progressively better individuals, until a stopping criterion is satisfied (FOGEL, 2006).

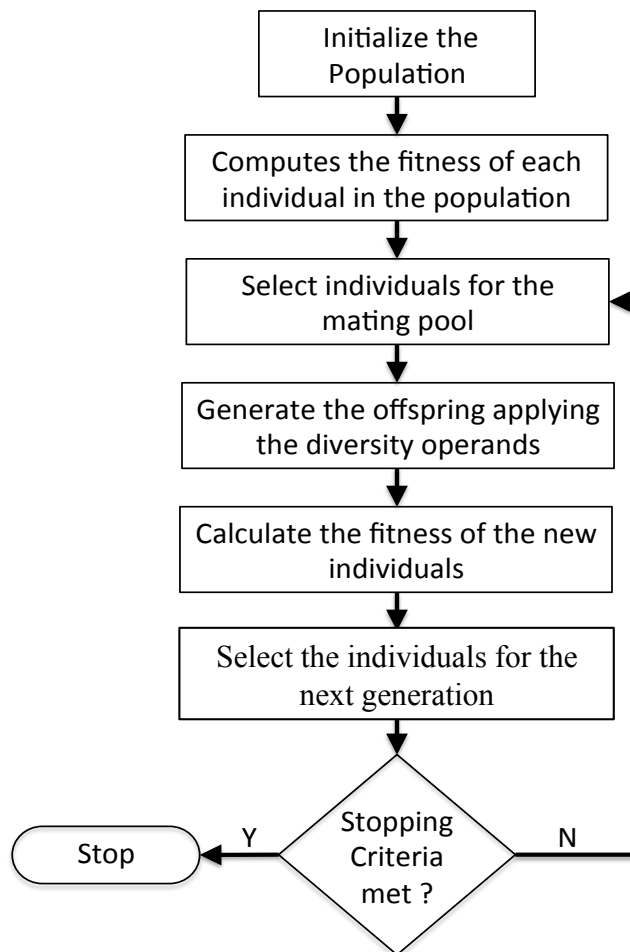


Figure 3.1 - Generic evolutionary algorithm flowchart.

When these algorithms are applied for optimization problems, the individuals in the population are, in fact, potential solutions for the problem, and the individual fitness is proportional to the merit function of the solution it represents.

In the specific case of optical design, each individual carries, in a codified form, the information of each variable of the optical system, such as the radius of curvature, the air and glass thickness, and the material properties of each surface. Lens design optimization is a minimization problem. In this case, as the MF (or OF) decreases, the individual fitness increases.

Evolutionary algorithms have some advantages over classical methods:

- a) Provide a much higher probability of finding the global minimum,
- b) Do not use either the gradient, Jacobian, or derivative information from the OF,
- c) Have large application domains requiring little to no information about the problem being solved,
- d) Can be applied in problems with any kind of variable: continuous, discrete, or a mix of both,
- e) Can be robust and well suited for complex search spaces without getting stuck in local minima,
- f) Do not require an initial solution for a good convergence,
- g) Are simple to implement and parallelize, and
- h) Can be applied to multi-objective problems without transforming them to a mono-objective problem.

This class of algorithms is considered computationally demanding; however, this drawback may not be a huge problem for modern computational systems.

The fast evolution in the performance of computers in the last decades enabled the successful use of evolutionary methods to solve optimization problems in different areas. In optical design, these methods have been used since the 1990s with the promise of addressing the limitations of classical methods.

Different evolutionary optimization approaches have been used in lens design: genetic algorithms (VAN LEIJENHORST *et al.*, 1996; ONO *et al.*, 1998; MOORE, 1999; CHEN; YAMAMOTO, 2000; VASILJEVIC, 2002; BEAULIEU *et al.*, 2002; SUKAMA; KOBAYASHI, 2005; FANG *et al.*, 2007), evolution strategy (VASILJEVIC, 2002; THIBAUT *et al.*, 2005; NAGATA, 2004), and genetic programming (BEAULIEU *et al.*, 2002; KOZA *et al.*, 2005; JONES *et al.*, 2006). All of these studies have reported good results.

However, by studying the previous research, we discovered an opportunity to improve the algorithms by designing from scratch, using a multi-objective approach, customizing the EA for the problem, and optimizing the glass selection before the system is optimized.

The multi-objective approach is infrequently used in lens design, but in our opinion, there are a number of possible applications. Some studies have reported the use of multi-objective optimization approaches in lens design (JOSEPH *et al.*, 2007; ONO *et al.*, 1998; GAGNÉ *et al.*, 2008). However, the previous research has not discussed the use of this technique in designing optical systems, foreseeing fabrication issues such as system sensitivity and complexity.

Despite many papers claiming the possibility of designing a lens system from scratch, we found only a single implementation (KOZA *et al.*, 2005; JONES *et al.*, 2006) where the number of lenses is used as design variable in the search. For a true from scratch design, only the system requirements must be provided. When the number of lenses is preset, there is a huge constraint in the design, which restricts the exploration of the design space.

Many of the studies applying EA in lens design made few or no customizations to the algorithm for the specific problem (JOSEPH *et al.*, 2007; BEAULIEU *et al.*, 2002; GAGNÉ *et al.*, 2008; THIBAUT *et al.*, 2005; CHEN; YAMAMOTO, 1996; MORRE, 1999; VAN LEIJENHORST *et al.*, 1996; NAGATA, 2004). This lack of adaptation limits the algorithm performance.

As we have already discussed, glasses are important design parameters for color correction, but they are discrete variables that cannot be directly optimized with classical methods. On the other hand, EAs have no limitations in dealing with discrete variables. In spite of that, many EO methods applied in lens design (CAGNÉ *et al.*, 2008; THIBAUT *et al.*, 2005; CHEN; YAMAMOTO, 1996; BEAULIEU *et al.*, 2002; SAKUMA; KOBAYASHI, 2005) do not take advantage of this. Furthermore, the studies that do report the use of glasses directly as a discrete variable (ONO *et al.*, 1999; FANG *et al.*, 2007; LI *et al.*, 2010; VAN LEIJENHORST *et al.*, 1996; KOZA *et al.*, 2005; VASILJEVIC, 2002) do not do so in an efficient way, as it will be pointed out in section 5.2.1.

Based on the weaknesses found in the methods presented in the literature, we present a new method that addresses all these discussed issues. The proposed method makes use during the exploration phase of a variant of the generalized extremal optimization (GEO) algorithm. In the next chapter, we present the background of the GEO algorithm and some of its variations before we discuss our proposed version of the GEO algorithm in Chapter 6.

4 GENERALIZED EXTREMAL OPTIMIZATION (GEO) ALGORITHM AND ITS VARIATIONS

In this chapter, we present the GEO algorithm in its canonical form as well as in some of its proposed variations: M-GEO and GEO_{real1}. Other GEO variations do exist; however, this text is restricted to the mentioned algorithms because they are necessary and sufficient for understanding the method we propose in this thesis.

4.1. Canonical GEO

De Sousa *et al.* (2003) presented the GEO as a generalization to the extremal optimization (EO) algorithm proposed by Boettcher (2000). Both are based on the simplified evolutionary model of Bak-Sneppen, which was developed to study self-organized criticality in ecosystems (BAK; SNEPPEN, 1993).

The codification used in GEO is binary. In a similar method to that used in GA, all design variables are stacked in a single string of bits representing a candidate solution for the problem as shown in

Figure 4.1. Nevertheless, GEO has some advantages over other evolutionary algorithms: it has only one free adjustable parameter τ , its implementation is very simple, and its performance is competitive for test functions as well as for real problems (DE SOUSA *et al.*, 2003; DE SOUSA *et al.*, 2004; GALSKI *et al.*, 2005; GALSKI, 2006; ABREU *et al.*, 2005; MURAOKA *et al.*, 2006; ABREU *et al.*, 2007; DE SOUSA *et al.*, 2007; GALSKI *et al.*, 2007; SWITALSKI; SEREDYNSKI, 2008; CUCO *et al.*, 2009; SCHNEIDER *et al.*, 2009; CASSOL *et al.*, 20011; SWITALSKI; SEREDYNSKI, 2012a, 2012b). Figure 4.2 shows the flowchart of the canonical GEO.

Unlike GA, the GEO bit string does not represent the chromosome of a candidate solution, but it represents different species coexisting in an ecosystem.

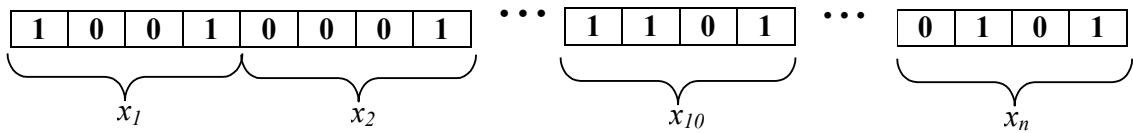


Figure 4.1 - GEO candidate solution representation. Each bit can be interpreted as a species within an ecosystem. Four bits representation were used here just as an example. The number of bits used by each variable can be defined according to the problem needs.

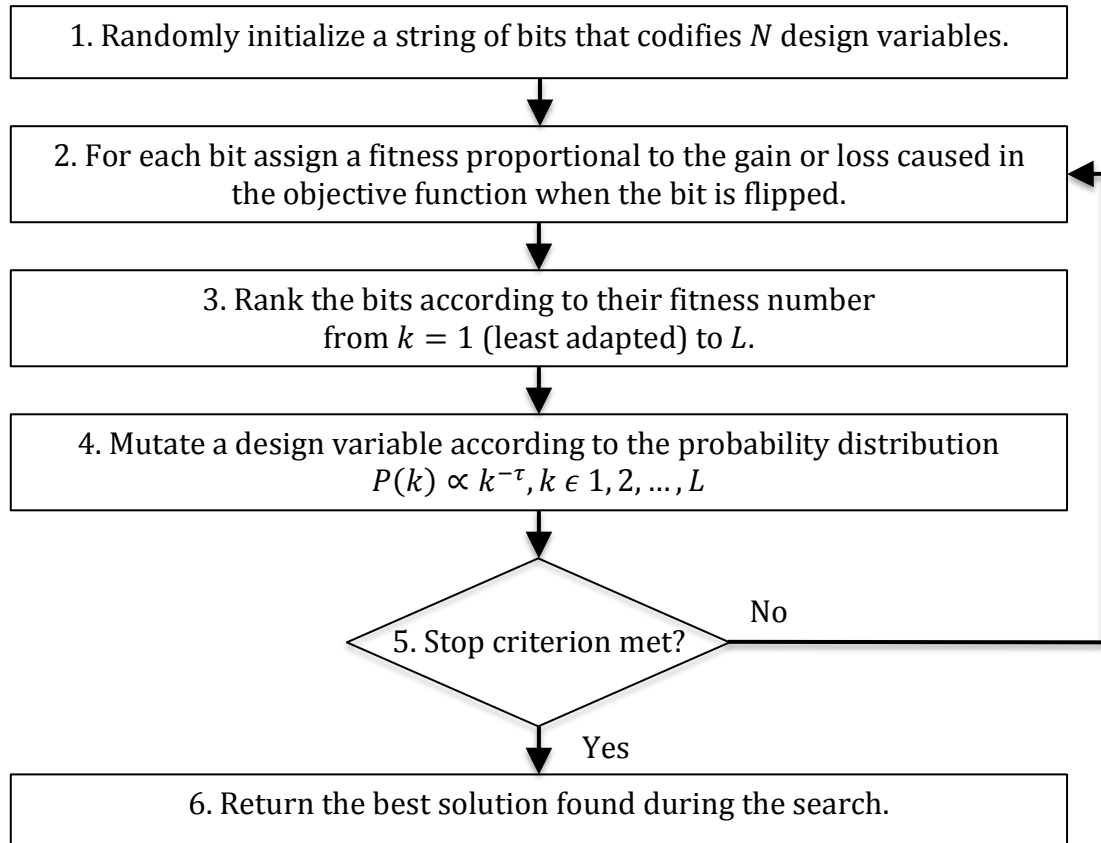


Figure 4.2 - Canonical GEO flowchart.

A fitness value is associated with each species of a candidate solution. The fitness is proportional to the gain or loss the objective function suffers when the bit is flipped. The bits are then ranked from the least adapted bit, $k = 1$, to the most adapted bit, $k = L$, where k is the rank position and L the number of bits in the string. Then, one bit is randomly selected with uniform probability. The selected bit has a probability of flipping given by

$$P(k) = k^{-\tau}, \quad (4.1)$$

where τ must be a non-negative real value.

If the selected bit is flipped, the resulting species set is transferred to the next generation where the fitness assignment, bit ranking, and random bit selection is repeated. Otherwise, a new bit is randomly selected until a bit is flipped. The process is repeated from generation to generation until the stopping criterion is fulfilled. The best bit configuration (solution) found during the search is saved and returned at the end of the data run.

4.1.1. Multi-objective approach and M-GEO algorithm

Before we introduce the multi-objective GEO version, it is necessary to explain some terms used in multi-objective approaches. Section 4.1.1.1 brings the basics of a multi-objective approach, while Section 4.1.1.2 explain the M-GEO algorithm.

4.1.1.1. Multi-Objective Problems

Despite being frequently considered as mono-objective, practical engineering optimization problems are normally of multi-objective nature. Many times these objectives or criteria are conflicting. In the design of a car engine for example, the main goal is to maximize performance and minimize fuel consumption simultaneously.

The most used methods to deal with these kinds of problem are based on scalarization approaches, which transform multi-objective problems into mono-objective. Among these scalarization methods the most common are the Weighted Sum Approach, the ϵ -Constraint Method, Goal Attainment, Lexicographic Ordering, Reference Point Approach and Goal Programming (BRANKE, *et al.*, 2008).

Scalarized methods are attractive approaches to deal with multi-objective problems due to the possibility of using one of the many available mono-objective optimization methods and tools out there. This is perhaps the reason why multi-objective approaches have not been extensively explored in optical design.

When an optimization problem is treated as multi-objective, usually it returns a set of solutions as a result, different from what happens in mono-objective approaches, which return a single solution. Any solution in the resulting set cannot be considered, in principle, better or worse than another solution in the same set because any solution will be worse than another solution in at least one aspect or objective, but never at all of them at the same time. This resultant set of solutions is known as non-dominated solutions. When these solutions are plotted in the objective functions space they form the thus called Pareto front.

Lets suppose we have a generic multi-objective problem where we want to minimize n functions, F_1, F_2, \dots, F_n . We say that a feasible solution X is non-dominated if and only if there is no other solution K in the feasible design space such that for all $i = 1, 2, \dots, n$, $F_i(K) \leq F_i(X)$. If at least one solution K exists, then solution X is dominated.

To illustrate the ideas of dominance, non-dominance and Pareto front consider Figure 4.3, where blue and red dots represent feasible solutions of a multi-objective min-min problem of two objective functions (F_1 and F_2), plotted in the objective-function space.

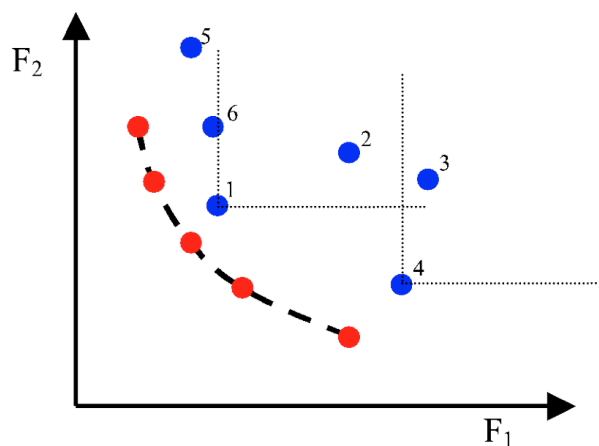


Figure 4.3- The graph shows solutions for a generic min-min multi-objective problem, plotted in the objective-functions space F_1 and F_2 . Dominated solutions are represented in blue, while red dots represent non-dominated solutions.

Blue points represent the dominated solutions. Red points denote the non-dominated ones. The set of red points form the Pareto front, represented by the dashed line in the graph.

The goal in a multi-objective problem is to find the non-dominated solutions that form the Pareto Front. This gives the designers a very clear idea of the compromises that can be made in the design considering the used metrics.

Evolutionary Optimization (EO) Algorithms are very powerful tools to directly solve multi-objective optimization problems. Multi-Objective Genetic Algorithm - MOGA (FONSECA; FLEMING, 1993), Non-dominated Sorting Genetic Algorithm-NSGA (SRINIVAS; DEB, 1994) and NSGAI (DEB *et al.*, 2002), Niche Pareto Genetic Algorithm-NPGA (HORN *et al.*, 1994), Strength Pareto Evolutionary Algorithm-SPEA (ZITZLER; THIELE, 1999) and SPEA-II (ZITZLER *et al.*, 2001), and Pareto Archived Evolution Strategy –PAES (KNOWLES; CORNE, 1999), can be quoted as the most outstanding multi-objective evolutionary algorithms.

In this work we use the multi-objective approach in two situations: i) in the glass selection phase, where an exhaustive search optimization method is applied, ii) in the exploration phase, where a M-GEO variant algorithm is used, which is a multi-objective method developed based on GEO;

In the following section the M-GEO algorithm is presented. M-GEO is used as background for the explanation of the algorithm developed for the exploration phase of the automatic lens design method.

4.1.1.2. The multi-objective GEO algorithm (M-GEO)

In the last few years, variations of the canonical GEO have been suggested and have also shown competitive results for both test functions and real problems (GALSKI *et al.*, 2005, 2009; GALSKI, 2006, 2012; MAINENTI-LOPES *et al.*, 2008, 2012; YANO *et al.*, 2010; CUCO *et al.*, 2011; GUO *et al.*, 2012). Galski *et al.* (2005) presented the multi-objective version of GEO called M-GEO. The primary change in the multi-objective version of the algorithm occurs in the bit

fitness calculation. For each generation in M-GEO, a single objective function from the N objective functions used to drive the search is randomly selected with a uniform distribution. Only the selected function is used in the current generation to assign the bit fitness and ranking. Additionally, all of the candidate solutions found during a generation are checked for dominance. All non-dominated solutions visited during the search are saved and returned at the end of the data run.

The version of M-GEO presented by Galski (2006) re-initializes the seed solution after a defined number of function calculations as an intrinsic step in the algorithm. This technique increases the statistical robustness of the algorithm and helps to spread the solutions over the whole Pareto front (GALSKI, 2006).

Figure 4.4 presents the M-GEO flowchart from Galski *et al.* (2005), which inspired our proposed algorithm. Despite not including the re-initialization intrinsically in our version, the proposed algorithm adopts independent re-initialization of the exploration phase as we will see in the next chapter.

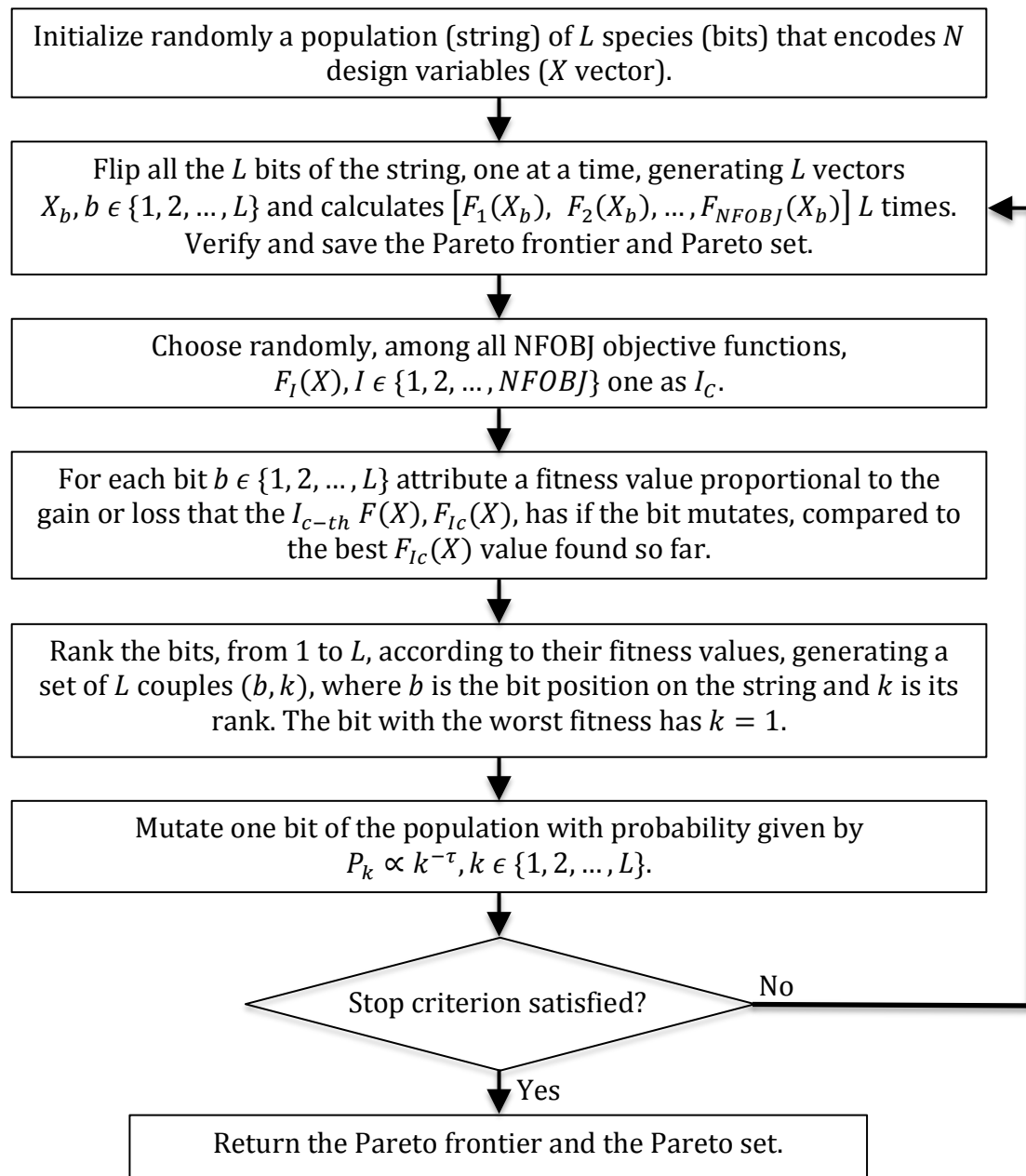


Figure 4.4 - M-GEO flowchart (GALSKI *et al.*, 2005)

4.1.2. Real-coded GEO (GEO_{real1})

Mainenti-Lopes *et al.* (2008) presented two variations of GEO using real codifications for the variables: GEO_{real1} and GEO_{real2} . These variations perform better for some test functions than the canonical versions. We only discuss GEO_{real1} herein because it provides the sufficient background for understanding the proposed method.

GEO_{real1} has the same basic principles of GEO, but it uses real codification. In other words, the candidate solutions are represented by a linear string formed by the stack of all variables in a real format rather than in a binary format. In this way, the perturbation made in each one of the i species (or variables) for a candidate solution is very similar to the perturbations used in the evolution strategy (ES), which is done by adding a random number $N(0, \sigma)$ to the variable x :

$$x'_i = x_i + x_i N(0, \sigma), \quad (4.2)$$

where x'_i is the value of the variable after the perturbation, and $N(0, \sigma)$ a random number with a Gaussian distribution, zero mean, and standard deviation σ . Equation (4.2) is applied individually to all variables. For each perturbation, the objective function is calculated and the fitness of the species is assigned. Then, the variables are ranked from the least adaptable to the most adaptable. From this point on, the algorithm is performed like the canonical GEO. One of the species (or variables) is randomly selected with a uniform probability. The selected species of rank k has a mutation probability given by Equation (4.1).

If the mutation occurs, the resulting species set is transferred to the next generation, where the whole process is repeated. Otherwise, a new variable is randomly selected until a mutation occurs. The process is repeated from generation to generation until a stopping criterion is satisfied. The best configuration of variables found during the search is saved and returned at the end of the data run. GEO_{real1} flowchart is presented in Figure 4.5.

In this thesis, we introduce a new variation of GEO named O-GEO. The O-GEO is used in the exploration phase of the proposed method. It is a tailored version resulting from the mix between M-GEO (GLASKI, 2005) and GEO_{real1} (MAINENTI-LOPES *et al.*, 2008) with the addition of specific diversity operand suitable for the problem of optical design. The O-GEO algorithm is explained in detail in Chapter 6.

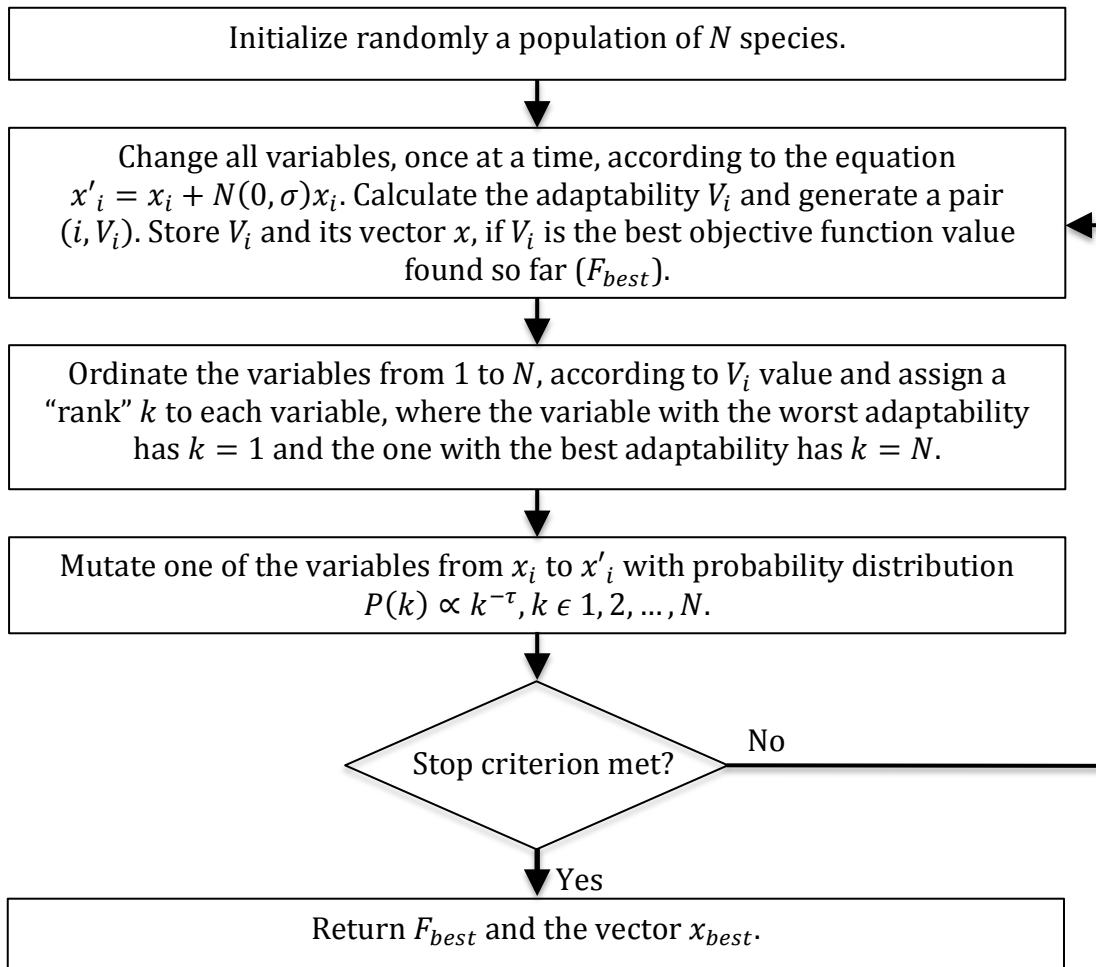


Figure 4.5 - GEO_{real1} flowchart (MAINENTI-LOPES *et al.*, 2008).

5 AN OVERVIEW OF THE PROPOSED AUTOMATIC OPTICAL DESIGN METHOD

In this chapter, we present an overview of the proposed automatic optical design method. As mentioned earlier, the method proposed in this thesis uses a multi-objective memetic approach. In addition to discussing the method overview, this chapter will discuss the key components of the method.

5.1. The multi-objective approach

The multi-objective approach proposed addresses the design, image quality, assembly tolerance, and system complexity.

Tolerancing is a crucial issue in optical design field due to the high sensitivity of imaging optical systems with respect to fabrication errors. The goal of an optical designer is to determine an insensitive optical system that complies with the image quality requirements after fabrication. Furthermore, the production costs of insensitive systems are reduced without significantly compromising the image quality.

Classical approaches for the design of insensitive optical system are based on a two-part interactive method. The first part is the design itself, which can be performed using first-order and third-order analysis, lens systems databank and optimization tools. As the second task, a tolerance analysis is carried out in order to determine the system error budget and the expected as-built performance. For high-performance optical systems, designers usually realize that some modifications to the system architecture are needed to improve the as-built system performance within the desired tolerances. In this way, an interactive process of design and tolerance analyses is performed to find an acceptable trade-off solution between the as-designed and the as-built system performance.

Some authors suggest that metrics estimating the system sensitivity should be included in the merit function (MF) as a penalty (ISSHIKI *et al.*, 2004; JEFFS, 2002). The challenge with this approach is balancing the weight between the

image quality and the sensitivity metrics in a single MF due to their differing physical meaning and units.

Other studies have used a multi-configuration approach to design insensitive system (FUSE, 2003). In this method, each configuration represents the nominal system with one of the design parameters perturbed. The final MF is formed by the average of the merit function of each configuration. In this way, the tolerancing can be considered during optimization process. This seems to be a very interesting and practical solution. However, the methodology quickly collapses as the number of elements in the system increases due to the increasing number of configurations needed to account for the fabrication errors of each surface.

Some approaches have taken advantage of global optimization algorithms to find many local minimums (MCGUIRE, 2006; ISSHIKI *et al.*, 2006). Then, the systems are ranked according to the sensitivity, which is accessed by means of a simple metric or a complete tolerance analysis. The drawback to these methodologies is that the optimization algorithm is not driven by the sensitivity but only by the image quality metric.

Epple and Wang (2008) suggested that aspherical surfaces should be included to reduce sensitivities in optical design. However, aspherical surfaces might have their own tolerance problems, which can conflict with the desensitization process.

Another important characteristic in the fabrication of an optical system is the system complexity. Herein, the system complexity is taken as the number of optical elements used in the system.

Normally, more complex systems require more expensive production in terms of man-hours and material. Likewise, increasing the number of optical elements in a system increases the number of degrees of freedom available to correct the optical aberrations, making better image correction possible. Furthermore, increasing the number of elements used in the system potentially lowers the

power of each element, making the system more insensitive to fabrication errors of each element. On the other hand, with more elements, the system has more potential sources of errors in the fabrication.

With this explanation, we see that defining the optimum number of elements used in an optical system is not a straightforward task even for an experienced optical designer, especially for high performance optical systems. As our research has determined, the variation of the number of optical elements during the automatic optimization is rarely explored.

A single study reports an optimization tool for optical systems, based on a genetic programming algorithm, where the number of lenses is considered as a design variable (KOZA *et al.*, 2005). In spite of that, the number of lenses is controlled by a penalty in the merit function, the more elements, the higher the penalty. In our opinion, the EO method used, as well as the way they control the number of lenses, result in a drawback to their implementation. The penalty to control the number of lenses restricts the exploration of the design space and genetic programming approach limits the method application and/or performance due to its computationally demanding nature. To execute his method, Koza *et al.* (2005) mention the use of a cluster with thousands of CPUs.

In this thesis, we explore a multi-objective approach for the lens design optimization problem. In this way of handling the problem, the image quality, system sensitivity, and number of lenses are simultaneously taken into consideration and drive the search. Furthermore, unlike any previously published methods in lens design, these criteria are not fused in a single merit function. As a result, non-dominated solutions can be obtained to generate the corresponding Pareto Front. This method yields better insight into the available trade-off solutions for the problem.

5.2. The memetic approach

Our method is characterized as a memetic approach (MOSCATO, 1989; MOSCATO; COTTA, 2003) because it breaks the search into three parts: (i) glass selection, (ii) exploration, and (iii) exploitation phases.

The glass selection phase is based on a detailed and general mathematical formulation of the residual chromatic aberration resultant from the combination of different types of glasses. The aim of this phase is to select the most appropriate set of glasses for the system under design. This information is then used as a priori knowledge into the exploration phase. The glass selection method uses a multi-objective approach and the final selection of the best set of glasses depends on the designer choice.

The exploration phase is based on a multi-objective metaheuristic algorithm, which is responsible for the global search aspect of the method. This algorithm incorporates problem-knowledge in the candidate solutions codification and in the diversity operands.

The exploitation phase on the other hand, consists of an exact deterministic algorithm, which is responsible for the local search or intensification of the candidate solutions.

In this section, we elucidate each one of these phases of the method. The details are then provided in Chapter 6.

5.2.1. Glass selection

According to Rayces and Rosete-Aguilar (2001), two barriers limit optical system performance: light diffraction and chromatic aberration. As pointed out in Chapter 2, glasses are important variables for correcting the chromatic aberration in optical systems. However, as we saw in Chapter 3, glasses are discrete variables and cannot be handled in a direct or effective manner using classical methods of optimization.

On the other hand, EO methods have no problems dealing with discrete variables. In spite of this, not all EO methods applied in lens design take advantage of this feature of the algorithm. In some studies (GAGNÉ *et al.*, 2008; THIBAUT *et al.*, 2005; CHEN; YAMAMOTO, 1996), glasses are transformed to continuous variables using glass model equations. This is the same technique used by classical optimization methods that consider glasses as variables; however, as already mentioned, these techniques do not produce satisfactory results. In other studies, glasses are not considered as variables (BEAULIEU *et al.*, 2002; SAKUMA; KOBAYASHI, 2005).

Indeed, it is possible to find lens design studies using EO that take advantage of the method to optimize glasses in a direct discrete way (ONO *et al.*, 1999; FANG *et al.*, 2007; LI *et al.*, 2010; VAN LEIJENHORST *et al.*, 1996; KOZA *et al.*, 2005; VASILJEVIC, 2002). Despite reporting excellent results, the dimensionality of the glass selection problem is huge, even for a reasonably simple optical system, as pointed out by Tesar (2000). Moreover, these methods do not guarantee that the best set of glasses has been found. Furthermore, the success of the design, especially for broadband systems, depends on a specific combination of glasses. In this way, the performance of the EO algorithm can be significantly increased if the number of glasses is constrained. This is confirmed by Tesar (2000) and Van Leijenhorst *et al.* (1996).

For this reason, in the proposed automatic design algorithm, we treat the glass selection as a separate optimization problem. Our proposal is to reduce the number of available glasses for a design from hundreds of glasses to just a few. The resulting information about the most appropriate glasses for a specific design will then be used as input for the exploration phase of the algorithm. The glasses in the exploration phase are then considered as discrete variables, but with significantly reduced number of possibilities.

Several graphical and mathematical methods have been proposed for the selection of optimal glass combinations for correcting chromatic aberration (RAYCES; ROSETE-AGUILAR, 2001; SINGLER, 1986; GRUESCU *et al.*, 2008;

HARIHARAN, 1997, 1999; MERCADO; ROBB, 1993; ROBB, 1985; LESSING, 1970; SLOAN, 1970; HERZBERGER; McCLURE, 1963; WILLEY, 1962; STEPHEN, 1960). However, the problem of glass selection is wide in scope, and in our opinion, the glass selection problem is not completely solved.

Even a recent study about optimal glass selection for doublets (SUN *et al.*, 2009) does not provide relevant contributions to the subject. The method used in Sun *et al.* (2009) is based on the chart of partial dispersion vs. abbe number for selecting the potential glass pairs, and on the use of secondary spectrum for evaluating the glass pair chromatic correction, which were presented by Ernst Karl Abbe more than 140 years ago (RAYCES; ROSETE-AGUILAR, 2000). Furthermore, the equations presented for the thin aplanatic doublet solution are well known (RAYCES; ROSETE-AGUILAR, 2000). The new metric suggested in the paper for evaluating the residual chromatic aberration, which is given by the area under the chromatic focal shift curve, does not, in fact, contribute any additional information that what we can determine from the standard secondary color metric. The only possible contribution in Sun *et al.* (2009) is the technique of thickening the thin design, which does not help in the glass selection process itself.

Fischer *et al.* (2004) mention that the glass selection in optical design has a mystique and tends to be both a science and an art. Our goal in this thesis is not only to use a glass selection technique in our automatic design method but also to present a new method that objectively systematizes the task of glass selection for the design of color corrected optical systems.

5.2.2. Exploration

As we discussed in Chapter 3, multi-objective optimizations and discrete variables can be easily handled with evolutionary methods of optimization, which have been successfully applied in lens design problems.

Despite studies reporting the use of multi-objective optimization approaches in lens design (JOSEPH *et al.*, 2007; ONO *et al.*, 1998; GAGNÉ *et al.*, 2008),

these works do not apply this technique in designing optical systems considering the sensitivity to fabrication errors and system complexity as proposed herein. Joseph *et al.* (2007) used a multi-objective method to optimize optical systems using three criteria: spherical aberration, distortion, and transverse ray aberration function. Ono *et al.* (1998) also applied a multi-objective optimization in lens design using both the image resolution and the distortion as attributes. Finally, Gagné *et al.* (2008) employed a multi-objective optimization in lens design by taking into account the glass material cost and image quality.

Very few studies in the use of EO in lens design customize the algorithm to the problem. In fact, most studies on this subject (JOSEPH *et al.*, 2007; BEAULIEU *et al.*, 2002; GAGNÉ *et al.*, 2008; THIBAUT *et al.*, 2005; CHEN; YAMAMOTO, 1996; MORRE, 1999; VAN LEIJENHORST *et al.*, 1996; NAGATA, 2004) simply apply EO methods to lens design without adapting the algorithm to the problem.

In this work, we propose a variant of the generalized extremal optimization (GEO) algorithm introduced by De Sousa *et al.* (2003). More precisely, the exploration algorithm suggested herein is a customized version resulting from a mix between the multi-objective version of GEO (M-GEO) (GLASKI, 2005) and the real codification version of GEO (GEO_{real1}) (MAINENTI-LOPES *et al.*, 2008) with an additional specific diversity operand suitable for the problem. By customizing the algorithm to the problem, we expect better performance from our method.

5.2.3. Exploitation

While the EO methods are useful for exploring different regions in the design space, without getting stuck in local minima, they are not efficient for tuning the design to determine a final solution. This occurs because optical design is a high-dimensional strong epistatic problem.

EO algorithms converge very slowly to the optimal solution in comparison with classical optimization methods. For this reason, many studies applying EO in

lens design use hybrid methods, combining both local search and EO methods to find good solutions (CHEN; YAMAMOTO, 1996; MORRE, 1999; JOSEPH *et al.*, 2007; GAGNÉ *et al.*, 2008; LI *et al.*, 2010). This hybridization combines the best characteristics of each method and overcomes their weaknesses.

In a hybridized process, the EO method is used for finding regions of solution space that are good candidates for locating the optimum candidate, and the classical optimization methods are used to actually find the optimum candidate. This means that the EO methods are used to find a set of good starting points and the classical methods use these identified starting points to find the optimum solution.

Our proposed method takes advantage of the EO and classical method hybridization. The local search conducted in the exploitation phase is applied to all feasible non-dominated solutions found in the exploration phase. The algorithm used in the exploitation phase is based on DLS method presented in Chapter 3.

5.3. The method overview

Now that we have identified each of the features of the proposed method, we present an overview of the proposed algorithm. Figure 5.1 illustrates the flowchart of the proposed method.

As input for the proposed method, the designer must provide only the optical system requirements and constraints. At first, the glass selection phase is executed. As a result, the most suitable set of optical glasses is selected for the problem and used as input for the next phase. The glass selection phase helps to reduce the design space, limiting the set of available glasses from hundreds to just a few, making the search for solutions more efficient.

Next, the exploration phase starts with a random solution and runs for a specified number of generations. The feasible non-dominated solutions found during the latest independent execution of this phase are transferred to the exploitation phase.

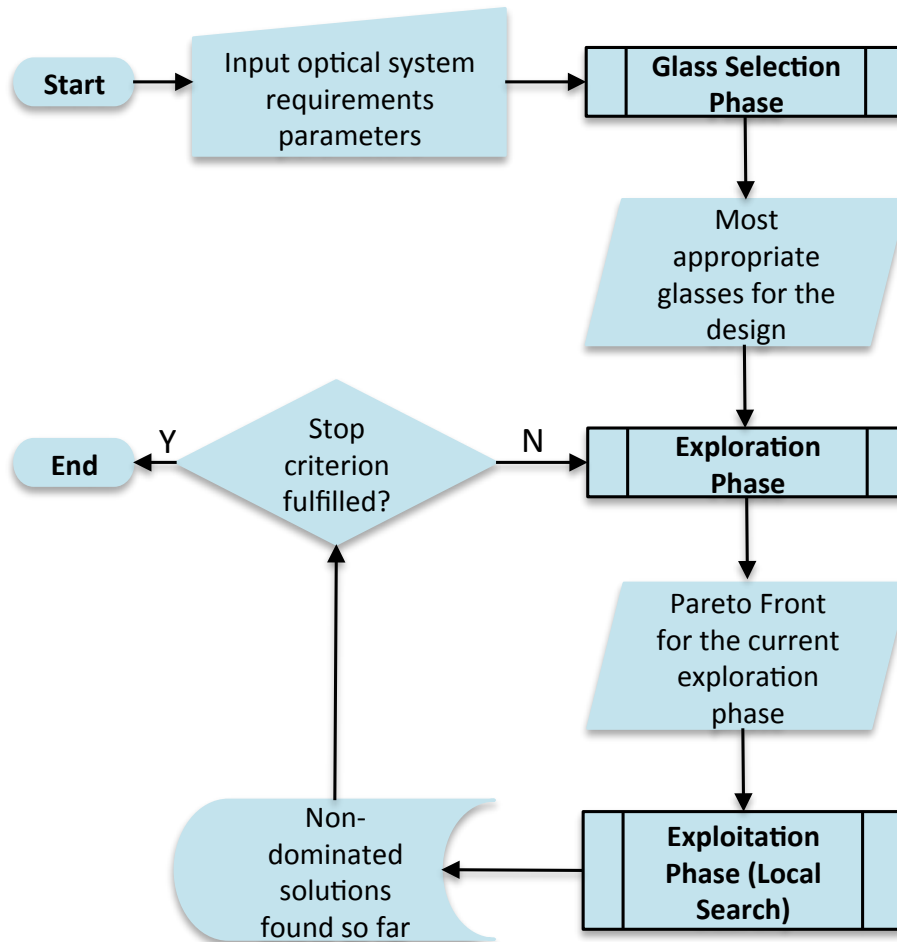


Figure 5.1 - Overview flowchart of the global search algorithm proposed for the automatic design of optical systems.

In the exploitation phase, a local search algorithm is applied for each one of input solutions until the stopping criterion is fulfilled. The non-dominated solutions found in this interaction are compared with the Pareto front solutions found by previous iterations of the algorithm. The remaining non-dominated solutions resulting from this comparison are used to develop a new Pareto front. If the stopping criterion is not reached, the algorithm returns to the exploration phase and the cycle is repeated until the stopping criterion is fulfilled.

In the next chapter, we present a more detailed description of each phase of the algorithm, following a discussion of the method overview starting with the glass selection phase, followed by the exploration phase, and concluding with the exploitation phase.

6 DETAILING THE METHOD PHASES

6.1.1. The glass selection phase

We only present a summary of the method for glass selection here. For more details, the readers are encouraged to study Appendix C which contains the full paper about the method published in the high-impact journal *Optics Express* Albuquerque *et al.* (2012).

The glass selection phase is performed first, and it is independent of the two subsequent phases in the process of automatic design. However, the results are very important in providing the input glass materials for the Exploration phase. This phase supports the selection of the most appropriate optical glass to be used in a specific design based on the input system requirements given by the designer.

The selection of the most appropriate glass materials significantly reduces the design space, decreasing the number of available glasses from hundreds to a few and increases the efficiency of the whole automatic design method as a consequence.

The method presented lies on the compatibility of the glass materials to minimize the chromatic aberration while simultaneously controlling other specific difficult-to-correct monochromatic aberrations.

6.1.2. Background for the method of glass selection

The proposed method is based on the unification of two methods proposed in the literature (RAYCES; ROSETE-AGUILAR, 2001; MERCADO; ROBB, 1993) with some additional contributions. We also developed a multi-objective approach for the problem.

After surveying many methods of glass selection available in the literature, we determined that the method proposed by Mercado and Robb (1993) is the most theoretically rigorous and general. The Mercado-Robb method allows different number of glasses in the set as well as different number of wavelengths for

which the minimization of chromatic aberration is desired. Despite the general formulation of the Mercado-Robb method and the excellent discussion provided in their work, Mercado and Robb only demonstrate a few practical examples of the solution technique.

The method of color correction proposed by Rayces and Rosete-Aguilar (2001) was limited to two glasses and three wavelengths. In spite of these limitations, the Rayces and Rosete-Aguilar method establishes and utilizes metrics, which have never been reported before in glass selection theory. These metrics are not related to color correction, but they verify if a set (in their case, a pair) of glasses has the potential to provide a successful design. In contrast to other glass selection methods, the Rayces and Rosete-Aguilar method uses not only the wavelength as input but also the desired focal length and the numerical aperture of the designed system.

The method presented in this thesis improves the Mercado-Robb method by addressing some of the practical implementations issues. It also incorporates the metrics proposed by Rayces and Rosete-Aguilar (2001). Because each possible glass arrangement has different metrics with dissimilar physical natures, we further included a multi-objective approach in the glass selection method. This is useful for filtering out the non-dominated solutions and organizing them with different Pareto rankings, assisting the selection of the most appropriate glass combination solution for the problem.

6.1.2.1. The Mercado and Robb method with some new contributions

The index of refraction of optical materials is a function of the wavelength. Several mathematical models have been proposed to describe this dependence. One of these models, proposed by Buchdahl (ROBB; MERCADO, 1983), is given by the following power series:

$$N(\lambda) = N_0 + v_1\omega(\lambda) + v_2\omega(\lambda)^2 + \dots + v_i\omega(\lambda)^i. \quad (6.1)$$

Here, N represents the refractive index for wavelength λ , N_0 is the refractive index for a reference wavelength λ_0 . The chromatic coordinate ω is a function of λ :

$$\omega = \frac{\delta\lambda}{1 + \alpha\delta\lambda} \quad (6.2)$$

where $\delta\lambda = \lambda - \lambda_0$, and α is a universal constant taken to be 2.5 (MERCADO; ROBB, 1993). The dispersion coefficients v_n are specific to a given glass.

If a set of glasses is needed to minimize the chromatic aberration for n wavelengths, Equation (6.1) is expanded up to the $n - 1^{th}$ order.

Moving N_0 to the left side of Equation (6.1) and dividing both sides by the constant $N_0 - 1$, we obtain

$$D(\lambda) = \sum_{i=1}^{n-1} \eta_i \omega(\lambda)^i, \quad (6.3)$$

where $D(\lambda) = \delta N(\lambda)/(N_0 - 1)$, $\delta N(\lambda) = N(\lambda) - N_0$, and $\eta_i = v_i/(N_0 - 1)$. The term $D(\lambda)$ is called the dispersive power. The method presented by Mercado and Robb (1993) is based on Equation (6.3)

The optical power $\phi(\lambda)$ of a single lens for wavelength λ is defined as the inverse of its focal length at the same wavelength $f(\lambda)$. For a system of k thin lenses in contact, the resulting optical power Φ for the reference wavelength λ_0 is computed by

$$\Phi(\lambda_0) = \sum_{j=1}^k \phi_j(\lambda_0). \quad (6.4)$$

Using Equations (6.3) and (6.4) and the lens maker equation it is possible to write:

$$\Phi(\lambda) = \Phi(\lambda_0) + \sum_{j=1}^k \phi_j(\lambda_0) D_j(\lambda). \quad (6.5)$$

Assuming that each of the k lenses is made from a different glass, where $k \geq 2$, it is possible to show that the conditions for an achromatized optical system in n wavelengths, where $n \geq 2$, can be given in a matrix form by (MERCADO; ROBB, 1993)

$$\Delta\bar{\Omega} \cdot \bar{\eta} \cdot \bar{\Phi} = \bar{0}, \quad (6.6)$$

where $\Delta\bar{\Omega}$ is a square matrix of order $n - 1 \times n - 1$:

$$\Delta\bar{\Omega} = \begin{bmatrix} (\omega_1 - \omega_2) & \cdots & (\omega_1^{n-1} - \omega_2^{n-1}) \\ \vdots & \ddots & \vdots \\ (\omega_{n-1} - \omega_n) & \cdots & (\omega_{n-1}^{n-1} - \omega_n^{n-1}) \end{bmatrix}, \quad (6.7)$$

Here, $\bar{\eta}$ is a matrix of order $n - 1 \times k$

$$\bar{\eta} = \begin{bmatrix} \eta_{11} & \cdots & \eta_{1k} \\ \vdots & \ddots & \vdots \\ \eta_{(n-1)1} & \cdots & \eta_{(n-1)k} \end{bmatrix}, \quad (6.8)$$

while $\bar{\Phi}$ is a matrix of order $k \times 1$,

$$\bar{\Phi} = \begin{bmatrix} \phi_1(\lambda_0) \\ \vdots \\ \phi_k(\lambda_0) \end{bmatrix}, \quad (6.9)$$

Finally, $\bar{0}$ is a matrix of order $n - 1 \times 1$:

$$\bar{0} = \begin{bmatrix} 0 \\ \vdots \\ 0 \end{bmatrix}. \quad (6.10)$$

Matrix $\Delta\bar{\Omega}$ is a square and doubtless nonsingular. In this case, Equation (6.6) can be reduced to

$$\bar{\eta} \cdot \bar{\Phi} = \bar{0}. \quad (6.11)$$

Equation (6.11) has a nontrivial solution (i.e., $\bar{\Phi} \neq \bar{0}$) if and only if the rank of matrix $\bar{\eta}$ is lower than k (i.e., k is not a full rank matrix). This happens when there is a perfectly linear dependence among the columns of matrix $\bar{\eta}$. Nevertheless, for any practical and meaningful situation where $k \leq n - 1$, the linear dependence is virtually never mathematically exact. As a consequence, the rank of matrix $\bar{\eta}$ will always be equal to k . This result makes the rank of matrix $\bar{\eta}$ an inefficient metric either to identify sets of glasses that are free from chromatic aberration in the defined wavelengths or to compare the residual chromatic aberration among the different possible glass combinations.

To solve this problem, Mercado and Robb provide a geometrical interpretation of Equation (6.11). In this way, they suggest a geometric metric to verify how well a set of glasses correct the chromatic aberration for a given set of wavelengths. The metric is easy to understand and visualize for the case of two glasses. Nevertheless, for more than two glasses the interpretation changes and becomes complicated. Furthermore, the metric has no physical meaning.

We propose a different metric for verifying how well a specific set of glasses minimizes the chromatic aberration for a given set of wavelengths. This metric has a general form, which does not depend on the number of glasses used in the combination, and it has a direct physical meaning. This new metric is presented and explained in the following paragraphs.

To minimize or correct the chromatic aberration, we must not only select a specific set of compatible glasses but also use the right optical power for the lenses made with each one of these materials. To calculate the optimum power of each glass that minimizes the chromatic aberration, both Equations (6.4) and (6.6) are used. To simplify the computation, we normalize the optical power of the system for λ_0 and write Equation (6.4) in its matrix form

$$\bar{S} \cdot \bar{\Phi} = 1, \quad (6.12)$$

where \bar{S} is a row vector of order $1 \times k$ with all elements equal to one.

Combining Equations (6.12) and (6.6) we obtain:

$$\bar{G} \cdot \bar{\Phi} = \hat{e}, \quad (6.13)$$

where $\bar{G} = \begin{bmatrix} \bar{S} \\ \Delta\bar{\Omega} \cdot \bar{\eta} \end{bmatrix}$ and \hat{e} is a column vector of order $n \times 1$ where the first element is equal to one and the other elements are equal to zero.

Solving Equation (6.13) for $\bar{\Phi}$ using the least square method results in the following equation:

$$\hat{\Phi} = (\bar{G}^t \cdot \bar{G})^{-1} \cdot \bar{G}^t \cdot \hat{e}. \quad (6.14)$$

Equation (6.14) computes the optimal power of the lenses made with each of the glasses considered in the set that minimizes the square sum of the chromatic change of power for the n defined wavelengths. It is important to note that the equations provided by Mercado and Robb (1993) used to compute the optical powers are only related to some specific situations and do not use all of the glass information available. In contrast, the equation presented herein is general, uses all of the glass dispersion coefficients available, and provides the minimum chromatic aberration for the glass set considered in the n given wavelengths.

Now, it is possible to use the vector $\hat{\Phi}$ in Equation (6.6), to obtain the minimum chromatic change of power \overline{CPP} :

$$\overline{CPP} = \Delta\bar{\Omega} \cdot \bar{\eta} \cdot \hat{\Phi}. \quad (6.15)$$

Our metric to verify how suitable a specific set of glasses is for minimizing chromatic aberration for a given set of n wavelengths is now established as the modulus of the vector \overline{CPP} .

An excellent approximation for the chromatic focal shift is given by multiplying the vector \overline{CPP} by the desired effective focal length F for the optical system:

$$\begin{bmatrix} f(\lambda_2) - f(\lambda_1) \\ \vdots \\ f(\lambda_n) - f(\lambda_{n-1}) \end{bmatrix} = \overline{CPP} \cdot F. \quad (6.16)$$

Because the chromatic focal shift is proportional to \overline{CPP} , it clearly gives physical meaning to our metric.

6.1.2.2. The Rayces and Rosete-Aguilar Method

Rayces and Rosete-Aguilar (2001) proposed a method of glass selection where not only the chromatic correction is considered but also aberrations that, according to the authors, cannot be corrected, namely spherochromatism and fifth order spherical aberration.

The Rayces and Rosete-Aguilar method is based on an exhaustive search of glass pairs able to minimize the chromatic aberration for three wavelengths. All possible arrangements of glasses derived from a glass catalog are tested. For each glass set possibility, the power of the glasses is computed to produce a thin achromatic doublet solution for two extreme wavelengths considered. Then, the chromatic aberration for the middle wavelength, also called the secondary spectrum, is computed. Based on the power of the elements of the doublet and on the desirable aperture of the system, the first set of potentially useless solutions are removed. This eliminates solutions with steep curves that are an indicator of high-order monochromatic aberrations, which are difficult to correct or balance. In the next step, the radius of each surface is computed to produce an aplanatic solution to the third-order approximation using structural aberration coefficients. Paraxial rays are then traced to compute third-order spherochromatism and fifth-order spherical aberration. Based on the magnitude of these aberrations, a second set of glass arrangements is eliminated.

The Rayces and Rosete-Aguilar method produces an output table containing solutions that comply with the limits imposed for each aberration ranked according to the secondary spectrum value. The first rows in the table supply glass combination pairs that potentially are able to provide successful optical systems design.

6.1.3. The synthesis method of glass selection

With the background presented in the last section, the explanation of our glass selection method is straightforward. Its implementation involves several steps.

Step 1. As input, the designer must provide the effective focal length F , the f number $F/\#$, the n wavelengths covering the desired spectral range, and the number of the primary wavelength λ_0 . A glass catalog and the number of glasses k used in the combination (i.e., 2, 3, 4, etc) must also be specified.

Step 2. At the outset, the first $n - 1$ dispersion coefficients η_i are calculated for each glass in the catalog. For the calculation, the n specified wavelengths and their respective refractive indexes in the corresponding glass are used in Equation (6.3). This results in a system of $n - 1$ linear equations with $n - 1$ unknowns, which when solved provides the η_i dispersion coefficients. With the specified wavelengths, the matrix $\Delta\bar{\Omega}$ is then calculated using Equation (6.7).

Step 3. Next, all possible arrangements for the glasses from the specified catalog are checked. For each possibility, the optimum normalized power of each glass is computed using Equation (6.14). The sum of the absolute power of each arrangement, which is given by Equation (6.17) below, is used as a metric for the first reduction of the solution set:

$$F_1 = \sum_{j=1}^k |\phi_j(\lambda_0)|. \quad (6.17)$$

As pointed out by Rayces and Rosete-Aguilar (2001), high power elements have steep surfaces resulting in large monochromatic aberrations that involve higher orders of aberration. This first cut eliminates potentially useless solutions. The metric used here is different from the one presented in Rayces and Rosete-Aguilar (2001). Our metric, first suggested by Herzberger and McClure (1962), is more general in terms of the number of glasses used in the combination.

The user must set the maximum value for F_1 . Glass arrangements with F_1 values larger than the specified value are discarded. This metric is used to eliminate potential useless solutions; moreover, this metric can be used as one of several metrics in the multi-objective approach proposed for this glass selection method. The next steps and calculations are performed only for arrangements that comply with the imposed F_1 limit.

The vector $\overline{\text{CPP}}$ is then calculated by Equation (6.15). The modulus of this vector, called F_2 ($F_2 = |\overline{\text{CPP}}|$), can also be used in the multi-objective analysis. The smaller the value of F_2 the better the color correction the set of glasses provides.

Step 4. Then, a thin lens aplanatic solution for wavelength λ_0 is found for each candidate glass arrangement. To find the aplanatic solution, the system structural coefficients for spherical aberration Ξ and coma X are set equal to zero, using the power of each glass element calculated by Equation (6.14). We developed the following set of equations:

$$\Xi = \sum_{j=1}^k \xi_j = 0, \quad (6.18)$$

$$X = \sum_{j=1}^k \chi_j = 0, \quad (6.19)$$

$$\begin{aligned} [N_1(\lambda_0) - 1] \left(\frac{1}{r_1} - \frac{1}{r_2} \right) &= \left(\frac{\phi_1(\lambda_0)}{F} \right) \\ &\vdots \\ [N_k(\lambda_0) - 1] \left(\frac{1}{r_{(2k)-1}} - \frac{1}{r_{2k}} \right) &= \left(\frac{\phi_k(\lambda_0)}{F} \right). \end{aligned} \quad (6.20)$$

To find the aplanatic solution, it is necessary to solve the above set of equations from r_1 to r_{2k} .

For the case of a doublet, or $k = 2$, there are four equations and four unknowns which result in a straightforward solution. Because Equation (6.18) has a

quadratic dependence as a function of the radius (see Appendix A in RAYCES; ROSETE-AGUILAR, 2000), we can obtain two different aplanatic solutions for each glass arrangement. The best solution is retained when the definition for a better solution is based on the metric F_3 as explained ahead.

For $k \geq 3$, there are more unknowns than equations. For quickly and analytically solving the set of equations, we add constraint equations to make the number of unknowns equal the number of equations. For example, in the case where $k = 3$ (triplet), there are two possible options for the constraint: $r_3 = r_2$ or $r_5 = r_4$. The system can then be solved for both cases, and in each case two solutions exist, resulting in four total possible solutions. Once more, we only retain the better solution. We can expand the technique for $k > 3$. Unfortunately, the solution for the set of equations where $k \geq 3$ is not trivial and must be determined with a computer.

For each one of the possible retained solutions, the fifth-order spherical $W_{060}(\lambda_0)$ and the spherochromatism $W_{040CL}(\lambda_1 \cdots \lambda_n)$ wave aberration coefficients are calculated according to the algorithm presented in Rayces and Rosete-Aguilar (2000). The fifth-order spherical coefficient is calculated for the reference wavelength λ_0 . The sphero-chromatism coefficient is calculated for all possible combinations of the input wavelengths, and the worst case is assigned to the set.

Step 5. The third and last metric used in the multi-objective analysis is computed by summing the normalized fifth-order spherical \bar{W}_{060} and normalized spherochromatism \bar{W}_{040CL} wave aberration coefficients according to the following equation:

$$F_3 = (\bar{W}_{040CL} + \bar{W}_{060}), \quad (6.21)$$

where Rayces and Rosete-Aguilar (2001) define

$$\bar{W}_{060} = \frac{14W_{060}(\lambda_0)}{20\sqrt{7}} \quad (6.22)$$

and

$$\bar{W}_{040CL} = \frac{14W_{040CL}(\lambda_1 \cdots \lambda_n)}{6\sqrt{5}}. \quad (6.23)$$

As mentioned above, we also use the metric F_3 to define which of the possible aplanatic solutions for a specific glass set is the best one.

Step 6. For all of the possible sets of glass arrangements complying with the maximum allowed metric F_1 , the best aplanatic solution is stored in a table with its respective F_1 , F_2 , and F_3 metric values. The data are organized in the table as shown in Figure 6.1. The r values are the radius of curvature of each surface, and the ϕ values are the normalized optical power of each thin lens.

N°	Glass 1	...	Glass k	r_1	...	r_{2k}	ϕ_1	...	ϕ_k	F_1	F_2	F_3
1												
2												
⋮	⋮	⋮	⋮	⋮	⋮	⋮	⋮	⋮	⋮	⋮	⋮	⋮

Figure 6.1 - Format of the table used to store the best aplanatic solution data for each glass arrangement.

Step 7. The solutions are then organized into different Pareto ranks using the metrics F_1 , F_2 , and F_3 .

Step 8. Finally, a post-Pareto analysis is applied to the first Pareto ranks, organizing the solutions in the output table from the best to the worse trade-off solutions.

In summary, we can treat the glass selection for the design of optical systems with reduced chromatic aberration as a multi-objective optimization problem. The goal is to simultaneously minimize the objective functions F_1 , F_2 , and F_3 , subjected to $F_1 \leq Constant$, to Equations (6.18), (6.19), and (6.20), and to additional constraints as necessary when $k \geq 3$ (e.g., $r_3 = r_2$ or $r_5 = r_4$ for the $k = 3$ case). To solve the problem, we used an exhaustive search method, testing all possible glass arrangements.

The glass selection method overview can be represented by the flowchart in Figure 6.2.

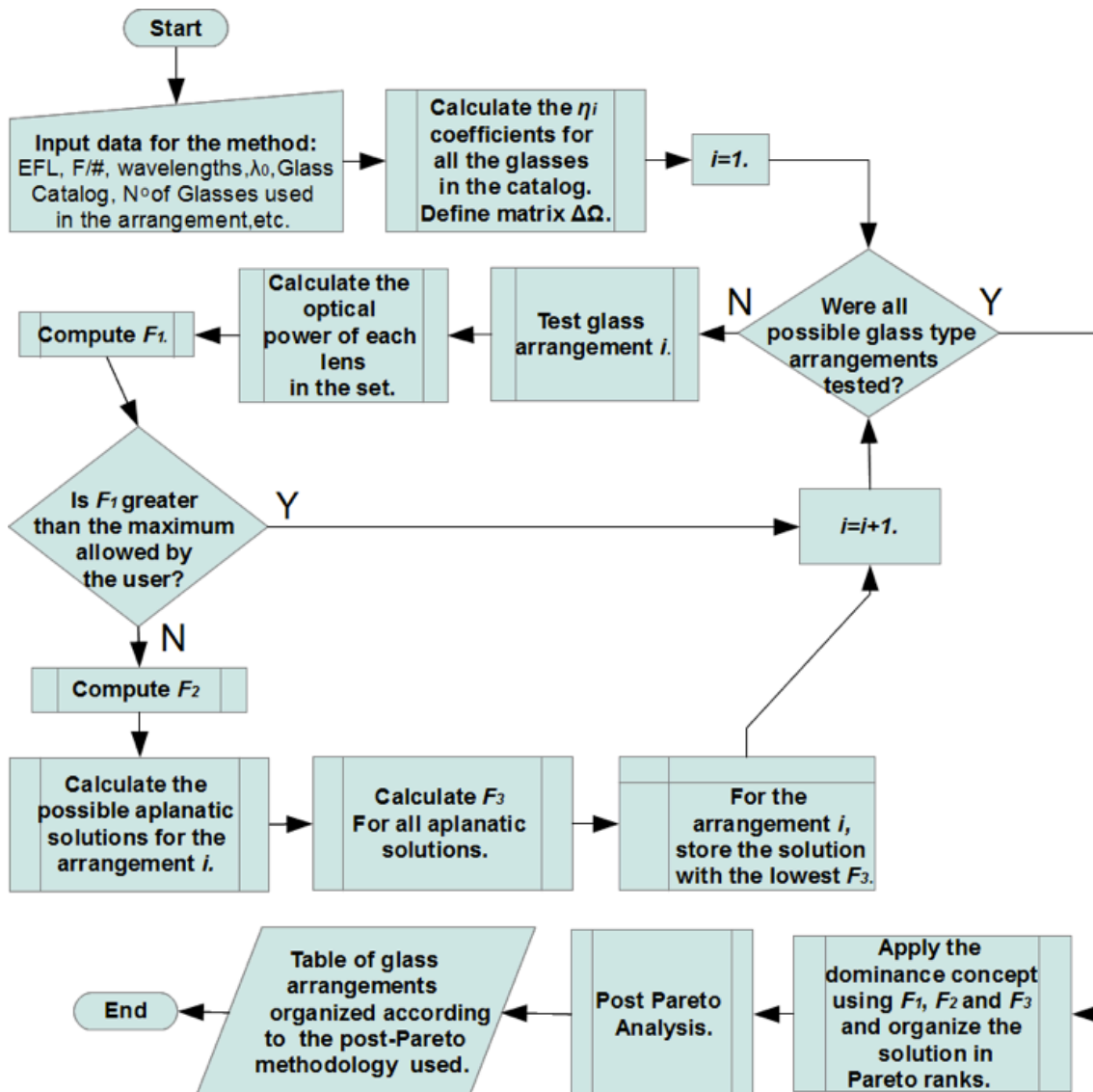


Figure 6.2 -. Flowchart of the proposed method of glass combination selection.

6.1.4. Post-Pareto analysis

The Pareto front, or Pareto rank 1, specifies the global non-dominated trade-off solutions for the problem. In practice, the designer has to choose one solution from this set as input for the exploration phase. Though one solution in the Pareto front may not, in principle, be considered better than another solution in the same front, it is possible to discriminate between the less satisfactory trade-offs and the most promising ones. This process of selecting a solution is called

decision making. There are many methods for supporting this post-Pareto analysis process, which can be found in the literature (LOPEZ *et al.*, 2011; AGUIRRE *et al.*, 2011; ZIO; BAZZO, 2011; BLASCO *et al.*, 2008; FERREIRA *et al.*, 2007; VENKAT *et al.*, 2004; COELLO COELLO, 2000).

The post-Pareto analysis is not easy, especially when the number of candidate solutions is large and the number of objectives is greater than two, which is often the case. Depending on the number of glasses in the catalog and the number of glasses used in the combination, hundreds of solutions are usually obtained in the Pareto front.

We recommend two techniques for the Post-Pareto analysis in this glass selection method. A detailed description of these techniques and a suggestion when each technique should be used is provided in Albuquerque *et al.* (2012). The final selection of the set of glasses used as input for the exploration phase is the only manual process made by the designer in the optical design method suggested in this thesis.

6.2. Exploration phase algorithm for optical GEO (O-GEO)

In this section, we present the GEO version developed for the exploration phase algorithm proposed for the automatic design method of optical systems. This version of the algorithm was named optical GEO or O-GEO.

The primary steps in O-GEO are similar to the steps followed by the M-GEO algorithm. We use real codification, and one of the many diversity operands is similar to the perturbations used in GEO_{real1} given by Equation (4.2).

With the specific problem of lens design in mind, other diversity operands were suggested for O-GEO aiming for a better exploration of the design space. The proposed diversity operands work to change some parameters in the optical system that normally are not considered as variables during the optimization process such as the number of lenses in the system, the lens glass type, and the aperture stop position. We discuss each of these diversity operands in this section.

6.2.1. O-GEO candidate solution representation

The candidate solution representation in O-GEO was customized for the problem allowing the application of the different diversity operands. A candidate solution in O-GEO has a string representation of the form shown in Figure 6.3.

The first two cells in the string provide general information about the optical system. The first cell contains the number of lenses in the system. The second cell provides the surface number where the system aperture stop (system diaphragm) is located.

We are not aware of any commercial optical design software that uses the number of lenses as a design variable. However, in our case, because we intend to design optical systems from scratch, a wide-ranging search in the design space, which returns all potential trade-off solutions, is necessary. Therefore, in this case, the number of lenses becomes a crucial variable. The aperture stop position is also not normally used as a variable; nevertheless, it can be converted into a continuous variable in commercial optical design software with some tricks. In our case, we treat the aperture stop position as a discrete variable.

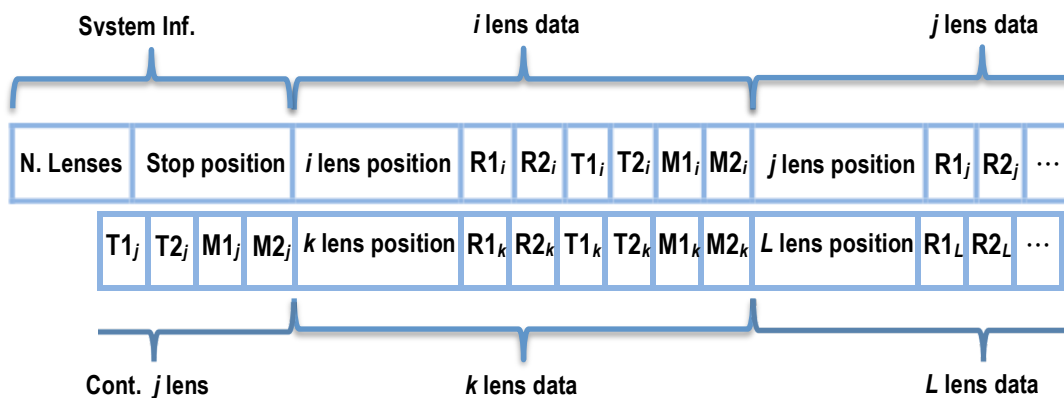


Figure 6.3 - O-GEO solution representation.

After the general system information, the codification string provides the data for each lens in the system starting with the lens position in the set, which is given by an integer number indicating its rank in the system, followed by its construction parameters: the first surface radius of curvature ($R1$), second

surface radius of curvature (R2), central thickness of the lens (T1) (the distance from the first lens surface to the second lens surface), central distance to the next lens (T2) (the distance from the second lens surface to the first surface of the following lens), lens material (M1), and medium material between the current lens and the following lens (M2).

Note that the lens position information has nothing to do with the lens sequence in the codification string. The lens position cell is important for facilitating the application of diversity operands proposed in the method such as the variation of the number of lenses in the system and the lens switching position as presented later in Section 6.2.4.

The lens radii and central thickness are real values, normally defined within a certain boundary provided by the designer. An integer number corresponding to a real glass in the catalog represents the material variables. If the material is set to zero, it is interpreted to be air.

Figure 6.4 provides an example of the O-GEO codification. In this example, the data represent the lens system shown in Figure 6.5. Note that the radius of the object, the radius of the image plane, and the distance from the object to the first lens is not codified in the string. These parameters are not considered to be variables and must be defined by the designer.

3	5	2	-4.502e-02	4.928E-02	1.000E+00	4.750E+00	43	0	...
		1	4.543e-02	-2.295e-03	3.259e+00	6.008e+00	301	0	...
		3	1.255E-02	-5.436E-02	2.952E+00	4.221E+01	301	0	

Figure 6.4 - O-GEO codification of the triplet lens shown in Figure 6.5.

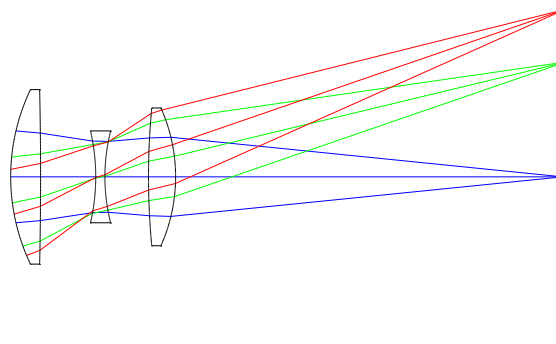


Figure 6.5 - Layout representations for the lens system codified in the string shown in Figure 6.4

6.2.2. O-GEO steps

An overview of the O-GEO algorithm is shown in Figure 6.6.

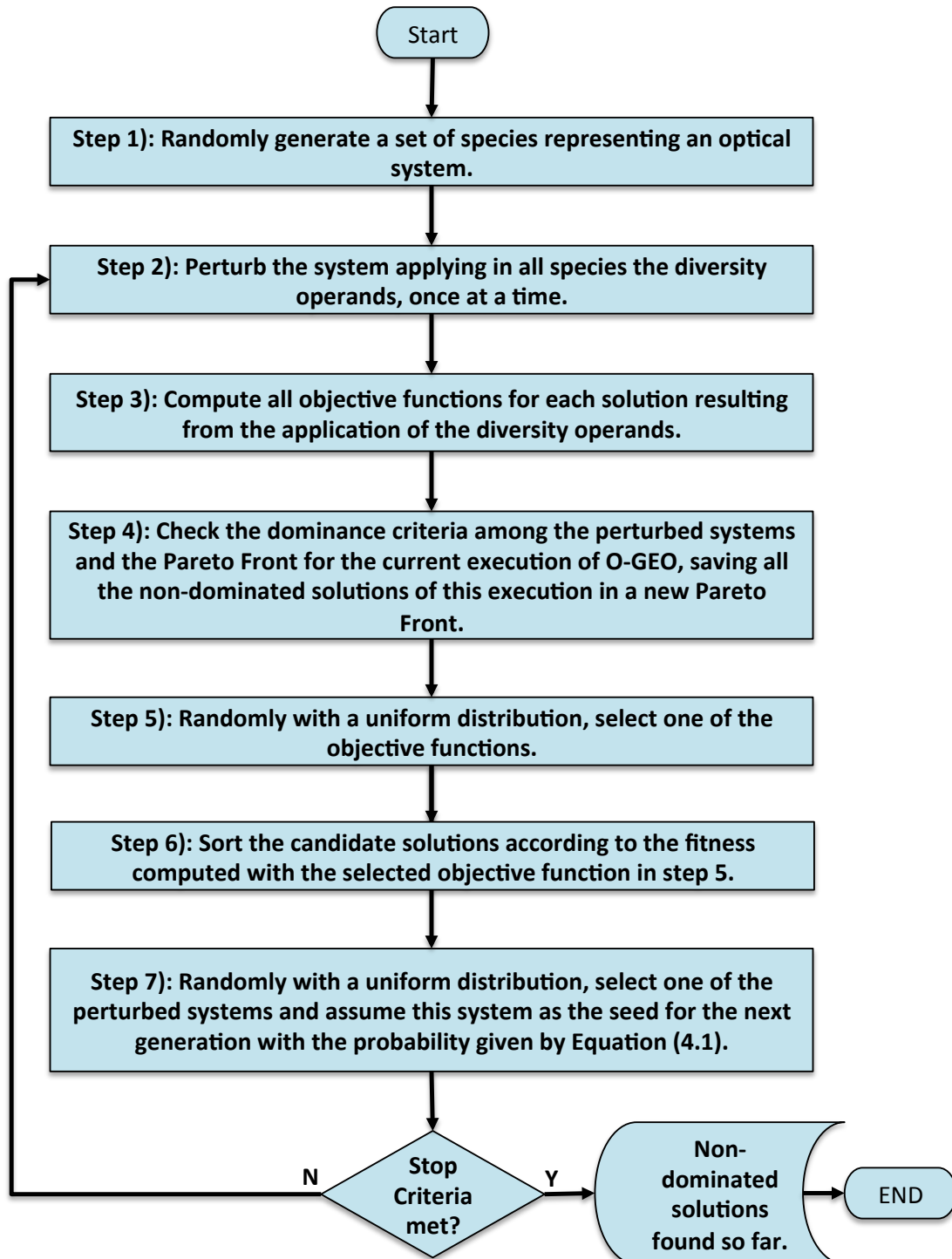


Figure 6.6- O-GEO flowchart.

The algorithm performs the following steps: 1) randomly generate a set of species representing an optical system, 2) perturb the system applying the diversity operands to all species, once at a time, 3) compute all objective functions for each solution resulting from the application of the diversity operands, 4) check the dominance criteria among the perturbed systems and the Pareto front for the current execution of O-GEO, saving all of the non-dominated solutions of this execution in a new Pareto front, 5) randomly select one of the objective functions, 6) sort the perturbed systems according to their fitness from the least to the most adaptable given by the selected objective function, 7) randomly select one of the perturbed systems and use this system as a seed for the next generation with the probability given by Equation(4.1), and 8) check if one of the stopping criteria is fulfilled. If one of the stopping criteria is verified, the algorithm stops and returns the last Pareto front of this independent execution of O-GEO. This Pareto front is sent to the exploitation phase as input. Otherwise, a new generation starts with the system selected in step 6, and the algorithm repeats steps 2 to 7.

6.2.3. O-GEO Step 1

The first set of species codifying an optical system is randomly generated in every independent execution of O-GEO. The first variable defines the number of lenses, which is randomly selected with a uniform distribution between the maximum and minimum number of lenses delimited by the designer (or user).

Next, the aperture stop position is set. The aperture stop position is also generated randomly with a uniform distribution by selecting any whole number between 2 and $NS - 1$, where NS is the number of surfaces in the system. The system aperture stop cannot be placed at the first or the last surfaces in the system corresponding to the object and image, respectively.

Then, the two radii of curvature and the central thicknesses of each lens are defined randomly with a uniform distribution between the maximum and minimum values defined as a constraint by the designer. The radii constraints

are given in the form of a positive or negative real number, allowing the surfaces to be either concave or convex, respectively.

The glass central thickness and the air central thickness have different boundaries. Cemented lenses are avoided in the proposed optimization algorithm. In this way, the thickness corresponding to the distance from the second surface of a lens to the next lens (T_2) is always considered to be the air central distance. As a consequence, the filling material between the current lens and the following lens (M_2) is not a variable; it is always set to zero.

The glass material for each lens (M_1) is randomly selected with a uniform distribution from one of the glasses available in the catalog considered.

The second radius of curvature of the last lens in the system as well as the related second central distance are not treated as variables. In both cases, a solver is used to calculate the value of these parameters. The last radius of curvature is solved to maintain the effective focal length of the system, while the central distance of the last lens is set to keep the image plane in the paraxial focus position. These solvers are applied after a random system is generated as well as after the application of any diversity operand.

6.2.4. O-GEO Step 2

In Step 2, the diversity operands are applied to the current candidate solution, once at a time, for each one of the species (or variables). Based on our knowledge of the problem, six diversity operands were developed for O-GEO. Each one of the operands actuates one type of variable. O-GEO has the following diversity operands: 1) continuous variable mutation, 2) lens flipping mutation, 3) lens position mutation, 4) glass mutation, 5) aperture stop shift mutation, and 6) number of lenses mutation.

1) Continuous variables mutation

This operand is applied to the continuous variables of the candidate solution string: radii of curvature (R_1 and R_2), glass thickness (T_1), and

lens air separation (T2). The continuous variable mutation works in a similar way to the diversity operand used in $\text{GEO}_{\text{real1}}$ implementations. We applied a small change because the continuous variables can represent different classes of physical parameters, which may have different numerical ranges and magnitudes. The perturbation for each one of the continuous variables is then given by Equation (6.24).

$$x'_i = x_i + x_i N(0, \delta_j), \quad (6.24)$$

where x'_i is the value of variable i after the perturbation, and $N(0, \delta_j)$ a random number with a Gaussian distribution, zero mean, and standard deviation δ_j . The standard deviation is different for each class j of variables given by

$$\delta_j = \sigma \cdot Vrange_j, \quad (6.25)$$

where $Vrange_j$ is the numerical range for the variables of class j . The range is calculated by finding the difference between the maximum and minimum value allowed for each class of variables, which are defined as a constraint by the designer. Defining the standard deviation in this way avoids the use of different adjustable parameters for each variable class in the algorithm. In this case, it is only necessary to define σ .

If, after the perturbation, the continuous variable is outside of the constraints defined, the algorithm fixes the value of the variable to the closest boundary.

The application of this operand will generate $4NL - 2$ different systems, where NL is the number of lenses in the input system. The -2 comes from the fact that the second radius of curvature of the last lens in the system as well as the related second central distance are not treated as variables.

2) Lens flipping mutation

The lens flipping operand mimics a method used by optical designers to escape from local minima. Smith (2004) suggests the technique of flipping over a lens in his book in one or more of the design examples.

With this operand, we can automate this technique applying it to all of the lenses in the system, one at a time. The implementation of this algorithm is very simple. For a specific lens in the system, the numerical values of R1 and R2 are swapped and their sign is changed. In this case, for a system with NL lenses, the application of this operand generates NL new systems, with each system containing one flipped lens.

3) Lens position mutation

This operand actuates the lens position cell of the codification string. The objective of this operand is to swap the lens positions in the system.

The lens position mutation operand works in the following way. The position of the first lens appearing in the codification string is swapped with the position of the second lens in the string. The position of the first lens in the string is swapped with the third lens in the string, and so on until it is swapped with the last lens in the string. Then, the second lens in the string is swapped with the position of the third, fourth, and so on until it is swapped with the last lens in the string. This process is repeated until the next-to-last lens in the string is swapped with the last lens in the string.

When this operand is used it generates $\frac{NL!}{2^{(NL-2)!}}$ new systems. Two things shall be noticed: (i) this operand does not generate all the possible lens permutation because this would be too costly, and (ii) the position a lens occupies in the string has nothing to do with its position in the system.

4) Glass mutation

The lens glass material is a very important variable in the design and optimization process. However, glass materials are not continuous

variables, and the designer is limited to the hundreds of glass types available from the vendors. Consequently, the use of descendent optimization methods is not suitable for glass optimization.

Some of the commercially available optical design software utilizes mathematical models to simulate the glasses, in this way transforming them into continuous variables. This technique together with a set of the glass parameters constraints allows the use of descendent methods to optimize the glass. However, before the designer can finish the drawing, all of the model glasses must be converted back to real (discrete) glasses. Many times, this process ruins the design, especially when glasses play an important role in the system performance, which is the case in broadband systems.

EO methods are advantageous because they can easily deal with discrete variables. In this way, the glasses can be used as variables, and we can always assume real glass data.

In the automatic design method present in this thesis, the selection of the most suitable glasses for the specific design is the first task executed as shown in Figure 5.1. In doing so, we can vary the glass while drastically reducing the design space. The number of glasses is reduced from hundreds to a few, and the glass mutation operand takes advantage of this. The mutation operand changes the glass type of each lens for each one of the available glasses selected by the method. This is done one lens at a time. With the application of this operand, $(N_{glass} - 1)NL$ new systems are generated, where N_{glass} is the number of glasses selected by the glass selection method.

5) Aperture stop shift mutation

This operand is applied to the aperture stop position cell, which is the second cell in the codification string. The aperture stop position cell is given in terms of the surface number, which is counted from the first

surface (the object) to the last surface (the image). The aperture stop can be placed at any surface but the object and image position. Because the possibilities are small and finite, this operand changes the aperture stop position by placing it at all possible surfaces. This operand produces a total of $2NL$ possible positions generating $2NL - 1$ new systems.

6) Number of lens mutation

This operand adds or deletes lenses in the system. To do that, it actuates the first cell of the codification string, increasing or decreasing the number. The perturbation in this variable was limited to plus or minus one lens.

For the case when one lens is added, the parameters of the new lens (R1, R2, T1, T2, and M1) are randomly generated. This new lens is then placed in all possible lens positions from 1 to $NL + 1$, where NL is the number of lenses before the application of this operand. For each position NP occupied by the new lens, the position of each one of the lenses with an index greater than or equal to NP is changed to their original position plus one.

For the case when one lens is deleted, all possibilities are also tested. All of the system lenses are deleted, one at a time. When the lens with index DL is deleted, all of the lenses with an index greater than DL are changed to their original position minus one.

Working in this way, the lens mutation operand generates $2NL + 1$ new systems with one more lens and NL new systems with one less lens.

6.2.5. O-GEO Step 3

Three objective functions drive the O-GEO search: one function measures the image quality, one function measures the sensitivity to alignment error, and the final function identifies the number of lenses in the system, interpreted as the system complexity.

We will discuss the image quality used in the exploration phase as well as the sensitivity objective functions in Chapter 7 given by Equation (7.3) and (7.34), respectively. The third objective function does not need to be computed, it is given directly by the number of lenses in the system, which is obtained from the first cell of the candidate solution codification string. The smaller the number of lenses, the more adapted the solution is in terms of this parameter.

All three functions are computed for every candidate solution that results from the application of the diversity operands. The numerical values of the three functions are assigned to the candidate solution.

6.2.6. O-GEO Step 4

In this step, the algorithm checks the dominance criteria between the systems created during the current generation and the systems saved in the Pareto front of the current independent execution of O-GEO. The resulting non-dominated solutions from this dominance check are saved as the new Pareto front to be used during the dominance check in next generation.

6.2.7. O-GEO Step 5

Though all three objective functions are computed for every solution visited during the current generation, only one of them is randomly selected with a uniform distribution to drive the search. The numerical value of the selected function computed for each candidate solution is used to calculate the adaptability or fitness of each candidate solution. The adaptability of a specific species is given by the current value of the selected objective function for the specific candidate subtracted from the value of the same objective function for the seed solution of this generation, i.e., the input system of this generation before the mutation in any species is applied.

6.2.8. O-GEO Step 6

The solutions are then sorted according to their fitness from the least adaptable $k = 1$ to the most adaptable $k = L$, where k is the rank position and L is the number of candidate solutions.

6.2.9. O-GEO Step 7

A solution with rank k is randomly selected with a uniform distribution. The probability of the selected solution becoming the seed for the next generation is given by Equation (4.1). If the selected solution is not assigned as the seed for the next generation, a new solution is randomly selected. This continues until one selected solution becomes the next generation seed.

6.2.10. O-GEO Step 8

The stopping criterion adopted for O-GEO is assigned as the number of generations. The maximum number of generations assumed for each O-GEO independent execution is linearly proportional to the number of lenses in the system produced in step 1.

In this step, the algorithm checks if the stopping criterion is fulfilled. If the stopping criterion is verified, the algorithm stops and returns the last Pareto front of this independent execution of O-GEO. This Pareto front is then used as input for the exploitation phase. Otherwise, a new generation starts with the system selected in step 6, and the algorithm repeats steps 2 through 7.

6.3. Exploitation phase

The exploitation phase, also known as the intensification phase, begins after each independent execution of the exploration phase terminates. The non-dominated solution found during the previous independent execution of O-GEO is used as input in this phase. A local search is conducted for every non-dominated system for which real rays can be traced.

The local search is based on a descendent optimization method. In the exploitation phase, the objective function contains only the image quality metric, given by the root square of Equation (7.12), and the static internal constraint penalty function. The image quality function was chosen in this phase because it is the most important objective function.

Because the method can only deal with continuous variables, the optimization in the exploitation phase only affects the radii (R1 and R2) and the thicknesses (T1 and T2) of all lenses in the system. All other parameters, i.e., the glass material, aperture stop position, number of lenses, lens sequence, etc., are fixed during this local optimization.

The local search is done with an embedded MATLAB function: `lsqnonlin`, which is in fact based on the Levenberg–Marquardt algorithm. The local optimization algorithm runs for each feasible system until a stopping criterion is reached.

Once the local search has been applied for all the feasible input solutions, the algorithm checks the dominance criteria. The dominance is verified between the current systems after the local search and the non-dominated solutions found so far by the automatic design algorithm. The new set of non-dominated solutions is saved in a file with the codification used by O-GEO.

7 SIMULATOR AND MERIT FUNCTIONS

In order to automatically design and optimize optical systems, we need to use an optical simulator. An optical simulator is defined herein as software capable of simulating the sequential light propagation through a set of optical elements, emulating the image formation of an optical system.

We also need to define a metric, or metrics, used to evaluate the system performance. As described earlier, the optimization process consists of changing the design parameters with the goal of minimizing or maximizing the metric or metrics provided while simultaneously respecting the constraints imposed by the problem.

This section presents the concept of the simulator, metrics, and merit functions used in this work for the automatic design of optical systems.

7.1. The simulator

In our first approach, we used a commercial lens design software program as the simulator. The lens design software was linked to preliminary versions of the automatic lens system design algorithm. We tested this methodology by linking the Zemax lens design software to the optimization algorithm coded in Matlab. Unfortunately, we found some limitations with this approach. In particular, we determined some of the weaknesses to be the low speed performance in the change of information between Zemax and Matlab and the inability to easily change the number of lenses in Zemax during the optimization processes. These, and other issues, led us to abandon the idea of using commercial lens design software for ray tracing purposes and develop our own simulator (ray tracing software) in Matlab.

The simulator we developed is intended only for research purposes and was not developed as a sophisticated tool like commercial optical design software solutions. Our simulator is only capable of simulating light propagation by means of a sequential geometrical ray trace through axial symmetrical systems

containing only spherical surfaces, which is satisfactory for the development of the thesis presented herein.

We used Matlab to developing the simulator because of its simplicity in programming and debugging and due to our familiarity with the language. We also transcribed a small part of the code to **C** for functions where higher speed performance was necessary.

The optical design software was developed following a component-based architectural design method, also known as the building block method. With this kind of architecture, the software is decomposed into independent subroutines (functions), which can be combined to execute specific and complex tasks. This architecture is flexible, facilitating debugging, integration, evolution, and extension. A small part of the code developed was based on subroutines developed by Dr. John S. Loomis from the University of Dayton, which are available on the web (<http://www.johnloomis.org/eop601/>). Dr. Lin-Yao Liao also collaborated on this work with the development and improvement of some subroutines under author supervision.

The main simulator subroutines are the material refractive index computation, surface paraxial ray trace, and the surface real ray trace. These subroutines are virtually called directly or indirectly from any other function. For instance, the surface paraxial ray trace is used to compute the basic characteristics of the optical system such as the effective focal length and the entrance and exit pupil position and diameter, which are the basic quantities necessary to simulate and compute the system performance. The real ray trace is essential to accurately compute the system image quality performance based on either the spot size or wavefront error. For any ray trace, the refraction index of the materials in each wavelength is necessary. Both the paraxial and real ray trace subroutines were implemented based on the equations provided respectively in Chapter 3 and Appendix A.3 from Smith (2007).

The simulator took about one year of work to become fully functional. Every function implemented was verified. Whenever possible, the results of the

functions were compared to reported quantities given by Zemax or other commercial optical design software.

7.1.1. Lens system and glass catalog representation in the simulator

In the developed code, the lens system is represented by a Matlab structure, which contains all of the information necessary for the system simulation.

Figure 7.1 shows the lens system variable representation. The values presented in Figure 7.1 are associated with the Cooke triplet lens shown in Figure 7.2. In the structure, the lens construction parameters are defined in LensData, which has three fields R, T, and M, containing the data for the radius of curvature, thickness, and optical material of each surface, respectively.

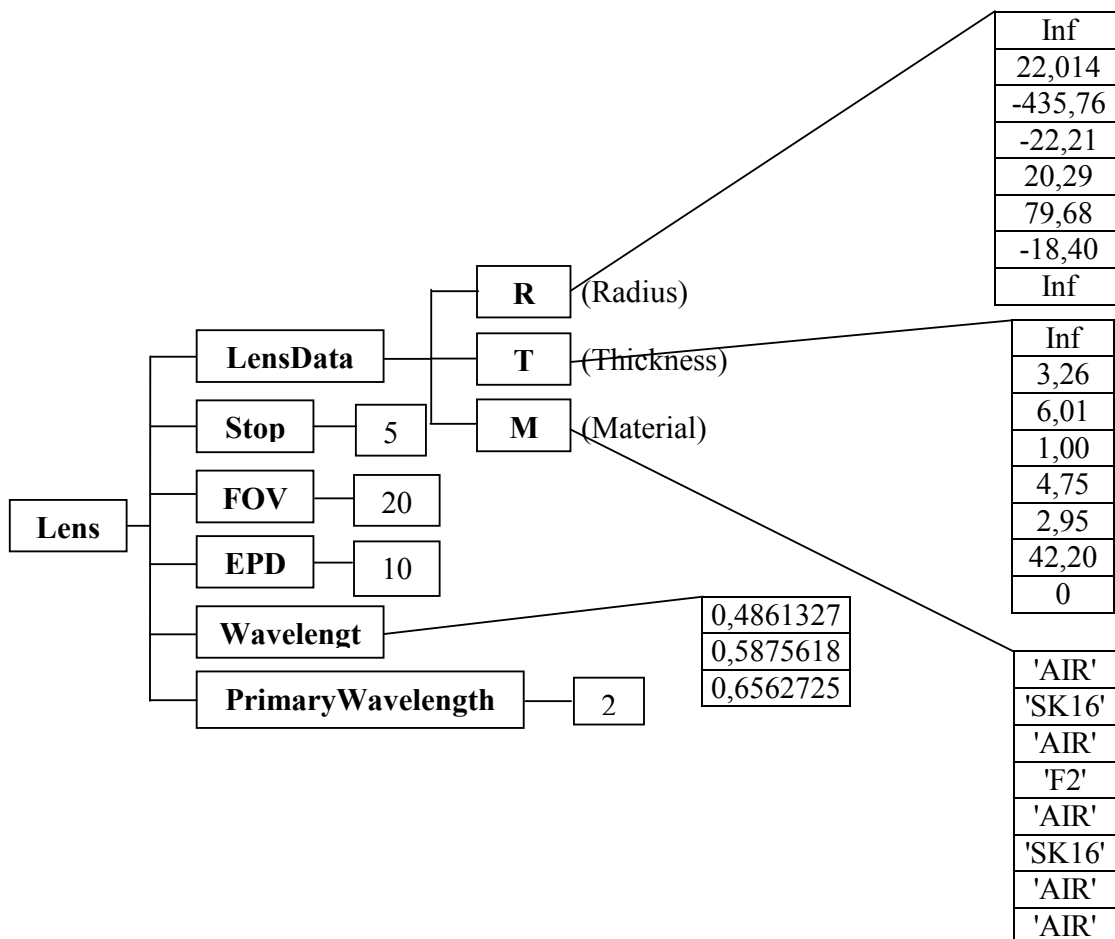


Figure 7.1 - Lens system variable representation in the Matlab simulator.

The Stop field contains the surface position in which the lens aperture stop (diaphragm) is located counting from the object (system surface number 1). The field of view (FOV) informs the maximum half-field angle of the system in degrees.

The entrance pupil diameter (EPD) defines the system aperture in millimeters. The wavelength defines the wavelength of the light in microns that will be propagated through the system during the simulation. Any number of wavelengths can be assigned. The field PrimaryWavelength provides the wavelength number taken as reference. The primary wavelength is used to compute the effective focal length, $F/\#$, exit pupil position and diameter, and other paraxial quantities.

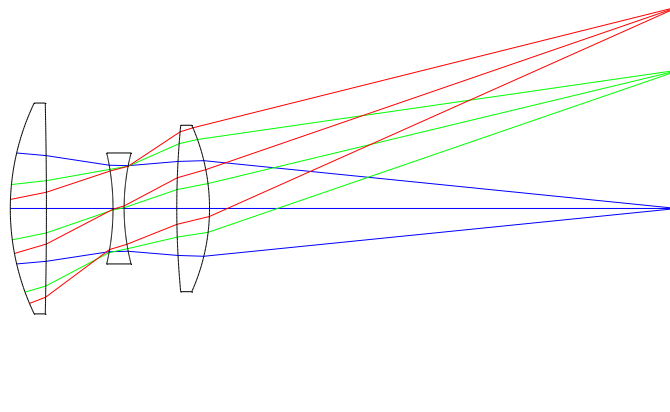


Figure 7.2 - Layout representation for the lens system data shown in the Matlab simulator variables in Figure 7.1.

The lens prescription is defined by the data in the LensData and Stop fields, and these parameters are changed during the optimization process. The LensData is recorded in millimeters. The LensData fields contain information about each surface in the system such as the radius of curvature thickness and material, going from the object to the image plane surface.

We can easily connect the data shown in Figure 7.1 with the system layout in Figure 7.2. The radius of the first surface, which represents the object (not shown in Figure 7.2), is infinity suggesting that the surface is flat. The first line in the T thickness field gives the distance from the object to the first optical surface in the optical system. Infinity represents a very far distance, which results in a

lack of divergence of rays coming from the same object point. The optical material filling the space between the object and the first optical surface is air.

Following the same rationale, the first optical surface (second surface of the system) has a radius of curvature of 22.014 mm, and the positive radius denotes a center of curvature to the right of the surface. The axial distance between the first and the second optical surfaces (third surface of the system) is 3.26 mm, which is filled with SK16, an optical glass from Schott AG. The second optical surface radius is -435.76 mm, and the negative radius indicates a center of curvature to the left of the surface. The material of the second surface is air, and its distance to the third optical surface (fourth surface of the system) is 6.01 mm. We can clearly see that the first and second optical surfaces, represented by the second and third surfaces in LensData, result in a biconvex singlet lens made of SK16 glass, and the axial distance to the next lens is 6.01 mm.

We represent the construction parameters of optical systems in the standard way used by most of optical design software. The representation in our simulator is not the same representation used by the evolutionary optimization algorithm discussed in section 6.2.1.

The remaining fields in the lens system structure (i.e., FOV, EPD, Wavelength, and PrimaryWavelength) identify the lens system specifications and are not variables of the problem.

Note that the material information in LensData is given by the actual glass name. To make this possible, we created glass catalogs in Matlab for the simulator. The glasses are also represented as a structure variable similar to the lens variable. All possible information for the glass is available in this structure. The glass catalog is given by an array of structures with each structure representing a glass. To trace rays for a specific wavelength, the glass name is interpreted, and the refractive index for the specific wavelength is computed using the dispersion equation data and coefficients available for the glass in the catalog.

We intend to share the codes implemented in the future.

7.2. The Optimization Metrics

In this section, we present the metrics used in the optimization algorithm proposed in this thesis. The developed algorithm uses a hybrid evolutionary multi-objective optimization approach, simultaneously, but separately, addressing the image quality, tolerance, and complexity of the system. In this case, we require three classes of metrics to evaluate the solutions: the image resolution, the system sensitivity to fabrication errors, and the system complexity. The system complexity is simply taken as the number of optical elements used. However, the other two metrics involve more elaborate considerations and computations, which we explain in detail in the following sections of this chapter.

7.2.1. Image resolution metrics

For the image resolution metric, we suggest two different merit functions: one for the exploration phase and one for exploitation phase. Each merit function has special characteristics that are appropriate to the phase where they are applied.

Both metrics are based on an estimation of the optical system wavefront error. In Chapter 2, we explained and derived the optical aberrations in terms of the ray aberrations $\delta X'$ and $\delta Y'$ (see Equations (2.3) and (2.4)), which are given by the error in the intersection coordinate of the ray related to the reference point $P_0'(X'; Y')$ on the focal plane. However, optical aberrations can also be expressed in terms of the optical path difference (OPD), described by the wavefront error function W . The rays are infinitesimally thin slices of waves, pointing in the direction of the energy flow, which is perpendicular to the wavefront. Therefore, a perfectly spherical wavefront will cause the rays collapse to a single point and no aberration will occur. In this way, the OPD is given by the difference between the actual (aberrated) wavefront W_{ab} produced by the optical system and the ideal spherical wavefront S at each point of the

exit pupil (EXP) of the system. Figure 7.3 shows the definition of the OPD, and its relation to the ray aberration.

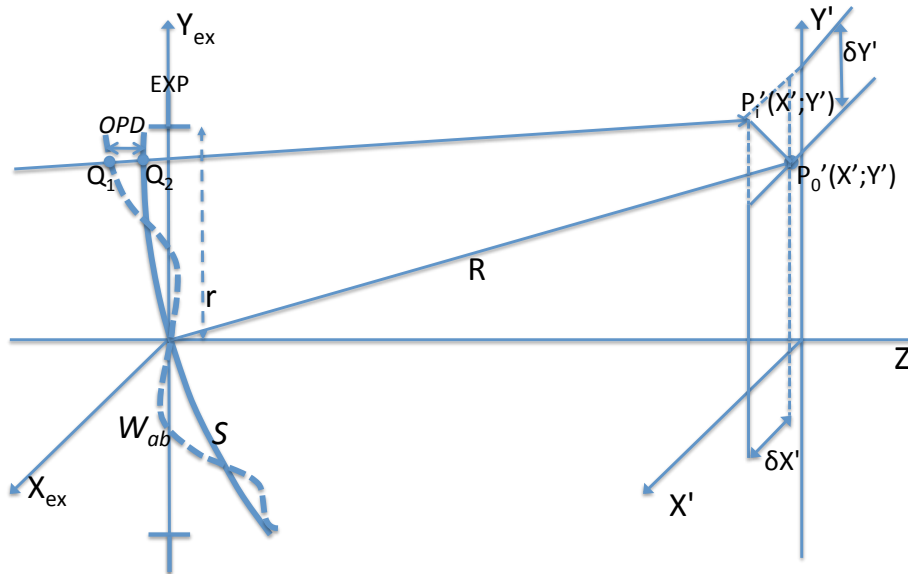


Figure 7.3 - Relationship between the OPD and ray transverse aberration.

The relation between the ray transverse aberration function and the wavefront error function is given by the following equations (MAHAJAN, 1998; KIDGER, 2002; SMITH, 2007):

$$\delta X' = -\frac{R}{n'} \frac{\partial W}{\partial x'}, \quad (7.1)$$

$$\delta Y' = -\frac{R}{n'} \frac{\partial W}{\partial y'}. \quad (7.2)$$

where n' is the refractive index in the image space.

7.2.1.1. Exploration phase image resolution metric

One of the key points for determining the performance and feasibility of evolutionary optimization methods applied to engineering problems is related to the computational cost necessary for calculating the merit function. These optimization methods are stochastic and must calculate the MF repeatedly for a large number of times to evolve the solution to a good point.

When personal computers were not available or when computers were not available at all, optical designers developed simple and fast methods to verify the quality of an optical system design. Perhaps the most efficient and famous is the Seidel aberration coefficients. These coefficients are calculated using a paraxial trace of only two meridional rays through the system. Several famous systems were designed using the Seidel coefficients, such as the Cooke triplet, Ritchey–Chrétien telescope, and others.

With the invention and evolution of computers, the design and optimization of optical systems using the Seidel coefficients declined. Since computers became fast enough to calculate real skew rays through an optical system, the traces of many rays has been preferred to construct the MF of optical systems because ray tracing is a more accurate image quality assessment technique than Seidel coefficients. However, even with very fast computers to trace rays, speed improvements in the MF computation are welcome for evolutionary optimization of optical systems, resulting in a better and faster exploration of complex design spaces intrinsic to the problem.

Another important issue in applying evolutionary optimization (EO) methods in the problem of lens design is related to feasibility of the systems. Many systems generated during the search are unfeasible, especially during random generation of the first population and by diversity operands (e.g., crossover or mutation) during early stage of the optimization. This issue is aggravated in large-scale problems (systems with many lenses). This is a consequence of the complex constraints involved in optical design problems. For unfeasible systems, standard image quality metrics, which depends on the trace of real rays such as spot size and wavefront error, are impossible to calculate due to the failure of real ray trace through the system.

These feasibility problems have been reported in several studies along with methods to circumvent these issues. Ono *et al.* (1998) proposed a method that systematically changes system variables until all of the necessary real rays can be traced through the system, allowing calculation of spot size. In order to accomplish this, marginal rays are traced from different FOV positions. Surfaces

causing the ray trace to fail are identified and the parameters from those surfaces are changed until a feasible system is achieved. Other studies, such as Chen and Yamamoto (1996) and Gagné *et al.* (2008), use a two-layer MF where one MF is used when the rays cannot be traced through the system and other MF is used when the system is feasible.

With speed and feasibility issues in mind, we proposed an image quality metric for the exploration phase given by Equation (7.3). This metric is computed by the square root of the sum of the root mean square (RMS) wavefront error for the whole FOV for each wavelength λ :

$$W_{RMS} = \sqrt{\sum_{\lambda=1}^{n_{\lambda}} W_{rms}^2(\lambda)}. \quad (7.3)$$

The RMS wavefront error for the whole field (W_{rms}) is calculated for each wavelength using the following equation:

$$W_{rms}(\lambda)^2 = \frac{\int_0^1 \sigma(H', \lambda)^2 dH'}{\int_0^1 H' dH'}. \quad (7.4)$$

Here, H' is the normalized image height, and $\sigma(H', \lambda)$ is given by Equation (7.5), which is the RMS wavefront error for a specific image position H' for wavelength λ :

$$\sigma(H', \lambda)^2 = \frac{1}{\pi} \int_0^{2\pi} \int_0^1 W^2(H', \rho, \theta, \lambda) \rho d\rho d\theta - \frac{1}{\pi^2} \left[\int_0^{2\pi} \int_0^1 W(H', \rho, \theta, \lambda) \rho d\rho d\theta \right]^2. \quad (7.5)$$

The wave aberration function W at the exit pupil can be written as an infinite power series in terms of the normalized image height H' and the exit pupil coordinates. Considering a rotationally symmetric system with circular exit pupils for which the normalized polar coordinates are (ρ, θ) , the wave aberration function can be written in the form:

$$\begin{aligned}
W(H', \rho, \theta, \lambda) = & W_{111}(\lambda)H'\rho \cos \theta + W_{020}(\lambda)\rho^2 + W_{040}(\lambda)\rho^4 \\
& + W_{131}(\lambda)H'\rho^3 \cos \theta \\
& + W_{222}(\lambda)H'^2\rho^2 \cos^2 \theta + W_{220}(\lambda)H'^2\rho^2 \\
& + W_{311}(\lambda)H'^3\rho \cos \theta + W_{240}(\lambda)H'^2\rho^4 \\
& + W_{331}(\lambda)H'^3\rho^3 \cos \theta + W_{422}(\lambda)H'^4\rho^2 \cos^2 \theta \quad (7.6) \\
& + W_{420}(\lambda)H'^4\rho^2 + W_{511}(\lambda)H'^5\rho \cos \theta + W_{060}(\lambda)\rho^6 \\
& + W_{151}(\lambda)H'\rho^5 \cos \theta \\
& + W_{242}(\lambda)H'^2\rho^4 \cos^2 \theta \\
& + W_{333}(\lambda)H'^3\rho^3 \cos^3 \theta + \text{higher order terms}
\end{aligned}$$

The W_{ijk} are peak-normalized wave aberration coefficients, which are normalized in image height and exit pupil. The first-order coefficients W_{111} and W_{020} are known respectively as the lateral magnification and defocus. The coefficients from W_{040} to W_{311} are the third-order (Seidel) coefficients and are called the third-order spherical, coma, astigmatism, field curvature and distortion, respectively. The fifth-order terms range from W_{240} to W_{333} . The first seven fifth-order terms are named: oblique spherical, fifth-order coma, astigmatism, field curvature, distortion, and spherical. The last three fifth-order coefficients have no formal or widely recognized names (SASIAN, 2010).

For the proposed metric, the wave aberration equation is expanded up to the fifth-order coefficients. The third-order coefficients in Equation (7.6) are the Seidel terms, and their calculations can be found in any optical design book. The algebraic equations used to calculate the fifth-order wave aberration coefficients were presented by Sasian (2010) in a recent publication. The fifth-order coefficient computation uses only the data from the two paraxial rays used to calculate the Seidel coefficients.

We ignore the distortion coefficients W_{311} to W_{511} in our metric because the distortion does not influence the image resolution. Furthermore, W_{020} and W_{111} are taken to be zero for the principal wavelength λ_0 because the lateral magnification is not an aberration, and the paraxial focal plane of λ_0 is taken as the observation plane. However, the chromatic change of magnification (known

as the lateral color) and the chromatic change of focus (also known as the axial color or simply chromatic aberration) are important aberrations and shall be considered in the calculation. In this way, for other wavelengths λ , W_{020} and W_{111} are given by the following two equations, respectively (MAHAJAN, 1998):

$$W_{020}(\lambda, \lambda_0) = -\frac{n'\Delta S(\lambda, \lambda_0)}{2R^2} r^2, \quad (7.7)$$

$$W_{111}(\lambda, \lambda_0) = -\frac{n'\Delta H'(\lambda, \lambda_0)}{R} r, \quad (7.8)$$

where n' is the index of refraction in the image space, r' is the exit pupil semi-diameter, R is the radius of curvature for the reference sphere S , $\Delta S(\lambda, \lambda_0)$ represents the difference in distance from the exit pupil position to the paraxial image plane respectively between the wavelengths λ_0 and λ , and $\Delta H'(\lambda, \lambda_0)$ is the difference in image height between paraxial principal (or chief) rays coming from the edge of the FOV respectively for λ_0 and λ .

With the proposed metric for image quality based on the third- and fifth-order aberration coefficients, we can obtain a very robust and fast technique for computing the metric. Because no trigonometric rays are traced, the metric is robust. The paraxial rays used to compute the desired coefficients are not subject to failure due to a ray missing a surface or encountering total internal reflection (SMITH, 2004). Only two paraxial rays from each wavelength are necessary to calculate the coefficients, resulting in a very computationally efficient function in the exploration phase of the algorithm.

7.2.1.2. The exploitation phase image resolution metric

For the exploitation phase, we use a different model to represent the wavefront error. For a given point object and wavelength, the aberration function of an optical system can be represented in terms of a complete set of Zernike circle polynomials as follows (MAHAJAN, 1998):

$$W(H', \rho, \theta, \lambda) = \sum_{n=0}^{\infty} \sum_{m=0}^n Z_{nm}(H', \lambda) R_n^m(\rho) \cos m\theta, \quad (7.9)$$

where Z_{nm} are the Zernike coefficients that depend on the image height H' and on the wavelength λ . The values n and m are positive integers (including zero), and $(n - m)$ must be a non-negative even number. Finally, $R_n^m(\rho)$ is given by

$$R_n^m(\rho) = \left[\frac{2(n+1)}{1 + \delta_{m0}} \right]^{1/2} \cdot \sum_{s=0}^{\frac{n-m}{2}} \frac{(-1)^s (n-s)!}{s! \left(\frac{n+m}{2} - s \right)! \left(\frac{n-m}{2} - s \right)!} \rho^{n-2s}, \quad (7.10)$$

where δ_{ij} is the Kronecker delta. Note that Equation (7.10) has no explicit dependence on the image height H' , and the coefficients change for every field point unlike Equation (7.6).

The Zernike polynomial presented in Equation (7.9) is an orthonormal polynomial over a unit circle. Therefore, the square RMS wavefront error for a specific field point H' and wavelength λ is given by the sum of squares of all of the Zernike coefficients except the piston (Z_{00}):

$$\sigma(H', \lambda)^2 = \sum_{n=1}^{\infty} \sum_{m=0}^n Z_{nm}^2(H', \lambda). \quad (7.11)$$

In this way, the square of the RMS wavefront error can be approximated by

$$W_{RMS}^2 = \sum_{H'=H_1}^{H_l} \sum_{\lambda=\lambda_1}^{\lambda_k} \sum_{n=1}^{\infty} \sum_{m=0}^n Z_{nm}^2(H', \lambda) \quad (7.12)$$

where l and k are the number of field points and number of wavelengths used to evaluate the system, respectively. The root mean square of Equation (7.12) is used as an image quality metric for the local search algorithm. Note that this equation can be easily modified to account for different wavelengths and field points using relative weights if necessary.

To calculate the Zernike coefficients, the polynomial must be truncated at some point $n = n_{max}$, and a set of real rays for each field position and wavelength defined must be traced through the system. The optical path difference (OPD) at the exit pupil with respect to the centroid is computed for each ray. The average polychromatic tilt is removed from the OPD data for each field point, leaving only the chromatic differential tilt. The tilt itself does not influence the image quality, but the chromatic differential tilt is the lateral color aberration (chromatic change of magnification).

With the OPD and the coordinate (ρ, θ) of each ray i in the exit pupil, a weighted least square fitting method is used to compute the Zernike coefficients for each field and wavelength:

$$Z(H', \lambda) = (R^T \cdot W_t \cdot R)^{-1} \cdot R^T \cdot W_t \cdot OPD(H', \lambda), \quad (7.13)$$

where

$$Z(H', \lambda) = \begin{bmatrix} Z_{00}(H', \lambda) \\ Z_{11}(H', \lambda) \\ Z_{20}(H', \lambda) \\ \vdots \\ Z_{n_{max}n_{max}}(H', \lambda) \end{bmatrix}, \quad (7.14)$$

$$R = \begin{bmatrix} 1 & R_1^1(\rho_1) \cos \theta_1 & R_2^0(\rho_1) & R_2^2(\rho_1) \cos 2\theta_1 & \cdots & R_{n_{max}}^{n_{max}}(\rho_1) \cos n_{max}\theta_1 \\ 1 & R_1^1(\rho_2) \cos \theta_2 & R_2^0(\rho_2) & R_2^2(\rho_2) \cos 2\theta_2 & \cdots & R_{n_{max}}^{n_{max}}(\rho_2) \cos n_{max}\theta_2 \\ \vdots & \vdots & \vdots & \vdots & \ddots & \vdots \\ 1 & R_1^1(\rho_i) \cos \theta_i & R_2^0(\rho_i) & R_2^2(\rho_i) \cos 2\theta_i & \cdots & R_{n_{max}}^{n_{max}}(\rho_i) \cos n_{max}\theta_i \end{bmatrix}, \quad (7.15)$$

$$W_t = \begin{bmatrix} w_1 & \cdots & 0 \\ \vdots & \ddots & \vdots \\ 0 & \cdots & w_i \end{bmatrix}, \quad (7.16)$$

$$OPD(H', \lambda) = \begin{bmatrix} opd_1(H', \lambda) \\ \vdots \\ opd_i(H', \lambda) \end{bmatrix}. \quad (7.17)$$

The weighting W_t is used in the Equation (7.13) because the Gaussian quadrature (GQ) ray distribution scheme was chosen to sample the pupil. Despite GQ being the most efficient sampling method to estimate either the wavefront error or the spot size, it uses different relative weights for each ray traced. With this scheme, only a few rays are necessary to obtain good accuracy for the image quality metrics. The number of rays used in a GQ scheme is defined by the number of **rings** (N_r) and the number of **arms** (N_θ), where the total number of rays is given by the multiplication of these values ($N_r \cdot N_\theta$) for plane symmetrical systems or by $1/2 (N_r \cdot N_\theta)$ for rotational symmetric systems. The efficiency of the GQ sampling scheme can be verified by the following comparison: if 30 rays ($N_r = 5$, $N_\theta = 6$) are used with GQ scheme for an optical system assessment, 10^6 rays would be necessary in the Cartesian uniform gridding sampling scheme to get the same accuracy. The GQ and the Cartesian uniform gridding ray distribution schemes are shown in Figure 7.4 and Figure 7.5, respectively (FORBES, 1988).

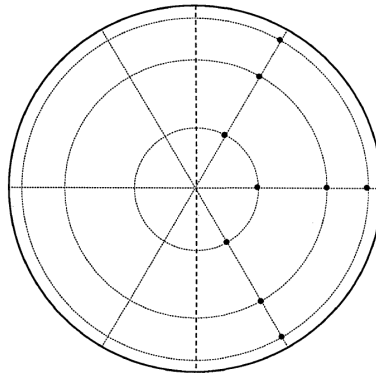


Figure 7.4 - Gaussian quadrature ray distribution scheme for $N_r = 3$ and $N_\theta = 6$ (FORBES, 1988).

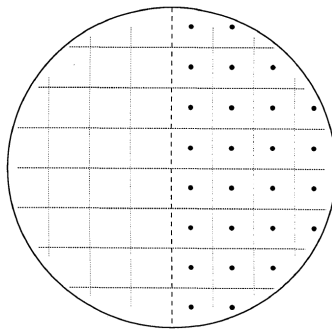


Figure 7.5 - Uniform Cartesian ray distribution scheme (FORBES, 1988).

The matrix $(R^T \cdot W_t \cdot R)$ is frequently ill conditioned (close to singular). To avoid problems inverting the matrix, we implemented the method described in (RILEY, 1955).

The RMS wavefront error of the system could be easily computed by the square root of the direct weighted square sum of the OPD of each ray. However, according to Rayces (2009), the relationship between the optical system variables and the Zernike coefficients is more linear than the relationship between the optical system variables and the OPD of each ray. In this way, utilizing the Zernike coefficients to compute the wavefront metric simplifies the design space topography. This results in better convergence when gradient-based optimization algorithms are used in the local search, which is the case for the DLS method used in this phase of the algorithm.

7.2.2. System sensitivity metrics

For the sensitivity metric, we followed the same principles used to define the image quality metric for the exploration phase. Therefore, the metric must be quickly evaluable, provide a good metric for tolerance, and computed in any situation.

In the literature it was possible to find some metrics that would work for our application, such as the power distribution metric proposed by Sasian and Descour (1998), the two sensitivity metrics proposed by Wang and Sasian (2010), and the metric proposed by Isshiki *et al.* (2004). All of these metrics can be calculated with paraxial rays. However, though the selected metrics are validated in an empirical way, there is a lack of theoretical background in the

metric derivations. In this way, we propose a new metric for the system sensitivity that fulfills our requirements and has a theoretical derivation.

In our case, our primary concern is the assembly tolerance, specifically related to the tilts and decentering of the surfaces or elements. These problems are the most pernicious, difficult to control, and the most difficult to debug when the system does not perform according to the image quality requirements.

When there are tilts and/or decenters, the system symmetry is broken, and the system might be completely asymmetric. Nevertheless, to simplify the metric without loss of generality, the decenter and/or the tilt are considered only for one direction (in our case, the tangential plane). This results in a plane-symmetric system, which is easier to treat than an asymmetric system. Once the estimated performance of a plane-symmetric system is known, the estimated performance of an asymmetric system can be computed by multiplying the estimated performance of a plane-symmetric system by the square root of two (SASIAN, 2011).

According to Mahajan (1998), if the contribution to the primary aberration function (third-order aberration) of a system by an unperturbed surface i is given by Equation (7.18), the change in the aberration function due to its decenter Δ_i (in the y -direction) or its tilt β_i (about the vertex in the tangential plane) is given by Equation (7.19).

$$W_i(h_i', r_i, \theta_i, \lambda) = a_{s_i}(\lambda)r_i^4 + a_{c_i}(\lambda)h_i'r_i^3 \cos \theta_i + a_{a_i}(\lambda)h_i'^2 r_i^2 \cos^2 \theta_i + a_{d_i}(\lambda)h_i'^2 r_i^2 + a_{t_i}(\lambda)h_i'^3 r_i \cos \theta_i, \quad (7.18)$$

$$\begin{aligned} \delta W_i(h_i', r_i, \theta_i, \lambda) = & - \left(E_i a_{c_i}(\lambda) + 4\varepsilon_i a_{s_i}(\lambda) \right) r^3 \cos \theta_i - \\ & 2 \left(E_i a_{a_i}(\lambda) + \varepsilon_i a_{c_i}(\lambda) \right) h_i' r_i^2 \cos^2 \theta_i - \\ & \left(2E_i a_{d_i}(\lambda) + \varepsilon_i a_{c_i}(\lambda) \right) h_i' r_i^2 - \\ & \left[3E_i a_{t_i}(\lambda) + 2\varepsilon_i \left(a_{a_i}(\lambda) + a_{d_i}(\lambda) \right) \right] h_i'^2 r_i \cos \theta_i \end{aligned} \quad (7.19)$$

where the a_i values are the third-order coefficients for the exit pupil of surface i (not for the exit pupil of the system), r_i and θ_i are the polar coordinates in exit pupil of surface i , h'_i is the object image height produced by surface i . Here, ε_i and E_i are given for decenter and tilt cases respectively by

$$E_i = M_i \Delta_i, \quad (7.20)$$

$$\varepsilon_i = m_i \Delta_i, \quad (7.21)$$

$$E_i = M_i S_i \beta_i, \quad (7.22)$$

$$\varepsilon_i = m_i s_i \beta_i. \quad (7.23)$$

Here, M_i and m_i are the object and exit pupil lateral magnification produced by surface i , respectively, and S_i and s_i are the axial distances of object and entrance pupil from the surface i , respectively.

We can rewrite Equation. (7.19) in the form:

$$\begin{aligned} \delta W_i(h'_i, r_i, \theta_i, \lambda) = & a_{cc_i}(\lambda) r_i^3 \cos \theta_i + a_{la_i}(\lambda) h'_i r_i^2 \cos^2 \theta_i + \\ & a_{fd_i}(\lambda) h'_i r_i^2 + a_{qt_i}(\lambda) h'^2_i r_i \cos \theta_i, \end{aligned} \quad (7.24)$$

where

$$a_{cc_i}(\lambda) = - \left(E_i a_{c_i}(\lambda) + 4 \varepsilon_i a_{s_i}(\lambda) \right), \quad (7.25)$$

$$a_{la_i}(\lambda) = -2 \left(E_i a_{a_i}(\lambda) + \varepsilon_i a_{c_i}(\lambda) \right), \quad (7.26)$$

$$a_{fd_i}(\lambda) = - \left(2 E_i a_{d_i}(\lambda) + \varepsilon_i a_{c_i}(\lambda) \right), \quad (7.27)$$

$$a_{qt_i}(\lambda) = - \left[3 E_i a_{t_i}(\lambda) + 2 \varepsilon_i \left(a_{a_i}(\lambda) + a_{d_i}(\lambda) \right) \right]. \quad (7.28)$$

The coefficients a_{cc_i} , a_{la_i} , a_{fd_i} , and a_{qt_i} are named, respectively, the constant or uniform coma, linear astigmatism, field tilt, and quadratic distortion

(MAHAJAN, 1998, SASIAN, 1994). The prefix adjective in the coefficient names gives the dependence of the aberration with the field, such as uniform, linear, or quadratic.

According to Mahajan (1998), for a multisurface system, the perturbation of a surface not only affects its aberration contribution but also the aberration contribution of the surfaces that follow it, even if the following surfaces are not perturbed. This happens because the location of the image point and the center of the exit pupil change for the perturbed surface, which are the object point and entrance pupil of the next surface. However, to simplify the definition of the metric and to increase the computation speed, we made the following assumptions. If the decenters and/ or tilts are considered small, on the order of the assembly errors (tens of microns), it is reasonable to assume that the change to the position of the image and exit pupil of the perturbed surface are so small that the aberrations induced by the unperturbed surfaces are unchanged when compared with the unperturbed system. In other words, only the intrinsic aberrations of a perturbed surface are considered, and the extrinsic aberrations of the following surfaces are ignored.

By making this assumption, we can perform a change of variables in Equation (7.24), rewriting it in terms of the system of normalized exit pupil coordinates and normalized field coordinates as follows:

$$\begin{aligned} \delta W_i(H', \rho, \theta, \lambda) = & W_{031_i}(\lambda) \rho^3 \cos \theta + W_{122_i}(\lambda) H' \rho^2 \cos^2 \theta + \\ & W_{120_i}(\lambda) H' \rho^2 + W_{211_i}(\lambda) H'^2 \rho \cos \theta, \end{aligned} \quad (7.29)$$

where

$$W_{031_i}(\lambda) = \frac{a_{cc_i}(\lambda) a^3}{\prod_{k=i+1}^j m_k^3}, \quad (7.30)$$

$$W_{122_i}(\lambda) = \frac{a_{la_i}(\lambda) h'_{max} a^2}{\prod_{k=i+1}^j M_k m_k^2}, \quad (7.31)$$

$$W_{120_i}(\lambda) = \frac{a_{fd_i}(\lambda) h'_{max} a^2}{\prod_{k=i+1}^j M_k m_k^2}, \quad (7.32)$$

$$W_{211_i}(\lambda) = \frac{a_{qt_i}(\lambda) h'_{max}{}^2 a}{\prod_{k=i+1}^j M_k^2 m_k}. \quad (7.33)$$

Here, j is the number of surfaces in the system, a is the exit pupil semi-diameter, and h'_{max} is the image height produced by the system.

With Equation (7.29), the sensitivity metric can be defined by the root square sum (RSS) of the RMS change in aberration function for wavelength λ_0 , which is induced by each surface tilt independently as follows:

$$\delta W_{RSS} = \sqrt{\sum_{i=1}^j \delta W_{rms_i}^2}, \quad (7.34)$$

where

$$\delta W_{rms_i}^2 = \frac{\int_0^1 \varsigma_i(H')^2 dH'}{\int_0^1 H' dH'}, \quad (7.35)$$

$$\varsigma_i(H')^2 = \frac{1}{\pi} \int_0^{2\pi} \int_0^1 \delta W_i^2(H', \rho, \theta, \lambda_0) \rho d\rho d\theta - \frac{1}{\pi^2} \left[\int_0^{2\pi} \int_0^1 \delta W_i(H', \rho, \theta, \lambda_0) \rho d\rho d\theta \right]^2. \quad (7.36)$$

For the metric computation, only the surface tilts are considered, and the amount of tilt is assumed to be the same for all of the surfaces. The decenter is equivalent to a thickness change and a surface tilt, where the thickness change is very small, normally negligible and below the tolerances. Therefore, the surface decenters are best treated as a surface tilt (SASIAN, 2011). The distortion coefficients W_{211_i} are assumed to be zero for the sensitivity metric. As mentioned before, the distortion does not affect the resolution of the image. The field tilt coefficients W_{120_i} may also be ignored if the focal plane tilt can be considered as a compensator

It is also possible to perform a change of variables in Equation (7.19), rewriting it in terms of a system of normalized exit pupil coordinates and normalized field. This gives rise to the following relationship between the aberration coefficients a_{ijk} and the peak normalized aberration coefficients W_{ijk} :

$$w_{040i}(\lambda) = a_{si}(\lambda) \left(\frac{a^4}{\prod_{k=i+1}^j m_k^4} \right), \quad (7.37)$$

$$w_{131i}(\lambda) = a_{ci}(\lambda) \left(\frac{h'_{max} a^3}{\prod_{k=i+1}^j M_k m_k^3} \right), \quad (7.38)$$

$$w_{222i}(\lambda) = a_{ai}(\lambda) \left(\frac{h'_{max}{}^2 a^2}{\prod_{k=i+1}^j M_k^2 m_k^2} \right), \quad (7.39)$$

$$w_{220i} = a_{di} \left(\frac{h'_{max}{}^2 a^2}{\prod_{k=i+1}^j M_k^2 m_k^2} \right), \quad (7.40)$$

$$w_{311i} = a_{ti} \left(\frac{h'_{max}{}^3 a}{\prod_{k=i+1}^j M_k^3 m_k} \right). \quad (7.41)$$

Now, we can substitute the Equations (7.37) to (7.40) into Equations (7.25) to (7.27), and we can substitute the results into Equations (7.30) to (7.32). These substitutions make it possible to write the wavefront peak normalized aberration coefficients from Equation (7.29) ($W_{031i}(\lambda)$, $W_{122i}(\lambda)$ and $W_{120i}(\lambda)$) in terms of the Seidel wavefront peak normalized aberration coefficients of each surface from the non-perturbed system as follows:

$$W_{031i}(\lambda) = - \left(\frac{W_{131i} \prod_{k=1}^j E_k a + 4 W_{040i} \prod_{k=1}^j \varepsilon_k h'_{max}}{h'_{max} a} \right), \quad (7.42)$$

$$W_{122i}(\lambda) = -2 \left(\frac{W_{222i} \prod_{k=1}^j E_k a + W_{131i} \prod_{k=1}^j \varepsilon_k h'_{max}}{h'_{max} a} \right), \quad (7.43)$$

$$W_{120i}(\lambda) = - \left(\frac{2W_{220i} \prod_{k=1}^j E_k a + W_{131i} \prod_{k=1}^j \varepsilon_k h'_{max}}{h'_{max} a} \right). \quad (7.44)$$

From these substitutions, we defined the sensitivity metric so that it is only dependent on the Seidel wavefront peak normalized aberration coefficients of each surface. These coefficients are a subset of the coefficients used in the image quality metric defined for the exploration phase. Therefore, our outlined metric complies with all of the defined requirements.

8 EXPERIMENTS RESULTS AND VERIFICATIONS

In this chapter, we describe the test of the global search algorithm developed for the automatic design of optical system. The results presented herein verify the efficiency of the algorithm, proving our proposed thesis.

We systematically tested and verified the algorithm. At first, the design of a very simple optical system is performed using a subset of the algorithm tools. We incrementally turned on the algorithm tools and the example optical system used became progressively more complicated. In this way, the experiments conducted range from a simple Cooke triplet design, which we tested with fixed number of lenses and a mono-objective approach, to an optical system design intended for a multi-spectral remote sensing camera, which we tested with a multi-objective approach, a variable number of lenses, and the glass selection tool.

8.1. The Cooke triplet problem

The Cooke triplet is a classical lens system designed for photographic cameras. H. Dennis Taylor proposed this design in 1893. It is an especially interesting design because it is the simplest lens system with the enough effective degrees of freedom to control or correct all seven third-order or Seidel aberrations (KIDGER, 2004; SMITH, 2004).

Due to the nonlinearity of the relationships between the aberrations and design variables, there are at least eight potential solutions (local minima) for the third-order aberrations, if a given choice of glass for each lens is assumed. By adding glass variables and high-order aberrations to balance the third-order aberrations, the number of local minima becomes enormous (KIDGER, 2004; SMITH, 2004).

The classical Cooke triplet solution, which provides the best aberration balancing, is a negative (diverging) flint glass lens between two positive (converging) crown glass lenses with the aperture stop located near the negative lens. Figure 8.1 shows three optimized Cook triplet examples. All of

examples were scaled to a 50 mm focal length set to F/5 and FOV +/-20 degree with no vignetting.

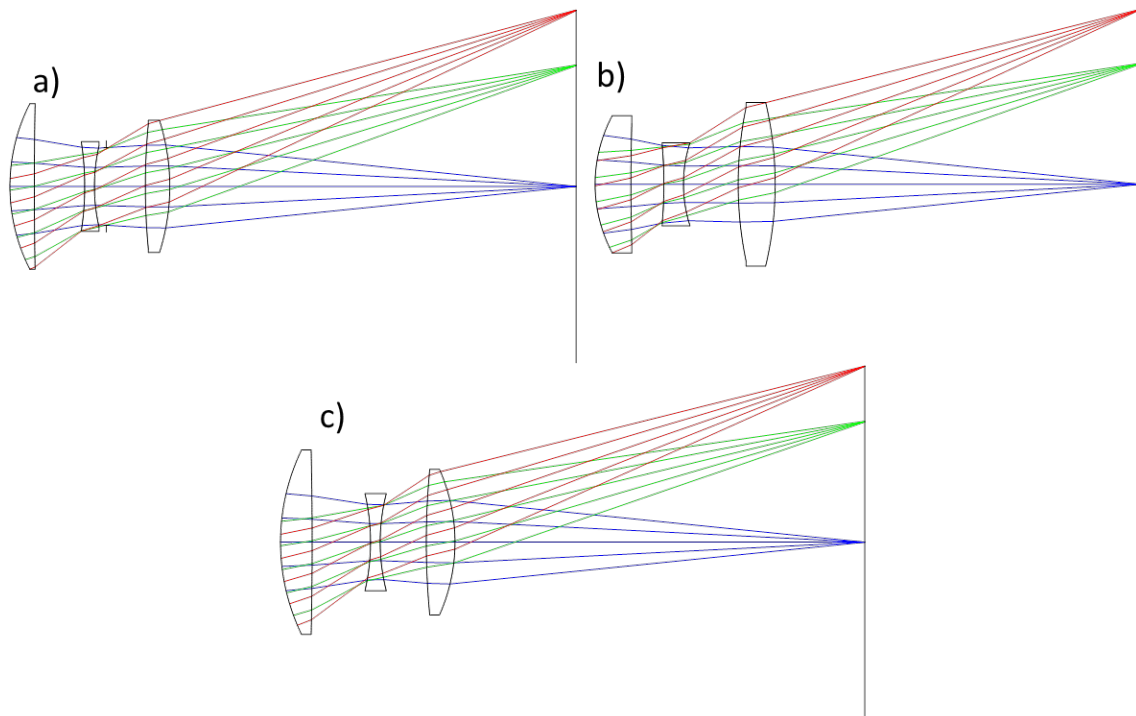


Figure 8.1 - Example of Cooke triplet solutions obtained from the following sources: a) Kidger (2004), b) Moore (1999), and c) ZEMAX (2011b).

The Cooke triplet solutions shown in parts a), b), and c) of Figure 8.1 were taken from Kidger (2004), Moore (1999), and Zemax (2011b), respectively. Figure 8.1b is the result of a global search algorithm. Figure 8.1c was taken from a ZEMAX samples data bank (ZEMAX, 2011b). All of the solutions are well-corrected systems, having polychromatic ($F-d-C$) RMS wavefront error equal to: 0.624, 0.464 and 0.453 waves, respectively. It is interesting to note that the second and third designs use the same glasses and have very similar performances in terms of RMS WFE. However, they have different shapes that can be visually detected, demonstrating that they are located in two different local minima in the design space.

Our goal in this first experiment is to test the performance of the proposed algorithm in designing a triplet system with the same optical requirements of the ones shown in Figure 8.1. In this first example, the proposed automatic design algorithm is set to work with a fixed number of lenses in the mono-objective

mode, optimizing only the image quality. Further, we bypass the glass selection phase limiting the available glasses in this design to the glasses used in the systems presented in Figure 8.1b and Figure 8.1c, which are SK16 and F2 from Schott Inc. By restricting our algorithm to work in the mono-objective mode with fixed number of lenses, the obtained results can be compared with the results obtained with the ZEMAX global search algorithm.

In Table 8.1, the system requirements and constraints used as input for the design are presented.

Table 8.1 - Triplet system requirements and constraints.

ITEM	REQUIREMENT
Effective Focal Length (EFL)	50 mm
F- Number (F#)	5
Field of View (FOV)	+/- 20 deg
Spectral band	Visible uniform weighting F (486,13nm), d (587.56nm) and C (656,27nm).
Available glasses	SK16 and F2
Minimum air edge thickness	2 mm
Minimum air central thickness	2 mm
Maximum air central thickness (excluding the back focal length)	25 mm
Minimum glass edge thickness	1 mm
Minimum glass central thickness	1 mm
Maximum central glass thickness	7.5 mm
Maximum system length (excluding the back focal length)	50 mm
Maximum total system length	75 mm

8.1.1. Tuning the exploration phase

Before running the experiment, it is necessary to tune the adjustment parameters used in the exploration phase algorithm. O-GEO has two adjustable parameters: τ and σ . The curves developed during the tuning studies also help to define the number of generations used in the exploration phase before entering the exploitation phase.

Once the best tradeoff combination for τ and σ is determined using the triplet design problem, these parameters will be fixed for all other optical design

experiments conducted herein. On the other hand, we assume that the number of generations used during the exploration has a linear relationship with the number of design variables and a quadratic relationship with the number of objective functions. In this case, the best tradeoff number of generations found for the triplet mono-objective example is used as a reference to calculate the number of generations for other experiments.

In the tuning experiment, τ was tested with the following values: 0.25, 0.5, 0.75, 1, 2, 3, 4, 5, 6, 7, 8, 9, and 10. For each value assumed for τ , σ was changed from 0.1 to 1 in increments of 0.1. The collected data was plotted and analyzed where we concluded that the best values for τ and σ are 1 and 0.6, respectively, and the number of generations for the mono-objective triplet is around 100 ± 50 . All of the details, data, graphs, and discussions about the tuning studies can be found in Appendix B.

8.1.2. Triplet experiment results

Due to the stochastic behavior of EA, we performed twenty independent executions of the proposed algorithm for this experiment. The stopping criterion for each run was established as when the RMS WFE gets smaller than 0.4 waves.

The algorithm found four types of systems that can be visually discriminated. The layout of each system is shown in Figure 8.2 and the results are shown in Table 8.2. All system types follow the classical triplet solution with a negative flint glass lens between two positive crown glass lenses and the aperture stop located near the negative lens. The difference between them is the shape of the lens and the exact position of the aperture stop. Systems of the same type, found in different executions of the algorithm, are not exactly the same but have very similar numerical values.

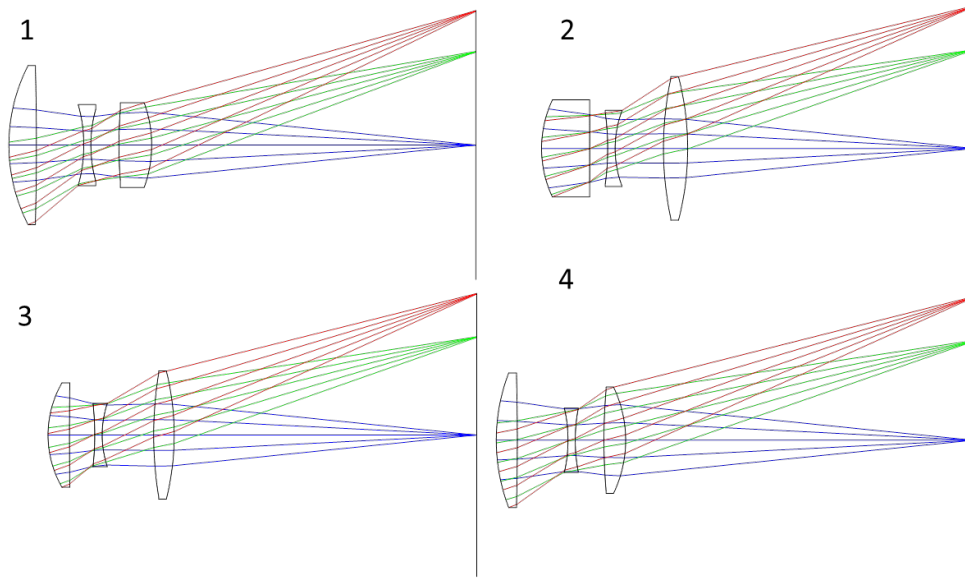


Figure 8.2 - Layout of the triplet system types found by the automatic lens design algorithm.

Table 8.2 - Cooke triplet experiment results using the automatic lens design algorithm. From left to right, the columns contain the execution number, the number of merit function evaluations in the exploration phase, the number of merit function evaluations during exploitation phase, the total number of merit function evaluations, the RMS WFE achieved in waves, and the system type obtained.

	GMFC	LMFC	TMFC	MF	Type
1	1.03E+05	4.39E+04	1.47E+05	0.366	1
2	4.80E+04	1.84E+04	6.64E+04	0.361	2
3	3.60E+04	1.45E+04	5.05E+04	0.384	3
4	5.52E+04	2.82E+04	8.34E+04	0.361	2
5	1.56E+05	6.91E+04	2.25E+05	0.384	3
6	3.29E+05	1.44E+05	4.72E+05	0.361	2
7	2.78E+05	1.17E+05	3.96E+05	0.361	2
8	2.64E+04	1.00E+04	3.64E+04	0.409	4
9	4.13E+05	1.84E+05	5.97E+05	0.409	4
10	1.44E+04	4.69E+03	1.91E+04	0.400	3
11	1.20E+04	4.68E+03	1.67E+04	0.384	3
12	2.09E+05	9.38E+04	3.03E+05	0.400	3
13	4.22E+05	1.92E+05	6.14E+05	0.384	3
14	2.64E+05	1.22E+05	3.86E+05	0.384	3
15	9.84E+04	4.18E+04	1.40E+05	0.409	4
16	1.06E+05	4.56E+04	1.51E+05	0.409	4
17	2.95E+05	1.26E+05	4.21E+05	0.384	3
18	8.40E+04	4.32E+04	1.27E+05	0.384	3
19	1.03E+05	4.15E+04	1.45E+05	0.384	3
20	6.72E+04	3.55E+04	1.03E+05	0.409	4
Average	1.56E+05	6.90E+04	2.25E+05	0.387	-

The same exact experiment was also conducted in ZEMAX using the built-in global search algorithm (Zemax, 2011a). According to Moore (1999), the ZEMAX global search is based on a hybrid GA.

In ZEMAX, a RMS WFE merit function was built with all of the system requirements and constraints. All of the lens parameters were set as variables and the glasses were set as substitution. A glass catalog containing only the allowed glasses for this design was defined. Solvers were used on the last surface curvature and air thickness in order to control the desired focal length and image plane positions, respectively.

Despite not using the user-provided starting point in the global search algorithm (MORRE, 1999), ZEMAX requires a feasible start solution in order to run the search. The initial solution defined is a set of plane parallel plates with 2 mm thickness and 2 mm air spacing. Due to the solvers, the last curvature of the system was set to preserve the desired focal length, and the distance to the image was set to 50 mm.

ZEMAX does not have an automatic stopping criterion for the global search algorithm; it keeps running until the user hits the STOP button. While running, ZEMAX informs the ten best MF found, the number of evaluated systems, and the elapsed time.

On this experiment, to compare ZEMAX results with the obtained results from the proposed algorithm, the user visually checks the best systems MF found by ZEMAX until the minimum required image quality is achieved. At that point, the user manually stops the ZEMAX search. The number of systems tested by ZEMAX, interpreted as the number of times the objective function was computed, is recorded. Likewise, the best system found is saved, and its RMS WFE is also recorded. Table 8.3 shows the obtained results for all twenty executions performed in ZEMAX.

The global search algorithm in ZEMAX found three visually distinct systems. The layout of each system is shown in Figure 8.3. All of the triplet systems found by ZEMAX also have the classical Cooke triplet architecture.

Table 8.3 - Cooke triplet experiment results using ZEMAX global search. The columns, from left to right, describe the execution number, the number of evaluations of the objective function, the RMS WFE value achieved in waves, and the system type.

	TMFC	MF	Type
1	3.65E+05	0.367	1
2	1.40E+05	0.367	1
3	2.75E+05	0.367	1
4	3.13E+06	0.367	1
5	1.89E+05	0.364	2
6	1.42E+06	0.367	1
7	6.64E+05	0.367	1
8	3.65E+05	0.367	1
9	7.49E+04	0.367	1
10	1.29E+06	0.367	1
11	4.52E+05	0.367	1
12	6.85E+05	0.364	2
13	1.38E+06	0.364	2
14	8.28E+05	0.364	2
15	5.49E+04	0.367	1
16	4.00E+05	0.367	1
17	1.27E+05	0.367	1
18	1.04E+06	0.367	1
19	1.83E+06	0.390	3
20	4.18E+05	0.367	1
Average	7.56E+05	0.368	-

A standard way of comparing the efficiency of EA is given by means of the average computation cost required to meet the defined stopping criterion. The average total number of the objective function evaluations provides the best metric for the computation cost. This metric is independent of the hardware, programming language, and the algorithm structure.

In this way, despite providing systems with slightly better average performance, the proposed algorithm was approximately 3.3 times more efficient than ZEMAX in terms of computation cost. Table 8.4 provides a summarized comparison for the experiment.

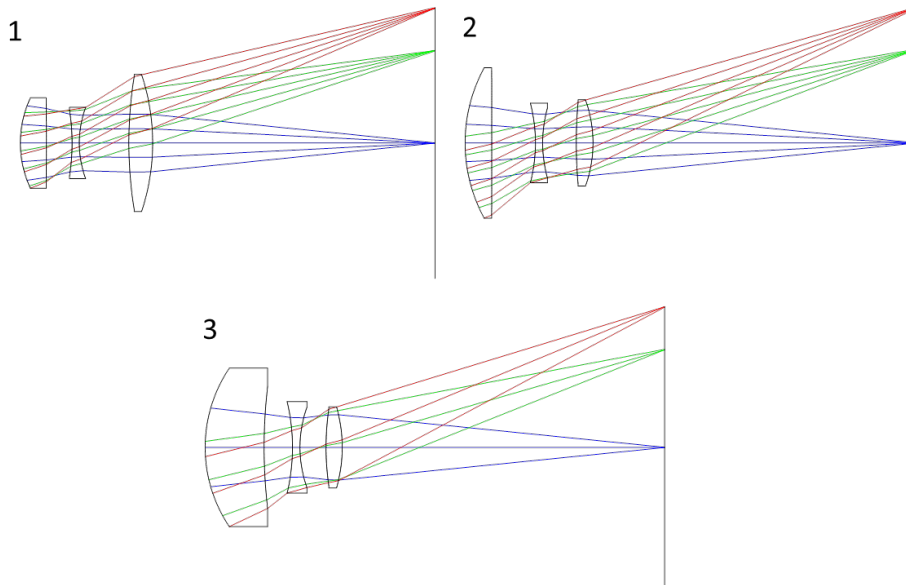


Figure 8.3 - Layout of the triplet system types found by ZEMAX.

Table 8.4 - Summarized results comparison for Cooke triplet experiment where TMFC describes the total number of merit function evaluations and MF describes the RMS WFE value achieved in waves.

	Proposed Method		ZEMAX	
	TMFC	MF	TMFC	MF
Maximum	6.14E+05	0.409	3.13E+06	0.390
Minimum	1.67E+04	0.361	5.49E+04	0.364
Average	2.25E+05	0.387	7.56E+05	0.368

The obtained results for the triplet experiment provide us with the necessary confidence to attempt a more complicated experiment.

8.2. The telephoto lens problem

The telephoto system is a classical photographic lens design characterized by the ratio between its overall length L and its focal length F , called telephoto ratio (L/F), which must be less than one and which is typically from 0.6 to 0.85. In other words, the system length is smaller than the effective focal length. The smaller the telephoto ratio, the more difficult the design. Normally, these systems have a long focal length. However, not all long-focal-length systems are telephoto designs, as they are frequently commercially misclassified (SMITH, 2004).

The classical design of a telephoto lens consists of two lens groups separated by a substantial air distance, where the first group is positive and the second group is negative. Therefore, the simplest telephoto designs could contain only one element in each group. In practice, however, more than one element is used in each group in order to control the various aberrations.

The telephoto design problem is interesting for this stage of tests for our proposed algorithm. In terms of number of lenses, telephoto systems can be much more complex optical systems than Cooke triplets, but depending on the first-order requirements, they might not be extremely complex systems. In optical design texts (KIDGER, 2004; SMITH, 2004; LAIKIN, 1995), telephoto designs contain from four to seven or more lenses, sometimes for systems with very similar first-order specifications. In this way, we can test the ability of the algorithm for finding solutions to a more complex problem than the earlier tested Cooke triplet. Furthermore, this problem can be used in subsequent experiments to test the algorithm expertise in finding trade-off solutions in terms of the number of lenses, image quality, and sensitivity.

A total of three experiments will be conducted with the telephoto problem. At first, the number of lenses is fixed, and the problem is executed in the mono-objective mode considering only the image quality. Second, the number of lenses is still fixed, but the problem is executed in the multi-objective mode considering both the image quality and tolerance. Finally, the number of lenses is allowed to vary, and the multi-objective approach considers the image quality, tolerance, and the number of lenses in the optimization process.

Table 8.5 shows the telephoto lens requirements and constraints used in this experiment. A commercial lens from Canon gave us the inspiration for the requirements and constraints in this problem. The Canon lens taken as a reference is the model EF 400 mm f/5.6L USM classified by Canon as a Super Telephoto Lens (CANON, 2013).

Table 8.5 - Telephoto system requirements and constraints.

ITEM	REQUIREMENT
Effective focal length (efl)	400 mm
F- number (f#)	5.6
Field of View (FOV)	+/- 3 deg
Maximum telephoto ratio	0.75
Spectral band	Visible uniform weighting F (486,13nm), d (587.56nm) and C (656,27nm).
Available glasses	N-LASF40 and N-PSK53A
Maximum RMS wavefront error	0.20 waves
Minimum air edge thickness	0 mm
Minimum air central thickness	0 mm
Maximum air central thickness (excluding the back focal length)	150 mm
Minimum glass edge thickness	2 mm
Minimum glass central thickness	4 mm
Maximum central glass thickness	15 mm
Minimum back focal length	44mm
Maximum system length (excluding the back focal length)	256 mm
Maximum total system length	300 mm

Some requirements are taken directly from the model specifications, while others are derived from the available information on the model. Likewise, some constraints are also derived from the Canon specifications, while others are simply defined by the rules-of-thumb used in lens design.

The glasses for the design were chosen using the glass selection method described above. The image quality in terms of the RMS wavefront error in waves was derived from an image quality in terms of the modulated transfer function (MTF) used as a rule-of-thumb for photographic objectives.

To perform the glass selection method, the newest available Schott glass catalog was used (SCHOTT, 2013). To avoid glasses with prohibitive cost, we applied an upper limit of 10 for the glass relative cost value. Glasses with no relative cost information in the catalog were not taken into account.

The three wavelengths shown in Table 8.5 were used as input to the glass selection method. The primary wavelength selected was d (587.56 nm). At first, arrangements of two glasses ($k = 2$) were used. The upper value for F_1 was set

as 10. The post-Pareto method used in this example was the minimum distance to the origin (ALBUQUERQUE *et al.*, 2012), where the distance metric $|\bar{g}_i|$ was computed using only F_2 and F_3 . The normalization factor \bar{O}_{ob} for each function was set as the value that accumulates 80% of the solutions in the Pareto front (ALBUQUERQUE *et al.*, 2012). Table 8.6 shows the first 10 output lines of the glass selection Pareto front organized from the lowest to the highest $|\bar{g}_i|$.

Table 8.6 - Telephoto lens problem output table from the glass selection method for 2 glasses sorted by $|\bar{g}_i|$.

N°	Glass 1	Glass 2	F1	F2	F3
2189	N-LASF40	N-PSK53A	3.81	4.77E-04	1.07
2423	N-LASF46A	N-PSK53A	2.92	5.33E-04	0.92
2582	N-PSK53A	N-LASF46A	2.92	5.33E-04	0.94
244	LAFN7	N-PSK53A	3.42	4.68E-04	1.17
2557	N-PSK53A	LAFN7	3.42	4.68E-04	1.17
2569	N-PSK53A	N-KZFS8	3.38	4.69E-04	1.20
1362	N-KZFS8	N-PSK53A	3.38	4.69E-04	1.21
2359	N-LASF45	N-PSK53A	3.42	5.18E-04	1.09
2602	N-PSK53A	SF4	2.51	5.69E-04	0.93
2599	N-PSK53A	SF1	2.71	5.54E-04	1.00

Based on the F_2 values, we notice that none of the glasses combinations found are able to give a diffraction limited color correction. In this case, for diffraction limited designs, more than two glasses should be used in combination. However, as the system requirements do not impose diffraction-limited quality, the glass pair in the first row of Table 8.6 was picked for the design. According to the applied post-Pareto analysis, the pair N-LASF40 and N-PSK53A provides the best tradeoff solution.

A rule-of-thumb for the image quality of photographic optical systems is given by the thirty-fifty, fifty-thirty rule. In other words, the MTF at thirty line pairs per millimeter (30 lp/mm) should be around fifty percent (50%), while at 50 lp/mm, it should be around 30% (SASIAN, 2011). However, the image quality metric used in our automatic design algorithm is given in terms of the RMS wavefront error. Shannon (1997) provides an approximate empirical equation to calculate the MTF curve for a given RMS wavefront error. Using this equation, the minimum MTF required is obtained when the RMS wavefront error is

approximately 0.2 waves. As this equation is empirical and provides only an approximation, this value for the RMS WFE is used as a reference only.

8.2.1. First telephoto design experiment

At this first telephoto experiment, the number of lenses is kept fixed and the algorithm is executed in the mono-objective mode. The number of lenses is set to seven, which is more than the double the number of lenses used in the first experiment. In this way, we can confirm the ability of the algorithm for finding competitive solutions in a much more complex design space and compare the results with the same experiment conducted using ZEMAX. Furthermore, the Canon commercial objective taken as reference for this experiment uses seven lenses as well.

The only things changed from the Cooke triplet experiment were the input requirements and constraints, the number of generations used during the exploration, and the stopping criterion.

As mentioned in Section 8.1.1, the necessary number of generations is assumed to be linear with the number of variables and quadratic with the number of objective functions. For this experiment, the number of generations is set to 300. The stopping criterion defined is 10^7 evaluations of the objective function, which includes both the exploration and exploitation objective functions. For this experiment, the objective function evaluation rate is 396.88 per second per core in an Intel quad core i5-2500 CPU.

A total of twenty independent executions of the algorithm were executed in order to obtain an average performance to compare with ZEMAX results. The total running time was 35 hours using the mentioned CPU running four instances in parallel. Table 8.7 shows the results for each execution of the proposed automatic design algorithm.

The image quality of the systems found is reasonable. Though the RMS WFE is slightly worse than desired, the MTF complies with the 30–50, 50–30 rule in almost all cases.

Table 8.7 - Results for each independent execution of the Telephoto problem using the proposed automatic design algorithm. From left to right, the columns describe the independent execution number, the number of exploration merit function evaluations, the number of exploitation merit function evaluations, the total number of merit functions required to determine the best solution, and the RMS WFE achieved in waves.

	GMFC	LMFC	TMFC	MF
1	4.16E+06	8.41E+05	5.00E+06	0.216
2	6.86E+06	2.08E+06	8.94E+06	0.240
3	3.54E+06	1.47E+06	5.01E+06	0.208
4	6.16E+06	3.33E+06	9.49E+06	0.213
5	1.51E+06	4.04E+05	1.91E+06	0.201
6	3.71E+06	1.09E+06	4.80E+06	0.206
7	6.37E+06	2.00E+06	8.37E+06	0.207
8	1.78E+06	5.18E+05	2.29E+06	0.207
9	1.89E+06	5.62E+05	2.45E+06	0.234
10	4.80E+06	1.50E+06	6.29E+06	0.209
11	3.97E+06	1.22E+06	5.19E+06	0.218
12	2.82E+06	8.04E+05	3.62E+06	0.212
13	4.55E+06	1.30E+06	5.85E+06	0.201
14	8.44E+05	2.37E+05	1.08E+06	0.221
15	2.40E+06	6.86E+05	3.08E+06	0.241
16	8.88E+05	2.78E+05	1.17E+06	0.207
17	1.73E+06	5.30E+05	2.26E+06	0.217
18	7.48E+06	2.29E+06	9.77E+06	0.226
19	4.66E+05	1.50E+05	6.16E+05	0.207
20	2.02E+06	5.65E+05	2.59E+06	0.225
Average	3.40E+06	1.09E+06	4.49E+06	0.216

Figure 8.4 and Figure 8.5 show the layout of each system found by the proposed automatic design algorithm. These designs have nice layouts; in general, we cannot identify unusually shaped lenses. It is important to note that the layouts and the image quality presented are exact from the systems determined by the automatic design software. We did not fix, change, or further optimize these designs. Almost all of the systems found by the algorithm have a positive group of lenses followed by a negative group as expected in a telephoto lens design, but they also have a group of lenses close to the image plane working as a field corrector.

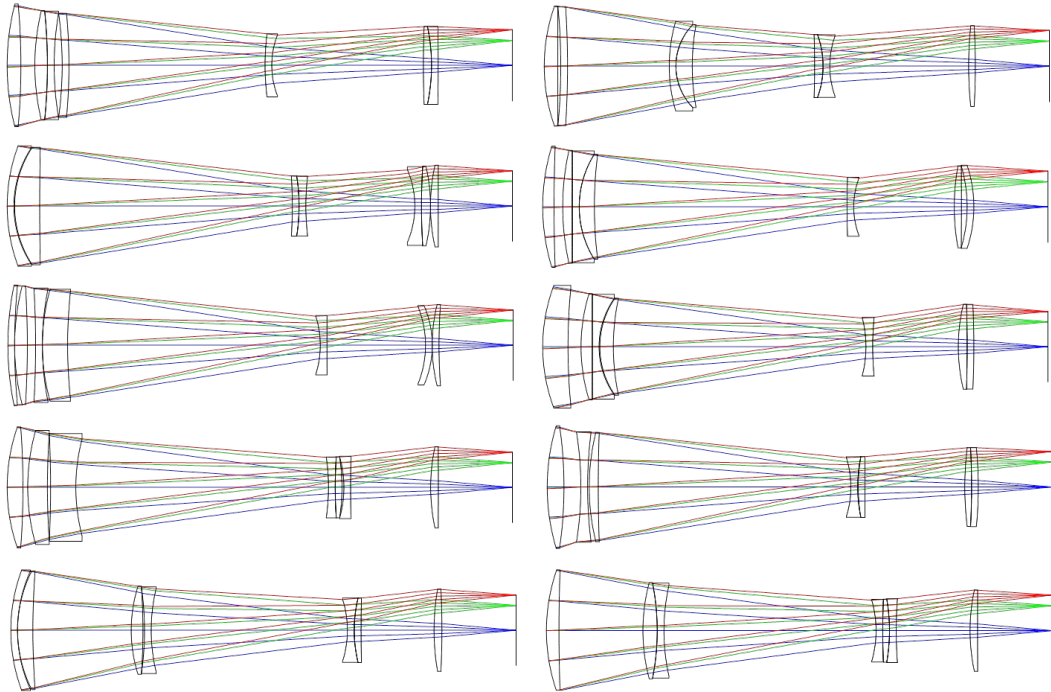


Figure 8.4 - Layout of the telephoto system found by the proposed automatic design algorithm during executions 1–10.

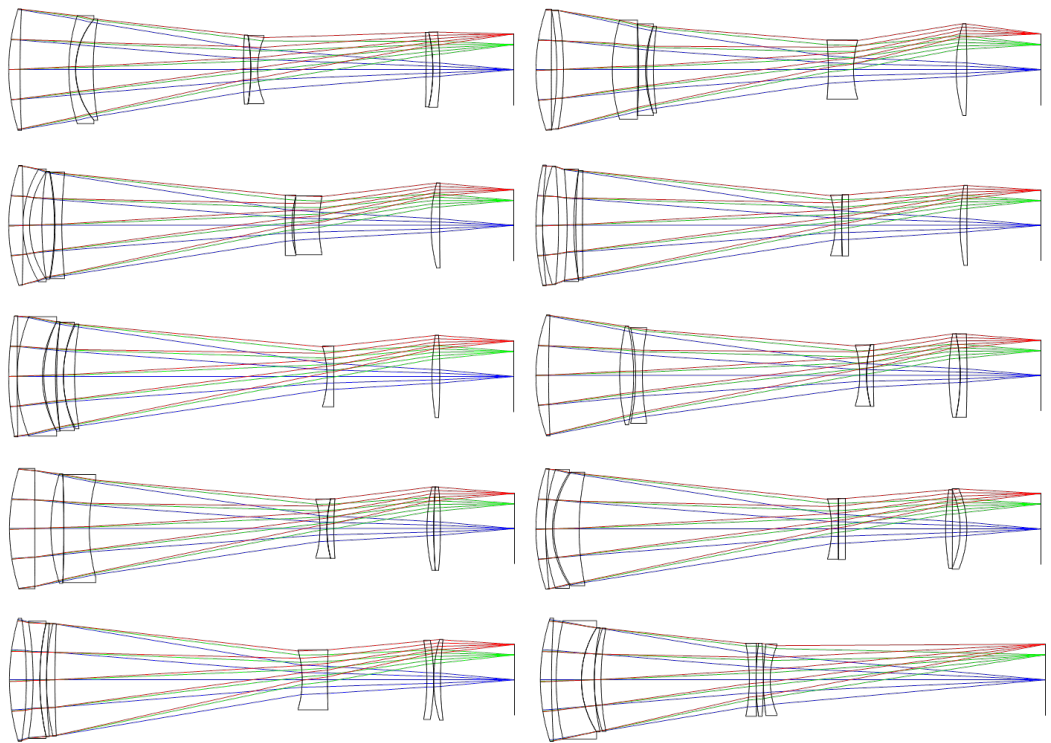


Figure 8.5 - Layout of the telephoto system found by the proposed automatic design algorithm during executions from 11–20.

Though each independent run of the algorithm stopped after 10^7 merit function calculations, the best solutions were found much earlier as reported in Table 8.7. The average number of merit function calculations to determine the best solution was approximately 4.49×10^6 , less than half of the stopping criterion.

To express the image quality of these systems in terms of the MTF, Figure 8.6 shows two polychromatic MTF curves up to 50 lp/mm for two different systems found. The left curve represents the MTF of the system with the lowest RMS WFE found. The right curve corresponds to the system with the highest RMS WFE.

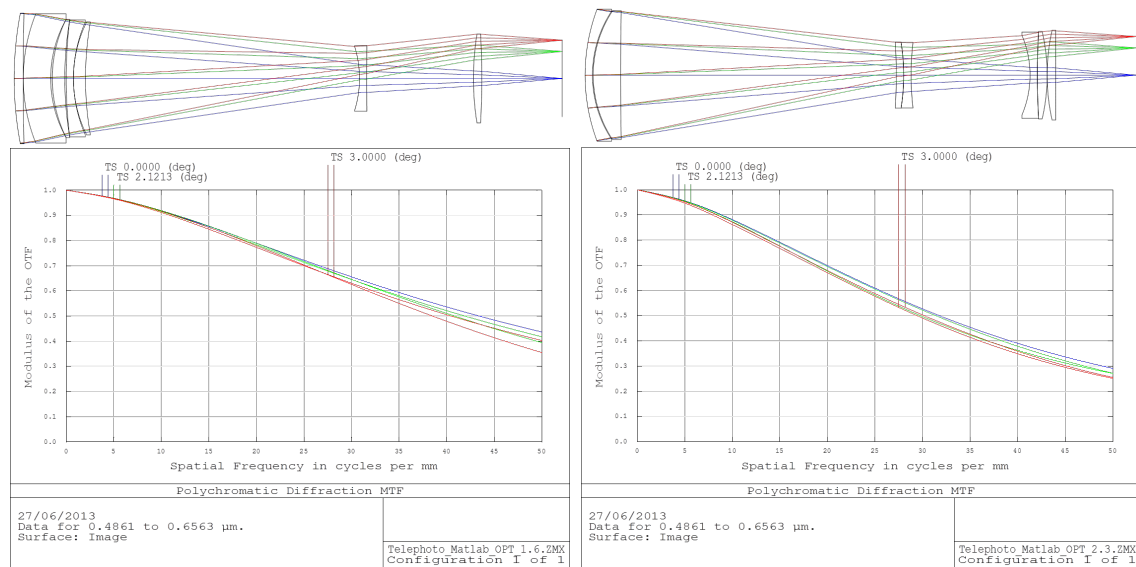


Figure 8.6 - Layout and MTF curves for the best and worst telephoto systems found during the twenty independent executions of the algorithm. The left-hand side corresponds to the worst system found and the right-hand side corresponds to the best system.

For comparison purposes, the same experiment with the same requirements, constraints, glasses, and stopping criterion was also executed in ZEMAX using its Global Search algorithm. To set the input system in ZEMAX, we used the same approach applied in the Cooke triplet problem.

The global search algorithm in ZEMAX does not have an automatic stopping criterion and keeps running until the user pushes the STOP button. Therefore, we estimated the approximate time it would take ZEMAX to reach the desired

number of MF calculations based on the elapsed time and the corresponding number of evaluated systems in the beginning of the search.

It is virtually impossible to stop ZEMAX global search with exactly 10^7 executions. The executions were stopped manually slightly after the defined stopping criterion. In some executions, the time was underestimated and the number of MF calculations became significantly higher. In ZEMAX, it is not possible to know when the algorithm found the best system.

Twenty independent executions were performed with ZEMAX global search. The results from this experiment using ZEMAX global search can be found in Table 8.8.

Table 8.8 - Results for each independent execution of the telephoto problem in ZEMAX. From left to right, the columns identify the independent execution number, the approximately number of MF calculations reported, and the best RMS WFE found during the execution.

	TMFC	MF
1	1.19E+07	0.408
2	1.00E+07	0.308
3	1.00E+07	1.237
4	1.00E+07	1.127
5	1.00E+07	0.921
6	1.00E+07	0.347
7	1.00E+07	0.772
8	1.00E+07	0.782
9	1.20E+07	0.707
10	1.20E+07	0.634
11	1.00E+07	0.373
12	1.00E+07	0.522
13	1.00E+07	0.856
14	1.00E+07	0.365
15	1.00E+07	0.877
16	1.00E+07	0.561
17	1.00E+07	0.587
18	1.00E+07	0.397
19	1.30E+07	1.293
20	1.30E+07	0.513
Average	1.06E+07	0.679

For this first telephoto lens problem, the image quality was the only goal in the optimization. In terms of image quality, the performance of ZEMAX was significantly worse than the performance of our proposed automatic design algorithm. Even permitting ZEMAX algorithm to continue above the stopping criterion in some runs, the average RMS WFE for the best systems found was approximately 0.679 waves, more than three times higher than the mean value found with our automatic design algorithm. Moreover, for our algorithm, it was not necessary to perform 10^7 MF calculations in any one of the experiments to reach the best lens systems found.

Figure 8.7 and Figure 8.8 show the layouts of the best systems achieved with each independent ZEMAX execution. By comparing the lens formats and design architectures between the ZEMAX solutions and our proposed method solutions, we conclude that our algorithm not only found much better image quality systems but also generated more feasible lens system layouts. Note that many of the ZEMAX solutions do not follow the typical telephoto lens architecture.

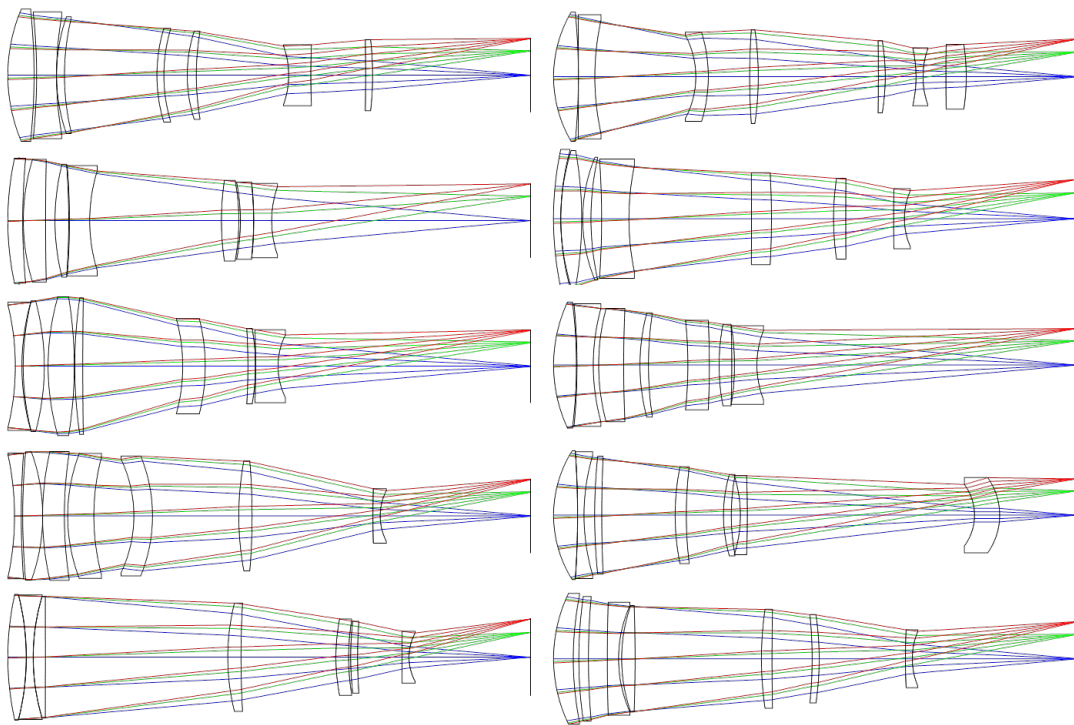


Figure 8.7- Layout of the telephoto system found by ZEMAX global search algorithm during executions 1–10.

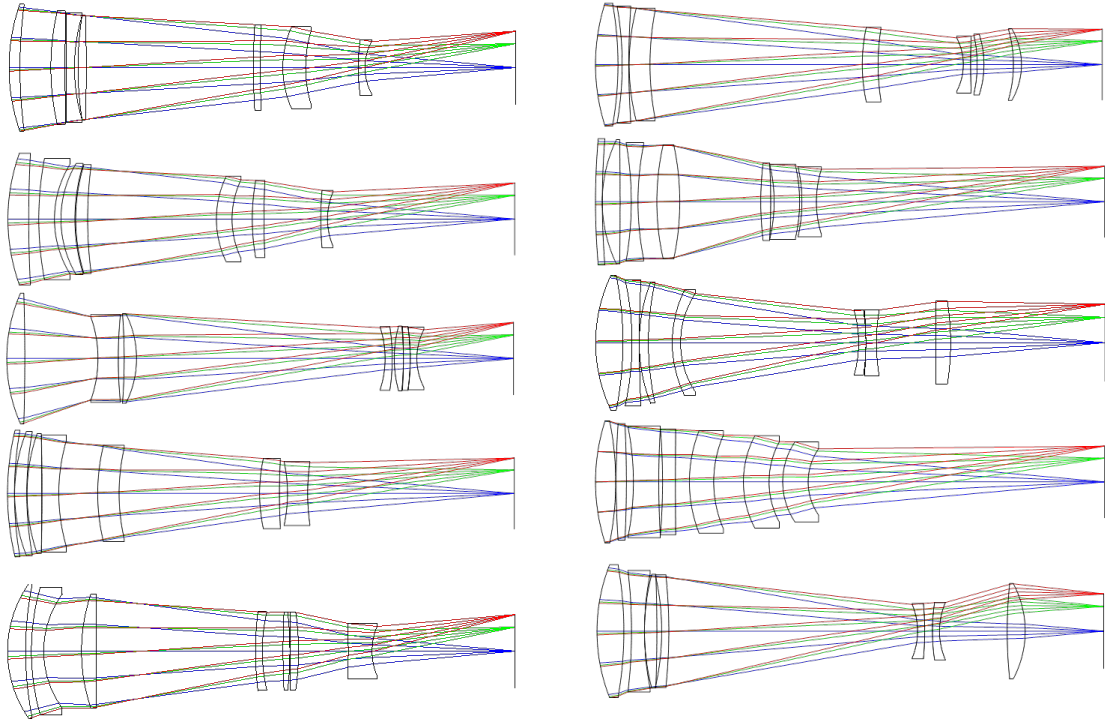


Figure 8.8- Layout of the telephoto system found by ZEMAX global search algorithm during executions 11–20.

For easy comparison, Table 8.9 summarizes the results for the current experiments executed by both tools.

Table 8.9 - Summarized results comparison for the first telephoto experiment.

	Proposed Method		ZEMAX	
	TMFC	MF	TMFC	MF
Maximu	9.77E+06	0.241	1.30E+07	1.293
Minimum	1.08E+06	0.201	1.00E+07	0.308
Average	4.49E+06	0.216	1.06E+07	0.679

To demonstrate how poor the image quality is for the systems found by ZEMAX, Figure 8.9 shows the MTF curve for one of the ZEMAX telephoto lens systems. This system has an RMS WFE of 0.6344, which is the closest to the average RMS WFE value.

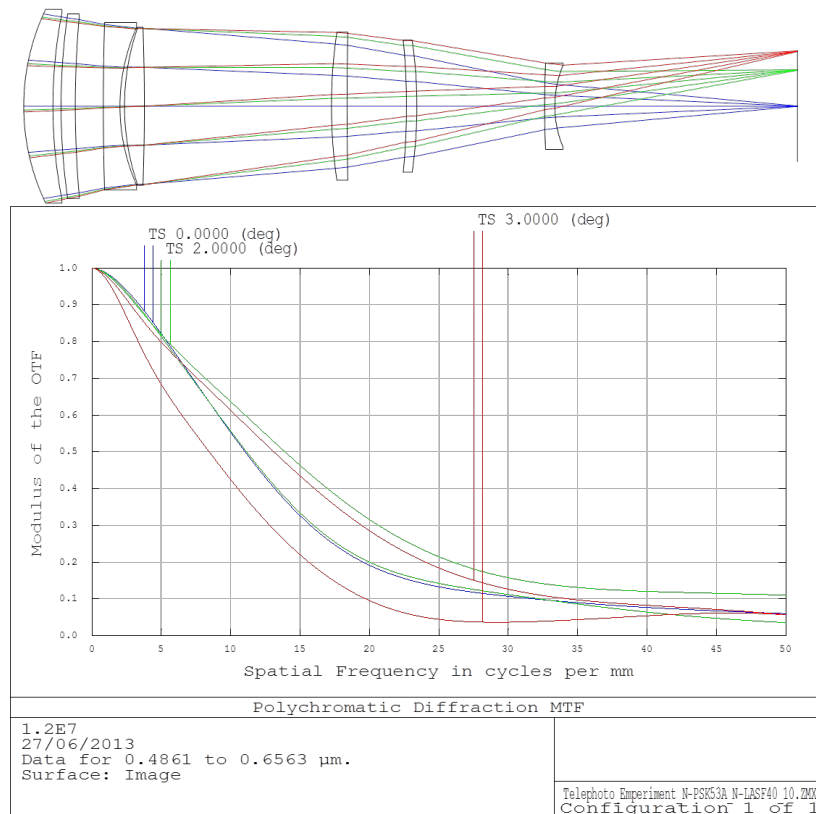


Figure 8.9 - Layout and MTF curve for the telephoto system found by ZEMAX with the RMS WFE closest to the average RMS WFE value.

8.2.2. Second telephoto design experiment

With the success in the previous experiments, we now take a step further. In the current experiment, we introduce the multi-objective approach taking into account both the image quality and tolerance.

The experiment is conducted on the exact same telephoto problem defined in the previous section. The only difference is that the automatic design algorithm is set to work in the multi-objective mode. As expected, the number of generations used during the exploration phase is increased from 300 generations to 1400 generations. Finally, the stopping criterion was changed so that the algorithm will run until the user stops the execution.

For this experiment, it is not possible to compare the performance with any commercial optical design software that we are aware of because no commercially available software utilizes a multi-objective approach.

Six instances of the algorithm were executed in parallel. The Pareto fronts resulting from each instance were combined and the non-dominated solutions were filtered out. As a result, we generated the Pareto front shown in Figure 8.10. To get these results it was necessary a total of $8.533E+08$ merit function calculations. For this experiment, the merit function evaluation rate is 357.2255 per second per core in an Intel quad core i5-2500 CPU. The total experiment time was around 5 ½ days, running the algorithm on 2 different computers.

Each dot in the graph of Figure 8.10 represents a trade-off solution. For some of the trade-off solutions, the respective system layout is displayed. The abscissa represents the image quality in terms of the RMS wavefront error, and the ordinate shows the tolerancing metric. The abscissa was truncated at 0.35 waves.

The best tradeoff solutions are located around the Pareto front knee region, circled in red. The layout and respective MTF and Seidel diagram plots of three systems inside the red circle are shown in Figure 8.11, Figure 8.12, and Figure 8.13.

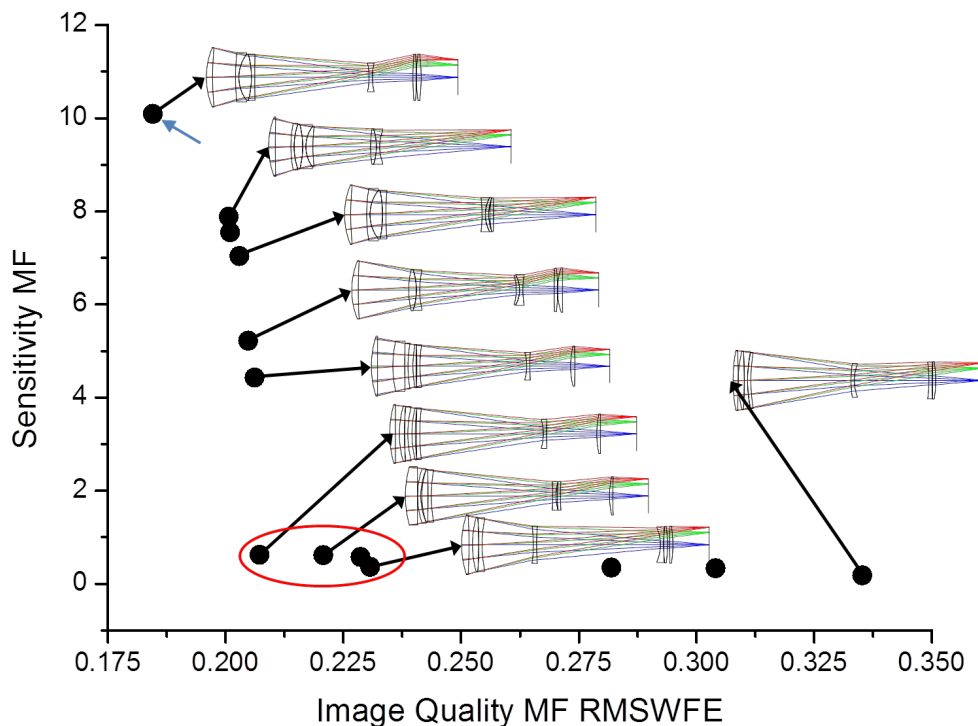


Figure 8.10 - Pareto front for the telephoto experiment using image quality and tolerance to drive the search.

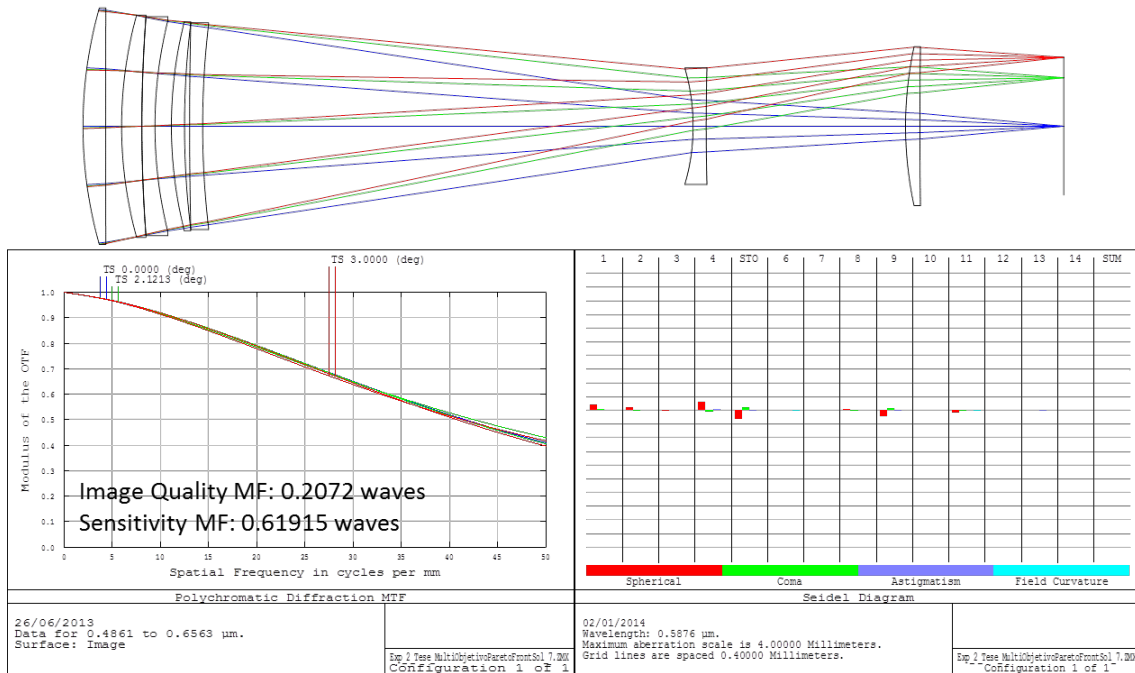


Figure 8.11 – Layout, MTF and Seidel diagram plots for one of the non-dominated telephoto designs close to the knee region in the Pareto front. This system has an image quality metric of 0.207 waves and a tolerancing metric of 0.619 waves.

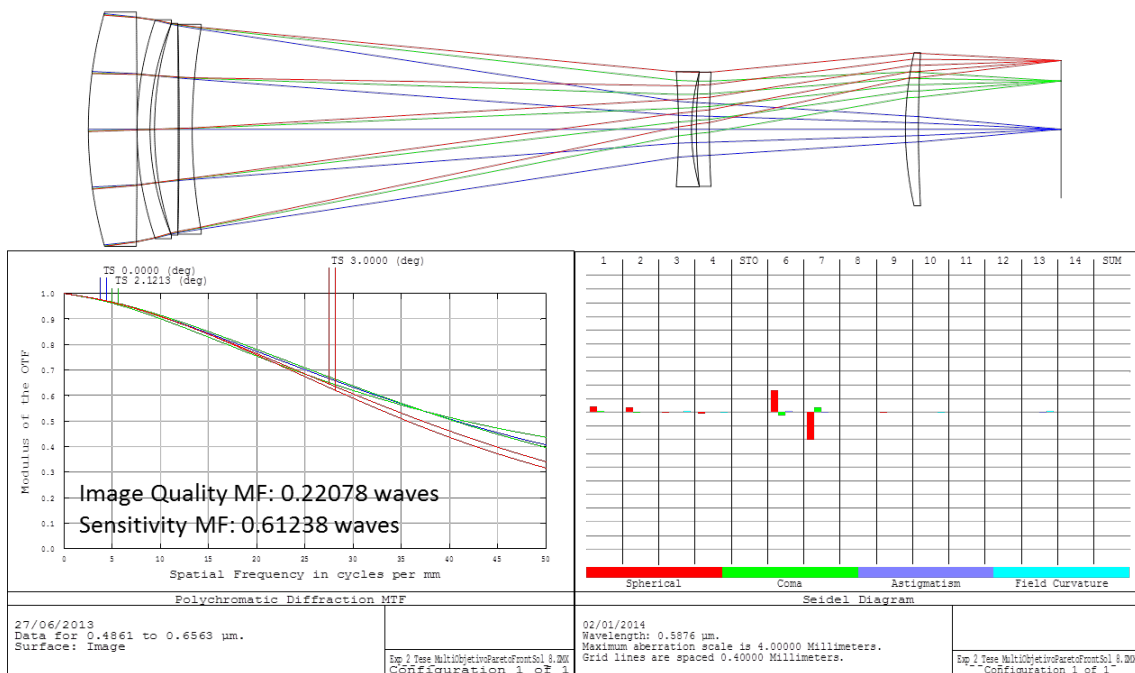


Figure 8.12 - Layout, MTF and Seidel diagram plots for one of the non-dominated telephoto designs close to the knee region in the Pareto front. This system has an image quality metric of 0.221 waves and a tolerancing metric of 0.612 waves.

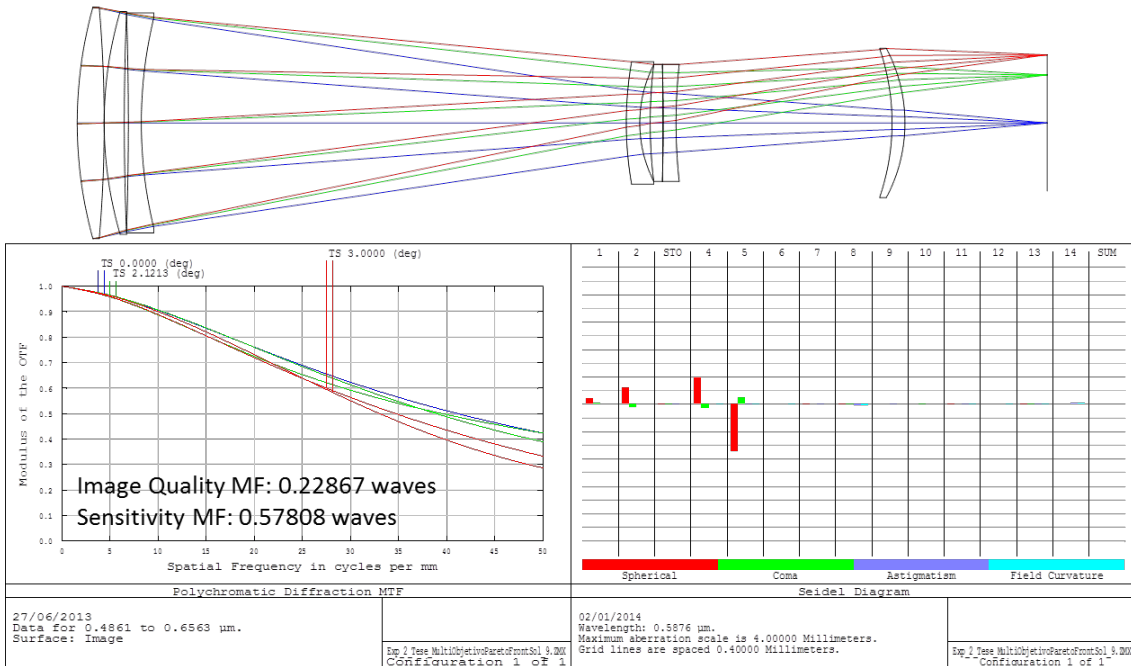


Figure 8.13 - Layout, MTF and Seidel diagram plots for one of the non-dominated telephoto designs close to the knee region in the Pareto front. This system has an image quality metric of 0.229 waves and a tolerancing metric of 0.578 waves.

The best image quality system, pointed by a blue arrow in of Figure 8.10, is also detailed in Figure 8.14 for comparison purposes.

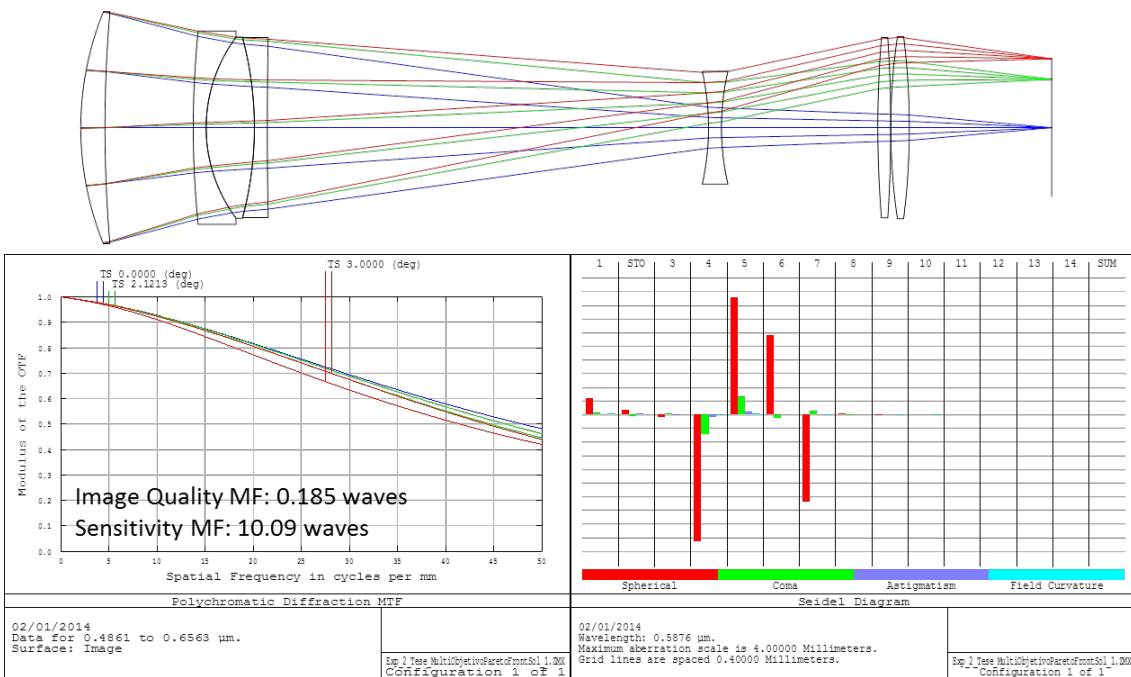


Figure 8.14 - Layout , MTF and Seidel diagram plots for the best image quality system found during the experiment. This system has an image quality metric of 0.185 waves and a tolerancing metric of 10.09 waves.

8.2.3. Third telephoto design experiment

In this last telephoto experiment, we use all of the automatic lens design software tools proposed in this thesis. The multi-objective approach considering image quality, tolerance and number of lenses is applied. The problem requirements and constraints are kept exactly the same as the previous two telephoto lens experiments. However, the number of lenses is now treated as a design variable and used as a third objective function.

We allow the number of lenses to vary from 4 to 9. The number of generations during the exploration phase is calculated from the number of lenses used in the randomly generated system at the beginning of each algorithm loop. No automatic stopping criterion is used in this experiment; the algorithm is allowed to run until the user stops the execution.

Eight instances of the algorithm were executed in parallel. The Pareto fronts resulting from each instance were combined and the non-dominated solutions were filtered out, resulting in the final Pareto front shown in Figure 8.15. Each bubble in this graph represents a trade-off solution in terms of the image quality (abscissa), tolerance (ordinate), and number of lenses (third axis represented by the dot color). The number of lenses used by the system is also printed inside the bubble representing its locus in the objective function space. Note that the bubble size is also proportional to the number of lenses.

This resultant Pareto front was obtained after $1.51E+9$ merit function calculations, including the exploration and exploitation phases from all instances. For this experiment, the merit function evaluation rate is 309.57 per second per core in an Intel quad core i5-2500 CPU. The total experiment time was around 7 days, running the algorithm on 3 different computers.

Some solutions close to the knee region of the Pareto front, which are considered to be preferable trade-offs, were picked visually. Red arrows in Figure 8.15 identify these selected solutions. The layout, MTF and Seidel

diagram plots of these selected solutions can be found in Figure 8.16, Figure 8.17, and Figure 8.18.

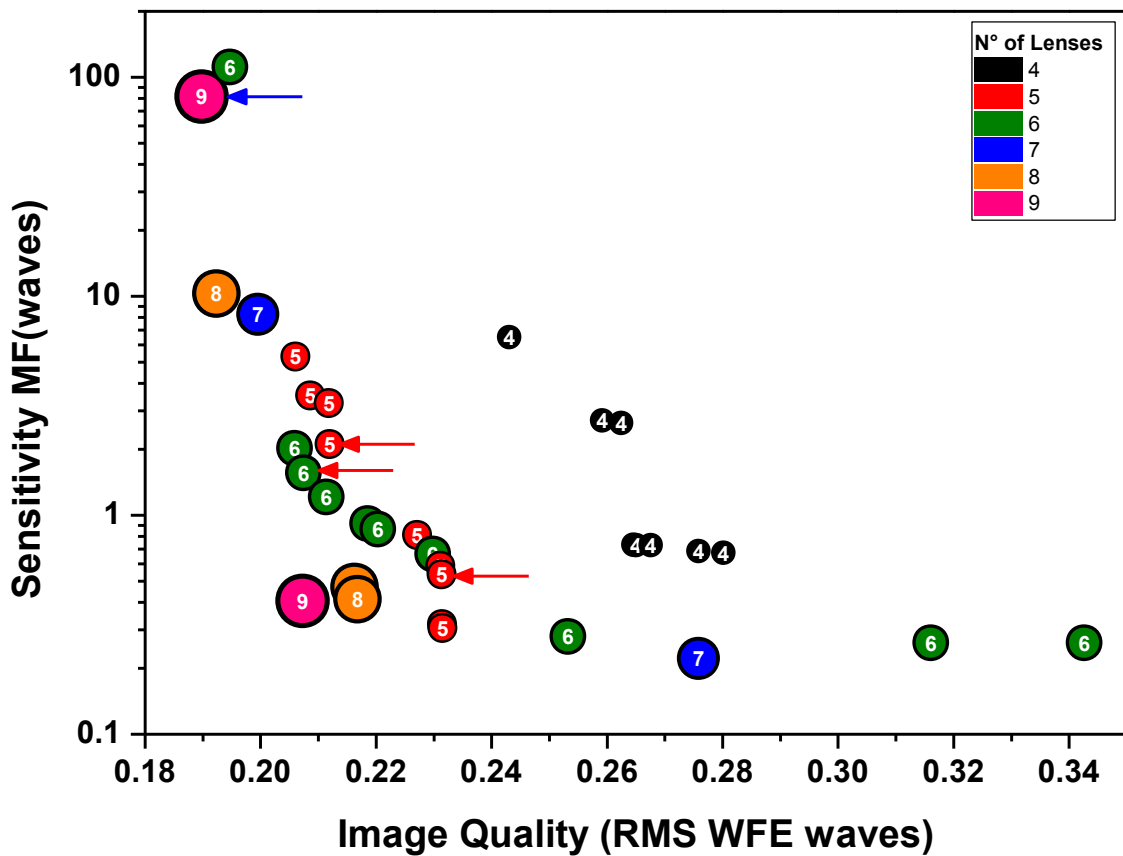


Figure 8.15 - Pareto front for the telephoto experiment using the image quality, tolerance, and number of lenses to drive the search.

For comparison purposes, we also show in Figure 8.19 the layout, MTF and Seidel diagram plots for the best image quality system resulting from this experiment, which is pointed in Figure 8.15 by a blue arrow.

In Figure 8.15, we observe a significant relative improvement between the solutions composed of four lenses with the solutions composed of five lenses. The distance from the front formed by the four lenses to the front formed by the five lenses solutions in the sensitivity by image quality Pareto front projection makes this clear. For systems with more than five lenses, the relative improvements are subtle. For solutions with more than six lenses, the compromises start to become very significant. Therefore, we conclude that systems with five to six lenses are the best trade-off solutions available for this problem.

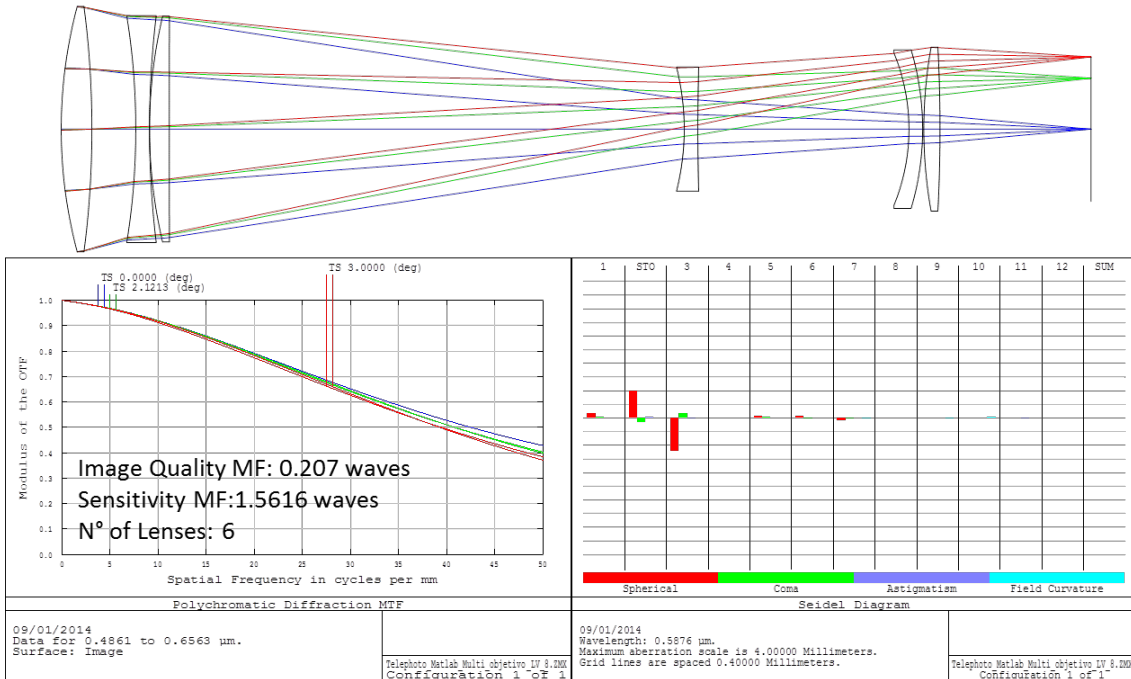


Figure 8.16 – Layout, MTF and Seidel diagram plots for one of the non-dominated telephoto designs selected from the Pareto front. This 6-lens system has an image quality metric of 0.207 waves and a tolerancing metric of 1.5616 waves.

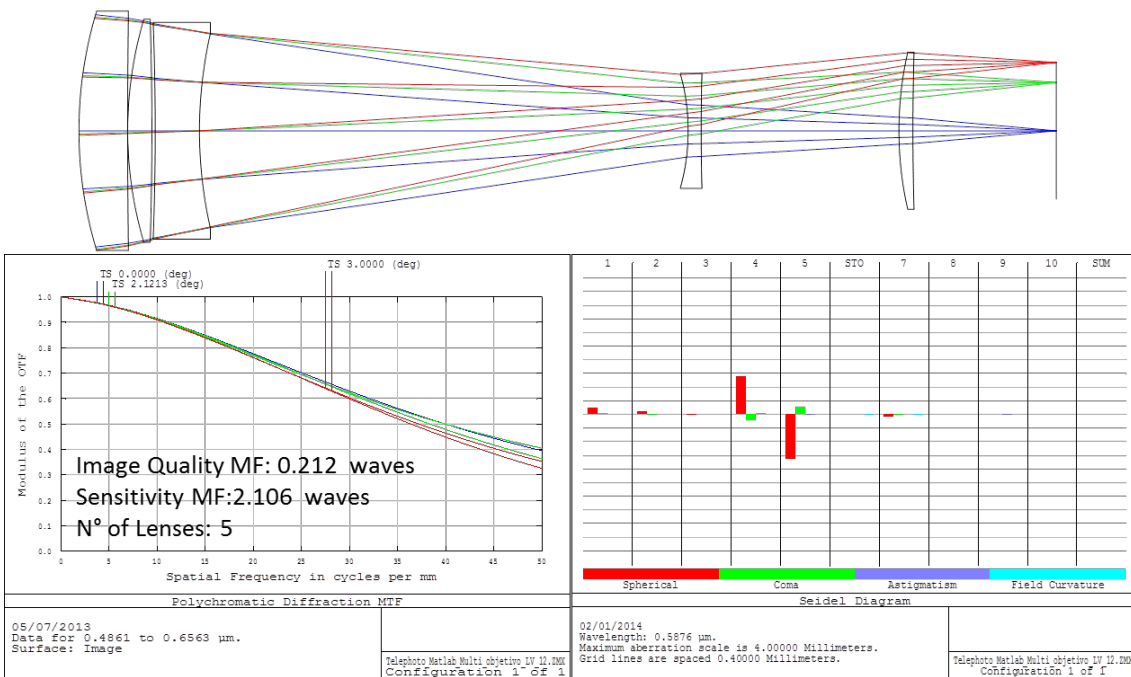


Figure 8.17 – Layout, MTF and Seidel plots for one of the non-dominated telephoto designs selected from the Pareto front. This 5-lens system has an image quality metric of: 0.212 waves and a tolerancing metric of 2.106 waves.

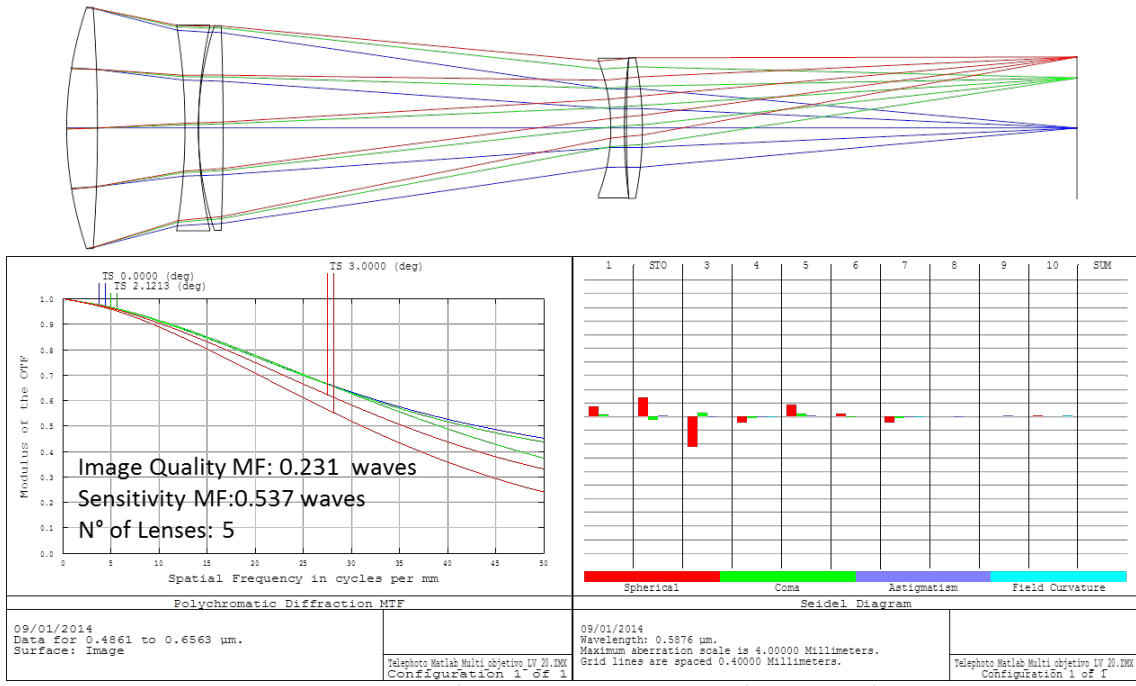


Figure 8.18 – Layout, MTF and Seidel diagram plots for one of the non-dominated telephoto designs selected from the Pareto front. This 5-lens system has an image quality metric of: 0.231 waves and a tolerancing metric of 0.537 waves.

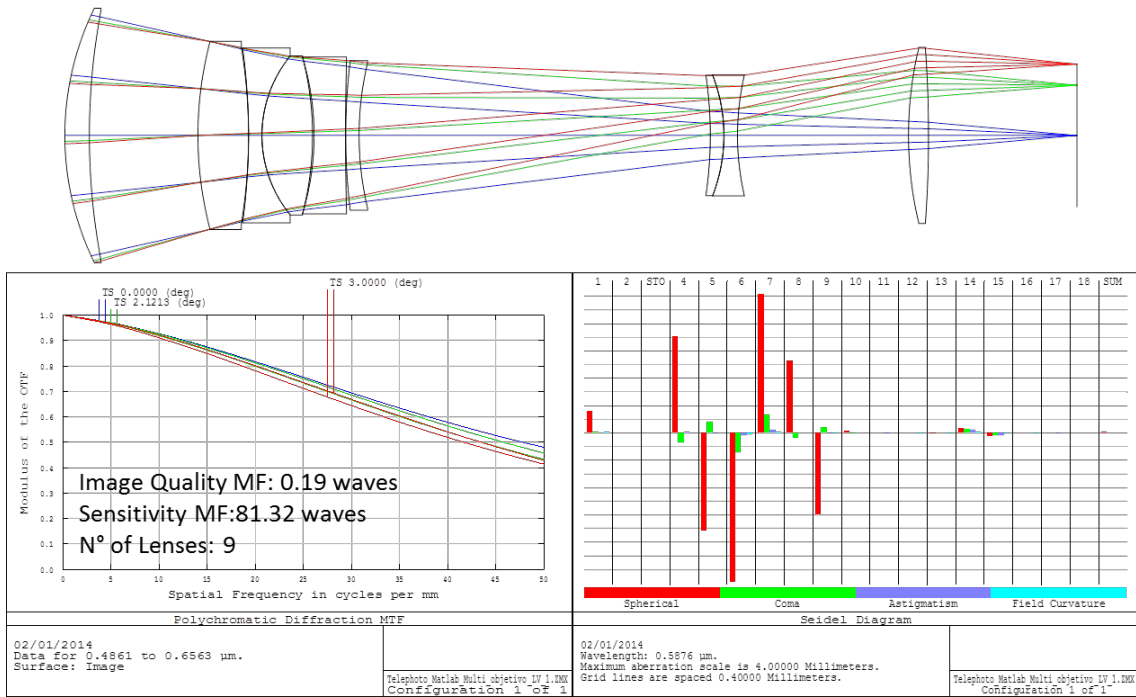


Figure 8.19 – Layout, MTF and Seidel diagram for the system pointed by a blue arrow in Figure 8.15. This nine-lens system corresponds to the best image quality system found in this experiment, with an image quality metric of: 0.19 waves and a tolerancing metric of 81.32 waves.

From the results of this experiment, we can observe the vast number of trade-off designs available for a single lens design problem. The multi-objective approach provides the designer with great visibility of the available possibilities. Knowing the available possibilities and the compromises involved is important for developing a solution to any engineering problem. This allows the designer to systematically choose the optimal solution. Consequently, this example illustrates the power of the automatic multi-objective design approach proposed in this thesis.

If one of these systems had to be selected for mass production, the system shown in Figure 8.18 would be a strong candidate. The image quality is fair for a photographic system, it requires only five lenses, and the system has loose tolerances. In addition, the fourth and fifth lenses in this system can be converted into a doublet, further reducing the system assembly tolerances and mounting costs.

8.3. The MUX lens design problem

In this experiment, we apply all of the automatic lens design software tools proposed in this thesis to a real case problem. The obtained results are then compared with the actual optical design of the instrument.

MUX is a multispectral optical remote sensing instrument that will be onboard the China Brazil Earth Resources Satellite (CBERS) 3&4. It is a medium spatial resolution camera (20 m on the ground) intended for natural resources monitoring. The instrument has four spectral bands ranging from 0.45 to 0.89 μm , covers a swath of 120 km using a push-broom scanning principle, and has an intended revisiting period of twenty-six days.

The MUX subsystem design, fabrication, and tests were contracted by INPE from a Brazilian company. The development has been a huge challenge to the local industry and has advanced the available technology in several different areas, especially in optics. The MUX is the most complex spaceborne subsystem ever contracted in the Brazilian industry.

The MUX contract is now reaching a successful end. The contracted company has already delivered the Qualification Model and two of the three Flight Models. Nevertheless, it has been challenging to this point. Many delays in the development were caused by the malfunction of the fabricated optical system. The designed optical system has a very high image quality; however, it is complex and very sensitive to fabrication and assembly errors. This sensitivity was responsible for a significant number of the problems and contract delays.

With this experiment, we intend to explore the design trade-off possibilities for the MUX optical system and to compare our results with the current MUX optical system design. Because the automatic design algorithm accounts for the tolerancing and system complexity during the design phase, we expected to find potentially better trade-off solutions for the problem. Further, by using the glass selection tool, we expect to reduce number of glass types used in the design without compromising the image quality, which can potentially reduce the system production cost, time, and complexity.

The primary MUX first-order optical requirements were gathered from INPE (2006) and are presented in Table 8.10.

Table 8.10 - Primary MUX first-order requirements from INPE (2006).

ITEM	REQUIREMENT
Effective focal length (efl)	505.8mm
F- number (f#)	4.5
Field of View (FOV)	+/- 4.4 deg
Nominal Spectral bands (central wavelength \pm half bandwidth).	485 \pm 35 μ m; 555 \pm 35 μ m; 660 \pm 30 μ m and 830 \pm 60 μ m.
Modulation Transfer Function (MTF)	> 0.65 at 38.5 lp/mm

The first step in our proposed automatic design method is the selection of the most appropriate set of glasses for the design. We used the newest available Schott glass catalog (SCHOTT, 2013); however, we discarded some specific glasses: Lithotec-CAF2, N-PK51, N-PK52A, N-FK51A, P-PK53, N-PSK53A and N-PSK53. While these glasses were very good options for color correction, they were rejected due to their undesirable thermal behavior. Optical systems

designed with these glasses are potentially sensitive to temperature changes. Normally, for small changes of temperature, the effect can be compensated with refocusing; however, MUX cannot afford a real-time automatic refocusing mechanism.

The central wavelengths for the four spectral bands shown in Table 8.10 were used as input for the glass selection method. The primary wavelength selected was 0.660 μm , which is near the median of the instrument spectral range. Due to the width of the instrument spectral range, we executed the glass selection method with three glasses ($k = 3$). The upper value for F_1 was set to 12. The post-Pareto method used in this problem was the minimum distance to the origin (ALBUQUERQUE *et al.*, 2012), where the distance metric $|\bar{g}_i|$ was computed using only F_2 and F_3 . The normalization factor \bar{O}_{ob} for each function was set to the value that accumulates 90% of the solutions in the Pareto front (ALBUQUERQUE *et al.*, 2012). Table 8.11 shows the first 10 output lines of the glass selection Pareto front organized from the lowest to the highest $|\bar{g}_i|$.

Table 8.11 - First 10 lines of the glass selection method output table applied to the MUX design using 3 glasses sorted by $|\bar{g}_i|$.

N°	Glass 1	Glass 2	Glass 3	F1	F2	F3
6175	N-KZFS11	N-BASF2	N-SK16	11.46	2.945E-05	2.33
7593	N-KZFS11	SF1	N-SK14	10.65	7.731E-05	2.64
906	KZFS12	N-SF66	N-SK2	9.62	2.540E-05	2.91
21909	N-SK5	SF57	N-KZFS11	10.68	2.394E-05	3.46
6703	N-KZFS11	N-SF1	N-SK14	10.86	1.616E-05	3.66
20450	N-SK14	N-SF4	N-KZFS11	10.63	1.744E-05	4.34
6721	N-KZFS11	N-SF10	N-SK14	10.75	1.535E-05	4.34
20437	N-SK14	N-SF14	N-KZFS11	10.60	1.188E-05	4.39
7534	N-KZFS11	P-SF69	N-SK14	10.89	9.942E-06	4.51
6834	N-KZFS11	N-SF5	N-SK14	11.11	3.178E-06	4.66

To achieve a potentially diffraction-limited color correction, F_2 must be less than 5.3×10^{-5} . The glass combination in the first row complies with this limit, and this would be the best trade-off choice of glasses according to the applied post-Pareto method. Therefore, to design the MUX system, we selected the following glasses: N-KZFS11, N-BASF2 and N-SK16.

The requirements in Table 8.10 were combined with some rules-of-thumb in optical design and together with the results from the glass selection method, we established the requirements and constraints for the MUX design as shown in Table 8.12.

Using the requirements and constraints shown in Table 8.12 as input, we executed eight instances of the algorithm in parallel. The Pareto fronts resulting from each instance were combined and the non-dominated solutions were filtered out, resulting in the final Pareto front shown in Figure 8.20. For a better visualization of the most promising designs, we truncated the image quality metric scale at 0.2 waves.

This resultant Pareto front in Figure 8.20 was obtained after $5.8E+8$ merit function calculations, including the exploration and exploitation phases from all instances. The merit function evaluation rate for this experiment is 188.3 per second per core running on an Intel quad core i5-2500 CPU. The total MUX experiment time execution was around 5 days, running the algorithm on 3 different computers.

Table 8.12 - MUX System Requirements and constraints.

ITEM	REQUIREMENT
Effective focal length (efl)	505.8mm
F- number (f#)	4.5
Field of View (FOV)	+/- 4.4 deg
Spectral bands central wavelengths.	485μm; 555μm; 660μm and 830μm.
Available glasses	N-BASF2, N-KZFS11 and N-SK16
Maximum RMS wavefront error	0.14 waves
Allowed number of lenses	From 7 to 13.
Minimum air edge thickness	3 mm
Minimum air central thickness	0.5 mm
Maximum air central thickness (excluding the back focal length)	150 mm
Minimum glass edge thickness	3 mm
Minimum glass central thickness	5 mm
Maximum central glass thickness	25 mm
Minimum back focal length	100mm
Maximum system length (excluding the back focal length)	650 mm
Maximum total system length	750 mm

Each bubble in Figure 8.20 represents a trade-off solution in terms of the image quality (abscissa), tolerance (ordinate), and number of lenses (third axis is represented by the dot color). The number of lenses used by each system is also printed inside the bubbles, and the bubble size is proportional to the number of lenses. For comparison, we also plot the actual MUX design characteristics from the engineering and qualification models in Figure 8.20 using diamonds. The number of lenses reported for the MUX QM and EM models excludes the floating/sliding lens used in the focusing mechanism.

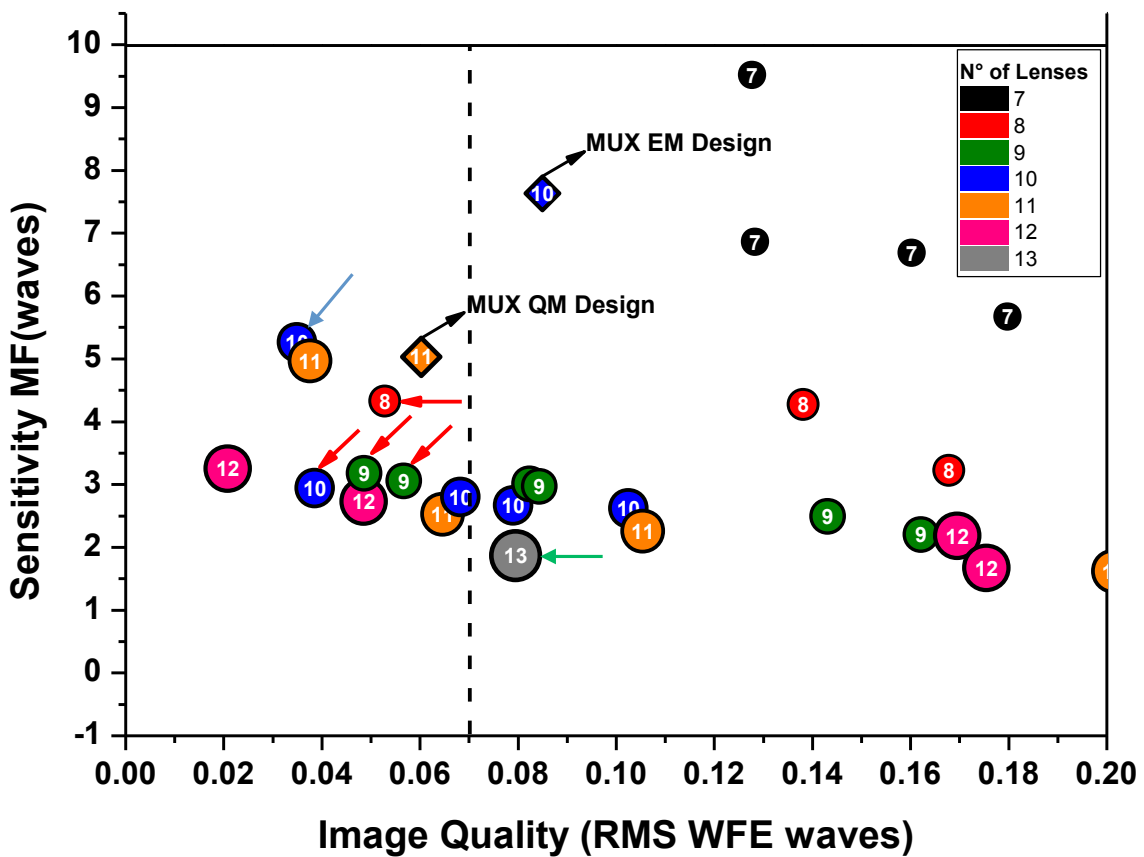


Figure 8.20 - Pareto front for the telephoto experiment using the image quality, tolerancing, and number of lenses to drive the search.

It is easy to see that both the MUX QM and EM designs are dominated by the designs found with the methodology proposed in this thesis. The designs located to the left of the dashed line are considered to be diffraction limited according to Strehl ratio criterion (SHANNON, 1997). The automatic design algorithm has identified 10 diffraction-limited solutions that comply with MUX first-order optical requirements. The upper limit for the image quality that

complies with the minimum MTF required for MUX optical system is an RMS WFE of 0.14 waves. We identified 19 systems with an RMS WFE better than 0.14 using the proposed methodology.

The red arrows in Figure 8.20 identify solutions that are considered to be good trade-offs. These solutions were visually selected by the position they hold in the Pareto front. The layout and respective MTF and Seidel diagram plots of these selected trade-off solutions are shown in Figure 8.21, Figure 8.22, Figure 8.23, and Figure 8.24. Note that the polychromatic MTF is very high in all cases.

For comparison purposes, we show in Figure 8.25 and Figure 8.26 the data for the best image quality system composed of less than twelve lenses, and for the least sensitive system, which complies with MUX image quality requirement, respectively. These two systems are identified in Figure 8.20 by the blue and green arrows respectively.

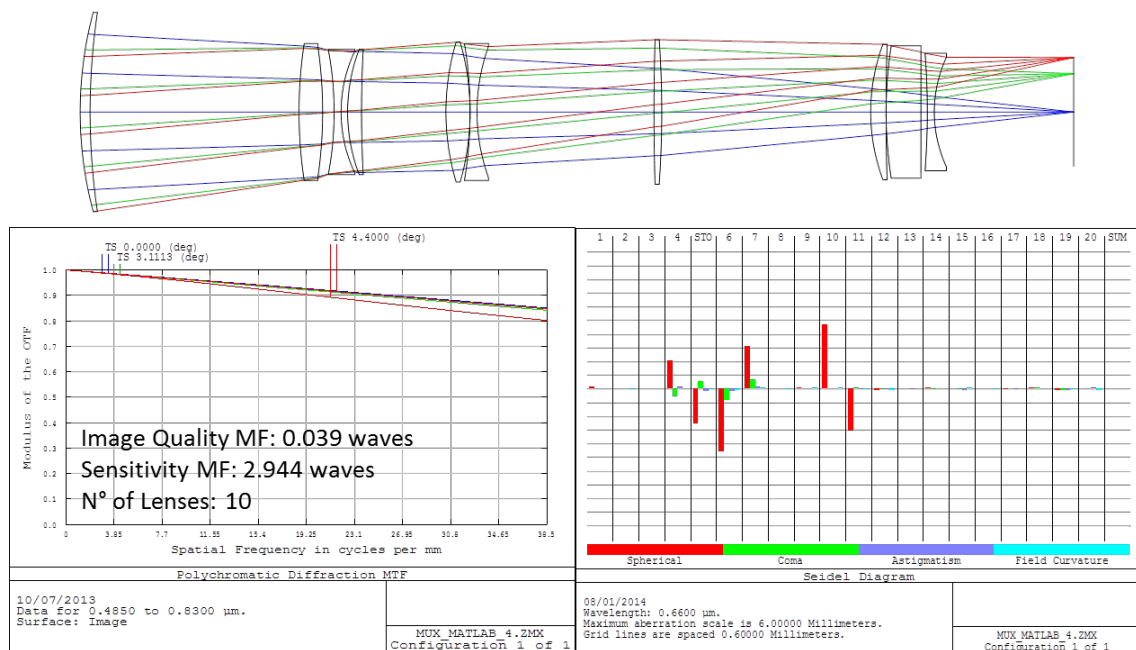


Figure 8.21 – Layout, MTF and Seidel diagram plots for one of the non-dominated MUX designs selected from the Pareto front. This 10-lens system has an image quality metric of 0.039 waves and a tolerancing metric of 2.944 waves.

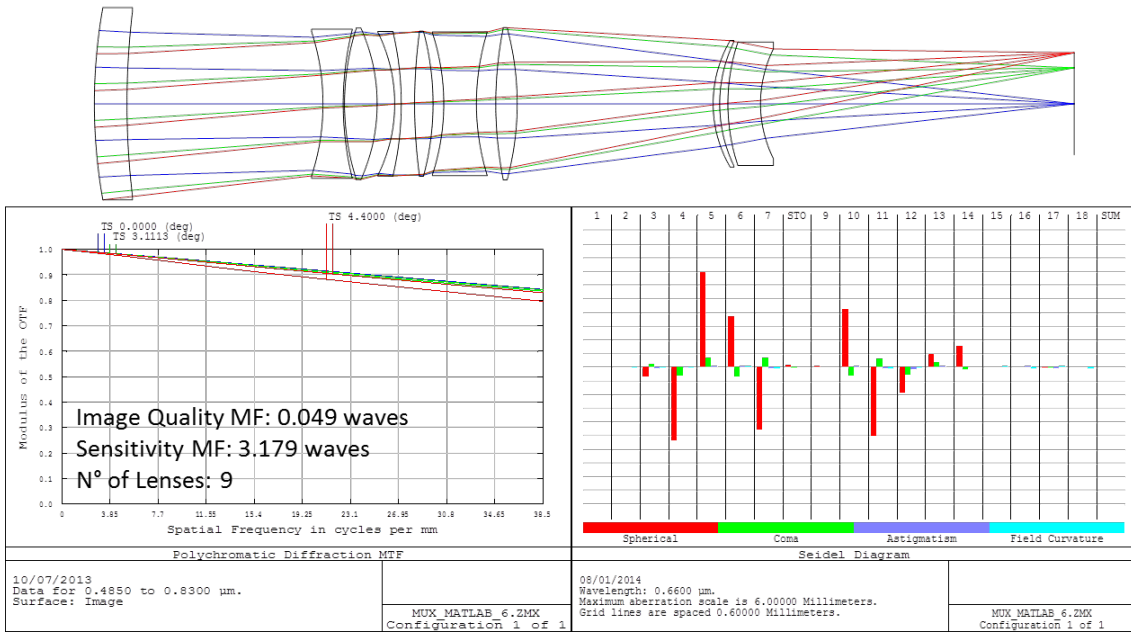


Figure 8.22 - Layout, MTF and Seidel diagram plots for one of the non-dominated MUX designs selected from the Pareto front. This 9-lens system has an image quality metric of 0.049 waves and a tolerancing metric of 3.179 waves.

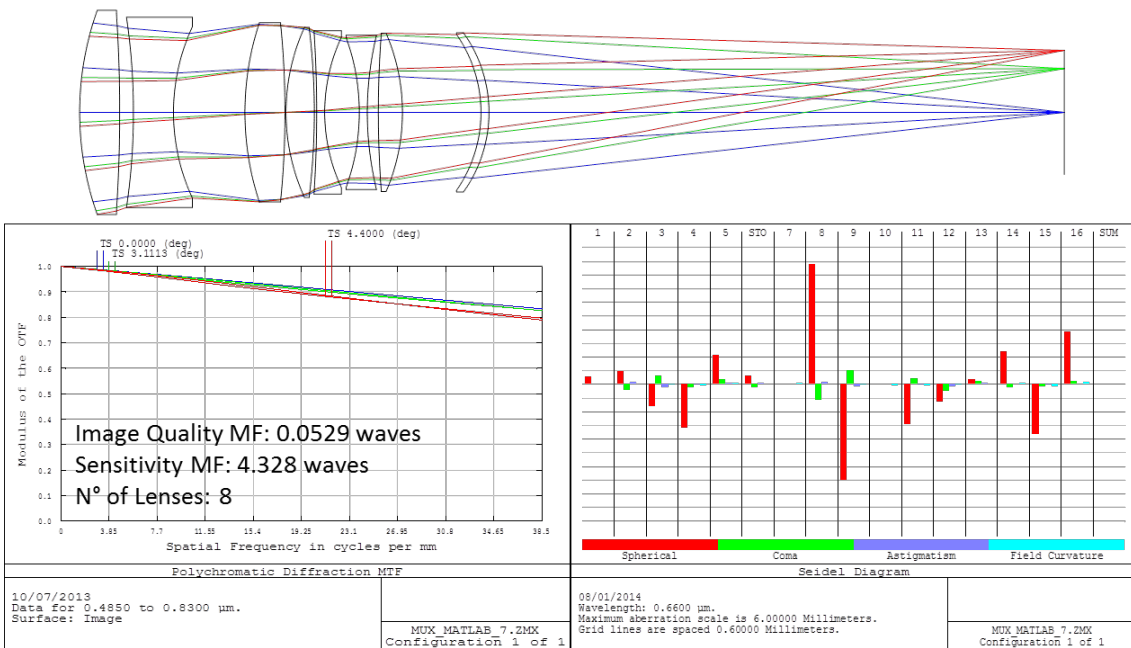


Figure 8.23 - Layout, MTF and Seidel diagram plots for one of the non-dominated MUX designs selected from the Pareto front. This 8-lens system has an image quality metric of 0.0529 waves and a tolerancing metric of 4.328 waves.

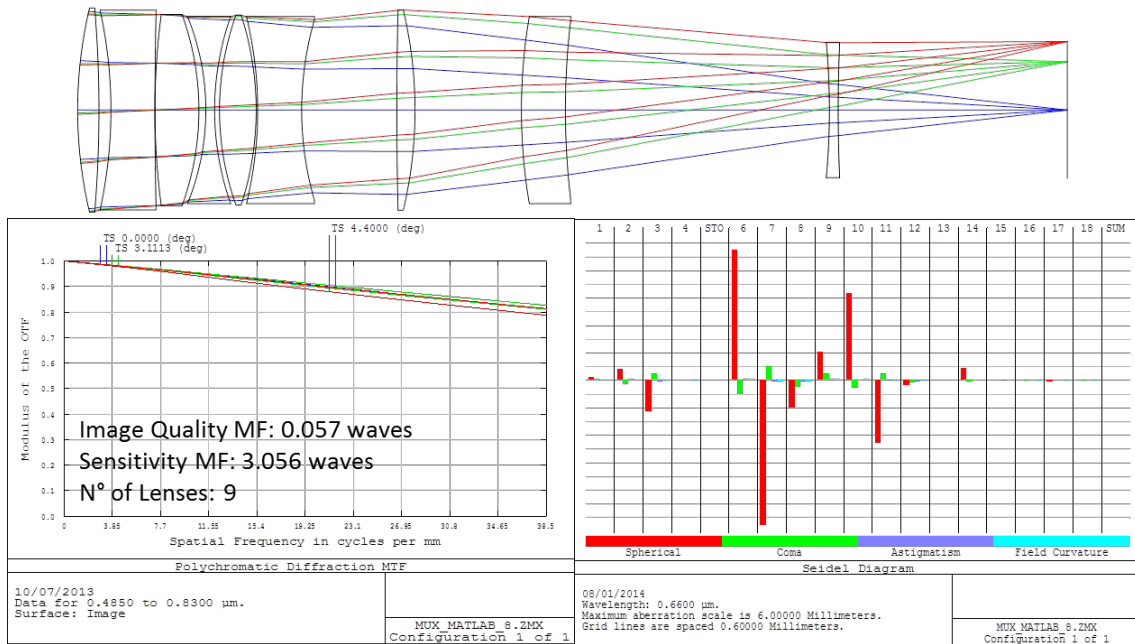


Figure 8.24 - Layout, MTF and Seidel diagram plots for one of the non-dominated MUX designs selected from the Pareto front. This 9-lens system has an image quality metric of 0.057 waves and a tolerancing metric of 3.056 waves.

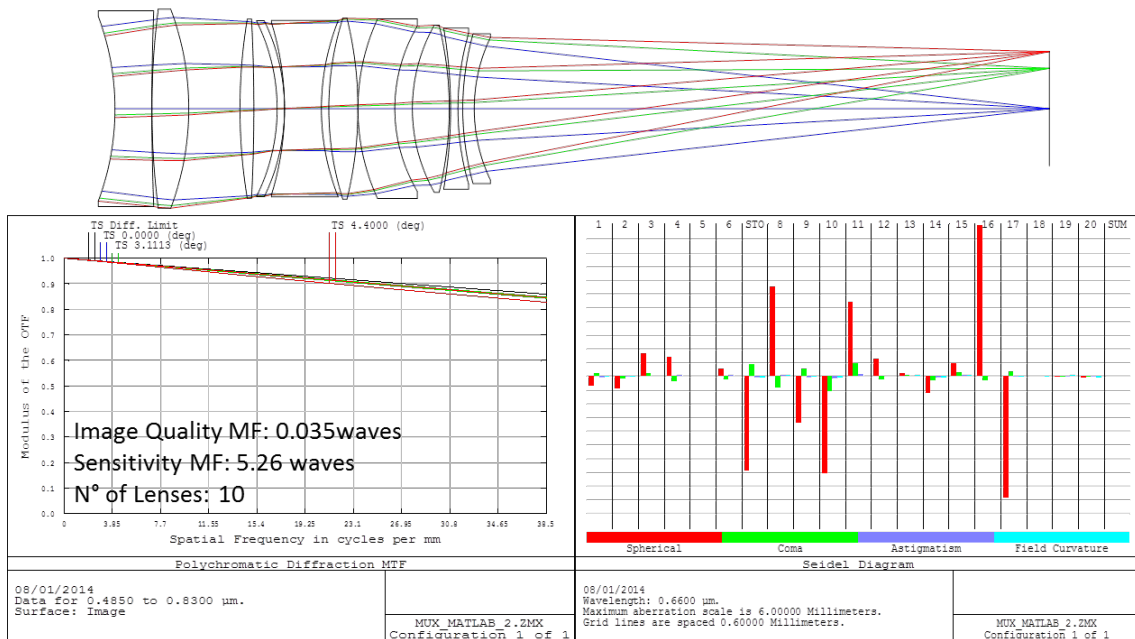


Figure 8.25 - Layout, MTF and Seidel diagram plots for the best image quality MUX system composed of less than twelve lenses. This 10-lens system has an image quality metric of 0.035 waves and a tolerancing metric of 5.26 waves.

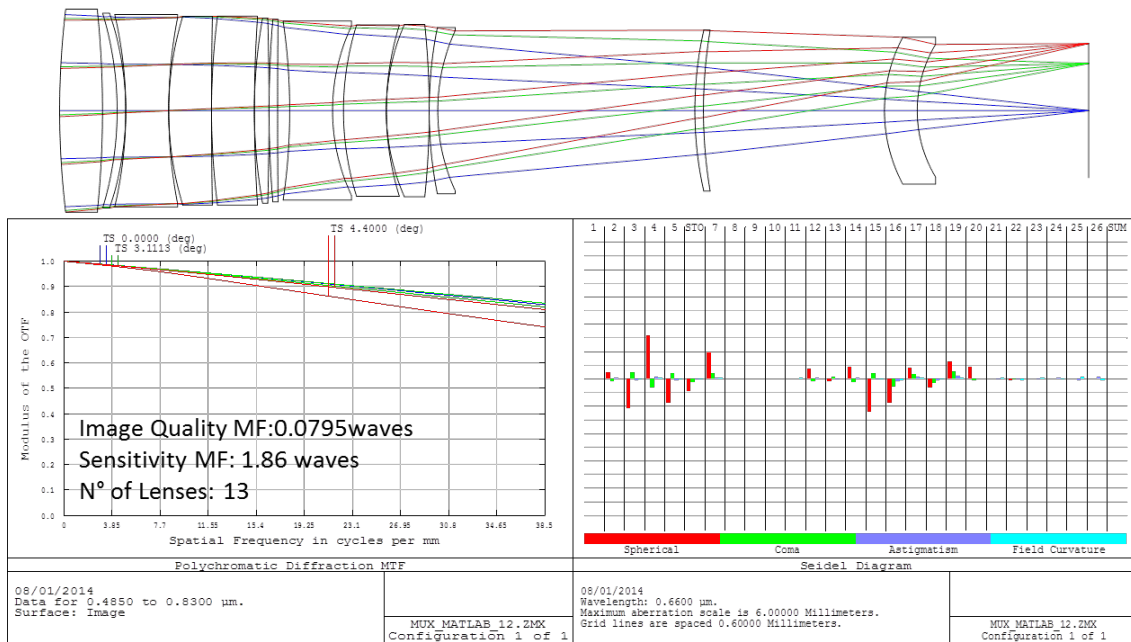


Figure 8.26 – Layout, MTF and Seidel plots for the least sensitive system that complies with MUX image quality requirement. This 9-lens system has an image quality metric of 0.0795 waves and a tolerancing metric of 1.86 waves.

Indeed some lens shapes in these designs are unusual. Some of the negative lenses are too thick, some positive and low power meniscus lenses are too thin, and some of the edge space between the lenses is too small. However, the designer can fix these small problems manually without significantly compromising either the image quality or the system sensitivity. These unusual lens shapes can be avoided by imposing more elaborate constraints during the automatic design.

Also for comparison purposes, we show the design layout and respective polychromatic MTF curves for both the MUX EM and QM in Figure 8.27 and Figure 8.28, respectively. Both the MUX EM and QM were designed using usual design methodologies: lens systems data banks, first and third order analysis and optimization tools from commercially available optical design software, combined with designer intervention as needed during the process. The company contracted to develop the MUX subsystem took many months to fully accomplish the design. In fact, the MUX optical design used in the EM was released in the September 2005 MUX monthly report (OPTO ELETRONICA SA, 2005) approximately eight months after the contract start.

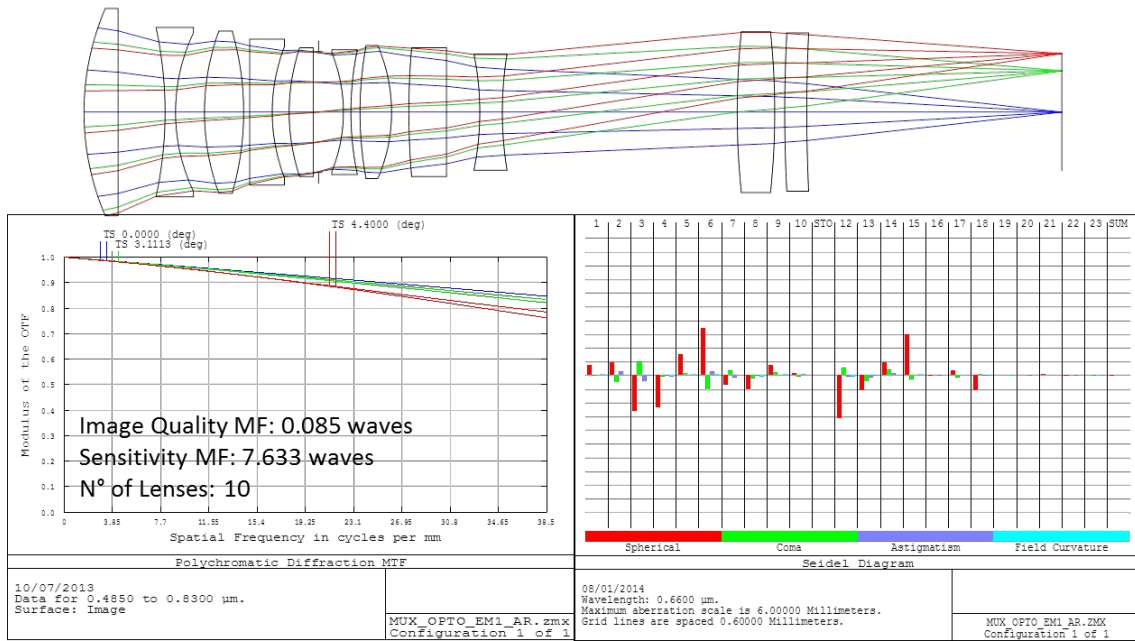


Figure 8.27 – Layout, MTF and Seidel diagram plots for the MUX EM design. This 10-lens system has an image quality metric of 0.085 waves and a tolerancing metric of 7.633 waves.

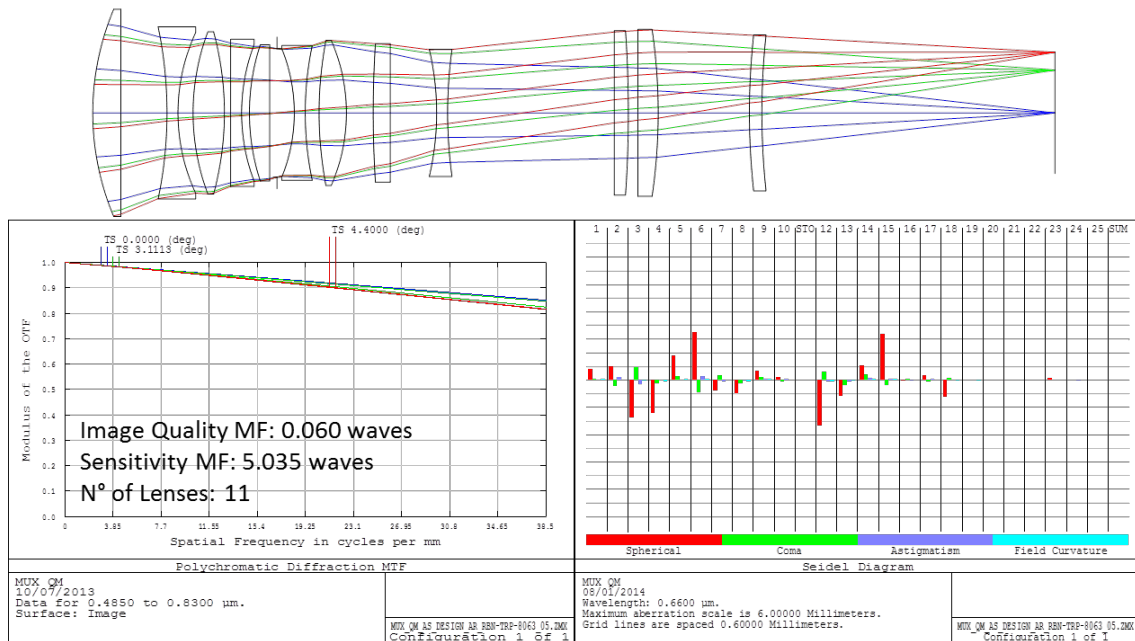


Figure 8.28 - Layout, MTF and Seidel diagram plots for the MUX QM design. This 11-lens system has an image quality metric of 0.060 waves and a tolerancing metric of 5.035 waves.

On the other hand, with our proposed automatic design method running for approximately one week on three different computing systems, we determined approximately ten diffraction-limited systems that comply with the MUX first-

order optical requirements. These systems are not final designs and the compliance with all the MUX subsystem requirements was not verified, for instance the thermal stability requirement, which was one of the important drivers in the MUX QM and EM designs. However, they provide great starting points for further optimizations by presenting an excellent overview for the designer about the available tradeoffs in terms of image quality, sensitivity and number of lenses. The potential systems are not dominated in terms of the image quality, sensitivity, and number of lenses by the actual MUX designs. Furthermore, our designs require only three glasses, while the MUX EM, for instance, requires eight different glasses from two different suppliers. When compared with a three glass system, the production of the eight glass system is more complicated, expensive, and time consuming.

With the success in applying our automatic design method to the MUX lens design, we can clearly see the great potential of our method when it is applied to real-world optical problems.

9 LIMITATIONS OF THE METHOD AND FUTURE WORK IDEAS.

The main goal of this thesis was to propose, develop and test a new methodology to automatically design optical systems from scratch that considers, during the design process, fabrication aspects. To achieve this goal in a time-limited scheduling, without loss of generality, it was necessary to restrict the implementation of the method to deal with only rotationally symmetrical optical systems composed of singlet spherical lenses, which are the most traditional kind of systems.

Now, that we have verified the efficiency of the new proposed methodology through the carried out experiments, it is time to discuss the method expansion and improvements ideas and insights for future work in order to incorporate more elaborated aspects to overcome the current restrictions: aspherical surfaces, reflective and catadioptric systems, non-rotationally symmetrical systems and cemented lens.

Some of these expansion and/or improvements are easy and straightforward to perform, others, on the other hand, requires significant amount of work to be implemented. In the following sections, each one of these aspects is discussed and ideas for future work are presented. Implementing or testing any of the improvements, extensions and upgrades of the method discussed in the following paragraphs, is out of the scope of this work.

9.1. Aspherical Surfaces

Aspherical lens is a lens with at least one of the surfaces with a non-spherical profile. Generally, the non-spherical profile is described by a conic or a polynomial with rotational symmetry but not necessarily. Aspherical lenses and mirrors are helpful for controlling aberrations in optical systems. The use of this type of surface can improve system performance and/or reduce the number of optical elements needed in a system. High quality aspherical surfaces are more complicated and expensive to fabricate as well as test, when compared to spherical lenses. Improvements in the fabrication and test techniques in the last

years made aspherical elements popular in commercial high-mass production products. Therefore, it is very important to consider aspherical surfaces in the future versions of the method.

The foreseen effort necessary for considering aspherical surfaces in the automatic design method presented herein is not huge. At least two different approaches can be tested in considering aspheres.

In the first approach, the aspherical surfaces are considered from the very beginning of the search to the end, going from the random first candidate solution creation, passing through the exploration phase and going to the exploitation phase of the method.

In this case, standard aspherical surfaces, described by even asphere polynomial, are preferable. The metrics used in the exploration phase are valid for aspherical surfaces of this type with order equal or lower than six, limited by the image quality metric (SASIAN, 2010). For this reason, the aspherical surfaces during the exploration phase have to be limited to sixth order, what is more than enough for finding rough solutions, which is the purpose of this phase. For the exploitation phase, such restriction does not exist, and the order of the polynomial can be increased if necessary.

In this approach, the representation of the candidate solutions in O-GEO needs to be changed. Each lens of the system in the candidate string representation (see Figure 6.3) shall be capable of bringing the aspherical information of each surface: conic constant (2nd order), 4th and 6th order coefficients. This can increase each lens codification in six cells, three for each surface.

During the exploration phase the change in the aspherical coefficients can be made by the continuous variables mutation diversity operand. Normally, the number of aspherical surfaces used in a system is limited due to cost. In such case, it might be necessary constraints to control the number of aspherical surfaces in the system and also other specific diversity operands to deal with

the aspherical surfaces, for instance, to transform a spherical surface in aspherical and vice-versa.

The second possible approach is considering aspherical surfaces only in the exploitation phase. In this approach, an automatic method to select the most appropriate surfaces to place an asphere can be used, something similar to the method described by Yabe, (2005; 2010) but customized for the method. This approach seems more straightforward and simpler to be implemented. It also makes easier the control of the number of aspheric surfaces and makes possible the use of any polynomial to describe aspherical surfaces, including the recently introduced orthogonal polynomial basis (FORBES, 2010).

9.2. Catoptric and Catadioptric Systems.

Catoptric and catadioptric optical systems are the ones who take advantage of mirrors with optical power. Catoptric systems are only composed of mirror elements. On the other hand, catadioptric combines mirrors and lenses in a single system.

Normally, catoptric systems are composed of just few elements, typically from one to four, each one with a single optical surface. Designs of this kind have representative closed-form analytical solutions in terms of image quality. They also involve complex constraints to guarantee the real path of the rays and to avoid mechanical interference of non-consecutive elements. Moreover, many of the useful catoptric designs take advantage of aspherical elements and non-rotational symmetric construction, complicating even more the physical constraints involved.

Catadioptric systems are normally formed by a subset with few elements containing reflective surfaces, one or two typically, and a dioptric group, which can be composed by many lenses. The subset containing the reflective surfaces normally has a specific architecture to perform a specific task, which can many times involve double pass ray path. As well as catoptric systems, this

group in the catadioptric system implicates complex constrains of the same nature.

The complexity required in the constrains definition, double-pass modeling and aspherical surfaces treatment, associated with small number of reflective elements and possible closed-form analytical solution, discourage the coverage of catoptric and catadioptric systems by the method proposed herein in this first stage of the development.

The expansion of the method to treat catoptric system would require the change in the solution representation in O-GEO, exclusion of the glass selection phase, and exclusion of the glass mutation diversity operand, which might not be complex tasks to accomplish. The biggest foreseen challenge is to write generic rules in the form of codes to control or even just to check the violation of the complex constrains involved in such systems.

The effort necessary to change the method in order to cover the design of catadioptric system might be considerable, if all the tools of the method are desired to work in this class of systems. For instance: i) the codification in O-GEO has to be changed to codify refractive and reflective elements in a single system; ii) the de-codification function that takes the O-GEO system to the simulator needs to be able to automatic identify double pass surfaces and model them properly in the simulator; iii) diversity operands needs to have the capability to transform a refractive element into a reflective element and vice-versa; iv) it is necessary to create functions to control the number of reflective surfaces in the system as well as the complex mechanical and ray path constrains involved in such systems; etc.

Nevertheless, if we sacrifice the exploration range of the method for catadioptric systems, the effort to cover such class of systems might be significantly reduced. In this case, a rough initial configuration for the system has to be supplied by the designer and the subgroups of the design containing the reflective surfaces and double pass elements have to be identified. In this approach, these identified subgroups are not allowed to suffer radical changes,

that mean: the number of elements and the type of surface (reflective or refractive) cannot be changed. For the other subgroups in the system, containing only refractive elements, the method can be applied with no restriction.

9.3. Non-rotationally Symmetrical Systems.

In optical design, a specific class of non-rotationally symmetrical system that has a particular interest is the plane-symmetric kind. In these systems there is at least one plane of symmetry, that is, one half of the system is a mirror image of the other. This includes: off-Axis, tilted, and decentered systems, and combination of them.

An off-axis optical system is an optical system in which the aperture stop or/and the field of view are shifted in relation to the mechanical center of the system surfaces. Tilted and decentered systems are the ones where the surfaces are tilted and/or decenter in relation to each other in the plane of symmetry. The main applications of non-rotationally optical systems are to avoid obstruction of the primary aperture by secondary optical elements and provide access to the image.

In order to make the method able to cover this class of optical system, it is necessary to change at least two things: the optical system representation in O-GEO; and the objective functions used in the exploration phase, either the Image quality and system sensitivity.

The representation of the candidate solutions in O-GEO needs to codify the surface tilt and decenter. As the systems of interest are plane symmetrical, two new fields for each surface would be necessary in the codification, that means four new fields for the refractive elements (two for each surface) and two for the reflective surface. These new fields in the system codification can be treated as continuous variables within a range defined by the designer, being perturbed by the continuous variables mutation.

These merit functions in the exploration phase were derived from the wave aberration function for the specific case of a rotationally symmetrical systems therefore, are not valid for non-rotational systems. In this case, new merit functions have to be defined. Fortunately there are some papers that discuss the wave aberration function coefficients for non-rotationally symmetrical systems (SAND, 1972; SASIAN, 1994; THOMPSON, 2005; MOORE *et al*, 2008; WANG *et al*, 2012).

Scanning these papers, it seems that the work from Thompson (2005) is a good point to start from. According to his developments and the works he uses as reference, the total system aberration field holds the same property for either rotationally or non-symmetrical optical systems. In both cases the total system aberration field is given by the sum of individual surfaces contributions. The difference is that in rotationally symmetrical systems, the centers of the aberration field contribution for each surface coincide with the optical axis in the image, and in non-symmetrical system they don't, being each surface j centered at a different point in the image, specified by the vector $\vec{\sigma}_j$. This point in the image plane is a function of the tilt and decenter of each surface, given by the projection of a line connecting the center of the pupil for the surface of interest with the center of curvature of that surface to the image plane.

It seems very reasonable that the image quality and sensitivity metric, for the exploration phase, can both be derived from Thompson (2005) work. In his paper he also derives, for non-symmetrical system, an expression for the RMS wave front error for a field point. This is one of the steps necessary to define the image quality metric following the same rationally used in the proposed method.

To finally get the image quality metric for the exploration phase, it is necessary to integrate the RMS wave front error over the whole field, which is not necessarily symmetric in this case. The sensitivity metric, on the other hand, can be derived through the differentiation of the wave front error function with respect to the vector $\vec{\sigma}_j$.

9.4. Cemented Lens.

Cemented lens are literally lenses that are stick together using a common radius of curvature surface as interface. The adhesives used are optically transparent. The most usual cemented lenses are doublet (composed of two lenses) and triplets (composed of three lenses). The glass materials used in two subsequent cemented lenses are different. Lenses are cemented mainly to reduce aberration (in most cases chromatic), surface reflection and assembling tolerance and costs.

Cemented lens are not allowed to happen in the automatic lens design method presented herein. However, as discussed in Chapter 8, Section 8.2.3, it was possible to observe some solutions that came out from the method, which suggests the cementing between some lenses in the system. These lenses are the ones that ended up becoming both, very close in distance and consecutive curvatures. In many of these cases the designer, in a later stage of the project, can change the lenses to cement without impacting the design performance and architecture.

Nevertheless, in some cases, cemented lens are used to bend relatively high angle optical rays without introducing too much aberration and avoiding total internal reflection of the light. In these cases, the cemented lens shall be considered since the beginning of the design process. To cover for these cases, the method needs some changes. The necessary modification on the method to cover for cemented lens doesn't seems to be very complex. Probably, there is more than one way of doing this but, here the method that seems the most straightforward is discussed.

If in the O-GEO codification the second surface material (M_2) of a lens is allowed to assume values different to zero, that means, it is allowed to assume optical materials different from air (vide section 6.2.1), we immediately get cemented lenses, triplets in this case. To get doublets, it would be necessary, apart from letting the M_2 assume different values, to force T_{2j} to be zero and R_{2j} to be equal to R_{1L} , for $M_{2j} \neq 0$, where j and L represent two consecutive

lenses in the system (not necessarily consecutive in the O-GEO lens codification).

New diversity operands are necessary to transform the lenses in the system in doublet or triplets and vice-versa. Also, it is necessary to control by penalty constrains the total allowed number of cemented lenses in a system.

9.5. System Thermal Stability

A very important aspect in optical design, mainly for spaceborne and infrared optical system, is the thermal image quality stability. The changes in the temperature modify not only the system geometry dimensions, but also change the index of refraction of the glasses. Depending on the design of the system and the optical material used, the changes caused by few degrees can drastically drop the image quality. For this reason, the thermal stability must be considered in the design of optical systems. The method proposed herein does not consider these aspects during the search. Nevertheless, there is the possibility of including these considerations in future versions of the method during the search process for uniform temperatures intervals (not considering gradients).

The thermal effects can be considered in all phases of the method. Starting in the glass selection, the thermal stability for each glass combination can be computed and used as a new metric in the multi-objective approach used for choosing the glasses combinations. The stability can be computed for each possible combination using the equations presented in Jamieson (1992) for two and three glasses, and if necessary, expanded for more glasses with the same rationally presented in the paper.

During the exploration phase, the equation also derived in Jamieson (1992) that gives the defocusing term in waves with respect to the temperature variation for a multiple lens system, can be used. The defocussing term W_{020} in the wave aberration function (vide Section 7.2.1.1; Equation. 7.6) is then not anymore considered zero for the principal wavelength λ_0 but is a function of the

temperature change. The designer needs to provide the temperature interval for which the system shall work. Half of this temperature range can be used as the delta in temperature to compute the defocussing term W_{020} . As the image quality metric during the exploration phase is calculated from the wave aberration function, it will then consider the temperature effects in the image quality metric.

During the exploitation phase, a multi-configuration approach can be used for the temperature effects consideration; just like is done in some commercial optical design software. In this approach two (or more) systems dependent to each other, are modeled and simulated at once. The temperature effects give the differences among these systems in each configuration. The radii, thicknesses and refractive index in each one of the configurations is slightly different, given as a function of the temperature in each configuration. The image quality metric can be then computed as the average of the individual image quality in each temperature or configuration. Doing so, the temperature effects are used during the exploitation optimization process.

10 CONCLUSIONS

Problems faced during the fabrication of high-performance optical systems for space applications motivated not only the investigation of available methods and techniques for fabrication and assembling, but also the exploration of methods and techniques of designing lens systems for fabrication by considering the final system as-built performance.

Studying the available methods of optical design and optimization, we realized that all presented approaches had drawbacks or missing points that could be improved or better explored. We selected several important points to investigate in this thesis: (i) design from scratch, (ii) multi-objective approach considering not only the image quality, but also the system complexity and sensitivity, (iii) optimum choice of lens materials for color correction, and (iv) broad exploration of the design space to find the best possible trade-off solutions.

With these points in mind, a novel automatic optical design method was born. The new automatic design method is based on a multi-objective memetic optimization algorithm. The multi-objective approach simultaneously, but separately, optimizes the image quality, tolerance, and complexity of the system. The memetic technique divides the search for optical designs into three different phases: glass selection; exploration; and exploitation. In this thesis, we concentrated the majority of our effort in the development of the glass selection and exploration phases.

The application of the automatic lens design method presented in this thesis only need the system requirements as input. As a result, our method provides a family of trade-off designs supplying the designer with a complete picture of the available possibilities.

The proposed method includes several scientific contributions on a number of different levels. The overall design strategy has particular characteristics: (i) the three phases involved, their sequences and loops (see Figure 5.1); the design

from scratch and the multi-objective approach considering fabrication issues are some of these particularities.

The glass selection method presented herein, merges two pre-published methods and integrates significant original contributions: (i) generalize the glass selection techniques in terms of number of glasses and wavelengths, (ii) repair practical implementation issues, (iii) and incorporates a multi-objective approach. This gives rise to a new method of glass selection that offers significant advantages, leading to an optimal choice of optical glasses for specific problems as demonstrated in Section 6.1.1 and verified in Chapter 8 and in Albuquerque *et al.* (2012).

The novel EO algorithm developed for the exploration phase was based on a customization of the GEO algorithm. The newly developed O-GEO algorithm incorporates many features into a single algorithm. The search is driven by three different metrics in a multi-objective approach: image quality, tolerance, and number of lenses. Our method allows variation of the number of lenses during the search, which has only been explored once before in a computationally demanding study (KOZA *et al.*, 2005). Furthermore, our O-GEO method is one of few EO algorithms customized for optical design, incorporating different diversity operands suitable for the problem by mimicking techniques that are traditionally applied manually by optical designers, which is a new strategy for EO algorithms applied to lens design problems. The codification proposed for the solutions in O-GEO makes many of the algorithm features possible.

The image quality and sensitivity metrics applied during the exploration phase are other major contributions to this work. These computationally efficient metrics provide a good approximation of the system characteristics and robustly handle the situation when a real ray cannot be traced through the system.

As we presented in Chapter 8, our proposed method is capable of finding competitive optical designs from scratch. It is a powerful method for designing simple, insensitive systems, providing the designer with many trade-off options

with systems presenting different architectures. In addition to providing great results, our method was demonstrated to be computationally efficient when compared to commercial optical design software.

Despite the proposed method has shown excellent results for the experiments carried out, it does have limitations and room for improvements. In Chapter 9 we discussed in details these limitations and gave ideas for future work implementations in order to improve the method and overcome its current restrictions. As shown, it is feasible to expand the method to incorporate:

- Aspherical Surfaces;
- Catoptric and catadioptric systems;
- Non-rotationally symmetrical systems;
- Cemented lenses;
- Thermal stability aspects.

During the whole Ph.D. program, the author participated in the publication of a total of seven papers, three conference papers and four journal papers. From these, three are directly related with the theme of this thesis, including a high impact journal paper. A list of the publications is given below in chronological sequence. The papers directly related with the thesis subject are marked with *.

PONZONI, F. J.; ALBUQUERQUE, B. F. C. Pre-launch absolute calibration of ccd/cbers-2b sensor. **Sensors**, MDPI, Switzerland, v. 8, n. 10, p. 6557–6565, Oct. 2008. ISSN 1424-8220.

ALBUQUERQUE, B. F. C.; LOPES, R. V. F.; KUGA, H. K.; CARVALHO, E. G. de; SCADUTO, L. C. N.; STEFANI, M. A. Misalignment parameters estimation in refractive optical systems. In: OPTICAL SYSTEM ALIGNMENT AND TOLERANCING, 2., 2008, San Diego, CA. **Proceedings...** Bellingham, WA: SPIE, 2008. v. 7068, p. 70680P–1–70680P–17.

BERNI, L. A.; ALBUQUERQUE, B. F. C. Stray light analysis for the thomson scattering diagnostic of the ete tokamak. **Review of Scientific Instruments**, AIP, Melville, NY, v. 81, n. 12, p. 123504–1–123504–6, Dec. 2010. ISSN 0034-6748.

*ALBUQUERQUE, B. F. C.; SOUSA, F. L. Preliminary results of the generalized extremal optimization algorithm applied in the design of optical systems. In: LATIN AMERICA OPTICS AND PHOTONICS CONFERENCE (LAOP), 2010, Recife, Brazil. **Proceedings...** Washington, DC: Optical Society of America, 2010. p. WE16. ISBN 9781557529.

*ALBUQUERQUE, B. F. C. de; LIAO, L.-Y.; MONTES, A. S.; SOUSA, F. L. de; SASIÁN, J. A multi-objective approach in the optimization of optical systems taking into account tolerancing. In: OPTICAL SYSTEM ALIGNMENT, TOLERANCING, AND VERIFICATION, 5., 2011, San Diego, CA. **Proceedings...** Bellingham, WA: SPIE, 2011. v. 8131, p. 813105–1–813105–9.

*ALBUQUERQUE, B. F. C.; SASIÁN, J.; DE SOUSA, F. L.; MONTES, A. S. Method of glass selection for color correction in optical system design. **Opt. Express**, OSA, v. 20, n. 13, p. 13592–13611, Jun. 2012. ISSN 1094-4087.

LIAO, L.-Y.; ALBUQUERQUE, B. F. C.; PARKS, R. E.; SASIAN, J. M. Precision focal-length measurement using imaging conjugates. **Optical Engineering**, v. 51, n. 11, p. 113604–113604, Nov. 2012. ISSN 0091-3286.

Also during the Ph.D. program, the author was awarded with the Michael Kidger memorial scholarship in optical design due to his achievements in the area.

REFERENCES

ABREU, B.; MARTINS, E.; DE SOUSA, F. L. Automatic test data generation for path testing using a new stochastic algorithm. In: SIMPÓSIO BRASILEIRO DE ENGENHARIA DE SOFTWARE (SBES), 19., 2005, Uberlândia. **Proceedings...** [S.l.]: SBC, 2005. p. 247–262. ISBN 85-7669-030-6.

ABREU, B. T. D.; MARTINS, E.; DE SOUSA, F. L. Generalized extremal optimization: a competitive algorithm for test data generation. In: SIMPÓSIO BRASILEIRO DE ENGENHARIA DE SOFTWARE (SBES), 21., 2007, João Pessoa. **Proceedings...** [S.l.]: SBC, 2007. p. 342–358.

AGÊNCIA ESPACIAL BRASILEIRA. **Programa nacional de atividades espaciais: PNAE** : 2012 - 2021. Brasília, 2012. 36 p. Available on: <<http://www.aeb.gov.br/wp-content/uploads/2013/01/PNAE-Portugues.pdf>>. Accessed on: 23 sep. 2013.

AGUIRRE, O.; TABOADA, H.; COIT, D.; WATTANAPONGSAKORN, N. Multiple objective system reliability post-Pareto optimality using self organizing trees. In: QUALITY AND RELIABILITY (ICQR), IEEE INTERNATIONAL CONFERENCE ON, 2011, Bangkok. **Proceedings...** New York: IEEE, 2011. p. 225–229. ISBN 978-1-4577-0626-4.

ALBUQUERQUE, B. F. C. de; SASIÁN, J.; DE SOUSA, F. L.; MONTES, A. S. Method of glass selection for color correction in optical system design. **Opt. Express**, OSA, v. 20, n. 13, p. 13592–13611, Jun. 2012. ISSN 1094-4087.

BACK, T.; HAMMEL, U.; SCHWEFEL, H.-P. Evolutionary computation: comments on the history and current state. **Evolutionary Computation, IEEE Transactions on**, v. 1, n. 1, p. 3–17, Apr. 1997. ISSN 1089-778X.

BAK, P.; SNEPPEN, K. Punctuated equilibrium and criticality in a simple model of evolution. **Phys. Rev. Lett.**, v. 71, n. 24, p. 4083–4086, Dec. 1993. ISSN 1079-7114.

BEAULIEU, J.; GAGNÉ, C.; PARIZEAU, M. Lens system design and re-engineering with evolutionary algorithms. In: GENETIC AND EVOLUTIONARY COMPUTATION CONFERENCE (GECCO), 2002, New York. **Proceedings...** San Francisco, CA, USA: Morgan Kaufmann Publishers Inc., 2002. p. 155–162. ISBN 1-55860-878-8.

BIANCHI, L.; DORIGO, M.; GAMBARDELLA, L.; GUTJAHR, W. A survey on metaheuristics for stochastic combinatorial optimization. **Natural Computing**, v. 8, n. 2, p. 239–287, Jun. 2009. ISSN 1567-7818.

BLASCO, X.; HERRERO, J. M.; SANCHIS, J.; MARTÍNEZ, M. A new graphical visualization of n-dimensional Pareto front for decision-making in multiobjective optimization. **Information Sciences**, v. 178, n. 20, p. 3908–3924, Oct. 2008. ISSN 0020-0255. Special Issue on Industrial Applications of Neural Networks 10th Engineering Applications of Neural Networks.

BLUM, C.; ROLI, A. Metaheuristics in combinatorial optimization: overview and conceptual comparison. **ACM Comput. Surv.**, v. 35, n. 3, p. 268–308, Sep. 2003. ISSN 0360-0300.

BOETTCHER, S. Extremal optimization: heuristics via coevolutionary avalanches.

Computing in Science and Engineering, v. 2, n. 6, p. 75–82, Nov.-Dec. 2000. ISSN 1521-9615.

BRANKE, J.; DEB, K.; MIETTINEN, K.; SLOWIŃSKI, R. **Multiobjective optimization**: interactive and evolutionary approaches. Berlin: Springer, 2008. 470 p. ISBN 978-3-540-88907-6.

CANON U.S.A., INC. **EF 400mm f/5.6L USM super telephoto**. Canon U.S.A., Inc. Canon lens specification. Available on:
<http://www.usa.canon.com/cusa/consumer/products/cameras/ef_lens_lineup/ef_400mm_f_5_6l_usm#Specifications>. Accessed on: 01 Jul. 2013.

CASSOL, F.; SCHNEIDER, P. S.; FRANÇA, F. H.; SILVA NETO, A. J. Multi-objective optimization as a new approach to illumination design of interior spaces. **Building and Environment**, v. 46, n. 2, p. 331–338, Feb. 2011. ISSN 0360-1323.

CAVAZZUTI, M. **Optimization methods**: From theory to design scientific and technological aspects in mechanics. Berlin: Springer, 2013. 350 p. ISBN 978-3-642-31186-4.

CHEN, X.; YAMAMOTO, K. Genetic algorithm and its application in lens design. In: CURRENT DEVELOPMENTS IN OPTICAL DESIGN AND ENGINEERING, 6., 1996, Denver, CO. **Proceedings...** Bellingham, WA: SPIE, 1996. v. 2863, p. 216–221.

COELLO COELLO, C. A. Handling preferences in evolutionary multiobjective optimization: a survey. In: EVOLUTIONARY COMPUTATION, CONGRESS ON, 2000, La Jolla, CA. **Proceedings...** New York: IEEE, 2000. v. 1, p. 30–37.

COLAÇO, M. J.; DULIKRAVICH, G. S. A survey of basic deterministic, heuristic and hybrid methods for single objective optimization and response surface generation. In: ORLANDE, H. R. B.; FUDYM, O.; MAILLET, D.; COTTA, R. M. (Ed.). **Thermal measurements and inverse techniques**: heat transfer. Boca Raton: CRC Press, 2011. p. 355–405. ISBN 978-1-4398-4555-4. Cap. 10.

CUCO, A. P. C.; DE SOUSA, F. L.; VLASSOV, V. V.; SILVA NETO, A. J. da. Multi-objective design optimization of a new space radiator. **Optimization and Engineering**, v. 12, p. 393–406, Sep. 2011. ISSN 1389-4420.

CUCO, A. P. C.; SILVA NETO, A. J.; VELHO, H. F. C.; DE SOUSA, F. L. Solution of an inverse adsorption problem with an epidemic genetic algorithm and the generalized extremal optimization algorithm. **Inverse Problems in Science and Engineering**, v. 17, n. 3, p. 289–302, Apr. 2009. ISSN 1741-5977.

DE SOUSA, F. L.; RAMOS, F. M.; PAGLIONE, P.; GIRARDI, R. M. New stochastic algorithm for design optimization. **AIAA Journal**, v. 41, n. 9, p. 1808–1818, Sep. 2003. ISSN 0001-1452.

DE SOUSA, F. L.; SOEIRO, F. J. C. P.; SILVA NETO, A. J.; RAMOS, F. M. Application of the generalized extremal optimization algorithm to an inverse radiative transfer problem. **Inverse Problems in Science and Engineering**, v. 15, n. 7, p. 699–714, Oct. 2007. ISSN 1741-5977.

DE SOUSA, F. L.; VLASSOV, V.; RAMOS, F. M. Generalized extremal optimization: an application in heat pipe design. **Applied Mathematical Modelling**, v. 28, n. 10, p. 911–931, Oct. 2004. ISSN 0307-904X.

- DEB, K.; PRATAP, A.; AGARWAL, S.; MEYARIVAN, T. A fast and elitist multiobjective genetic algorithm: NSGA-II. **Evolutionary Computation, IEEE Transactions on**, v. 6, n. 2, p. 182–197, Apr. 2002. ISSN 1089-778X.
- EIBEN, A. E.; SMITH, J. E. **Introduction to evolutionary computing**: natural computing series. 1st. ed. Berlin: Springer, 2003. 299 p. (Natural computing series). ISBN 3-540-40184-9.
- EPPLE, A.; WANG, H. Design to manufacture: from the perspective of optical design and fabrication. In: OPTICAL FABRICATION AND TESTING, 2008, Rochester, New York. **Proceedings...** Washington, D.C: Optical Society of America, 2008. p. OFB1.
- FANG, Y.-C.; TSAI, C.-M.; MACDONALD, J.; PAI, Y.-C. Eliminating chromatic aberration in gauss-type lens design using a novel genetic algorithm. **Appl. Opt.**, OSA, v. 46, n. 13, p. 2401–2410, May. 2007.
- FERREIRA, J. C.; FONSECA, C. M.; GASPAR-CUNHA, A. Methodology to select solutions from the Pareto-optimal set: a comparative study. In: ANNUAL CONFERENCE ON GENETIC AND EVOLUTIONARY COMPUTATION (GECCO), 9., 2007, London, England. **Proceedings...** New York: ACM, 2007. p. 789–796. ISBN 978-1-59593-697-4.
- FISCHER, R. E.; GRANT, A. J.; FOTHERINGHAM, U.; HARTMANN, P.; REICHEL, S. Removing the mystique of glass selection. In: NOVEL OPTICAL SYSTEMS DESIGN AND OPTIMIZATION, 7., 2004, Denver, CO. **Proceedings...** Bellingham, WA: SPIE, 2004. v. 5524, p. 134–146.
- FOGEL, D. B. Foundations of evolutionary computation. In: MODELING AND SIMULATION FOR MILITARY APPLICATIONS, 2006, Kissimmee, FL. **Proceedings...** Bellingham, WA: SPIE, 2006. v. 6228, p. 801–814.
- FONSECA, C. M.; FLEMING, P. J. Genetic algorithms for multiobjective optimization: Formulation, discussion and generalization. In: INTERNATIONAL CONFERENCE ON GENETIC ALGORITHMS (ICGA), 5., 1993, Urbana-Champaign, IL. **Proceedings...** San Francisco: Morgan Kaufmann Publishers Inc., 1993. p. 416–423.
- FORBES, G. W. Robust, efficient computational methods for axially symmetric optical aspheres. **Opt. Express**, OSA, v. 18, n. 19, p. 19700–19712, Sep. 2010. ISSN 1094-4087.
- FORBES, G. W. Optical system assessment for design: numerical ray tracing in the Gaussian pupil. **J. Opt. Soc. Am. A**, OSA, v. 11, n. 15, p. 1943–1956, Nov. 1988. ISSN 1084-7529.
- FRIEDLAND, B. **Control system design**: an introduction to state-space methods. New York: McGraw-Hill, 1986. 513 p. (McGraw-Hill series in electrical engineering: Control theory). ISBN 9780070224414.
- SUMITOMO ELECTRIC INDUSTRIES, LTD. Keiji Fuse. **Method for designing a refractive or reflective optical system and method for designing a diffraction optical element**. US 6567226, 1 Mar. 1999, 20 may 2003.
- GAGNÉ, C.; BEAULIEU, J.; PARIZEAU, M.; THIBAUT, S. Human-competitive lens system design with evolution strategies. **Applied Soft Computing**, WFSC, v. 8, n. 4, p. 1439–1452, Sep. 2008. ISSN 1568-4946.

GALSKI, R. L. **Desenvolvimento de versões aprimoradas híbridas, paralela e multiobjetivo do método da otimização extrema generalizada e sua aplicação no projeto de sistemas espaciais**. 2006. 279 p. (INPE-14795-TDI/1238). Tese (Doutorado em Computação Aplicada) — Instituto Nacional de Pesquisas Espaciais (INPE), São José dos Campos, 2006.

GALSKI, R. L. Preliminary design of satellite constellations for a Brazilian regional positioning system by means of an evolutionary algorithm. **Journal of Aerospace Engineering, Sciences and Applications**, v. 4, n. 1, p. 52–59, Jan./Mar. 2012. ISSN 2236-577X.

GALSKI, R. L.; DE SOUSA, F. L.; RAMOS, F. M. Application of a new evolutionary algorithm to the optimum design of a remote sensing satellite constellation. In: INTERNATIONAL CONFERENCE ON INVERSE PROBLEMS IN ENGINEERING: THEORY AND PRACTICE. **Proceedings...** [S.l.], 2005. v. 2, p. G01.

GALSKI, R. L.; DE SOUSA, F. L.; RAMOS, F. M.; MURAOKA, I. Spacecraft thermal design with the generalized extremal optimization algorithm. **Inverse Problems in Science & Engineering**, Taylor & Francis, v. 15, n. 1, p. 61–75, Jan. 2007. ISSN 1741-5977. 1

GALSKI, R. L.; DE SOUSA, F. L.; RAMOS, F. M.; SILVA NETO, A. J. Application of a GEO + SA hybrid optimization algorithm to the solution of an inverse radiative transfer problem. **Inverse Problems in Science & Engineering**, v. 17, n. 3, p. 321–334, Apr. 2009. ISSN 1741-5977 and 1741-5985.

GIRARD, A. Calcul automatique en optique geometrique. **Revue d'optique théorique et instrumentale**, v. 37, p. 225–241, 1958.

GLATZEL, E.; WILSON, R. Adaptive automatic correction in optical design. **Appl. Opt.**, OSA, v. 7, n. 2, p. 265–276, Feb. 1968. ISSN 1559-128X.

GONZALEZ, T. F. **Handbook of approximation algorithms and metaheuristics**. Boca Raton: Chapman & Hall/CRC, 2007. 1432 p. (Computer & Information Science Series). ISBN 978-1-58488-550-4.

GRUESCU, C.; NICOARA, I.; POPOV, D.; BODEA, R.; HORA, H. Optical glass compatibility for the design of apochromatic systems. **Science of Sintering**, IISS, v. 40, n. 2, p. 131–140, Jun. 2008. ISSN 0350–820X.

GUO, P.; CHEN, W.; WANG, Y. A hybrid generalized extremal optimization algorithm for the quay crane scheduling problem with interference constraints. 2012. Available on: <<http://arxiv.org/abs/1210.6896>>. Accessed on: 07 Jan. 2012. 2

HARIHARAN, P. Superachromatic lens combinations. **Optics and Laser Technology**, v. 31, n. 2, p. 115–118, Mar. 1999. ISSN 0030-3992.

HECHT, E. **Optics**. 2. ed. Massachusetts: Addison-Wesley, 1987. 676 p. ISBN 978-0201116090.

HERZBERGER, M.; MCCLURE, N. R. The design of superachromatic lenses. **Appl. Opt.**, OSA, v. 2, n. 6, p. 553–560, Jun. 1963. ISSN 1559-128X.

HORN, J.; NAFPLIOTIS, N.; GOLDBERG, D. A niched Pareto genetic algorithm for multiobjective optimization. In: EVOLUTIONARY COMPUTATION, CONFERENCE

- ON, 1., 1994, Orlando, FL. **Proceedings...** New York: IEEE, 1994. v. 1, p. 82–87.
- INSTITUTO NACIONAL DE PESQUISAS ESPACIAIS (INPE). **CBERS 3&4: MUX** subsystem specification. São José dos Campos, 2006. (RBN-HDS-0014/03).
- INSTITUTO NACIONAL DE PESQUISAS ESPACIAIS (INPE). **Plano diretor 2011 - 2015: planejamento estratégico do INPE**. São José dos Campos, 2013. 57 p. Available on: <http://www.inpe.br/noticias/arquivos/pdf/Plano_diretor_miolo.pdf>. Accessed on: 23 sep. 2013.
- ISSHIKI, M.; GARDNER, L.; GREGORY, G. G. Automated control of manufacturing sensitivity during optimization. In: OPTICAL DESIGN AND ENGINEERING, 2003, St. Etienne, France. **Proceedings...** Bellingham, WA: SPIE, 2004. v. 5249, p. 343–352.
- ISSHIKI, M.; SINCLAIR, D.; KANEKO, S. Lens design: Global optimization of both performance and tolerance sensitivity. In: INTERNATIONAL OPTICAL DESIGN CONFERENCE, 2006, Vancouver. **Proceedings...** Washington, D.C: Optical Society of America, 2006. p. TuA5.
- JEFFS, M. Reduced manufacturing sensitivity in multi-element lens systems. In: INTERNATIONAL OPTICAL DESIGN CONFERENCE, 2002, Tucson, Arizona. **Proceedings...** Washington, D.C: Optical Society of America, 2002. p. IMC4.
- JONES, L. W.; AL-SAKRAN, S. H.; KOZA, J. R. Automated synthesis of a human-competitive solution to the challenge problem of the 2002 international optical design conference by means of genetic programming and a multi-dimensional mutation operation. In: **Proceedings...** New York: ACM, 2006. p. 823–830.
- JOSEPH, S.; KANG, H. W.; CHAKRABORTY, U. K. Optical design with epsilon-dominated multi-objective evolutionary algorithm. In: BELICZYNSKI, B.; DZIELINSKI, A.; IWANOWSKI, M.; RIBEIRO, B. (Ed.). **Adaptive and Natural Computing Algorithms**. Berlin: Springer, 2007, (Lecture Notes in Computer Science, v. 4431). p. 77–84. ISBN 978-3-540-71589-4.
- KIDGER, M. **Fundamental optical design**. Bellingham, WA: SPIE Press, 2002. 290 p. (Press Monographs). ISBN 9780819439154.
- KIDGER, M. **Intermediate optical design**. Bellingham, WA: SPIE Press, 2004. 227 p. (Press Monographs). ISBN 9780819452177.
- KNOWLES, J.; CORNE, D. The Pareto archived evolution strategy: A new baseline algorithm for Pareto multiobjective optimization. In: EVOLUTIONARY COMPUTATION, CONGRESS ON (CEC), 1999, Washington, DC. **Proceedings...** New York: IEEE, 1999. v. 1, p. 98–105.
- KOZA, J. R.; AL-SAKRAN, S. H.; JONES, L. W. Automated re-invention of six patented optical lens systems using genetic programming. In: CONFERENCE ON GENETIC AND EVOLUTIONARY COMPUTATION (GECCO), 2005, Washington, DC. **Proceedings...** New York, NY, USA: ACM, 2005. (GECCO '05), p. 1953–1960. ISBN 1-59593-010-8.
- LACERDA, E. G. M.; CARVALHO, A. C. P. L. F. Introdução aos algoritmos genéticos. In: GALVÃO, C. O.; VALENÇA, M. (Ed.). **Sistemas inteligentes: aplicações a recursos hídricos e ciências ambientais**. Porto Alegre, RS: UFRGS: Associação Brasileira de Recursos Hídricos, 1999, (Coleção ABRH de Recursos

Hidricos; 7). p. 99–150.

LAIKIN, M. **Lens design**. 2nd. ed. New York: Marcel Dekker, Inc, 1995. 446 p. (Optical Engineering). ISBN 9780824796020.

LESSING, N. v.d. W. Selection of optical glasses in superachromats. **Appl. Opt.**, OSA, v. 9, n. 7, p. 1665–1668, Jul. 1970. ISSN 1559-128X.

LI, L.; WANG, Q.-H.; XU, X.-Q.; LI, D.-H. Two-step method for lens system design. **Opt. Express**, OSA, v. 18, n. 12, p. 13285–13300, Jun. 2010. ISSN 1094-4087.

LIN, M.-H.; TSAI, J.-F.; YU, C.-S. A review of deterministic optimization methods in engineering and management. **Mathematical Problems in Engineering**, Hindawi Publishing Corporation, v. 2012, p. 756023–1–756023–15, 2012. ISSN 1024-123X.

LOPEZ, N.; AGUIRRE, O.; ESPIRITU, J.; TABOADA, H. Using game theory as a post-Pareto analysis for renewable energy integration problems considering multiple objectives. In: INTERNATIONAL CONFERENCE ON COMPUTERS & INDUSTRIAL ENGINEERING, 41., 2001, Los Angeles. **Proceedings...** 2011. p. 678–683. Available on:<

[http://www.usc.edu/dept/ise/caie/Checked%20Papers%20\[ruhi%2012th%20sept\]/word%20format%20papers/REGISTRATION%20PAID%20PAPERS%20FOR%20PROCEEDINGS/pdf/211%204%20USING%20GAME%20THEORY%20AS%20A%20POST-PARETO%20ANALYSIS%20FOR%20RENEWABLE%20ENERGY.pdf](http://www.usc.edu/dept/ise/caie/Checked%20Papers%20[ruhi%2012th%20sept]/word%20format%20papers/REGISTRATION%20PAID%20PAPERS%20FOR%20PROCEEDINGS/pdf/211%204%20USING%20GAME%20THEORY%20AS%20A%20POST-PARETO%20ANALYSIS%20FOR%20RENEWABLE%20ENERGY.pdf)>. Accessed on: 07 Jan. 2012.

MAHAJAN, V. N. **Optical imaging and aberration: part 1: ray geometrical optics**. Bellingham, WA: SPIE Press, 1998. 470 p. ISBN 0-8194-2515-X.

MAIENTI-LOPES, I.; DE SOUSA, F. L.; SOUZA, L. C. G. de. The generalized extremal optimization with real codification. In: INTERNATIONAL CONFERENCE ON ENGINEERING OPTIMIZATION (ENGOPT), 1., 2008, Rio de Janeiro. **Proceedings...** Rio de Janeiro: EngOpt, 2008. ISBN 978-85-7650-344-6.

MAIENTI-LOPES, I.; SOUZA, L. C. G. de; DE SOUSA, F. L. Design of a nonlinear controller for a rigid-flexible satellite using multi-objective generalized extremal optimization with real codification. **Shock and Vibration**, IOS Press, v. 19, n. 5, p. 947–956, 2012. ISSN 1070-9622.

MALACARA, D.; MALACARA, Z. **Handbook of optical design**. 2. ed. New York: Marcel Dekker Incorporated, 2004. 533 p. (Optical Science and Engineering). ISBN 9780824746131.

MCGUIRE, J. J. P. Designing easily manufactured lenses using a global method. In: INTERNATIONAL OPTICAL DESIGN CONFERENCE, 2006, Vancouver. **Proceedings...** Washington, D.C: Optical Society of America, 2006. p. TuA6.

LOCKHEED MISSILES & SPACE COMPANY, INC. Romeo I. Mercado; Paul N. Robb. **Color-corrected optical systems and method of selecting optical materials therefor**. US 5210646,, 19 Nov. 1990, 11 May 1993.

MOORE, K. E. Algorithm for global optimization of optical systems based on genetic competition. In: OPTICAL DESIGN AND ANALYSIS SOFTWARE, 1999, Denver, CO. **Proceedings...** Bellingham, WA: SPIE, 1999. v. 3780, p. 40–47.

MOORE, L. B.; HVISC, A. M.; SASIÁN, J. Aberration fields of a combination of plane

symmetric systems. **Opt. Express**, OSA, v. 16, n. 20, p. 15655–15670, Sep. 2008. ISSN 1094-4087.

MOSCATO, P. **On evolution, search, optimization, genetic algorithms and martial arts: towards memetic algorithms**. Pasadena, CA, 1989. 67 p. (CALTECH Report 826). Available on:

<<http://citeseerx.ist.psu.edu/viewdoc/download?doi=10.1.1.27.9474&rep=rep1&type=pdf>>. Accessed on: 03 Jan. 2014.

MOSCATO, P.; COTTA, C. A gentle introduction to memetic algorithms. In: GLOVER, F.; KOCHENBERGER, G. A. (Ed.). **Handbook of Metaheuristics**. New York: Springer US, 2003, (International Series in Operations Research & Management Science, v. 57). p. 105–144. ISBN 978-1-4020-7263-5. Cap. 5.

MURAOKA, I.; GALSKI, R. L.; DE SOUSA, F. L.; RAMOS, F. M. Stochastic spacecraft thermal design optimization with low computational cost. **Journal of Spacecraft and Rockets**, AIAA, v. 43, n. 6, p. 1248–1257, Nov./Dec. 2006. ISSN 1533-6794.

NAGATA, Y. The lens design using the CMA-ES algorithm. In: DEB, K. (Ed.). **Genetic and Evolutionary Computation-GECCO 2004**. Berlin: Springer, 2004, (Lecture Notes in Computer Science, v. 3103). p. 1189–1200. ISBN 978-3-540-22343-6.

NIELSEN, H. B. **Introduction to vector and matrix differentiation**. Copenhagen, Denmark, 2005. 5 p. Available on: <http://www.econ.ku.dk/metrics/Econometrics2_04_II/LectureNotes/matrixdiff.pdf>. Accessed on: 19 Nov. 2009.

OGATA, K. **Engenharia de controle moderno**. 2. ed. Rio de Janeiro: Prentice/Hall do Brasil, 1990. 781 p. ISBN 85-7054-045-0.

ONO, I.; KOBAYASHI, S.; YOSHIDA, K. Global and multi-objective optimization for lens design by real-coded genetic algorithms. In: INTERNATIONAL OPTICAL DESIGN CONFERENCE, 1998, Kona, HI. **Proceedings...** Bellingham, WA: SPIE, 1998. v. 3482, p. 110–121.

ONO, I.; TATSUZAWA, Y.; KOBAYASHI, S.; YOSHIDA, K. Designing lens systems taking account of glass selection by real-coded genetic algorithms. In: INTERNATIONAL CONFERENCE ON SYSTEMS, MAN, AND CYBERNETICS (SMS), 1999, Tokyo. **Proceedings...** New York: IEEE, 1999. v. 3, p. 592–597.

OPTICAL RESEARCH ASSOCIATES (ORA). **CODE V: Reference manual**. Pasadena, California, Dec. 2009. v. 1, 496 p. Cap. 5 (CODE V 10.2).

OPTO ELETRONICA SA. **CBERS 3&4: MUX subsystem monthly progress report**. São Carlos, Sep. 2005. (RBN-PRP-8006/00).

POLASHENSKI, M. J. **A brief history of the telescope and ideas for use in the high school physics classroom**: Astr 699 - Topics in astronomy education - Prof. Karen Meech. Manoa, HI: Institute for Astronomy/University of Hawaii, 2001. 28 p. Available on: <http://www.ifa.hawaii.edu/~meech/mp/A_Brief_History.pdf>. Accessed on: 07 Jul. 2010.

RADIANT ZEMAX LLC. **ZEMAX**: optical design program, user's manual. Bellevue,

- WA: Radiant ZEMAX LLC, Jul. 2011a. 786 p. Cap. 17.
- RADIANT ZEMAX LLC. **Cooke 40 degree field**. Bellevue, WA: Radiant ZEMAX LLC, Jul. 2011b. Zemax Lens objective data bank.
- RAYCES, J. L.; ROSETE-AGUILAR, M. Differential equation for normal glass dispersion and evaluation of the secondary spectrum. **Appl. Opt.**, OSA, v. 38, n. 10, p. 2028–2039, Apr. 1999. ISSN 1559-128X.
- RAYCES, J. L.; ROSETE-AGUILAR, M. Selection of glasses for achromatic doublets with reduced secondary color. In: CURRENT DEVELOPMENTS IN LENS DESIGN AND OPTICAL SYSTEMS ENGINEERING, 2000, San Diego, CA. **Proceedings...** Bellingham, WA: SPIE, 2000. v. 4093, p. 36–46.
- RAYCES, J. L.; ROSETE-AGUILAR, M. Selection of glasses for achromatic doublets with reduced secondary spectrum: I. tolerance conditions for secondary spectrum, spherochromatism, and fifth-order spherical aberration. **Appl. Opt.**, OSA, v. 40, n. 31, p. 5663–5676, Nov. 2001. ISSN 1559-128X.
- RAYCES, J. L.; ROSETE-AGUILAR, M. Critical view of three lens design methods: damped least squares, Spencer's and Glatzel's. In: OPTICAL DESIGN AND TESTING, 2002, Shanghai, China. **Proceedings...** Bellingham, WA: SPIE, 2002. v. 4927, p. 77–89.
- RAYCES, J. L.; ROSETE-AGUILAR, M. A discontinuity in the constrained damped least squares (DLS) method of optimization. In: NOVEL OPTICAL SYSTEMS DESIGN AND OPTIMIZATION, 7., 2004, Denver, CO. **Proceedings...** Bellingham, WA: SPIE, 2004. v. 5524, p. 250–260.
- RILEY, J. D. Solving systems of linear equations with a positive definite, symmetric, but possibly ill-conditioned matrix. **Mathematical Tables and Other Aids to Computation**, American Mathematical Society, v. 9, n. 51, p. 96–101, Jul. 1955. ISSN 0891-6837.
- ROBB, P. N.; MERCADO, R. I. Calculation of refractive indices using Buchdahl's chromatic coordinate. **Appl. Opt.**, OSA, v. 22, n. 8, p. 1198–1215, Apr. 1983. ISSN 1559-128X.
- ROSEN, S.; ELDERT, C. Least-squares method for optical correction. **J. Opt. Soc. Am.**, OSA, v. 44, n. 3, p. 250–251, Mar. 1954. ISSN 1084-7529.
- SAKUMA, J.; KOBAYASHI, S. Latent variable crossover for k-tablet structures and its application to lens design problems. In: CONFERENCE ON GENETIC AND EVOLUTIONARY COMPUTATION (GECCO), 2005, Washington, DC. **Proceedings...** New York, NY, USA: ACM, 2005. (GECCO '05), p. 1347–1354. ISBN 1-59593-010-8.
- SANDS, P. J. Aberration coefficients of plane symmetric systems. **J. Opt. Soc. Am.**, OSA, v. 62, n. 10, p. 1211–1220, Oct. 1972. ISSN 1084-7529.
- SASIÁN, J. How to approach the design of a bilateral symmetric optical system. **Optical Engineering**, v. 33, n. 6, p. 2045–2061, Jun. 1994. ISSN 0091-3286.
- SASIÁN, J. Theory of sixth-order wave aberrations. **Appl. Opt.**, OSA, v. 49, n. 16, p. D69–D95, Jun. 2010. ISSN 1559-128X.

- SASIÁN, J. **Tolerance II: Opt 517 lens design**. Tucson, AZ: College of Optical Sciences, The University of Arizona, Fall 2011. Lecture notes.
- SASIÁN, J.; DESCOUR, M. R. Power distribution and symmetry in lens systems. **Optical Engineering**, v. 37, n. 3, p. 1001–1004, Mar. 1998. ISSN 0091-3286.
- SCHNEIDER, P. S.; MOSSI, A. C.; FRANÇA, F. H. R.; DE SOUSA, F. L.; SILVA NETO, A. J. da. Application of inverse analysis to illumination design. **Inverse Problems in Science and Engineering**, v. 17, n. 6, p. 737–753, Aug. 2009. ISSN 1741-5977.
- SCHOTT N. AMERICA, INC. **Optical glass catalogue**: Zemax format. Elmsford, NY, 2013. Available on: <http://www.us.schott.com/advanced_optics/english/download/schottzemax-20130425.zip>. Accessed on: 1 Jul. 2013.
- SHANNON, R. R. **The Art and science of optical design**. Cambridge: Cambridge University Press, 1997. 630 p. ISBN 9780521588683.
- SIGLER, R. D. Glass selection for airspaced apochromats using the Buchdahl dispersion equation. **Appl. Opt.**, OSA, v. 25, n. 23, p. 4311–4320, Dec. 1986. ISSN 1559-128X.
- SLOAN, T. R. Analysis and correction of secondary color in optical systems. **Appl. Opt.**, OSA, v. 9, n. 4, p. 853–858, Apr. 1970. ISSN 1559-128X.
- SMITH, W. **Modern lens design**. 2nd. ed. New York: McGraw-Hill, 2004. 631 p. (Electronic engineering). ISBN 978-0-07-143830-8.
- SMITH, W. **Modern optical engineering: the design of optical systems**. 4th. ed. New York: McGraw-Hill Education, 2007. 754 p. (McGraw Hill professional). ISBN 978-0-07-147687-4.
- SPENCER, G. H. A flexible automatic lens correction procedure. **Appl. Opt.**, OSA, v. 2, n. 12, p. 1257–1264, Dec. 1963. ISSN 1559-128X.
- SRINIVAS, N.; DEB, K. Multiobjective optimization using nondominated sorting in genetic algorithms. **Evol. Comput.**, MIT Press, Cambridge, MA, USA, v. 2, n. 3, p. 221–248, Sep. 1994. ISSN 1063-6560.
- STEPHENS, R. E. Four-color achromats and superchromats. **J. Opt. Soc. Am.**, OSA, v. 50, n. 10, p. 1016–1019, Oct. 1960. ISSN 1084-7529.
- SUN, W.-S.; CHU, C.-H.; TIEN, C.-L. Well-chosen method for an optimal design of doublet lens design. **Opt. Express**, OSA, v. 17, n. 3, p. 1414–1428, Feb. 2009. ISSN 1094-4087.
- SWITALSKI, P.; SEREDYNSKI, F. Generalized extremal optimization for solving multiprocessor task scheduling problem. In: LI, X.; KIRLEY, M.; ZHANG, M.; GREEN, D.; CIESIELSKI, V.; ABBASS, H.; MICHALEWICZ, Z.; HENDTLASS, T.; DEB, K.; TAN, K.; BRANKE, J.; SHI, Y. (Ed.). **Simulated Evolution and Learning**. Berlin: Springer, 2008, (Lecture Notes in Computer Science, v. 5361). p. 161–169. ISBN 978-3-540-89693-7.
- SWITALSKI, P.; SEREDYNSKI, F. An effective multiprocessor scheduling with use of geo metaheuristic. **International Journal of Foundations of Computer Science**, v. 23, n. 02, p. 465–481, Feb. 2012a. ISSN 0129-0541.

SWITALSKI, P.; SEREDYNSKI, F. A grid scheduling based on generalized extremal optimization for parallel job model. In: WYRZYKOWSKI, R.; DONGARRA, J.; KARCZEWSKI, K.; WASNIEWSKI, J. (Ed.). **Parallel Processing and Applied Mathematics**. Berlin: Springer, 2012b, (Lecture Notes in Computer Science, v. 7204). p. 41–50. ISBN 978-3-642-31499-5. 9th International Conference on Parallel Processing and Applied Mathematics.

TALBI, E.-G. **Metaheuristics**: from design to implementation. Hoboken, N.J.: J. Wiley & Sons, 2009. 593 p. ISBN 978-0-470-27858-1.

TESAR, J. C. Mozart, dice, and glass selection. In: NOVEL OPTICAL SYSTEMS DESIGN AND OPTIMIZATION, 3., 2000, San Diego, CA. **Proceedings...** Bellingham, WA: SPIE, 2000. v. 4092, p. 1–6.

THIBAULT, S.; GAGNÉ, C.; BEAULIEU, J.; PARIZEAU, M. Evolutionary algorithms applied to lens design: case study and analysis. In: OPTICAL DESIGN AND ENGINEERING, 2., 2005, Jena, Germany. **Proceedings...** Bellingham, WA: SPIE, 2005. v. 5962, p. 66–76.

THOMPSON, K. Description of the third-order optical aberrations of near-circular pupil optical systems without symmetry. **J. Opt. Soc. Am. A**, OSA, v. 22, n. 7, p. 1389–1401, Jul. 2005. ISSN 1084-7529.

VAN LEIJENHORST, D. C.; LUCASIUS, C. B.; THIJSSSEN, J. M. Optical design with the aid of a genetic algorithm. **Biosystems**, Elsevier, v. 37, n. 3, p. 177–187, 1996. ISSN 0303-2647.

VASILJEVIĆ, D. **Classical and evolutionary algorithms in the optimization of optical systems**. 1st. ed. Boston: Kluwer Academic Publishers, 2002. 296 p. (Genetic Algorithms and Evolutionary Computation Series). ISBN 9781402071409.

VENKAT, V.; JACOBSON, S.; STORI, J. A post-optimality analysis algorithm for multi-objective optimization. **Computational Optimization and Applications**, Kluwer Academic Publishers, v. 28, n. 3, p. 357–372, Sep. 2004. ISSN 0926-6003.

WANG, J.; GUO, B.; SUN, Q.; LU, Z. Third-order aberration fields of pupil decentered optical systems. **Opt. Express**, OSA, v. 20, n. 11, p. 11652–11658, May. 2012. ISSN 1094-4087.

WANG, L.; SASIÁN, J. Merit figures for fast estimating tolerance sensitivity in lens systems. In: INTERNATIONAL OPTICAL DESIGN CONFERENCE, 2010, Jackson Hole, WY. **Proceedings...** Bellingham, WA: SPIE, 2010. v. 7652, p. 76521P–1–76521P–8.

WILLEY, R. R. Machine-aided selection of optical glasses for two-element, three-color achromats. **Appl. Opt.**, OSA, v. 1, n. 3, p. 368–369, May. 1962. ISSN 1559-128X.

YABE, A. Optimal selection of aspheric surfaces in optical design. **Opt. Express**, OSA, v. 13, n. 18, p. 7233–7242, Sep. 2005. ISSN 1094-4087.

YABE, A. Global optimization with traveling aspherics: aspheric surface number as continuous variable. In: INTERNATIONAL OPTICAL DESIGN CONFERENCE, 2010, Jackson Hole, WY. **Proceedings...** Bellingham, WA: SPIE, 2010. v. 7652, p. 76522P–1–76522P–9.

YANO, T.; MARTINS, E.; DE SOUSA, F. L. Generating feasible test paths from an executable model using a multi-objective approach. In: INTERNATIONAL CONFERENCE ON SOFTWARE TESTING, VERIFICATION, AND VALIDATION WORKSHOPS (ICSTW), 3., 2010, Paris. **Proceedings...** New York: IEEE, 2010. p. 236–239.

ZIO, E.; BAZZO, R. A clustering procedure for reducing the number of representative solutions in the Pareto front of multiobjective optimization problems. **European Journal of Operational Research**, elsevier, v. 210, n. 3, p. 624–634, May. 2011. ISSN 0377-2217.

ZITZLER, E.; LAUMANN, M.; BLEULER, S. A tutorial on evolutionary multiobjective optimization. In: GANDIBLEUX, X.; SEVAUX, M.; SORENSEN, K.; T'KINDT, V. (Ed.). **Metaheuristics for multiobjective optimization**. Berlin: Springer, 2004, (Lecture Notes in Economics and Mathematical Systems, v. 535). p. 3–37. ISBN 978-3-540-20637-8. Cap. 1.

ZITZLER, E.; LAUMANN, M.; THIELE, L. **SPEA2**: Improving the strength Pareto evolutionary algorithm. Zurich: [s.n.], 2001. 21 p. Computer Engineering and Network Laboratory Technical Report-103. Available on: <<http://www.kddresearch.org/Courses/Spring-2007/CIS830/Handouts/P8.pdf>>. Accessed on: 07 Jan. 2012.

ZITZLER, E.; THIELE, L. Multiobjective evolutionary algorithms: a comparative case study and the strength Pareto approach. **Evolutionary Computation, IEEE Transactions on**, v. 3, n. 4, p. 257–271, Nov. 1999. ISSN 1089-778X.

GLOSSARY

The definitions in this glossary were taken from the glossary in Smith, 2008.

Abbe V-number	The reciprocal relative dispersion of an optical material. For visual work $V = (n_d - 1)/(n_F - n_C)$, where d , F and C indicate the Fraunhofer wavelengths: 0.5876, 0.4861, and 0.6563 μm , respectively. Often called V -value or u -value, or nu -number.
aberration	An image defect whereby all rays from a point source do not converge to a point image at the desired location. An aberrated wave front departs from a perfect sphere centered on the desired image point. The primary aberrations are: spherical, coma, astigmatism, field curvature, distortion, axial chromatic (axial color), and lateral color. Relative to the ideal paraxial image, the aberration of a ray may be measured as a transverse displacement, a longitudinal displacement, an angular deviation, or a wavefront deformation.
achromat	An optical system free of primary chromatic aberration. Usually defined as a system where two different wavelengths (e.g., C - and F -light) are brought to a focus at the same location. Usually accomplished by the use of materials of differing V -numbers.
Airy disk	The central bright patch of the diffraction pattern which is formed as the image of a point source. The disk size is defined by the diameter of the first dark ring of the pattern, equal to $1.21\lambda/NA$ (or, very approximately, equal to the f -number in microns). Usually implies a perfect or near-perfect lens with a circular aperture.
anastigmat	Strictly, without astigmatism. The term is usually applied to a lens system where an effort has been made to flatten the field and reduce the third-order spherical coma and astigmatism aberration to zero.
aperture stop	That feature of an optical system which most severely limits the diameter of the axial light beam which can pass through the system. The feature is usually the clear aperture of a lens element or a mechanical aperture, such as the iris diameter in a camera lens. The chief or principal ray crosses the axis at, and passes through the center of, the aperture stop. In many compound optical systems (e.g., a telescope or microscope) the aperture stop is located at the objective lens. Note that for off-axis object points the beam size may be limited (vignetted) by more than one physical feature of the system.
aplanat(ic)	A lens or surface which is free of both spherical aberration and coma.
aspheric surface	A surface which departs from a true spherical shape. The conic section surfaces (paraboloid, ellipsoid, and hyperboloid) are aspherics, as are more general aspheric surfaces. Aspheric surfaces are often used to correct aberrations.
axial chromatic	An aberration which causes light of different wavelengths to be focused at different distances from the lens.
axis, optical	The common axis of rotational symmetry for an optical system. For a spherically surfaced lens element, the line connecting the centers of curvature of the surfaces.
back focal	The distance from the vertex of the last surface of a system to the second focal

length (bfl)	point.
Cassegrain	A two-mirror objective with a concave primary mirror (classically a paraboloid) and a convex secondary mirror (a hyperboloid), corrected for spherical aberration.
catadioptric and catoptric	Optical systems consisting of only mirrors (catoptric), or of mirrors and refracting surfaces (catadioptric). A purely refracting system is called dioptric.
chief or principal ray	Theoretically the oblique ray which passes through the center of the aperture stop, entrance and exit pupil.
chromatic aberration	An aberration which results from the dispersion of the materials used in an optical system. See axial chromatic (axial color) and lateral chromatic.
coma	An off-axis aberration where annular zones of the aperture have different magnifications. The resulting image of a point looks like a comet.
concave surface	A hollow curved surface, i.e., one which is lower in the center, sunken. The inner surface of a hollow sphere.
converging lens or surface(positive lens or surface)	One which bends rays toward the optical axis. A positive lens or surface.
convex surface	A surface which is higher at the center than at the edge, outward curving, and bulging. The outer surface of a sphere.
Cooke triplet	A triplet anastigmat with two outer positive crown elements and an inner negative flint element, all spaced apart.
cosine fourth	The illumination in the image plane of a nominal optical system varies approximately as the fourth power of the cosine of the angle of obliquity of the chief ray. Assumes no distortion of the image or of the pupil, and a small NA.
crown glass	A low dispersion glass. A glass with a V -value of more than 50 (for an index 1.6) or more than 55 (for an index 1.6).
curvature of field	The departure of the image surface from a desired flat surface. Measured longitudinally, or as the Petzval radius.
curvature of field	The departure of the image surface from a desired flat surface. Measured longitudinally, or as the Petzval radius.
decentered lens	A lens whose the line connecting the centers of curvature of its surfaces are displaced from the optical axis.
decentered surface	A surface the center of curvature or axis of symmetry of which is not on the optical axis.
diffraction	The cause of the spreading or divergence of a wave front which occurs when it encounters an obstruction such as an aperture or an opaque edge. The Airy disk and the associated rings are caused by the diffraction resulting from the aperture of the optical system.
diffraction	Strictly, when system performance is limited solely by diffraction. Often

limited	colloquially applied to a system with a Strehl ratio of 0.8 or more, or an OPD of one quarter wave or less.
dispersion	The change of index with wavelength. For visual work it is usually taken as the index difference between the red and blue Fraunhofer hydrogen lines C (656.3 nm) and F (486.1 nm), thus $(n_F - n_C)$. This is total or principal dispersion. See also partial dispersion.
distortion	An aberration in which the magnification varies over the field of view. It is called pincushion or positive if the magnification increases toward the edge of the field, and barrel or negative if it decreases. Note that distortion reverses sign if the object and image are interchanged.
diverging lens or surface (negative lens or surface)	One which bends light rays away from the optical axis. A negative lens or surface. A lens with a negative focal length. A surface where $(n' - n)/r$ is negative, n and n' are the refraction indices of media in which the incident and refracted rays travel respectively and r is the surface radius of curvature.
doublet lens	A closely spaced or cemented pair of elements, one positive and one negative.
effective focal length (efl)	See focal length.
element	A lens which is a single piece of glass (or a mirror).
entrance or exit pupil	The image of the aperture stop which is seen from object or image space. All light rays passing through the system must enter through the entrance pupil and exit through the exit pupil. The principal ray passes through the center of both pupils.
exit pupil	The image of the aperture stop as seen from image space. All light rays passing through the optical system must emerge through the exit pupil. In a visual system, the eye must be placed at the exit pupil to see the full field of view.
f-number	The "speed" or relative aperture of a lens system. The ratio of the effective focal length to the diameter of the entrance pupil. A measure of the illuminating capability of a lens. Usually written f/n where n is the <i>f-number</i> , e.g., $f/6.3$; or $1:6.3$, or $f:6.3$. Sometimes abbreviated as $f/\#$ or f/no . For an aplanatic system with the object at infinity, the f-number equals $0.5/NA$.
field curvature	The departure of the image surface from a plane, when the image is formed as a curved surface due to astigmatism and/or Petzval aberrations. See curvature of field.
field of view	The area or angle visible through an optical system.
flint glass	An optical glass with a V -value less than 50 (for index 1.6), or less than 55 (for index 1.6). Named for the broken flints added to the melt in making fine glass for tableware.
floating lens	An element or component which moves independently of the balance of the system, usually to maintain good aberration correction while focusing, or as a focusing device.

focal length	The effective (or equivalent) focal length, often abbreviated efl or simply f , is the limiting value of $h' / \tan \theta$, as θ approach zero, where h' is the image height of an infinitely distant object and θ is the angle subtended by the object.
focal point	The image of an infinitely distant axial point source object. The second or back focal point is the image of a point which is to the left of the lens, and the first or front focal point is the image of a point to the right.
focus (noun)	The (usually longitudinal) location of the sharpest image.
focus (verb)	The act of changing the relative positions of elements and sensor in order to get a sharp image.
image	A pictorial representation of an object, formed by the distribution of light at the focus of an optical system.
iris diaphragm	A mechanically adjustable aperture formed by thin pivoting arcuate leaves.
lateral color (chromatic change of magnification)	The variation of image height or magnification with wavelength.
magnification: lateral, linear, or transverse	The ratio of image height to object height, measured normal to the axis.
marginal ray	The ray (usually from an axial object point) which passes through the edge or margin of the lens aperture. An axial ray.
meridional plane	Any plane which includes the optical axis. Also called the tangential plane.
meridional ray	A ray which lies in the meridional plane; a ray which intersects the optical axis. A tangential ray.
modulation	The contrast in an object or image the luminance or illuminance of which varies sinusoidally. Defined as $M = (max. - min.) / (max. + min.)$, where $max.$ and $min.$ are the maximum and minimum levels of luminance or illuminance.
MTF (Modulation Transfer Function)	The ratio of the image modulation (or contrast) to that of the object, expressed as a function of the spatial frequency, where the object modulation is a sinusoidal variation of brightness/luminance/radiance and the image modulation is a sinusoidal variation of the illuminance/irradiance. $MTF = (M_{image}) / (M_{object})$. MTF is the real part of the complex optical transfer function (OTF), in which the imaginary part is the phase transfer function (PTF). It was originally known as the sine-wave response, the frequency response and the contrast transfer function.
numerical aperture, NA	The numerical aperture, $NA = n \sin U$, where n is the index of the medium in which the image is formed, and U is the half angle of the imaging cone. For an infinitely distant object, $NA = 1 / (2 f / \#)$, and $f / \# = 1 / (2 NA)$.
Nyquist frequency	The spatial frequency resolution limit imposed by the size of the pixels in a digital sensor (e.g., CCD). The Nyquist frequency is equal to the reciprocal of twice the pixel spacing d , or $freq = 1 / 2d$.

object	That which is being imaged by the optical system.
objective lens	In a camera, telescope, microscope, or other optical system, the lens which is closest to the object.
oblique beam or ray	A beam or ray which originates from an off-axis object point.
optical axis	The common axis of symmetry of a lens or optical system. See axis, optical.
optical glass	An amorphous, clear, highly transmissive material, made with accurately controlled index of refraction and chromatic dispersion.
optical path difference (OPD)	Wave-front aberration. The departure of the actual wave front from an ideal spherical wavefront. The difference between the total optical paths of two rays measured from their common point of origin in the object to their intersection with a reference sphere centered on the ideal object point. Usually measured in wavelengths, or fractions thereof.
optical path length	The sum of the index n times the path distance D along a ray in each medium i the rays, has gone through, $OP = \sum_i (n_i D_i)$. Related to the transit time of light along a ray through a system.
optical transfer function (OTF)	The complex function of spatial frequency used to describe the imagery of an optical system. It consists of the real part (the MTF, or Modulation Transfer Function), and the imaginary part (the PTF, or Phase Transfer Function).
paraxial	A region where all angles are treated as infinitesimals, so that $\phi = \sin \phi = \tan \phi$, and the equations for raytracing are simple linear (i.e., nontrigonometric) expressions.
paraxial ray	A raytraced according to the paraxial rules, where the ray heights and angles are infinitesimals. The linearity of the paraxial raytracing equations allows the use of fictitious, real, finite values for height and slope.
partial dispersion	The difference in refractive index for two wavelengths, expressed as a fraction of the total dispersion, e.g., $P_{F,d} = (n_F - n_d)/(n_F - n_C)$.
point spread function	The distribution of illumination in the image of a point.
power	The power of a lens is the reciprocal of its effective focal length. The power of a surface is equal to $(n' - n)/r$, where n and n' are the refraction indices of media in which the incident and refracted rays travel respectively and r is the surface radius of curvature. If the dimensions are in meters, the unit of power is the diopter. A positive power converging lens, or surface bends rays toward the axis; a negative power, diverging lens bends rays away from the axis.
pupil	Any image of the aperture stop. See also entrance pupil and exit pupil.
refraction	The bending or directional change of a light ray upon passing from one medium to another. Refraction follows Snell's Law.
refractive index	The ratio of the velocity of light in vacuum c (or, commonly, in air) to its velocity v in the medium being characterized ($n = c/v$).

Ritchey-Chretien	A Cassegrain system with both mirrors hyperbolic, shaped to correct both spherical and coma.
Seidel aberrations	The third-order aberrations, which are: spherical, coma, astigmatism, Petzval, and distortion. Also called the primary aberrations.
Siedel Diagram	The Seidel diagram, sometimes called Pagel (or Pegel) Diagram, gives a graphical representation of the surface by surface contribution to the third-order aberrations in a system.
skew ray	A general ray, not limited to the tangential/meridional plane.
Snell's law	The change in direction of a ray crossing the boundary between two media, is governed by Snell's law, which is: $n \sin l = n' \sin l'$, where n and n' are the refractive indices of the two media, and l and l' are the angles of incidence and refraction (the angle between the ray and the surface normal).
spherical aberration	The difference between the focus location of rays through the center of a lens aperture (i.e., paraxial rays) and those through the margin (or other parts) of the aperture.
spherochromatism	The variation of spherical aberration with wavelength, or the variation of axial chromatic with ray height.
Strehl ratio	The ratio of the peak intensity of the point spread function for an aberrated lens to the peak for an aberration-free lens. A Strehl ratio of 80 percent (called the Marechal criterion) corresponds to the quarter-wave Rayleigh criterion (exactly for defocusing, approximately for the other aberrations). The Strehl ratio has an excellent correlation with other image quality metrics for well corrected systems.
symmetrical lens	Most lenses are rotationally, axially symmetrical. Another type of symmetry is "front-to-back" or "mirror" symmetry where the elements before the aperture stop are the same as those which follow it. Front-to-back symmetry eliminates coma, distortion, and lateral color aberrations.
telephoto lens	A lens the length from the first surface of which to the focal point is shorter than its effective focal length. The ratio of the two is called the telephoto ratio which, for a true telephoto, is less than one. The lens consists of a positive front component followed by a negative rear component. The name is sometimes incorrectly applied to an ordinary lens of long focal length.
thin lens	A concept which is useful in preliminary optical system layout. It assumes that the optical components have zero axial thickness, so that the principal points and the lens are coincident.
vignetting	The mechanical clipping or obscuration of the edges of oblique beams by the apertures of elements which are spaced away from the stop. It reduces the off-axis illumination (in addition to the cosine-fourth reduction). Often introduced to reduce manufacturing cost and/or to eliminate aberrated portions of the beam. In visual or photographic systems, as much as 50 percent vignetting is not uncommon.
visible light	Light to which the human eye is sensitive and which can be perceived. Usually considered to include wavelengths from 380 nm to 780 nm, at which wavelengths the photopic response is less than 0.0001 of the peak photopic

response at 555 nm.

wave front A surface wherein all points have the same optical path distance from the object point, i.e., where the light has the same phase.

wave front aberration The departure of the wave front from a perfectly spherical surface. See optical path difference (OPD).

APPENDIX A DETAILED SOLUTION FOR THE DLS METHOD

A.1 Introduction

This appendix discusses the details of the general solution for the unconstrained damped least square method.

For the solution derivation, we assume the following proprieties without demonstrating (FRIEDLAND, 1986; OGATA, 1990 and NIELSEN, 2004):

Assuming A, B and C are matrixes with the respective dimensions of $m \times n$, $m \times n$, and $n \times l$, we have:

$$(A + B)^T = A^T + B^T, \quad (\text{A.1})$$

$$(A \cdot C)^T = C^T \cdot A^T. \quad (\text{A.2})$$

Now, we accept D and E as invertible matrixes with dimensions $m \times n$:

$$(D \cdot E)^{-1} = E^{-1} \cdot D^{-1}. \quad (\text{A.3})$$

Suppose c and X are vectors of dimension $k \times 1$ where X is a vector of variables. We can define a scalar function $f(X) = c^T \cdot X$, which maps the vector X into a single number scale. In this case, we find:

$$\frac{\partial(c^T \cdot X)}{\partial X} = c, \quad (\text{A.4})$$

$$\frac{\partial(X^T \cdot c)}{\partial X} = c. \quad (\text{A.5})$$

Now, assume G as a matrix of $n \times k$ dimensions. In this case, it is possible to demonstrate that

$$\frac{\partial(G \cdot X)}{\partial X^T} = G, \quad (\text{A.6})$$

$$\frac{\partial(X^T \cdot G^T)}{\partial X} = G^T, \quad (\text{A.7})$$

$$\frac{\partial(G \cdot X)}{\partial X} = G^T. \quad (\text{A.8})$$

Consider a square matrix V with dimensions $k \times k$ such that

$$\frac{\partial(X^T \cdot V \cdot X)}{\partial X} = (V + V^T)X, \quad (\text{A.9})$$

$$\frac{\partial(X^T \cdot V \cdot X)}{\partial X^T} = X^T(V + V^T). \quad (\text{A.10})$$

A.2 Unconstrained damped least square solution

For an unconstrained DLS problem, we want to minimize the following objective function:

$$\Psi = (F_0 + A \cdot \Delta X)^T W_e (F_0 + A \cdot \Delta X) + p \cdot \Delta X^T \cdot Q \cdot \Delta X. \quad (\text{A.11})$$

This objective function was written in the most general way by considering both the additive (p) and the multiplicative (Q) damping factors. If only the additive damping is desired, Q should be replaced by the identity matrix.

We can separate Equation (A.11) into two parts as follows:

$$\Psi = \underbrace{(F_0 + A \cdot \Delta X)^T W_e (F_0 + A \cdot \Delta X)}_{(i)} + \underbrace{p \cdot \Delta X^T \cdot Q \cdot \Delta X}_{(ii)}. \quad (\text{A.12})$$

Working out the denominator (I), we find

$$(I) = F_0^T \cdot W_e \cdot F_0 + (X - X_0)^T \cdot A^T \cdot W_e \cdot F_0 + F_0^T \cdot W_e \cdot A \cdot (X - X_0) + (X - X_0)^T \cdot A^T \cdot W_e \cdot A \cdot (X - X_0), \quad (\text{A.13})$$

where $\Delta X = (X - X_0)$.

Because $(X - X_0)^T \cdot A^T \cdot W_e \cdot F_0$ and $F_0^T \cdot W_e \cdot A \cdot (X - X_0)$ are identical scalar quantities, we can rewrite (A.13) as

$$(I) = F_0^T \cdot W_e \cdot F_0 - 2 \cdot F_0^T \cdot W_e \cdot A \cdot X_0 - X_0^T \cdot A^T \cdot W_e \cdot A \cdot X_0 + 2 \cdot F_0^T \cdot W_e \cdot A \cdot X + X^T \cdot A^T \cdot W_e \cdot A \cdot X - X^T \cdot A^T \cdot W \cdot A \cdot X_0 - X_0^T \cdot A^T \cdot W_e \cdot A \cdot X, \quad (\text{A.14})$$

$$(I) = F_0^T \cdot W_e \cdot F_0 - 2 \cdot F_0^T \cdot W_e \cdot A \cdot X_0 - X_0^T \cdot A^T \cdot W_e \cdot A \cdot X_0 + 2 \cdot F_0^T \cdot W_e \cdot A \cdot X + X^T \cdot A^T \cdot W_e \cdot A \cdot X - X^T \cdot A^T \cdot W \cdot A \cdot X_0 - X_0^T \cdot A^T \cdot W_e \cdot A \cdot X.$$

In the same way, we can determine (II):

$$(II) = p \cdot (X^T \cdot Q \cdot X - X^T \cdot Q \cdot X_0 - X_0^T \cdot Q \cdot X + X_0^T \cdot Q \cdot X_0). \quad (\text{A.15})$$

To solve the problem, it is necessary that $\frac{\partial(\Psi)}{\partial X} = 0$, which is equivalent to

$$\frac{\partial(I)}{\partial X} + \frac{\partial(II)}{\partial X} = 0.$$

Differentiating (I), we find

$$\begin{aligned} \frac{\partial(I)}{\partial X} = & \frac{\partial(F_0^T \cdot W_e \cdot F_0 - 2 \cdot F_0^T \cdot W_e \cdot A \cdot X_0 - X_0^T \cdot A^T \cdot W_e \cdot A \cdot X_0)}{\partial X} \\ & + \frac{\partial(2 \cdot F_0^T \cdot W_e \cdot A \cdot X)}{\partial X} + \frac{\partial(X^T \cdot A^T \cdot W_e \cdot A \cdot X)}{\partial X} \\ & - \frac{\partial(X^T \cdot A^T \cdot W \cdot A \cdot X_0)}{\partial X} - \frac{\partial(X_0^T \cdot A^T \cdot W_e \cdot A \cdot X)}{\partial X}. \end{aligned} \quad (\text{A.16})$$

To make things easier, we can differentiate each part of (A.16) individually. Because $F_0^T \cdot W_e \cdot F_0 - 2 \cdot F_0^T \cdot W_e \cdot A \cdot X_0 - X_0^T \cdot A^T \cdot W_e \cdot A \cdot X_0$ is a constant, its derivation is equal to zero:

$$\frac{\partial(F_0^T \cdot W_e \cdot F_0 - 2 \cdot F_0^T \cdot W_e \cdot A \cdot X_0 - X_0^T \cdot A^T \cdot W_e \cdot A \cdot X_0)}{\partial X} = 0. \quad (\text{A.17})$$

We determine the other parts of Equation (A.16) as follows:

$$\text{From (A.4)} \quad \frac{\partial(2 \cdot F_0^T \cdot W_e \cdot A \cdot X)}{\partial X} = 2 \cdot A^T \cdot W_e \cdot F_0, \quad (\text{A.18})$$

$$\text{From (A.4)} \quad \frac{\partial(X^T \cdot A^T \cdot W_e \cdot A \cdot X)}{\partial X} = 2 \cdot A^T \cdot W_e \cdot A \cdot X, \quad (\text{A.19})$$

$$\text{From (A.5)} \quad -\frac{\partial(X^T \cdot A^T \cdot W_e \cdot A \cdot X_0)}{\partial X} = -A^T \cdot W_e \cdot A \cdot X_0, \quad (\text{A.20})$$

$$\text{From (A.4)} \quad -\frac{\partial(X_0^T \cdot A^T \cdot W_e \cdot A \cdot X)}{\partial X} = -A^T \cdot W_e \cdot A \cdot X_0. \quad (\text{A.21})$$

Combining Equations (A.17) to (A.21) and substituting them into (A.16) we get:

$$\frac{\partial(I)}{\partial X} = 2 \cdot A^T \cdot W_e^T \cdot F_0 + 2 \cdot A^T \cdot W_e \cdot A \cdot (X - X_0). \quad (\text{A.22})$$

Now, differentiating (II), we find

$$\begin{aligned} \frac{\partial(II)}{\partial X} = p \cdot & \frac{\partial(X^T \cdot Q \cdot X)}{\partial X} - \frac{\partial(X^T \cdot Q \cdot X_0)}{\partial X} - \frac{\partial(X_0^T \cdot Q \cdot X)}{\partial X} \\ & + \frac{\partial(X_0^T \cdot Q \cdot X_0)}{\partial X}. \end{aligned} \quad (\text{A.23})$$

Again, because $X_0^T \cdot Q \cdot X_0$ is a constant, its derivative is zero:

$$\frac{\partial(X_0^T \cdot Q \cdot X_0)}{\partial X} = 0. \quad (\text{A.24})$$

We determine the other parts of Eq. (A.23) as follows:

$$\text{From (A.8)} \quad \frac{\partial(X^T \cdot Q \cdot X)}{\partial X} = 2 \cdot Q \cdot X, \quad (\text{A.25})$$

$$\text{From (A.5)} \quad -\frac{\partial(X^T \cdot Q \cdot X_0)}{\partial X} = -Q \cdot X_0, \quad (\text{A.26})$$

$$\text{From (A.4)} \quad -\frac{\partial(X_0^T \cdot Q \cdot X)}{\partial X} = (X_0^T \cdot Q)^T = -Q \cdot X_0. \quad (\text{A.27})$$

Combining Equations (A.24) to (A.27) and substituting them into (A.23), we get

$$\frac{\partial(II)}{\partial X} = p \cdot 2 \cdot Q \cdot X - Q \cdot X_0 - Q \cdot X_0 = p \cdot 2 \cdot Q \cdot (X - X_0). \quad (\text{A.28})$$

Now, with (A.22) and (A.28) and the minimum condition, we find

$$\begin{aligned}
\frac{\partial(\Psi)}{\partial X} = 0 &\Rightarrow \frac{\partial(I)}{\partial X} + \frac{\partial(II)}{\partial X} = 0 \\
&\Rightarrow 2 \cdot A^T \cdot W_e^T \cdot F_0 + 2 \cdot A^T \cdot W_e \cdot A \cdot (X - X_0) + p \cdot 2 \\
&\quad \cdot Q \cdot (X - X_0) = 0.
\end{aligned} \tag{A.29}$$

Isolating $(X - X_0)$ and dividing both sides of the equation by 2, we obtain the problem solution:

$$\Delta X = -(A^T \cdot W_e \cdot A + p \cdot I)^{-1} \cdot A^T \cdot W_e \cdot F_0. \tag{A.30}$$

APPENDIX B TUNING O-GEO

This appendix provides the description and detailed data resulting from the O-GEO free adjustment parameters experiment. Moreover, this appendix also includes the description and data for the experiment used to define the reference number of generations executed by O-GEO before entering the exploitation phase of the method.

The free parameters adjustment of an evolutionary algorithm is a crucial step in the development and application of the algorithm. The correct value selection parameters can have a significant impact in the algorithm convergence performance. The O-GEO algorithm has two adjustable parameters: τ , σ .

The main parameter for all GEO based algorithms is τ . This parameter defines the probability of selecting a candidate solution according to its position in the adaptability ranking, which is sorted by the objective function value. As the value of τ increases, the algorithm becomes more deterministic, increasing the probability of selecting the most adapted solution. As the value of τ decreases, the algorithm becomes more stochastic, increasing the probability of selecting less adapted solutions. The normalized standard deviation of the Gaussian perturbation applied in each continuous variable during the search is σ , defining the variable step change.

In O-GEO, the adjustable parameters are static. They are defined before the algorithm is run and remains fixed during the optimization process. For static parameters, the values are typically set using a parameter tuning approach.

Parameter tuning is performed by experimenting with different values and selecting the values, which give the best results for the test problem. Unfortunately, this task can be very time consuming because the parameter dependence is high, making the number of combinations extremely large even with a limited parameter range and significant step size.

In this case, the parameter values selected using this method are not necessarily optimal. Though the best values for the parameters are problem

dependent, it is practically impossible to define different parameters for different problems.

In this work, we perform a systematic search for the parameters of a very simple optical design problem, assuming a fixed number of lenses and running the algorithm in the mono-objective mode. We selected the Cooke triplet problem for tuning. The adjustable parameter values found for this problem are then utilized for every other lens design problem in this thesis. The Cooke triplet was selected for the tuning process because it has a known design space and runs fast in the available computer machines due to its simplicity, allowing in a feasible time interval, the test of many different adjustable parameter configurations.

Once τ and σ have been defined, we performed a search to establish the best number of generations to execute before entering the exploitation phase. We also used the Cooke triplet problem for this search. Unlike τ and σ , the number of generations is assumed to be linearly proportional to the number of design variables and quadratic with the number of objective functions.

B.1 Tuning τ and σ

The following values were tested for τ : 0.25, 0.5, 0.75, 1, 2, 3, 4, 5, 6, 7, 8, 9, and 10. For each value assumed for τ , σ was changed from 0.1 to 1 in increments of 0.1. For each combination, the algorithm was executed 50 times for 10^4 objective function calls.

We collected the data for each tested σ value and plotted the results in

Figure B.1 to Figure B.10. The plots on the left-hand side of these figures show the evolution of the objective function value with the accumulated number of objective function calculations. The curve colors differ for each τ value. The plots on the right-hand side show the final objective function value as a function of τ . In both plots, the values are the average of fifty independent executions.

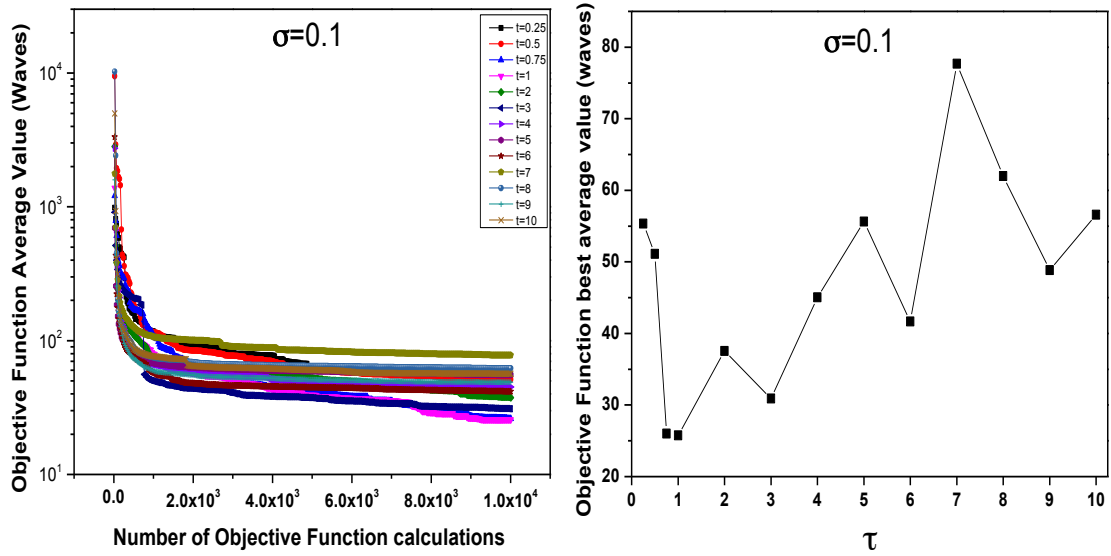


Figure B.1 - Tuning experiment curves for $\sigma = 0.1$. The left-hand side shows the average objective function value evolution for the number of objective function calculations. The right-hand side shows final performance of the average objective function as a function of τ .

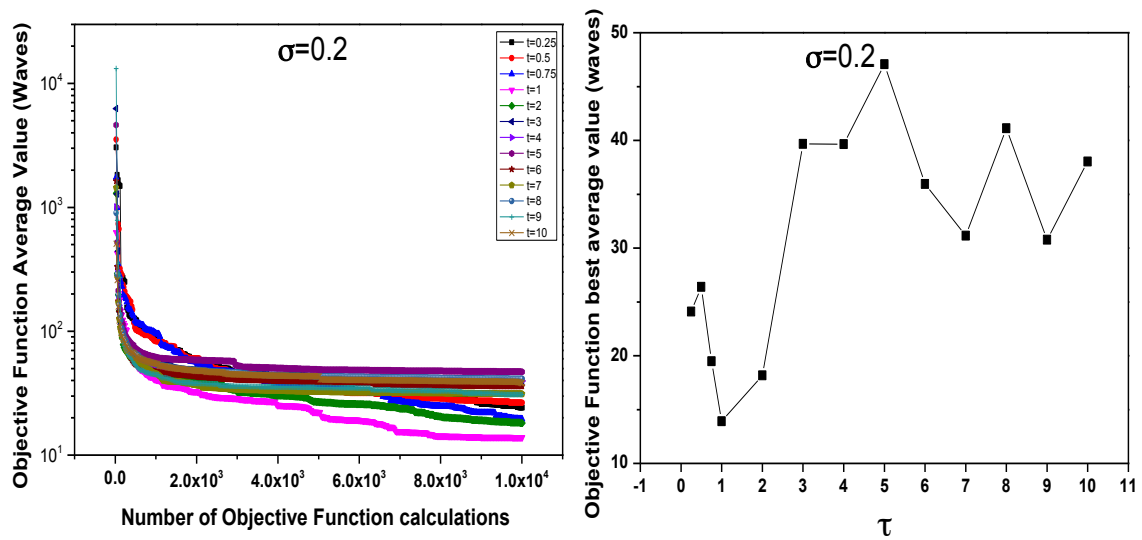


Figure B.2 - Tuning experiment curves for $\sigma = 0.2$. The left-hand side shows the average objective function value evolution for the number of objective function calculations. The right-hand side shows the final performance of the average objective function as a function of τ .

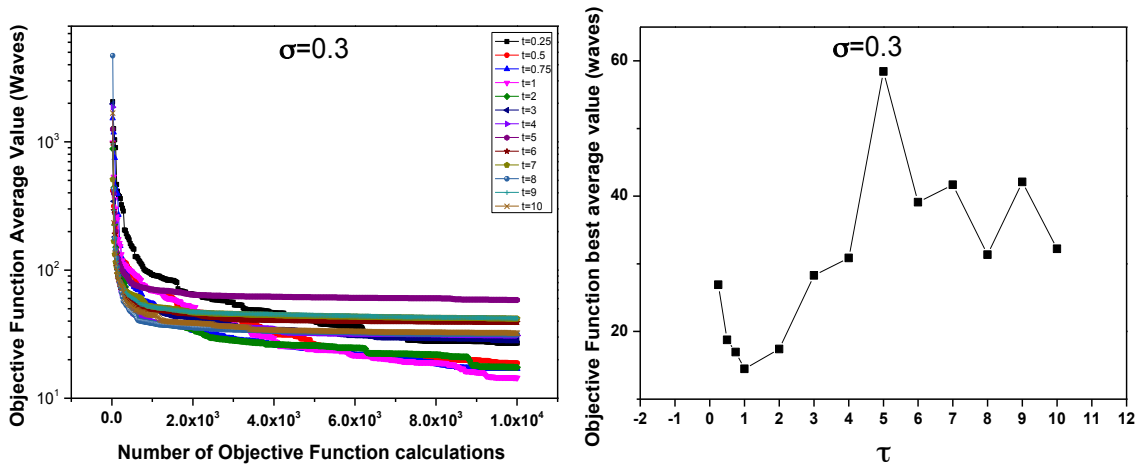


Figure B.3 - Tuning experiment curves for $\sigma = 0.3$. The left-hand side shows the average objective function value evolution for the number of objective function calculations. The right-hand side shows the final performance of the average objective function as a function of τ .

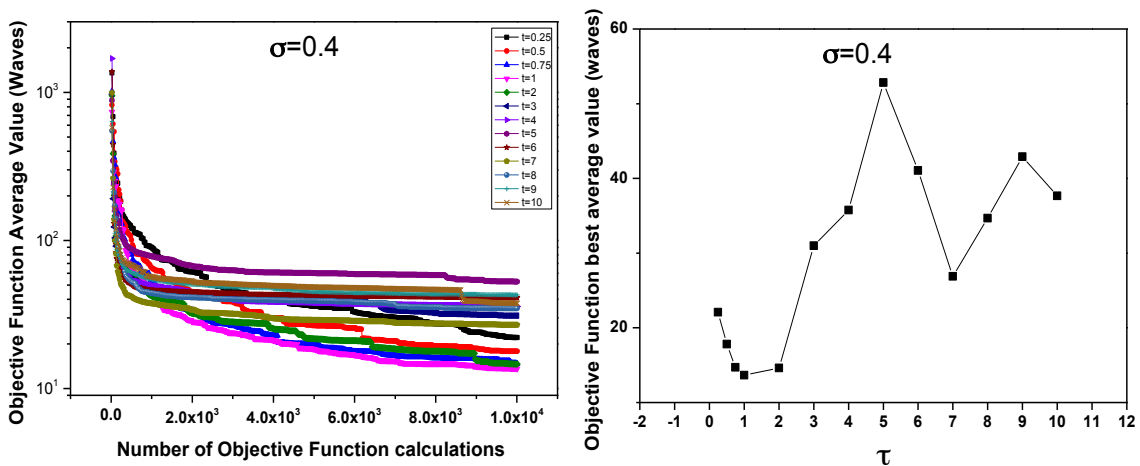


Figure B.4 - Tuning experiment curves for $\sigma = 0.4$. The left-hand side shows the average objective function value evolution for the number of objective function calculations. The right-hand side shows the final performance of the average objective function as a function of τ .

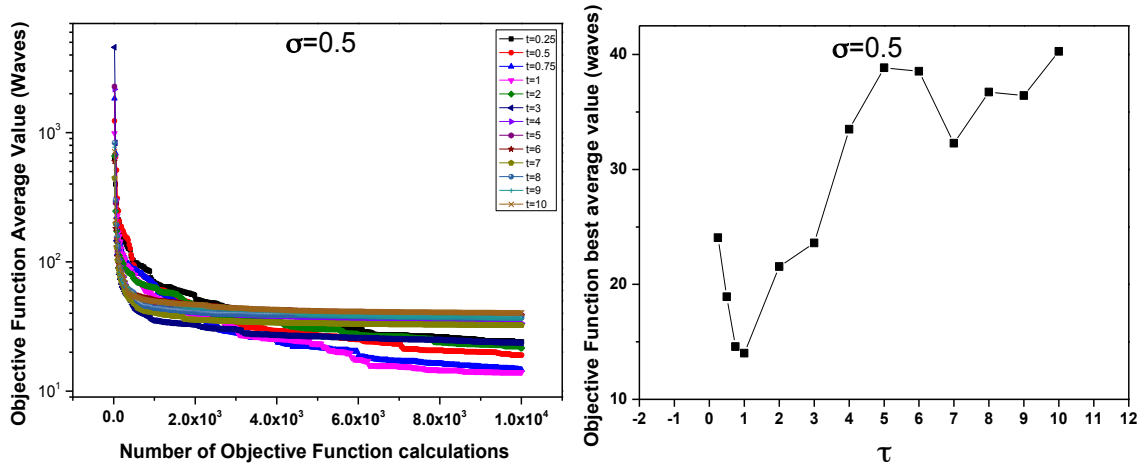


Figure B.5 - Tuning experiment curves for $\sigma = 0.5$. The left-hand side shows the average objective function value evolution for the number of objective function calculations. The right-hand side shows the final performance of the average objective function as a function of τ .

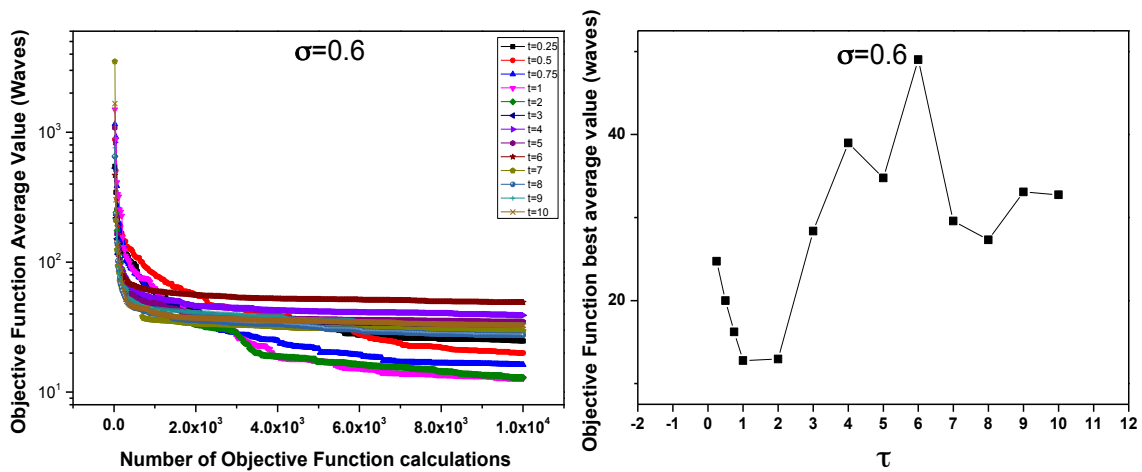


Figure B.6 - Tuning experiment curves for $\sigma = 0.6$. The left-hand side shows the average objective function value evolution for the number of objective function calculations. The right-hand side shows the final performance of the average objective function as a function of τ .

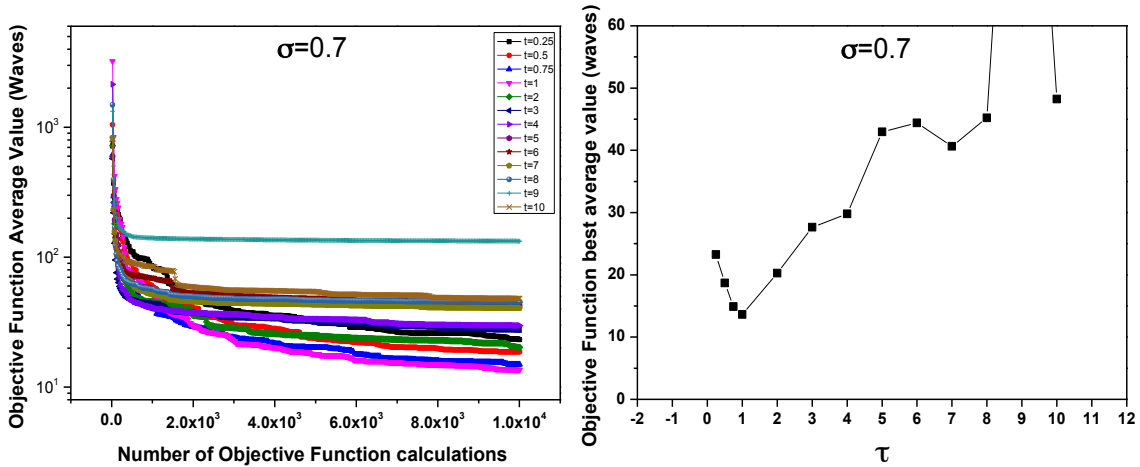


Figure B.7 - Tuning experiment curves for $\sigma = 0.7$. The left-hand side shows the average objective function value evolution for the number of objective function calculations. The right-hand side shows the final performance of the average objective function as a function of τ .

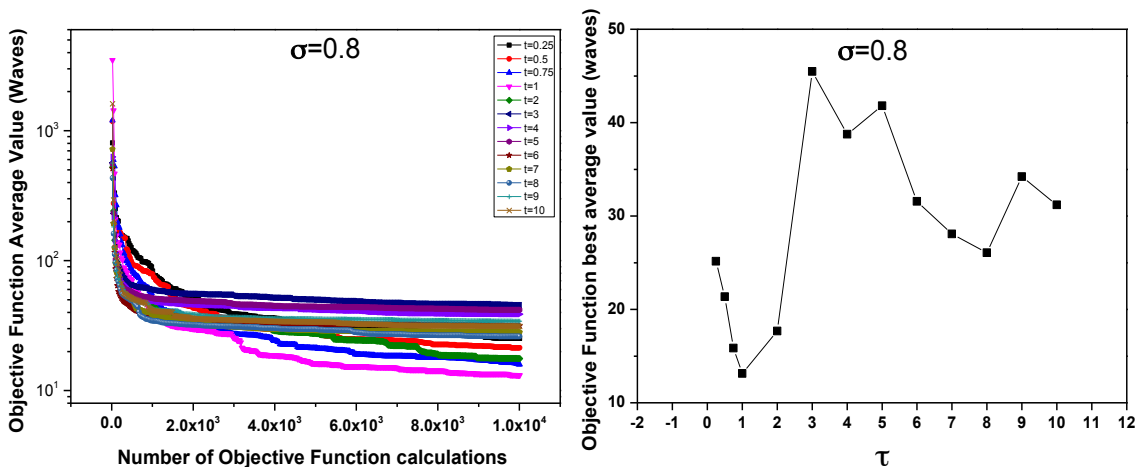


Figure B.8 - Tuning experiment curves for $\sigma = 0.8$. The left-hand side shows the average objective function value evolution for the number of objective function calculations. The right-hand side shows the final performance of the average objective function as a function of τ .

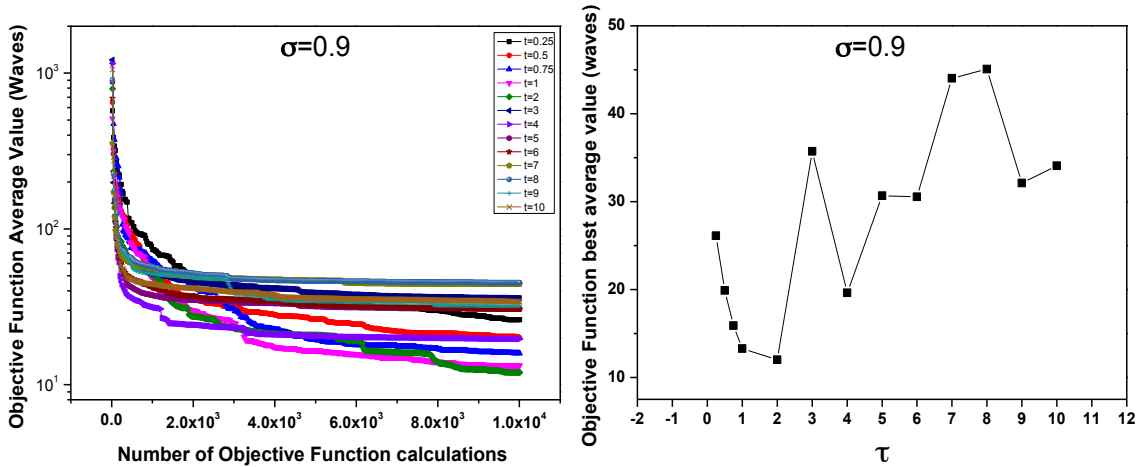


Figure B.9 - Tuning experiment curves for $\sigma = 0.9$. The left-hand side shows the average objective function value evolution for the number of objective function calculations. The right-hand side shows the final performance of the average objective function as a function of τ .

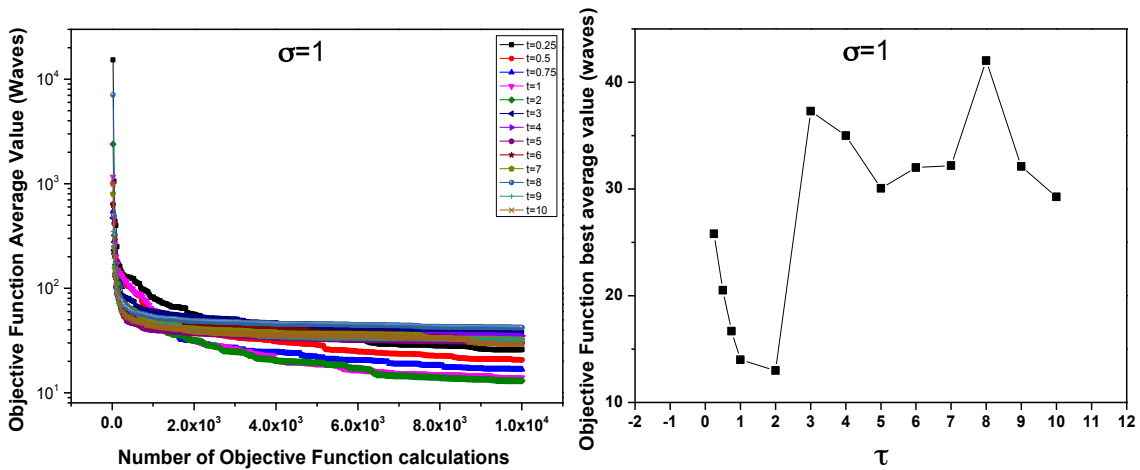


Figure B.10 - Tuning experiment curves for $\sigma = 1$. The left-hand side shows the average objective function value evolution for the number of objective function calculations. The right-hand side shows the final performance of the average objective function as a function of τ .

Analyzing Figures 1 through 10, we observe that for almost all σ values tested, $\tau = 1$ was the best value. However, this was not true for $\sigma = 0.9$ and $\sigma = 1$, for which $\tau = 2$ was the best value. These curves demonstrate that the best τ value is not very sensitive with respect to the σ value.

Now, to analyze the best σ value, we plot the curves for the best MF average value as a function of σ for the two best τ values: $\tau = 1$ and $\tau = 2$. Figure B.11 shows these results.

Analyzing the curves in Figure B.11, the best σ values are 0.6 and 0.9 for $\tau = 1$ and $\tau = 2$, respectively. From the $\tau = 1$ curve, despite the small fluctuations, we observe that the algorithm performance improves as σ approaches 0.6 and degrades for higher values. On the other hand, the $\tau = 2$ curve does not present a clear tendency despite providing best performances for $\sigma = 0.9$ and $\sigma = 1$, which was surprising because these values for σ are very high.

Analyzing all of the curves and data, we chose to set $\tau = 1$ due to the fact that this value was appropriate for the majority of the experiments and because the curve as a function of σ has the best behavior. As a consequence, σ was set equal to 0.6.

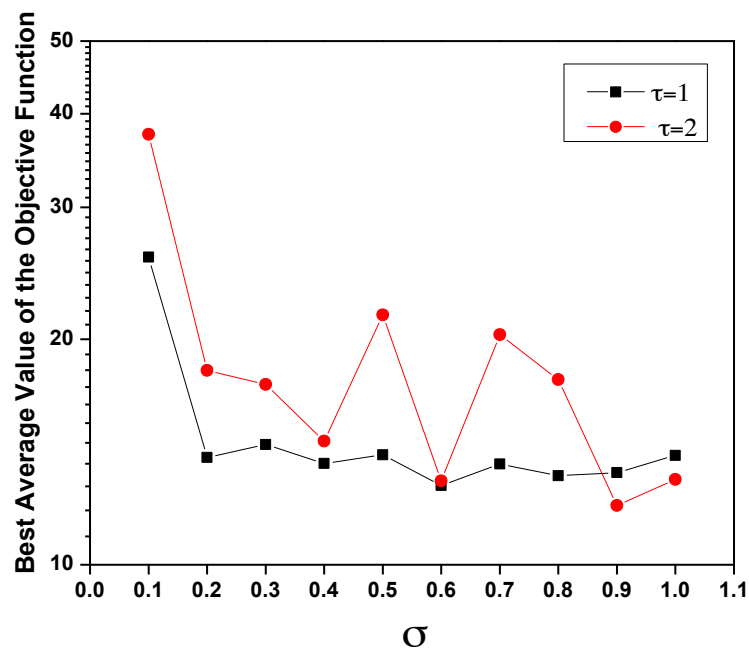


Figure B.11 - Performance of the algorithm as a function of σ for $\tau = 1$ and $\tau = 2$.

B.2 Defining the reference value for the number of generations

Once σ and τ are defined, we performed an experiment to define a good reference number of generations used for each call of O-GEO. In these experiments, we used the same Cooke triplet problem again.

In this experiment, O-GEO (exploration phase) runs for a predefined number of generations. After the maximum number of generations is complete, the exploitation phase (local search) is called. If the algorithm does not fulfill the stopping criterion, which is given by a minimum image quality for the system in this case, O-GEO is reinitialized and the loop continues until the stopping criterion is achieved. For this experiment, the image quality specified was 0.4 waves.

Once the stopping criterion is fulfilled, the total number of MF calculations in the current independent execution is logged. For each number of generations defined, this process is repeated 20 times.

The number of generations varied from 50 to 450 in steps of 50. To analyze the data, we plotted histograms for the total number of objective function calls in each independent execution for each number of generations tested.

We selected the most appropriate reference number of generations by analyzing these histogram plots. The analysis could have been done based on the average value of the total number of objective function calculation; however, because we only performed 20 independent executions, the average number could mislead the analysis. Therefore, the histograms shown in Figure B.12 provides a better representation of the algorithm performance.

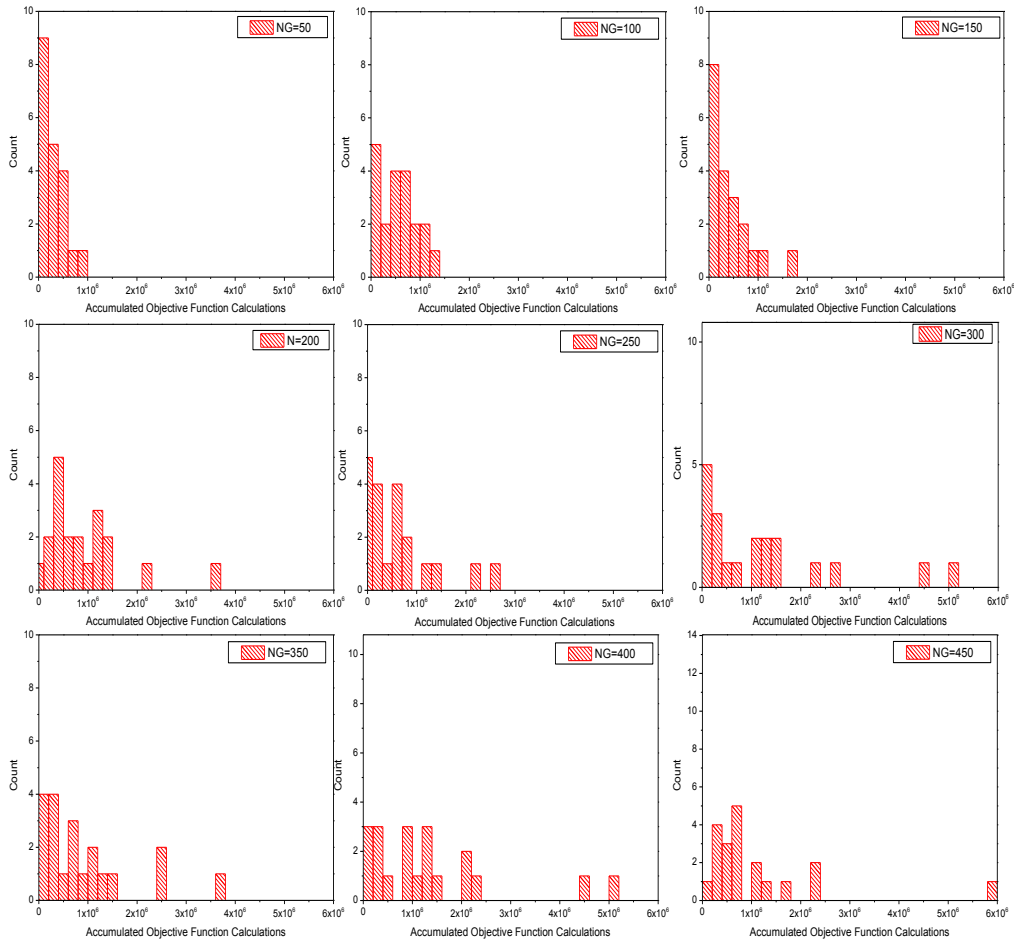


Figure B.12 - Histograms for the number of objective function calculations necessary to achieve the minimum image quality defined in the Cooke triplet experiment.

Analyzing the histograms in Figure B.12, a good number of generations for this experiment is between 50 and 150 generations. For these generation numbers, the stopping criterion is regularly satisfied with a low number of objective function calculations. For higher generation numbers, we see an increase in occurrences that require a much higher number of objective function calculations.

Method of glass selection for color correction in optical system design

Bráulio Fonseca Carneiro de Albuquerque,^{1,2*} Jose Sasian,² Fabiano Luis de Sousa,¹
and Amauri Silva Montes¹

¹National Institute for Space Research –Engineering and Space Technology (INPE/ETE), Av dos Astronautas, 1.758,
12227-010 São José dos Campos – SP-Brazil

² College of Optical Science, University of Arizona, 1630 East University Boulevard, Tucson, Arizona 85721, USA
[*braulio@dea.inpe.br](mailto:braulio@dea.inpe.br)

Abstract: A method of glass selection for the design of optical systems with reduced chromatic aberration is presented. This method is based on the unification of two previously published methods adding new contributions and using a multi-objective approach. This new method makes it possible to select sets of compatible glasses suitable for the design of super-apochromatic optical systems. As an example, we present the selection of compatible glasses and the effective designs for all-refractive optical systems corrected in five spectral bands, with central wavelengths going from 485 nm to 1600 nm.

©2012 Optical Society of America

OCIS codes: (220.0220) Optical design and fabrication; (220.3620) (080.3620) Lens system design; (220.1000) Aberration compensation; (080.0080) Geometric optics; (080.2720) Mathematical methods (general).

References and links

1. P. Mouroulis "Broadband achromatic telecentric lens," Nasa Tech Briefs, **NPO-44059**, (2007).
2. J. Rayces and M. R. Aguilar, "Selection of glasses for achromatic doublets with reduced secondary spectrum. I Tolerance conditions for secondary spectrum, spherochromatism, and fifth-order spherical aberration," *Appl. Opt.* **40**, 5663-5676 (2001).
3. R. D. Sigler, "Glass selection for airspaced apochromats using the Buchdahl dispersion equation," *Appl. Opt.* **25**, 4311-4320 (1986).
4. C. Gruescu, I. Nicoara, D. Popov, R. Bodea, and H. Hora, "Optical glass compatibility for the design of apochromatic systems," *Sci. Sinter.* **40**, 131-140 (2008).
5. P. Hariharan, "Superachromatic lens combination," *Opt. & Laser Tech.* **31**, 115-118 (1999).
6. P. Hariharan, "Apochromatic lens combinations, a novel design approach," *Opt. & Laser Tech.* **29**, 217-219 (1997).
7. R. I. Mercado and P. N. Robb, "Color corrected optical systems and method of selecting optical materials therefor," U.S Patent, **5,210,646**, (1993).
8. P. N. Robb, "Selection of optical glasses. 1: Two materials," *Appl. Opt.* **24**, 1864-1877 (1985).
9. N. V. D. W. Lessing, "Selection of optical glasses in superachromats," *Appl. Opt.* **9**, 1665-1668 (1970).
10. T. R. Sloan, "Analysis and correction of secondary color in optical systems," *Appl. Opt.* **9**, 853-858 (1970).
11. M. Herzberger and N. R. McClure, "The design of superachromatic lenses," *Appl. Opt.* **2**, 553-560 (1963).
12. R. R. Willey, "Machine-aided selection of optical glasses for two-elements, three-color achromats," *Appl. Opt.* **1**, 368-369 (1962).
13. R. E. Stephen, "Four-color achromats and superchromats," *J. Opt. Soc. Am.* **50**, 1016-1019, (1960).
14. W. S. Sun, C. H. Chu, and C. L. Tien, "Well-chosen method for an optimal design of doublet lens design," *Opt. Express* **17**, 1414-1428 (2009).
15. I. Ono, Y. Tatsuzawa, S. Kobayashi, and K. Yoshida, "Designing lens systems taking account of glass selection by real-coded genetic algorithms," in *Proceedings of IEEE International Conference on Systems, Man and Cybernetics* (Institute of Electrical and Electronics Engineers, New York, 1999), 7803-7831.
16. Y. C. Fang, C. M. Tsai, J. Macdonald, and Y. C. Pai, "Eliminating chromatic aberration in Gauss-type lens design using a novel genetic algorithm," *Appl. Opt.* **46**, 2401-2410 (2007).
17. L. Li, Q. H. Wang, X. Q. Xu, and D. H. Li, "Two-step method for lens system design," *Opt. Express* **18**, 13285-13300 (2010).
18. R. E. Fischer, A. J. Grant, U. Fotheringham, P. Hartmann, and S. Reichel, "Removing the mystique of glass selection," *Proc. SPIE* **5524**, 134-146 (2004).
19. W. J. Smith, *Modern Optical Engineering* (McGraw-Hill, Inc., 1990).

20. P. N. Robb and R. I. Mercado "Calculation of refractive indices using Buchdahl's chromatic coordinate," *Appl. Opt.* **22**, 1198-1215 (1983).
 21. J. Branke, K. Deb, K. Miettinen, and R. Slowinski, *Multiobjective Optimization: Interactive and Evolutionary Approaches* (Springer-Verlag, Berlin, 2008).
 22. N. Srinivas and K. Deb "Multi-objective function optimization using non-dominated sorting genetic algorithm," *Evol. Comput.* **2**, 221-248 (1994).
 23. N. Lopez, O. Aguirre, J. F. Espiritu, and H. A. Taboada "Using game theory as a post-Pareto analysis for renewable energy integration problems considering multiple objectives," in *Proceedings of the 41st International Conference on Computers & Industrial Engineering*, 678-683 Los Angeles, (2011).
 24. O. Aguirre, H. Taboada, D. Coit, and N. Wattanapongsakorn, "Multiple objective system reliability post-Pareto optimality using self organizing trees," in *Proceedings of IEEE International Conference on Quality and Reliability* (Institute of Electrical and Electronics Engineers, New York, 2011), 225-229.
 25. E. Zio and R. Bazzo, "Clustering procedure for reducing the number of representative solutions in the Pareto front of multiobjective optimization problems," *Eur. J. Oper. Res.* **210**, 624-634 (2011).
 26. X. Blasco, J. M. Herrero, J. Sanchis, and M. Martínez, "A new graphical visualization of n-dimensional Pareto front for decision-making in multiobjective optimization," *Inf. Sci.* **178**, 3908-3924 (2008).
 27. J. C. Ferreira, C. M. Fonseca, and A. Gaspar-Cunha, "Methodology to select solutions from the Pareto-optimal set: A comparative study," in *Proceedings of the 9th annual conference on Genetic and evolutionary computation*, (ACM, New York, NY, 2007), 789-796.
 28. V. Venkat, S. H. Jacobson, and J. A. Stori, "A Post-optimality analysis algorithm for multi-objective optimization," *Comput. Optim. Appl.* **28**, 357-372 (2004).
 29. C. A. Coello Coello, "Handling preferences in evolutionary multiobjective optimization: a survey," in *Proceedings of the 2000 Congress on Evolutionary Computation* (Institute of Electrical and Electronics Engineers, New York, 2000), 30-37.
 30. J. Rayces and M. R. Aguilar, "Selection of glasses for achromatic doublets with reduced secondary color," *Proc. SPIE* **4093**, 36-46 (2000).
 31. SCHOTT N. America, Inc., "Optical glass catalogue- ZEMAX format, status as of 13th September 2011, http://www.us.schott.com/advanced_optics/english/tools_downloads/download/index.html?PHPSESSID=utt2cbk96nlk3gf7gipb7ggt54#Optical%20Glass
-

1. Introduction

Multi-spectral imaging instruments are widely used in scientific instrumentation. The different spectral bands, which frequently go beyond the visible region of spectrum, can allow extraction of many important features and chemical-physical information from the objects been imaged.

Common examples of this kind of instrument are multispectral satellite remote sensing cameras, multispectral microscopes, and astronomical telescope multispectral cameras. These instruments sometimes cover spectral bands from the UV to the thermal IR. Depending on the instrument specification, an all-reflective solution for the optical system, which would be chromatic aberration-free, is not always feasible, due to some disadvantages of this kind of solution [1]. The design of a refractive optical system that can cover a wide spectral band providing good image quality is not an easy task. According to Rayces and Aguilar [2], two barriers impose limitations on an optical system performance, light diffraction and chromatic aberration.

The chromatic aberration in imaging forming optical systems is a well-known issue studied since the XVII century. As pointed out by Sigler [3], this topic has been one of most investigated in optical design.

Several graphical and mathematical methods for the selection of optimum glass combinations for the correction of chromatic aberration have been proposed [2,3-13]. However, the problem of glass selection is wide in scope and in our opinion is not yet completely solved. Even a recent publication about optimum glass selection [14] brings no relevant contributions for the subject in our opinion.

Some contemporary methods propose the use of evolutionary [15,16] and hybrid [17] optimization algorithms for the optimal glass selection. Despite of reporting excellent results, we believe these techniques can be computationally demanding due to the extremely huge number of different possibilities available even for a reasonable simple optical system. Moreover, these methods do not guaranty that the best set of glasses has been found.

Fischer *et al* [18] mention that the glass selection in optical design has a mystique and tends to be both a science and an art. Our goal in this paper is to present a synthesis method that systematizes the task of glass selection for the design of color corrected optical systems, making this an objective task. The proposed method is based on the unification of two other methods proposed in the literature [2,7] with some important contributions added, and a multi-objective approach for the problem.

In the next Section we present the motivation that conducted us to the development of this new method of glass selection. In the Section 3 we present the background for the proposed method, in Section 4 we explain the proposed method itself. In Section 5 we present one example of the application of the method. Concluding this work in Section 6.

2. Motivation

The studies presented herein were motivated by the request for the feasibility study of a single refractive optical system capable of covering and providing excellent image quality in five spectral bands, going from the blue (0.45-0.485-0.52 μm), passing through green (0.52-55-0.59 μm), red (0.63-0.66-0.69 μm), NIR (0.77-0.83-0.89 μm) and reaching the SWIR (1.5-1.6-1.7 μm) spectral region.

Optical system covering wide band with good image quality is a challenge due to the chromatic aberration. In this case a detailed study of how to design a broadband system like this had to be conducted. The success of such system lies on the selection of the right set of optical glasses used in the design [2,7,9,11,16]. For this purpose we started to study the available methods of glass selection in the literature. During this survey, we identified points that could be better developed in the available methods and we ended up with an improved technique that we present in this paper.

Using the developed method it was possible to design a preliminary system for the five spectral bands camera, which complies with the main requirements imposed to the system, as we show in Section 5.

3. Background of the proposed method

After studying many methods of glass selection available in the literature [2-13], we realized that the one proposed by Mercado and Robb [7] is the most theoretically rigorous and general. The Mercado-Robb method considers in the formulation different number of glasses used in the set, as well as different number of wavelengths for which the minimization of chromatic aberration is desired. It is possible to affirm that other methods presented in the literature [e.g. 4-6,9,11,13] can be seen as special cases of this method.

Despite the general formulation of the Mercado-Robb method and the excellent discussion provided in reference [7], the authors solve the problem for practical purposes just in some specific cases. The cases for two glasses corrected from 2 to n wavelengths are very well presented with all the necessary details. Nevertheless, for more than two glasses, only some particular cases are discussed. One reason is that for more than two glasses, the metric adopted to define how good a specific set of glasses is at color correction for n specific wavelengths, becomes difficult to define and interpret geometrically. Furthermore, the adopted method to calculate the optical power of each glass type does not have a general equation, also becoming complicated in these cases. The method presented in this paper improves the Mercado-Robb method with contributions that address some of the practical implementations issues.

In spite of the method of color correction proposed by Rayces and Aguilar [2] being limited to two glasses and three wavelengths, it establishes and makes use of some metrics that appear not to have been reported before in glass selection theory. These metrics are not related to color correction but are important for verifying if a set (in their case a pair) of glasses can provide a successful design. In contrast to other glass selection methods, the Rayces-Aguilar method uses as input not only the wavelengths, but also the focal length and

the numerical aperture of the designed system. In the method presented in this paper, we incorporate this metrics proposed by Rayces and Aguilar [2].

With different metrics of dissimilar physical natures for each possible glass arrangement, the use of a multi-objective approach was very convenient and helpful to filter out the non-dominated solutions and organize them in different Pareto rankings, helping the selection of the most appropriate glass combination solution for the problem.

3.1-The Mercado and Robb method with some new contributions

The index of refraction of optical materials is a function of the wavelength. Several mathematical models have been proposed to describe this dependence. Some are based in physical models other are simply empirical functions [19]. One of these models, proposed by Buchdahl [20] is given by Eq. (1).

$$N(\lambda) = N_0 + v_1\omega(\lambda) + v_2\omega(\lambda)^2 + \dots + v_n\omega(\lambda)^n \quad (1)$$

This model, as many others, is based on a Taylor series. N represents the refraction index for wavelength λ . N_0 is the refraction index in a reference wavelength λ_0 , and ω is a function of the wavelength λ that is called chromatic coordinate:

$$\omega = \frac{\delta\lambda}{1 + \alpha\delta\lambda} \quad (2)$$

where $\delta\lambda = \lambda - \lambda_0$, and α is a universal constant taken as 2.5 [7]. The dispersion coefficients v_n , are particular to a given glass. This dispersion equation proposed by Buchdahl converges rapidly and can model optical glasses to a very good accuracy using only a few terms in the series [20].

The develop method of glass selection for color correction takes advantage of this dispersion equation. If a set of glasses is needed to minimize the chromatic aberration for n wavelengths, Eq. (1) is expanded to include up to the $n-1^{\text{th}}$ algebraic power term. Then a system of linear equations is obtained to compute the dispersion coefficients v_n of each glass were the number of unknowns is equal to the number of equations.

By passing N_0 to the left side of Eq. (1) and by dividing both sides by the constant $N_0 - 1$, we obtain:

$$D(\lambda) = \sum_{i=1}^{n-1} \eta_i \omega(\lambda)^i \quad (3)$$

where: $D(\lambda) = \delta N(\lambda) / (N_0 - 1)$; $\delta N(\lambda) = N(\lambda) - N_0$ and $\eta_i = v_i / (N_0 - 1)$. The term $D(\lambda)$ is called dispersive power.

This equation is very important since the method presented in [7] is mainly based on it.

The optical power ϕ of a lens is defined as the inverse of the it's focal length f :

$$\phi = \frac{1}{f} \quad (4)$$

The optical power of a single thin lens for a wave λ is given by the relationship:

$$\phi(\lambda) = [N(\lambda) - 1](C_1 - C_2) \quad (5)$$

where C_1 and C_2 are the lens curvature.

For a specific optical material and a defined optical power, the quantity $(C_1 - C_2)$ must be a constant, conveniently called K . Thus we can write:

$$\phi(\lambda) = [N(\lambda) - 1]K \quad (6)$$

As a consequence, the power of a thin lens at λ_0 can be expressed by:

$$\phi(\lambda_0) = [N(\lambda_0) - 1]K \quad (7)$$

By use of $D(\lambda) = \delta N(\lambda)/(N_0 - 1)$, and $\delta N(\lambda) = N(\lambda) - N_0$, together with Eq. (7), we can write for the optical power:

$$\phi(\lambda) = \phi(\lambda_0)[1 + D(\lambda)] \quad (8)$$

For a system of k thin lenses in contact, the resulting optical power for the reference wavelength λ_0 is computed by:

$$\Phi(\lambda_0) = \sum_{j=1}^k \phi_j(\lambda_0) \quad (9)$$

Using Eq. (8) and Eq. (9), the total optical power for any wavelength λ can be written as:

$$\Phi(\lambda) = \Phi(\lambda_0) + \sum_{j=1}^k \phi_j(\lambda_0) D_j(\lambda) \quad (10)$$

Assuming that each one of the k lenses is made out of a different glass, where $k \geq 2$, the mathematical conditions for having an achromatized optical system in n wavelengths, where $n \geq 2$, can be given by:

$$\begin{aligned} \Phi(\lambda_1) &= \Phi(\lambda_2) \\ \Phi(\lambda_2) &= \Phi(\lambda_3) \\ &\vdots \\ \Phi(\lambda_{n-1}) &= \Phi(\lambda_n) \end{aligned} \quad (11)$$

Using Eq. (10), $\Phi(\lambda_1)$, $\Phi(\lambda_2)$, $\Phi(\lambda_3)$, ..., $\Phi(\lambda_n)$ can be transcribed in the following form:

$$\begin{aligned} \Phi(\lambda_1) &= \Phi(\lambda_0) + \phi_1(\lambda_0) D_1(\lambda_1) + \dots + \phi_k(\lambda_0) D_k(\lambda_1) \\ \Phi(\lambda_2) &= \Phi(\lambda_0) + \phi_1(\lambda_0) D_1(\lambda_2) + \dots + \phi_k(\lambda_0) D_k(\lambda_2) \\ &\vdots \\ \Phi(\lambda_n) &= \Phi(\lambda_0) + \phi_1(\lambda_0) D_1(\lambda_n) + \dots + \phi_k(\lambda_0) D_k(\lambda_n) \end{aligned} \quad (12)$$

Using the set of Eq. (12), the conditions for achromatized optical systems are:

$$\begin{aligned} \phi_1(\lambda_0) \cdot (D_1(\lambda_1) - D_1(\lambda_2)) + \dots + \phi_k(\lambda_0) \cdot (D_k(\lambda_1) - D_k(\lambda_2)) &= 0 \\ \phi_1(\lambda_0) \cdot (D_1(\lambda_2) - D_1(\lambda_3)) + \dots + \phi_k(\lambda_0) \cdot (D_k(\lambda_2) - D_k(\lambda_3)) &= 0 \\ &\vdots \\ \phi_1(\lambda_0) \cdot (D_1(\lambda_{n-1}) - D_1(\lambda_n)) + \dots + \phi_k(\lambda_0) \cdot (D_k(\lambda_{n-1}) - D_k(\lambda_n)) &= 0 \end{aligned} \quad (13)$$

The difference in the dispersive power of a particular glass j over the wavelength range $\lambda_1 < \lambda < \lambda_2$, can be written in simplified form as:

$$D_j(\lambda_1, \lambda_2) = D_j(\lambda_1) - D_j(\lambda_2) \quad (14)$$

By using the dispersive power definition in Eq. (3), we can rewrite Eq. (14) in terms of the chromatic coordinate ω as:

$$D_j(\lambda_1, \lambda_2) = \sum_{i=1}^{n-1} \eta_{ij} [\omega^i(\lambda_1) - \omega^i(\lambda_2)] \quad (15)$$

Thus we can write the conditions for achromatized optical systems, expressed in Eq. (13), in matrix form as:

$$\Delta\bar{\Omega} \cdot \bar{\eta} \cdot \bar{\Phi} = \bar{0} \quad (16)$$

where, $\Delta\bar{\Omega}$ is a square matrix of order $n-1 \times n-1$:

$$\Delta\bar{\Omega} = \begin{bmatrix} (\omega_1 - \omega_2) & (\omega_1^2 - \omega_2^2) & \cdots & (\omega_1^{n-1} - \omega_2^{n-1}) \\ (\omega_2 - \omega_3) & (\omega_2^2 - \omega_3^2) & \cdots & (\omega_2^{n-1} - \omega_3^{n-1}) \\ \vdots & \vdots & \ddots & \vdots \\ (\omega_{n-1} - \omega_n) & (\omega_{n-1}^2 - \omega_n^2) & \cdots & (\omega_{n-1}^{n-1} - \omega_n^{n-1}) \end{bmatrix} \quad (17)$$

$\bar{\eta}$ is a matrix of order $n-1 \times k$:

$$\bar{\eta} = \begin{bmatrix} \eta_{11} & \eta_{12} & \cdots & \eta_{1k} \\ \eta_{21} & \eta_{22} & \cdots & \eta_{2k} \\ \eta_{31} & \eta_{32} & \cdots & \eta_{3k} \\ \vdots & \vdots & \ddots & \vdots \\ \eta_{(n-1)1} & \eta_{(n-1)2} & \cdots & \eta_{(n-1)k} \end{bmatrix} \quad (18)$$

$\bar{\Phi}$ is a matrix of order $k \times 1$:

$$\bar{\Phi} = \begin{bmatrix} \phi_1(\lambda_0) \\ \phi_2(\lambda_0) \\ \vdots \\ \phi_k(\lambda_0) \end{bmatrix} \quad (19)$$

and $\bar{0}$ is a matrix of the $n-1 \times 1$ order:

$$\bar{0} = \begin{bmatrix} 0 \\ 0 \\ 0 \\ \vdots \\ 0 \end{bmatrix} \quad (20)$$

The matrix $\Delta\bar{\Omega}$ is a square and doubtless nonsingular. As a consequence its inverse ($\Delta\bar{\Omega}^{-1}$) exists. Multiplying both sides of Eq. (16) by $\Delta\bar{\Omega}^{-1}$ results in a condition to obtain a solution free from chromatic aberration for all the wavelengths defined:

$$\bar{\eta} \cdot \bar{\Phi} = \bar{0} \quad (21)$$

Equation (21) has a nontrivial solution (i.e. $\bar{\Phi} \neq \bar{0}$) if and only if the matrix $\bar{\eta}$ rank is lower than k (i.e. not a full rank matrix). This happens when there is a perfectly linear dependence among the columns of matrix $\bar{\eta}$. Nevertheless, for any practical and meaningful situation, where $k \leq n-1$, the linear dependence will virtually never be mathematically exact. As a consequence, the matrix $\bar{\eta}$ rank will always be equal to k . This result makes the rank of matrix $\bar{\eta}$ an inefficient metric either to identify sets of glasses that are free from chromatic

aberration in the defined wavelengths, or to compare the residual chromatic aberration among the different possible combination of glasses.

To solve this problem, Mercado and Robb provide a geometrical interpretation of the Eq. (21). In this way, they suggest a geometric metric to verify how good a set of glass is at color correction for a given set of wavelengths. The metric is easy to understand and visualize for the case of two glasses. Nevertheless, for more than two glasses the interpretation changes and becomes complicated. Another drawback is that the metric has no physical meaning.

In this paper we propose a different metric to verify how good a specific set of glasses is at minimizing the chromatic aberration for a given set of wavelengths. The proposed metric has a general form, not depending on the number of glasses used in the combination, and has a direct physical meaning. This new metric is presented and explained in some paragraphs ahead.

To minimize or correct the chromatic aberration, not only a specific set of compatible glasses must be selected, but also the right optical power for the lenses made with each one of these materials must be used. To calculate the optimum power of each glass that minimizes the chromatic aberration, both Eq. (16) and Eq. (9) are used. To simplify the computation, we normalize the focal length of the optical lens system for λ_0 . As a consequence Eq. (9) becomes:

$$\sum_{j=1}^k \phi_j(\lambda_0) = 1 \quad (22)$$

This equation can be written in a matrix form as:

$$\bar{S} \cdot \bar{\Phi} = 1 \quad (23)$$

where \bar{S} is a row vector of order $1 \times k$, with all elements equal to one.

Putting together Eq. (16) and Eq. (22) we obtain:

$$\begin{bmatrix} \bar{S} \\ \Delta\bar{\Omega} \cdot \bar{\eta} \end{bmatrix} \cdot \bar{\Phi} = \hat{e} \quad (24)$$

where \hat{e} is a column vector of order $n \times 1$ with the first element equal to one and the others zero as shown below :

$$\hat{e} = \begin{bmatrix} 1 \\ 0 \\ 0 \\ \vdots \\ 0 \end{bmatrix} \quad (25)$$

Defining $\bar{G} = \begin{bmatrix} \bar{S} \\ \Delta\bar{\Omega} \cdot \bar{\eta} \end{bmatrix}$, and assuming that $n \geq k$ and $k \geq 2$, we estimate an optimum $\bar{\Phi}$ applying in Eq. (24) the least square method, what results the following equation:

$$\hat{\bar{\Phi}} = (\bar{G}^t \cdot \bar{G})^{-1} \cdot \bar{G}^t \cdot \hat{e} \quad (26)$$

Equation (26) computes the optimum power of the lenses made with each one of the glasses considered in the set that minimizes the square sum of the chromatic change of power for the n defined wavelengths. We point out that the equations provided by Mercado and Robb, to compute the optical powers, are only related to some specific situations and do not use all the glass information available. In contrast, the equation presented herein is general,

uses all the glass dispersion coefficients available, and provides the minimum chromatic aberrations for the glass set considered, in the n given wavelengths.

Now, it is possible to use the vector $\hat{\Phi}$ in Eq. (16), to obtain the minimum chromatic change of power \overline{CCP} , as expressed in Eq. (27).

$$\overline{CCP} = \Delta\bar{\Omega} \cdot \bar{\eta} \cdot \hat{\Phi} \quad (27)$$

Our metric to verify how suitable a specific set of glasses is for minimizing chromatic aberration, for a given set of n wavelengths, is now established as the modulus of the vector \overline{CCP} .

As we have normalized the optical power (see Eq. (22)), we obtain an excellent approximation for the chromatic focal shift by multiplying the vector \overline{CCP} by the desired effective focal length F for the optical system.

$$\begin{bmatrix} f(\lambda_2) - f(\lambda_1) \\ f(\lambda_3) - f(\lambda_2) \\ \vdots \\ f(\lambda_n) - f(\lambda_{n-1}) \end{bmatrix} \approx \overline{CCP} \cdot F \quad (28)$$

As the chromatic focal shift is proportional to \overline{CCP} it clearly gives physical meaning to our metric.

3.2-The Rayces-Aguilar method

Rayces and Aguilar [2] proposed a method of glass selection where not only the chromatic correction is considered, but also aberrations, that according to the authors, cannot be corrected, namely spherochromatism and fifth order spherical aberration.

The Rayces-Aguilar method is based on an exhaustive search of combination of pairs of glasses. The possible arrangements of glasses, deriving from a glass catalog, are tested. For each glass set possibility the power of the glasses are computed to produce a thin achromatic doublet solution for the two extreme wavelengths considered. The chromatic aberration for the middle wavelength, also called the secondary spectrum, is computed. Based on the power of the elements of the doublet and on the desirable aperture of the system, a first weeding out of potentially useless solutions is carried out. This eliminates solutions with steep curves, what is an indication of high-order monochromatic aberrations, which are difficult to correct or balance. In the next step, the radius of each surface is computed to produce an aplanatic solution to third-order approximation using structural aberration coefficients. Paraxial rays are then traced to compute third-order sphero-chromatism and fifth-order spherical aberration. Based on the magnitude of these aberrations, a second glass arrangement elimination is carried out.

The output of the Rayces-Aguilar method is a table with solutions that comply with the limits imposed for each aberration, ranked according to the secondary spectrum value. The method provides a certain level of confidence for glass combinations solutions that may provide a successful design.

3.3-The multi-objective approach

Despite being frequently considered as mono-objective, practical optimization problems have in general more than one objective or criteria, which usually are conflicting. In the problem of finding the best glass combinations for color correction we pursue more than one objective and therefore the use of a multi-objective approach [21] is appropriate.

When a problem is treated as multi-objective, usually there is a set of solutions, and not only one solution. One solution in this set cannot be considered, in principle, better than

another solution in the same set, because at least it will be worse than another solution in one aspect or objective. This set of solutions is known as non-dominated solutions. When these solutions are plotted in the objective-functions space they form the thus called Pareto front.

To illustrate the ideas of dominance, non-dominance and Pareto front consider Fig. 1 where blue and red dots represent solutions of a multi-objective problem as plotted in the objective-function space F_1 and F_2 .

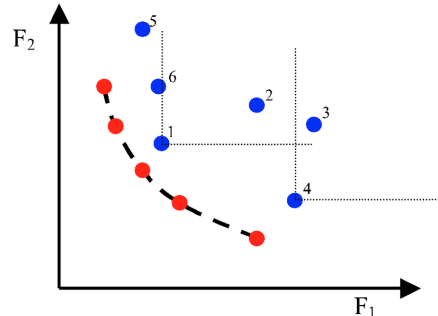


Fig. 1. The graph shows solutions for a generic min-min multi-objective problem, plotted in the objective-functions space F_1 and F_2 . Dominated solutions are represented in blue, while red dots represent non-dominated solutions.

Objective functions are metrics used to evaluate a specific characteristic of a solution. The example considered in Fig. 1 represents a two objective minimum-minimum problem. This means that the smaller the values of F_1 and F_2 the better the solution is.

The red dots represent the non-dominated solutions while the blue dots represent the dominated solutions. A given solution “A” is considered dominated when there is a solution “B” with at least one of objectives better than the objectives at solution “A”. The dominance relationship among the dominated solutions can also be considered; for example, the solution 1 dominates solutions 2 and 3 [21].

When the non-dominated solutions are plotted on the objective function space, they form the so-called Pareto front, represented in the Fig. 1 by the dashed line connecting the red dots.

Another useful concept used in this paper is the Pareto rank [22]. For a set of possible solutions of a specific problem the dominance definition can be applied several times. Each time the previous non-dominated solutions are removed, giving place to the formation of a new Pareto front. The different Pareto fronts that result are classified by ranking. For example, in Fig. 1 the red dots forming the Pareto ranking equal to 1. Solutions 5, 6, 1 and 4 are the ones forming the Pareto ranking 2 and so on.

The dominance, non-dominance, Pareto front and Pareto rank concepts can be used for multi-objective problems containing any number of objectives.

4. The synthesis method of glass selection

With the background presented in the last section, the explanation of our method of glass selection becomes straightforward. Its implementation involves several steps.

Step 1. As input data for the method, the designer must provide the effective focal length F , the f number $F/\#$, the n wavelengths that covers the desired spectral range, and the number of the primary wavelength λ_0 . A glass catalog and the number of glasses used in the combination (i.e. 2, 3, 4, etc) must also be specified.

Step 2. At the outset, the first $n-1$ dispersion coefficients η_i , are calculated for each glass in the catalog. For that, the n specified wavelengths and their respective refractive index in the corresponding glass are used in Eq. (3). This results in a system of linear equations with $n-1$

equations and $n-1$ unknowns, that when solved provides the η_i dispersion coefficients. With the specified wavelengths, the matrix $\Delta\bar{\Omega}$ is then calculated using Eq. (17).

Step 3. Next, all possible arrangements for the glasses from the specified catalog are performed. For each possibility the optimum normalized power of each glass is computed using Eq. (26). The sum of the absolute power of each arrangement, given by Eq. (29) below, is used as a metric for the first weeding out. As pointed out by Rayces and Aguilar [2], high power elements have steep surfaces that result in large monochromatic aberrations, involving higher orders of aberration. This first cut eliminates potentially useless solutions. The metric used here is different from the one presented in [2]. It is more general in terms of the number of glasses used in the combination. This metric has been suggested in [11].

$$F_1 = \sum_{j=1}^k |\phi_j(\lambda_0)| \quad (29)$$

The user must set the maximum value for F_1 . The glass arrangements that have F_1 values larger than the specified value are discarded. This metric is not just used to eliminate potential useless solutions but can also be used as one of the metrics in the multi-objective approach proposed in this work. The next steps and calculations are only performed for the arrangements that comply with the F_1 limit imposed.

The vector \overline{CCP} is then calculated by Eq. (27). The modulus of this vector, called F_2 ($F_2 = |\overline{CCP}|$) can also be used in the multi-objective analysis. The smaller the value of F_2 the better the color correction the set of glasses provides as explained in Section 3.1.

Step 4. Following, a thin lens aplanatic solution for wavelength λ_0 is found for each candidate glass arrangement. To find the aplanatic solution, the system structural coefficient for spherical aberration Ξ and coma X are set equal to zero, with the power of each glass element calculated using Eq. (26). We ended up with the following set of equations.

$$\Xi = \sum_{j=1}^k \xi_j = 0; \quad (30)$$

$$X = \sum_{j=1}^k \chi_j = 0; \quad (31)$$

$$\begin{aligned} [N_1(\lambda_0) - 1] \left(\frac{1}{r_1} - \frac{1}{r_2} \right) &= \left(\frac{\phi_1(\lambda_0)}{F} \right) \\ &\vdots \\ [N_k(\lambda_0) - 1] \left(\frac{1}{r_{(2k-1)}} - \frac{1}{r_{(2k)}} \right) &= \left(\frac{\phi_k(\lambda_0)}{F} \right) \end{aligned} \quad (32)$$

To find the aplanatic solution it is necessary to solve the above set of equations for r_1 to r_{2k} .

For the case of a doublet, $k=2$, there are four equations and four unknowns resulting in a straightforward solution. As Eq. (30) has a quadratic dependence as a function of the radius (see appendix A in [30]), two different aplanatic solutions can be obtained for each glass arrangement. The best solution is retained where the definition for a better solution is based in the metric F_3 as explained ahead.

For $k \geq 3$ there are more unknowns than equations. For solving the set of equations in an analytic and fast way, some constraint equations are added to make the number of unknowns equal to the number of equations. For example, the case where $k=3$ (triplet), two options for the constraint equations are possible $r_3=r_2$, or $r_5=r_4$. The system can then be solved for both

cases; in each case two solutions exist, which means four total possible solutions. Once more only the better solution is retained. This same idea can be expanded for $k>3$. The solution for the set of equations where $k\geq 3$ is not so trivial and is made with the help of a computer.

For each one of the possible retained solutions, the fifth-order spherical $W_{060}(\lambda_0)$ and the sphero-chromatism $W_{040CL}(\lambda_1 \dots \lambda_n)$ wave aberration coefficients are calculated according to the algorithm presented in [30]. The fifth-order spherical is calculated for the reference wavelength λ_0 . The sphero-chromatism is calculated for all possible combinations of the input wavelengths, and the worse case is assigned for the set.

Step 5. The third and last metric used in the multi-objective analysis is then computed by the sum of the normalized fifth-order spherical \bar{W}_{060} and normalized sphero-chromatism \bar{W}_{040CL} wave aberration coefficients according to Eq. (33).

$$F_3 = (\bar{W}_{040CL} + \bar{W}_{060}) \quad (33)$$

where [2]:

$$\bar{W}_{060} = \frac{14 \cdot W_{060}(\lambda_0)}{20\sqrt{7}} \quad (34)$$

and

$$\bar{W}_{040CL} = \frac{14 \cdot W_{040CL}(\lambda_1 \dots \lambda_n)}{6\sqrt{5}} \quad (35)$$

The metric F_3 is also used to define which of the possible aplanatic solutions for a specific glass set is the best one, as mentioned above.

Step 6. For all the possible set of glass arrangements complying with the maximum allowed metric F_1 , the best aplanatic solution is stored in a table with its respective F_1 , F_2 and F_3 metric values. The data stored in the table are organized as shown in the Fig. 2. The r 's are the radius of curvature of each surface and ϕ 's are the normalized optical power of each thin lens.

N°	Glass 1	...	Glass k	Γ_1	...	Γ_{2k}	Φ_1	...	Φ_k	F_1	F_2	F_3
1												
2												
⋮	⋮	⋮	⋮	⋮	⋮	⋮	⋮	⋮	⋮	⋮	⋮	⋮

Fig. 2. Format of the table where the data for each glass arrangement best aplanatic solution is stored.

Step 7. The solutions are then organized into different Pareto ranks using the metrics F_1 , F_2 and F_3 .

Step 8. At last, a post-Pareto analysis is applied in the first or in the firsts Pareto ranks, organizing the solutions in the out-put table from the best to the worse trade-off solutions.

In summary, the glass selection for the design of optical systems with reduced chromatic aberration can be seen as a multi-objective optimization problem where the goal is to minimize at the same time the objective functions F_1 , F_2 and F_3 , subjected to: $F_1 \leq Constant$; to Eq. (30), (31) and (32), and to some additional constrains when $k\geq 3$ (e.g. $r_3=r_2$, or $r_5=r_4$, for the case when $k=3$). The method we used here to solve the problem was an exhaustive search.

The method is also represented in a flowchart form in Fig. 3.

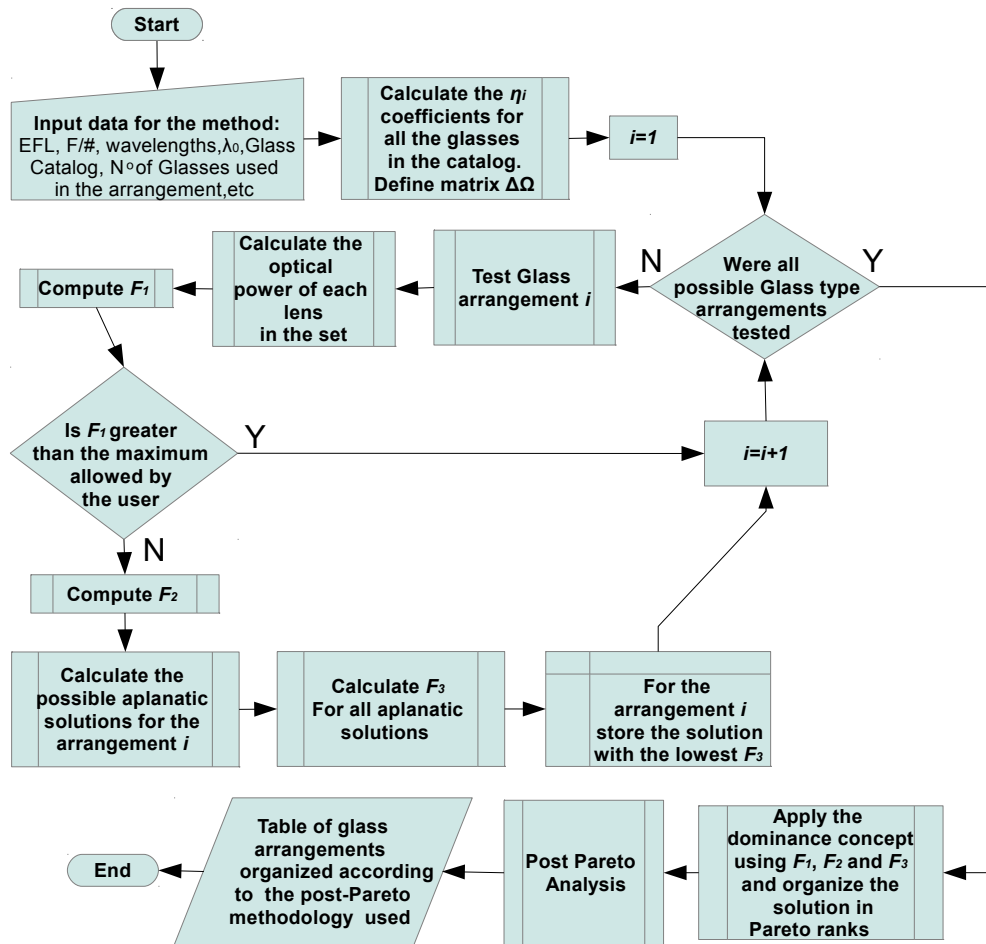


Fig. 3. Flowchart of the proposed method of glass combination selection.

4.1-Post Pareto analysis

The Pareto front, or the Pareto rank 1, specifies the global non-dominated trade-off solutions for the problem. In practice, the designer has to pick one solution from this set for designing the optical system. Despite one solution in the Pareto front not being in principle considered better than other solution in the same front, it is evident and intuitive that a discrimination among the less satisfactory trade-offs and the most promising solution can be done. This process of selecting a solution is called decision-making. Many methods for supporting this process, also known as Post-Pareto analysis, can be found in the literature [23-29].

The task of post-Pareto analysis is not so easy; especially when the number of candidate solutions is large and the number of objectives is greater than two, which is the case. Depending on the number of glasses in the catalog and the number of glasses used in the combination, hundreds of solutions are usually obtained in the Pareto front.

For this work, we used two methods of post-Pareto analysis described in sub-sections 4.1.1 and 4.1.2.

4.1.1-Minimum F_2

Organizing the solutions in the Pareto front by the most important metric is intuitive to perform the post Pareto analysis. In this paper the color correction is the most important

metric, given by F_2 . Rayces and Aguilar [2, 30] also propose the organization of the output table of their method by the color correction index, in their case given by the secondary color. We recommend the use of this method if the number of glasses used in the set is much lower than the number of wavelengths defined and the spectral band is broad, covering different regions of the spectrum. The best glass combination is not necessarily in the first line of this table but probably among the first ones. The final choice will be made by the designer, in this case, it is important to look for a solution with a low F_3 but at the same time keeping F_2 as low as possible. Other glass parameters can also be considered in this final choice.

4.1.2-Minimum distance to the origin

Suppose a generic multi-objective problem with two objective functions O_1 and O_2 , where the goal is to minimize both functions. Suppose also that the Pareto front for this problem in the objective function space can be represented as the line plotted in Fig. 4. This is in fact a very usual shape for a Pareto front in a min-min problem. In this Figure we highlight the “knee”, a region where the best trade-off solutions lays.

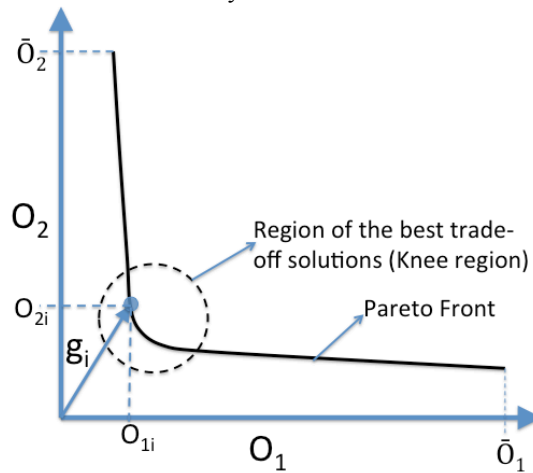


Fig. 4. Typical Pareto front for 2 objective min-min problem, showing the attributes used in the post-Pareto analysis.

Looking at Fig. 4, it is possible to say that the bigger the length of vector g_i the less satisfactory trade-offs solution i provides. This vector g_i connects the origin of the system to a solution i on the Pareto front, having objectives values O_{1i} and O_{2i} . Due to possible different physical meanings of the objective functions, completely different numerical values ranges may be represented in each axis. This difference in range can be a problem for the use of the vector numerical length as a metric. However, we can work out this issue through the normalization of each one of the objectives. This can be done dividing O_{1i} by \bar{O}_1 , O_{2i} by \bar{O}_2 , and so on, for each solution i . The solutions can than be organized according to the value $|\bar{g}_i|$, given in its general form by Eq. (36).

$$|\bar{g}_i| = \sqrt{\sum_{ob=1}^m \left(\frac{O_{ob,i}}{\bar{O}_{ob}} \right)^2} \quad (36)$$

These \bar{O}_{ob} values are not necessarily the highest values in the range of the solutions for each objective as we show in Fig. 4. For instance, in this work we defined this normalization factor for each variable as the value that accumulates 90% of the solutions used in the analysis. Organizing the solutions in the Pareto front in a new table using the metric given by Eq. (36), from the lowest to the highest, supports in a very nice way the decision-making.

keeping the final choice for the designer that should be limited among the firsts lines in the table.

We recommend the use of this method if the number of glasses k is within $n \geq k > n/2$. For the case when n is equal to k , F_2 is zero, so only functions F_1 and F_3 are used to calculate $|\bar{g}_i|$. When k is lower than n , the use of only F_2 and F_3 to compute $|\bar{g}_i|$ is recommended. Again, the best glass combination does not necessarily lie in the very first line of this table but probably among the first ones, and the designer must make the final choice.

5. Example

In this section it is presented an example for the application of the glass selection method proposed in this work. The specification of the lens system that motivated this development, described in Section 2, is used as the example. Our intention is not to present a final design for the problem but to show how the method can be used to effectively design a multi-spectral lens system. In Table 13 it is shown the most important features specified for the optical system.

Table 13-Basic Requirements for the optical system used as example.

ITEM	REQUIREMENT
Effective Focal Length	250mm
F/ Number (f#)	5
Field of view	± 9 degrees
Spectral Bands	0.450-0.520; 0.520-0.590; 0.630-0.690; 0.770-0.890 e 1.5-1.7 μ m
Maximal Distortion	3%
Field relative illumination	Constant $\pm 3\%$
Back focal length (BFL)	Large enough to fit the spectral bands beamsplitter (more than 50mm).
Design Resolution (MTF)	Close to diffraction limit for all bands in sagittal and tangential directions.

The inputs for the method can be extracted from the spec in Table 13. The focal length and the F/# are taken directly from the table. For the wavelengths, the central values for each spectral band were used: 0.485, 0.55, 0.66, 0.83 and 1.6 microns. The primary wavelength λ_0 was set to 0.83 microns the due to its proximity to the central wave of the whole spectrum covered by the instrument.

The newest available Schott glass catalog was selected [31] to run the method. However, some specific glasses from this catalog were discarded: Lithotec-CAF2, N-PK51, N-PK52A, N-FK51A, P-PK53, N-PSK53A and N-PSK53. Despite these glasses being very good options for color correction, they were rejected due to their undesirable thermal behavior. Optical systems designed with these glasses are potentially sensitive to temperature changes. Normally, for small changes of temperature, the effect can be compensated with refocusing, however, the application of the instrument object of this example, cannot afford either a manual or an automatic refocus mechanism.

At first we ran the method for arrangements of two glasses. The limit F_1 defined for this case was 9. The post-Pareto analysis was applied only for the solutions in the Pareto ranking 1, using the method presented in Section 4.1.1.

In Table 14 we can see the first 10 rows of the output table, sorted from the smallest to the biggest F_2 .

Table 14- Output table from the glass selection method for 2 glasses sorted by F_2 .

N°	Glass 1	Glass 2	r_1	r_2	r_3	r_4	ϕ_1	ϕ_2	F_1	F_2	F_3
771	N-BALF4	N-KZFS11	170.91	-37.58	-38.36	-351.12	4.63	-3.63	8.27	5.46E-04	16.28
606	N-BAK1	N-KZFS11	163.36	-47.77	-48.80	-403.20	3.82	-2.82	6.64	5.75E-04	8.69
1383	N-KZFS11	N-BAK1	111.63	37.08	36.53	3124.93	-2.82	3.82	6.64	5.75E-04	8.59
1417	N-KZFS11	N-SK2	129.72	38.16	37.98	3141.56	-2.90	3.90	6.79	7.36E-04	6.94
4394	N-SSK5	KZFS12	168.54	-58.44	-58.88	-1078.81	3.74	-2.74	6.47	2.50E-03	6.12
216	KZFS12	N-SSK5	134.49	42.57	42.37	1796.69	-2.74	3.74	6.47	2.50E-03	5.91
2092	N-LAK12	KZFS12	168.51	-74.49	-74.20	-2741.16	3.23	-2.23	5.47	3.72E-03	4.35
191	KZFS12	N-LAK12	145.49	50.04	50.19	1765.35	-2.23	3.23	5.47	3.72E-03	4.29
212	KZFS12	N-SK2	118.05	48.24	47.64	2732.27	-2.09	3.09	5.18	3.80E-03	4.32
596	N-BAK1	KZFS12	160.66	-65.53	-67.81	-355.23	3.03	-2.03	5.07	4.20E-03	4.92

We believe that the fourth line of Table 14 brings the best trade-off option for the combination of 2 glasses for the problem. Solutions above the fourth line have F_2 values slightly smaller, however, the F_3 values are significantly higher. Below the fourth line the F_2 values increase very fast.

Before we go for the design of the optical system with the selected pair of glass, we can perform a roughly check to see if it is promising in terms of the color correction. It is known that the tolerable depth of focus of a system can be given by [19]:

$$\varepsilon = \pm 2\lambda(f\#)^2 \quad (37)$$

Calculating Eq. (37), using the $f\#$ provided in the Table 13 and the selected primary wavelength λ_0 (0.83 μm), results in $\varepsilon = \pm 0.0415\text{mm}$. We can compare this value to the result from the multiplication between F_2 and the focal length F , which for the selected pair gives 0.184mm. This number is much higher than the calculated ε , telling us that the design with the selected pair is not promising. Even with the lowest F_2 value shown in the first line of Table 14, we cannot even get close to the calculated ε . The conclusion is that more glasses to the set are necessary to design the desirable system with the glass catalog used.

In this case, we ran the method again with the same parameters but now for three glasses in the set. With more glasses, the F_1 limit was changed to 11. The most suitable post-Pareto method in this situation is the one presented in Section 4.1.2, where the metric $|\bar{g}_i|$ is calculated using only F_2 and F_3 .

In Table 15 we can see the first 15 rows of the output table resulted from the application of the method using 3 glasses in the set. The solutions are sorted from the smallest to the biggest $|\bar{g}_i|$.

For the case of three glasses, we selected two solutions among the first lines that we believe to be good trade-offs. The chosen solutions are located in the fifth and thirteenth lines of Table 15. The first one has a smaller F_3 than the second one and also a better power distribution among the lenses. On the other hand the second has a smaller F_2 . Calculating the multiplication between F_2 and the focal length for both solutions we get 0.047mm and 0.014mm respectively. These numbers reveals that these glass combinations are promising in terms of color correction.

Figure 5 shows the chromatic focal shift for the two aplanatic thin triplet obtained from the glass combination chosen from Table 15. The one in the left side of the Fig. 5 corresponds to the glasses on the fifth line of Table 15 (N-BAF52, N-KZFS11 and N-BAK2) while the one in the right side corresponds to the ones on the thirteenth line of Table 15 (N-KZFS8, P-SF68 and N-SK2). This graphs reveals that despite not crossing the axis five times in the center of all spectral bands, the shift is not greater than 33 microns for the combination N-BAF52, N-KZFS11 and N-BAK2 and less than 13 microns for the combination N-KZFS8, P-SF68 and N-SK2 for the central wavelength of each spectral band. This gives us confidence that the design of the objective can be done. The residual chromatic focal shift can be compensated with a slightly change on the position of each spectral band image plane, as each band will focus in a different detector. In this case we can go for the design.

Table 15- Output table from the glass selection method for 3 glasses sorted by $|\bar{g}_i|$.

N°	Glass 1	Glass 2	Glass 3	r_1	...	r_c	φ_1	φ_2	φ_3	F_1	F_2	F_3
5317	N-BAF52	N-KZFS11	N-SK4	145.26	...	-1056.62	3.12	-4.68	2.56	10.37	2.15E-04	2.98
35786	N-SK4	N-KZFS11	N-BAF52	135.68	...	-2128.74	2.56	-4.68	3.12	10.37	2.15E-04	2.99
11387	N-KZFS11	N-BAF52	N-SK4	-42.02	...	-55.13	-4.68	3.12	2.56	10.37	2.15E-04	3.03
25496	N-LAK8	N-KZFS11	N-BAK2	-20.89	...	-23.05	-3.21	-1.58	5.79	10.59	4.61E-04	1.49
5310	N-BAF52	N-KZFS11	N-BAK2	110.35	...	-1266.01	3.34	-4.71	2.38	10.43	1.88E-04	3.14
26091	N-LASF31A	N-KZFS2	N-BAK1	-16.58	...	-17.83	-2.09	-2.03	5.13	9.26	5.11E-04	0.67
13718	N-KZFS11	N-SSK8	N-SK4	-45.56	...	-62.64	-3.71	2.41	2.29	8.41	4.28E-04	2.04
13672	N-KZFS11	N-SSK8	N-BAK2	-47.45	...	-65.80	-3.67	2.56	2.11	8.35	4.17E-04	2.14
9960	N-FK5	N-KZFS11	N-BAF51	165.17	...	-264.64	2.02	-4.37	3.35	9.74	3.18E-04	2.84
11541	N-KZFS11	N-BAK2	N-SSK8	-43.54	...	-58.25	-3.67	2.11	2.56	8.35	4.17E-04	2.23
6824	N-BAK2	N-KZFS11	N-SSK8	142.16	...	-444.22	2.11	-3.67	2.56	8.35	4.17E-04	2.28
37966	N-SSK8	N-KZFS11	N-BAK2	115.23	...	-1534.96	2.56	-3.67	2.11	8.35	4.17E-04	2.31
20485	N-KZFS8	P-SF68	N-SK2	98.06	...	812.98	-4.73	1.17	4.56	10.46	5.66E-05	3.56
2283	KZFS12	N-SF4	N-SK4	112.05	...	1464.73	-4.48	1.54	3.94	9.96	3.67E-04	2.68
11237	N-KZFS11	LLF1	N-SK14	-42.00	...	-54.57	-4.20	2.49	2.70	9.39	3.75E-04	2.63

The output glass combination chosen after the application of the method proposed can then be used to design an optical system either applying classical or evolutionary methods. In this last one the advantage is the significantly reduction of the design space, decreasing the number of glasses from thousands to just a few.

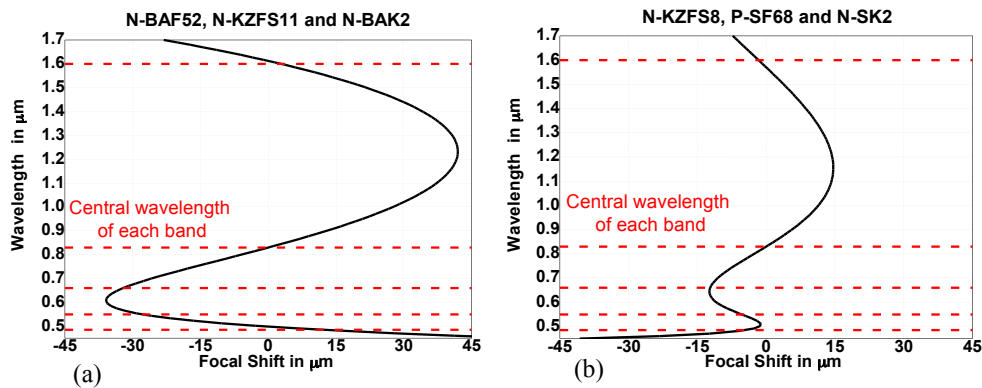


Fig. 5. Chromatic focal Shift for the applanatic triplets designed with glass combination (a) N-BAF52, N-KZFS11 and N-BAK2, and combination (b) N-KZFS8, P-SF68 and N-SK2.

The lens design lay out for the glass combination N-BAF52, N-KZFS11 and N-BAK2 can be seen in the top left side of Fig. 6, where each lens glass is identified. The system complies with all the basic requirements presented in Table 15. The image quality is also shown in Fig. 6 through the MTF curves. The Quality is fair for the blue band and great for the other bands.

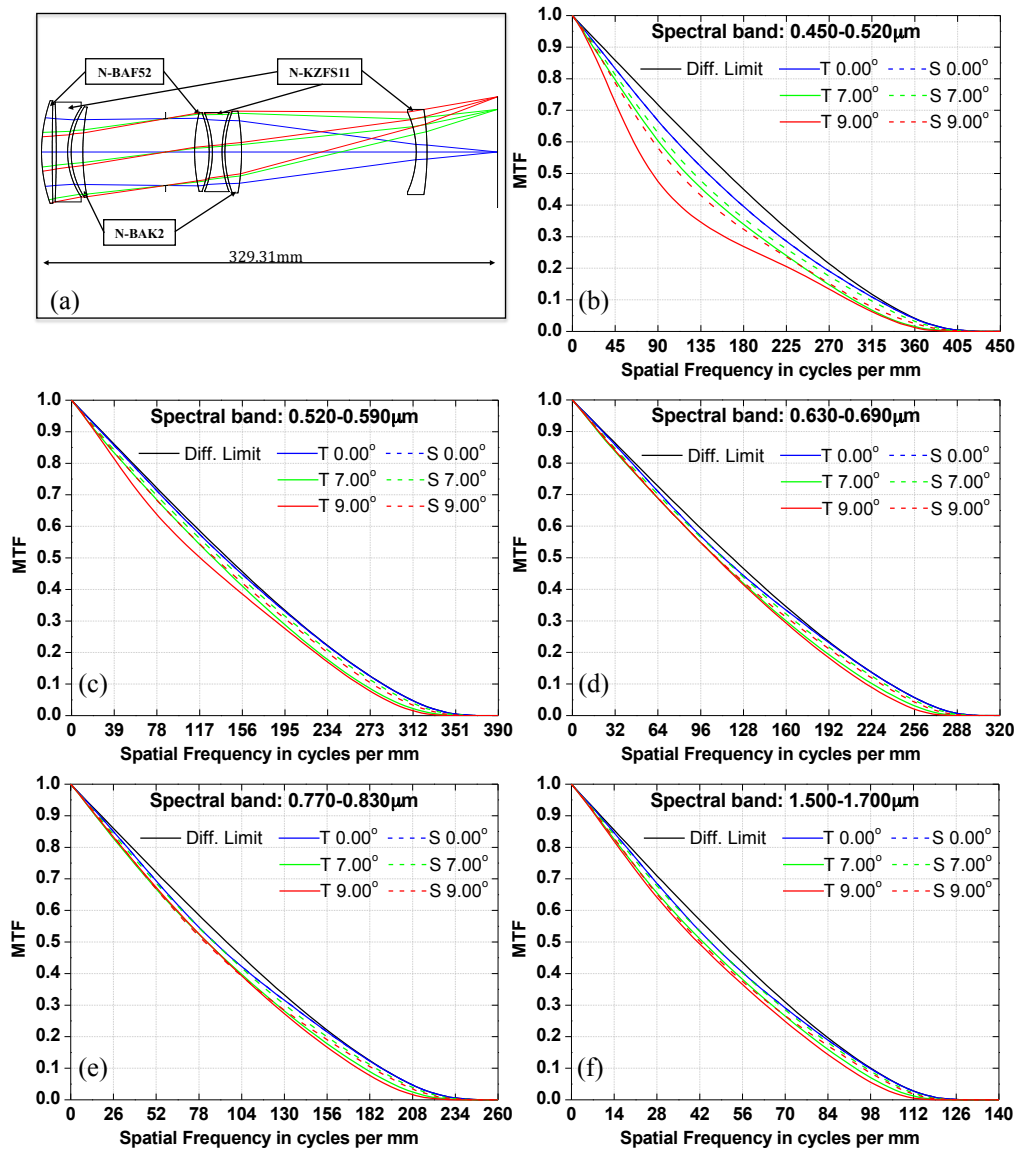


Fig. 6. Layout (a) and MTFs (b)(c)(d)(e)(f) for each spectral band and field position for the design made with glass combination N-BAF52, N-KZFS11 and N-BAK2.

In Fig. 7 the layout for the lens system designed with the glass combination N-KZFS8, P-SF68 and N-SK2 is shown in the top left side. The glass of each one of the lenses is identified in the layout. Notice that the glass P-SF68 is present only in one lens. This reflects the big difference in the power distribution between the 2 positive lenses as shown in Table 15.

The MTF curves for each one of the spectral bands for this system is also presented in Fig. 7. Again the image quality is fair for the blue band and excellent for the other bands for the whole field of view.

For both systems presented, the MTF curves reported were obtained with each spectral band focusing in its best focus. The prescription data for the lens shown in Fig. 6 and Fig. 7 are presented in Table 16 and Table 17 in the end of this section. The systems were designed using only spherical lenses.

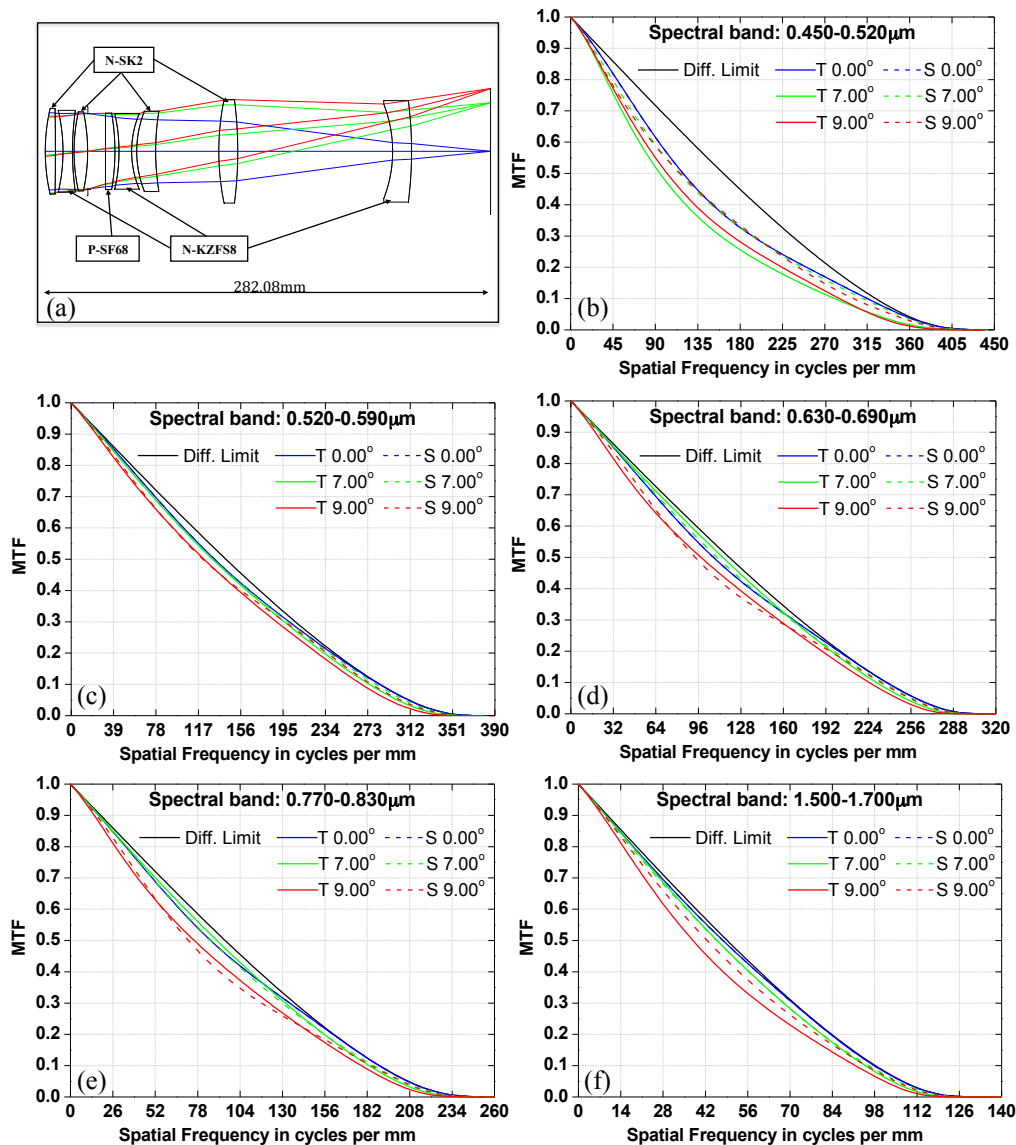


Fig. 7. Layout (a) and MTFs (b)(c)(d)(e)(f) for each spectral band and field position for the design made with glass combination N-KZFS8 P-SF68 and N-SK2.

Despite being very good designs, the systems presented in this example might not represent final designs for the system that motivated the development of the glass selection method proposed herein. Probably more elements in the system will be needed in order to comply with all the detailed optical requirements necessary for the system, as well as to accommodate the beam splitters necessary for the spectral bands separation in the different detectors. Although, care was taken to design systems that are very representative in order to show the feasibility of the project. For example we avoided the use of some glasses with potential thermal problems, and also cemented lens that would facilitate the design, controlling easier the lateral color, but would not be desired for the final system due to some thermo mechanical constraints.

Table 16-Prescription data for the system shown in Fig. 6.

System 1. EFL=250mm; F/# =5.			
Surf	Radius (mm)	Thickness (mm)	Glass
OBJ	Infinity	Infinity	
1	114.506	7.737	N-BAF52
2	1551.850	2.887	
3	-787.580	8.220	N-KZFS11
4	58.764	2.534	
5	60.880	8.455	N-BAK2
6	173.824	59.804	
STO	Infinity	20.929	
8	125.540	10.496	N-BAF52
9	-80.372	2.299	
10	-75.012	7.000	N-KZFS11
11	84.061	2.084	
12	84.729	12.000	N-BAK2
13	-170.627	126.151	
14	-69.911	7.833	N-KZFS11
15	-207.232	50.887	

Table 17- Prescription data for the system shown in Fig. 7.

System 2. EFL=250mm; F/# =5.			
Surf	Radius (mm)	Thickness (mm)	Glass
OBJ	Infinity	Infinity	
1	120.751	6.425	N-SK2
2	-1753.068	4.809	
3	-112.487	6.002	N-KZFS8
4	179.109	1.011	
5	115.631	8.594	N-SK2
6	-119.451	0.130	
STO	Infinity	11.169	
8	12071.420	6.000	P-SF68
9	-141.327	2.586	
10	-107.188	8.000	N-KZFS8
11	62.025	3.207	
12	68.587	12.000	N-SK2
13	159.482	40.000	
14	163.086	12.000	N-SK2
15	-257.749	98.105	
16	-82.596	12.000	N-KZFS8
17	-253.127	50.000	

6. Conclusion

In the research of available methods and techniques of glass selection for color correction in lens design, we realized that all presented approaches in the literature had some drawbacks and/or missing points. During the literature survey two of the reviewed methods called our attention: the Mercado and Robb method [7] and the Rayces and Aguilar method [2]. The first one presents a technique in a very general form in terms of the number of wavelengths where the achromatization is desired, spectral region, and number of glass material used in the set. However, it has some practical implementation issues that limit its use to some specific cases. The second is limited to the combination of only two glasses and three wavelengths. Nevertheless, it proposes the use of some metrics very important in the identification of promising glass combinations that can potentially provide good final designs.

Unifying these two mention methods, providing some original contributions to Mercado and Robb technique that repair its practical issues, and using a multi-objective approach, a

new method of glass selection for color correction was developed. This new method offers significant advantages in the task of glass selection, leading to optimum choice of optical glasses for specific problems, as pointed out and demonstrated here.

Along this paper we went from the background theory, passing through a detailed description of the new proposed method and finally wrapped it up with a practical example. The design examples demonstrated the power of the proposed method in fiddling compatible glasses that are able to conduct to excellent final designs. The results of this paper offer significant improvements to the problem of glass selection in lens design when color correction is an important matter, converting this task into a systematic and objective work. The efficiency of this new method will be investigated in future papers for other lens design problems, involving different spectral bands and types of lens systems.

We intend to incorporate the presented method of glass selection together with evolutionary optimization methods in lens design that we have been working on. The glass selection method has the ability to identify the most promising glasses to be used in a certain design, reducing the glass options from hundreds to just a few. As a consequence the design space is reduced and simplified, what is a significant advantage for global search heuristic methods.

In a near future, free stand-alone version of the software with the method presented here will be provided. The software will be found in the site: <http://www.optics.arizona.edu/glassselectiontool>. Meanwhile, we can provide free of charge tables of glass combinations upon request for specific input data provided. The request can be done by e-mail: braulio@dea.inpe.br.

Acknowledgments

B. F. C. Albuquerque gratefully acknowledges the Brazilian Research Council (CNPq) for supporting these studies and the Kidger Optics Associates for also supporting these studies through the 2010 Michael Kidger Memorial Scholarship in Optical Design.